DIRECT OBSERVATION AND REACTIONS OF ORGANIC BIRADICALS GENERATED FROM NOVEL BICYCLIC AZOALKANES

Thesis by

RAKESH JAIN

In Partial Fulfillment of the Requirements
for the Degree of
Doctor of Philosophy

California Institute of Technology
Pasadena, California

1987

(Submitted October 3, 1986)

TO MY FAMILY

ACKNOWLEDGEMENTS

It was a pleasure to work for my advisor Dennis Dougherty, and I extend my sincerest thanks for his scientific guidance, encouragement and friendship during my stay at Caltech. Being a member of the Dougherty group was a wonderful experience, and everyone in the group was extremely helpful. Special thanks go to Gary Snyder and Lisa McElwee-White, without whom ESR studies would have been a lot tougher. Mike Sponsler, Mike Petti and Tim Shepodd, with whom I shared my first laboratory at Caltech, will always be remembered with especially fond memories. Of course, all my other colleagues in the Dougherty, Dervan and Grubbs groups will never be forgotten either.

Tom Dunn in the electronic shop was a great help. Without his expertise and willingness to fix almost anything, I would have been left in the lurch on innumerable occasions.

I also gratefully acknowledge Dave Stauffer's help in proofreading this thesis.

ABSTRACT

Thermolysis of 2,3-diazabicyclo[2.1.1]hex-2-ene (**14**) in the gas phase produces highly vibrationally excited (chemically activated) bicyclo[1.1.0]butane (**30**). The excited **30** rearranges to butadiene, in competition with collisional deactivation by a bath gas. Quantitative modeling using RRKM theory and a stepladder model for collisional deactivation indicates that of the substantial amount of excess energy available to the products of thermolysis of **14**, the great majority lies in the hydrocarbon fragment (**30**). Within the framework of a mechanistic criterion developed previously by Bauer, this result suggests that **14** decomposes by a stepwise, one-bond cleavage involving an intermediate diazenyl biradical. We have also synthesized **16**, the dimethyl derivative of **14**, and studied its thermal decomposition. As predicted by RRKM calculations, gas phase thermolysis of **16** does not produce chemically activated 1,3-dimethylbicyclobutane (**31**).

Irradiation of frozen solutions of 1,4-dialkyl-2,3-diazabicyclo[2.1.1]hex-2-enes (**16**–**19**) in the cavity of an ESR spectrometer between 4 and 25 K produces the corresponding triplet 1,3-dialkyl-1,3-cyclobutanediyls (**20**–**23**). The spectra display zero-field splitting parameters, $|D/hc| = 0.112\ \mathrm{cm}^{-1}$ and $|E/hc| = 0.005\ \mathrm{cm}^{-1}$. Hyperfine coupling can be resolved in some of these spectra and can be simulated using a computer program which has been developed for the purpose. The decay of the ESR signals between 4 and 25 K is nonexponential and shows very little dependence on temperature. A novel approach for analyzing the matrix-site effect is used and evidence is provided for quantum-mechanical tunneling in the decay process.

Matrix isolation photolysis of 2,3-diazabicyclo[2.2.1]hept-2-ene-7-spirocyclopropane (**24**) and 2,3-diazabicyclo[2.2.1]hept-2-ene-7,5′-spirobicyclo[2.1.0]-pentane (**25**) between 4 and 35 K produces triplet ESR signals which are thermally stable up to 150 K. Independent generation from direct precursors 7-ethylidene-2,3-diazabicyclo[2.2.1]hept-2-ene (**71**) and 7-cyclobutylidene-2,3-diazabicyclo[2.2.1]hept-2-ene (**72**) confirms the assignment of the ESR signals to triplet biradicals 2-ethylidene-1,3-cyclopentanediyl (**28**) and 2-cyclobutylidene-1,3-cyclopentanediyl (**29**), respectively. Interpretable hyperfine coupling is observed and can be simulated, providing direct information about the electronic structures of these biradicals. The mechanism proposed for the formation of **28** and **29** from **24** and **25** involves two biradical rearrangements; a cyclopropylcarbinyl-type ring opening followed by a 1,2-H shift. Neither of these rearrangements can occur via thermal activation at such low temperatures. Chemical activation and quantum-mechanical tunneling are proposed to explain the reactivity of the intermediary biradicals.

TABLE OF CONTENTS

LIST OF FIGURES

LIST OF TABLES

CHAPTER I

INTRODUCTION

The study of organic biradicals[1] has been at the forefront of research in physical organic chemistry in recent years. Interest in the field has stemmed from the desire to better understand reaction mechanisms and electronic structure. For example, biradicals are often invoked as reactive intermediates in thermal[2] and photochemical[3] transformations. Direct evidence for their existence and a study of their reactivity can not only help chemists understand these reactions but can also improve their predictive ability. Additionally, the relative ordering of the singlet and triplet energy levels of such species has led to a particularly effective synergism between theoretical and experimental chemistry.

A biradical can be defined as an even electron species with one fewer bond than allowed by the standard rules of valence.[4] Thus they are often referred to as "open-shell" structures. In molecular orbital terms this translates to the presence of a pair of singly occupied degenerate or nearly degenerate non-bonding orbitals (Figure 1). The two electron spins can either be paired (spin quantum number S=0, singlet) or parallel (S=1, triplet). The magnitude and sign of the energy gap between these two states is highly dependent on electron correlation and even state-of-the-art calculations provide only very crude estimates. On the other hand, experimental techniques have been used successfully in determining this fundamentally important number with some confidence.

Thermodynamically, biradicals lie quite close to transition states for reactions involving the formation or homolytic cleavage of C–C single bonds. Direct observation can thus provide important information about the structure and properties of transition states. A number of triplet biradicals have been shown to occupy local minima on potential surfaces and their chemistry

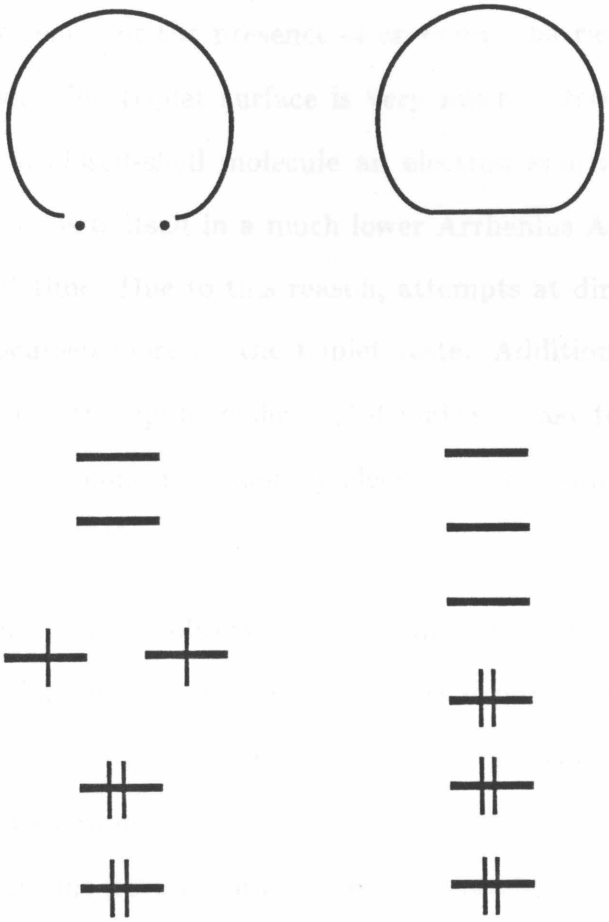

Figure 1. Molecular Orbital picture of an organic biradical and its closed-shell form.

has been investigated. However, it is still not clear whether singlet biradicals are best thought of as transition states or as true intermediates.[5] Theoretical calculations[6] and experimental stereochemical studies[7] have failed to provide any conclusive evidence for the presence of an energy barrier to the closure of a singlet biradical. The triplet surface is very much different in this regard. In order to form a closed-shell molecule an electron spin must invert. This "spin protection" reflects itself in a much lower Arrhenius A-factor and thus a longer biradical lifetime. Due to this reason, attempts at direct observation of biradicals have focussed more on the triplet state. Additionally, the presence of a permanent magnetic dipole in the triplet makes it easy to detect and characterize extremely low concentrations by electron spin resonance spectroscopy (ESR).

Interest in the direct observation and characterization of biradicals has also led to the development of some important new experimental techniques and to the synthesis of several novel target molecules with special features designed to increase their chances of detection. First, matrix-isolation experiments under cryogenic conditions have become increasingly useful. The strategy here is to use the rigid medium to suppress bimolecular chemistry and the very low temperatures to make even the smallest energy barrier insurmountable. Second, biradicals themselves can be conjugatively stabilized by delocalization of the radical centers over a π-system. Third, the closed shell reaction product can be destabilized by the introduction of ring strain and this can be easily accomplished by using small polycyclic molecular frameworks. Perhaps the most striking example of the use of these techniques is the study of a family of trimethylenemethane derivatives reported by Berson and coworkers.[4,8,9] A combination of ESR spectroscopy, flash photolysis and trapping studies has led

Scheme I

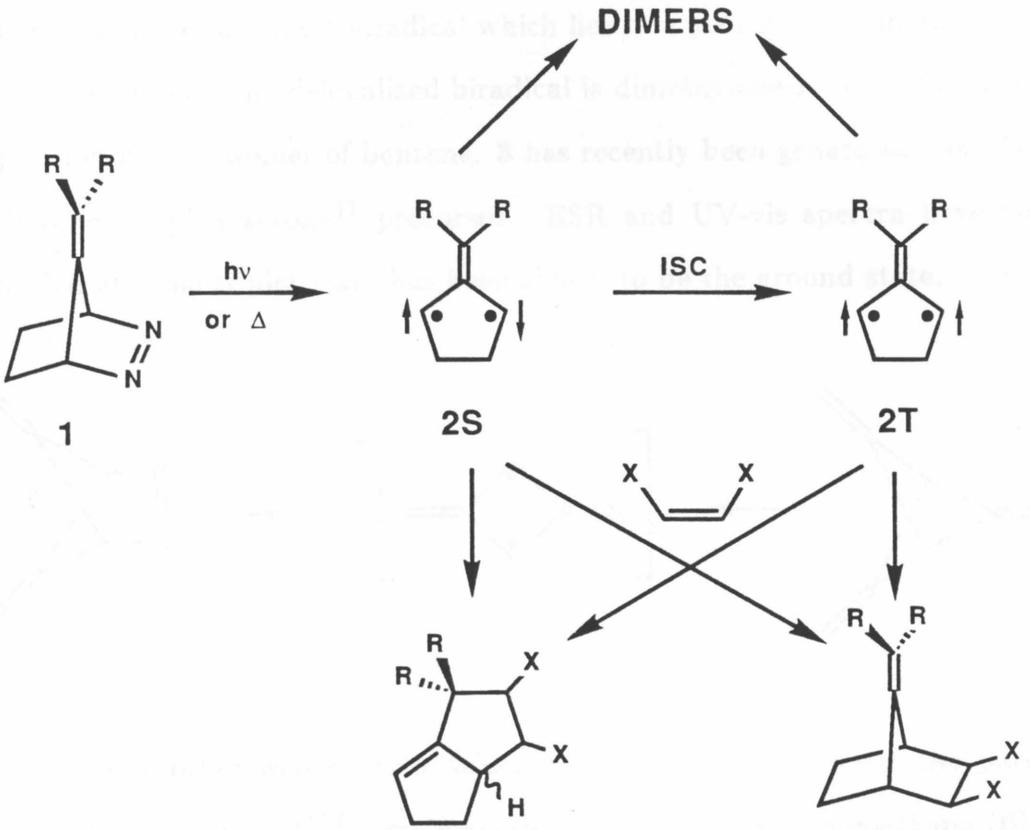

to the development of Scheme I for their generation and reactivity. It has been shown that for a variety of substituents (R), the triplet state is lower than the singlet and a reasonably accurate value for the S–T gap has been obtained. It has also been shown by trapping studies and transient spectroscopy[9] that **2**S is one example of a singlet biradical which lies in a potential minimum.

An interesting delocalized biradical is dimethylene-1,3-cyclobutanediyl (**3**), a non-Kekulé isomer of benzene. **3** has recently been generated from both a diazene[10] and a ketone[11] precursor. ESR and UV-vis spectra have been recorded and the triplet state has been shown to be the ground state.

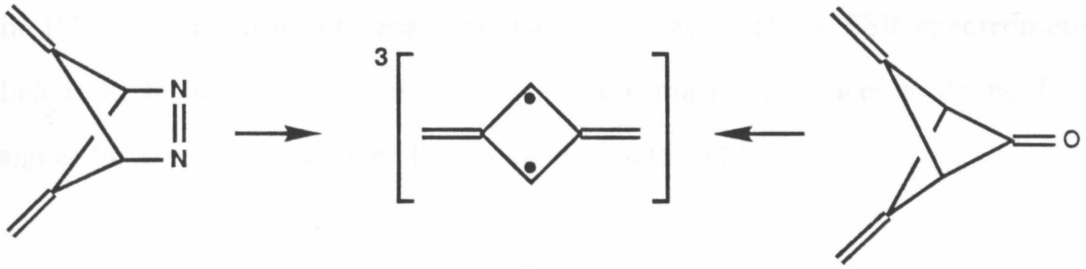

3

Some other well studied delocalized triplet biradicals are the parent trimethylenemethane (**4**)[12], *meta*-xylylene (**5**)[13], *meta*-quinomethane (**6**)[13], naphthoquinodimethane (**7**)[14] and tetramethyleneethanes (**8** and **9**).[15,16]

4

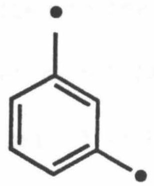

5

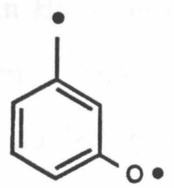

6

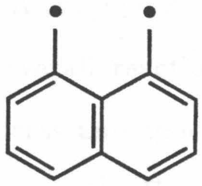

7

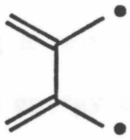

8

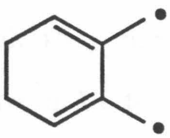

9

Biradicals which are not stabilized by conjugation have presented an even more challenging problem, and until our present work the only localized biradical to be spectroscopically observed was reported by Buchwalter and Closs in 1975.[17] Irradiation of azoalkane **10** in the cavity of an ESR spectrometer below 40 K in a polycrystalline cyclohexane matrix produces a strong ESR signal for the triplet state of 1,3-cyclopentanediyl (**11**).

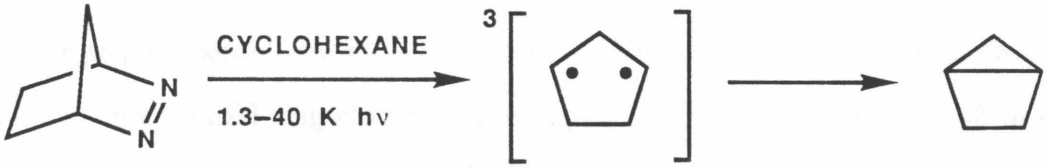

10 **11** **12**

The spectrum can be fitted to the triplet state spin Hamiltonian with zero-field splitting (zfs) parameters of $|D/hc| = 0.084\ \mathrm{cm}^{-1}$ and $|E/hc| = 0.0020\ \mathrm{cm}^{-1}$.[18] An interesting aspect of the chemistry of **11** is the fact that the ESR signal slowly decays even at 4 K and it was noted by Buchwalter and Closs that this reaction involves ring closure to bicyclopentane (**12**). They also found the decay behavior to be essentially temperature independent between 4 and 40 K, implying a substantial contribution due to a tunneling component to the overall reaction rate. Using a relatively crude model, they modeled this process and concluded that the energy barrier in going from **11** to **12** is 2.3 kcal mol^{-1}. For a decade **11** remained the only localized biradical to be studied and extension to related systems proved unfruitful. In an attempt to better understand the electronic structure of **11**, Schaefer[19] performed ab-initio calculations showing that in the case of **11** the triplet state was lower in energy than the singlet. Goldberg and Dougherty[20] further showed that this effect was the result of a fortuitous balance between "through-bond" and "through-space" interactions. Unfortunately, attempts to observe 1,3-cyclobutanediyl (**13**) upon irradiation of 2,3-diazabicyclo[2.1.1]hex-2-ene (**14**)[21] in a variety of matrices proved unsuccessful, although the same calculations predict that **13** should also have a triplet ground state. It was speculated that failure to observe an ESR signal for **13** was due to the unusual photochemistry of the azoalkane precursor **14** which undergoes β C–C bond cleavage (to give **15**) instead of nitrogen loss from the triplet excited state.[21] Of course, another possible explanation could be an extremely rapid ring-closure reaction preventing accumulation of **13** in a concentration high enough to allow detection.

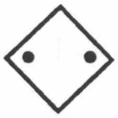

13

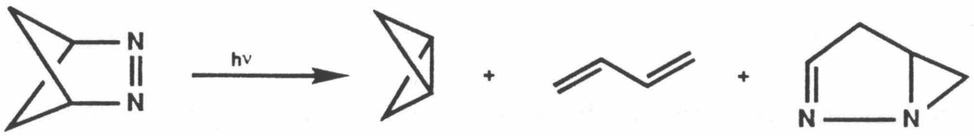

14 **30** **15**

The present study is aimed at modification of the parent cyclobutanediyl to improve chances of detection. Reasoning that stabilization of the radical centers in **13** might encourage nitrogen loss relative to β-cleavage, a series of bridgehead substituted azoalkanes (**16**–**19**) was synthesized. The study of these bridgehead substituted derivatives has now revealed that a series of localized biradicals (**20**–**23**) can be observed and substituent effects studied for the first time.

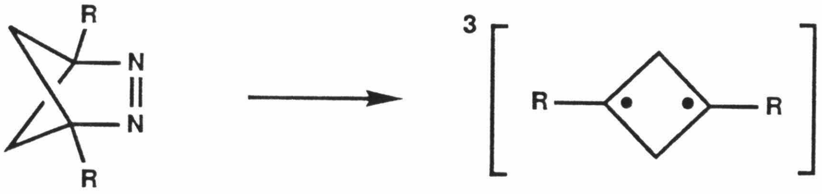

16	R = CH_3	**20**
17	R = CD_3	**21**
18	R = C_2H_5	**22**
19	R = C_3H_7	**23**

A comparative study of the decay behavior of these biradicals (**20**–**23**) and **11** has been performed using a novel approach which explicitly considers the distribution of matrix sites. However, obtaining accurate kinetic data turns out to be extremely difficult due to high reaction rates. Qualitatively, the decay behavior is once again temperature independent and computer modeling strongly suggests that quantum mechanical tunneling plays an important part in these reactions.

In our study of localized biradicals we also investigated matrix-isolation photolyses of diazenes **24** and **25** as possible methods for generation of biradicals

26 and **27**. However, a remarkable series of transformations takes place and the final products are triplet trimethylenemethane (TMM) derivatives **28** and **29**. Generation from authentic precursors and comparison of interpretable hyperfine coupling has been used in structure proof. The proposed route to these TMM's involves two sequential biradical-to-biradical rearrangements. The final analysis emphasizes the substantial thermodynamic driving force for obtaining a TMM-like structure and the opportunities for following novel chemical pathways under matrix-isolation conditions.

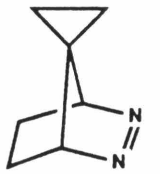

24

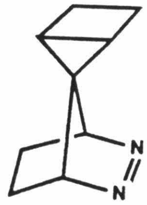

25

26

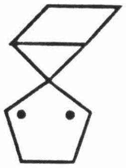

27

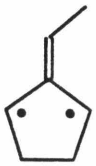

28

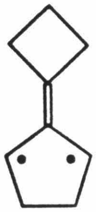

29

An important part of the present work involves the synthesis of novel azoalkanes (1,2-diazenes). Their chemistry has been utilized quite effectively for a long time as a potential source for various radicals, biradicals, sterically crowded structures and other highly strained ring systems.[22,23] However, despite intensive investigation, there is still considerable controversy over the mechanism of deazetation. The central issue is whether cleavage of the two C–N bonds occurs synchronously with direct loss of N_2 or whether cleavage is sequential and produces a diazenyl radical as an intermediate. We have used a novel approach based on the observation of chemical activation in an attempt to solve this problem.

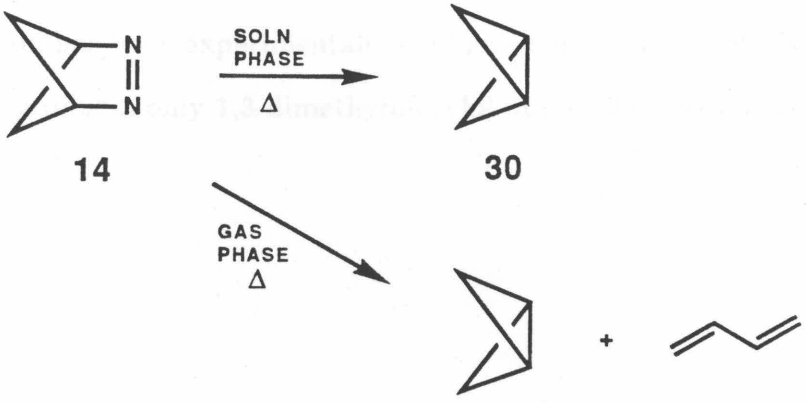

14 **30**

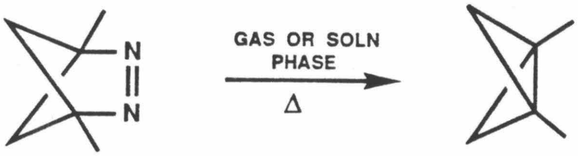

16 **31**

Solution phase thermolysis of both **14** and its bridgehead dimethyl derivative **16** produces only the corresponding bicyclobutanes **30** and **31**. In the gas phase, however, **14** gives both **30** and 1,3-butadiene and the relative ratio of the two is dependent on the pressure. This suggests that **30** is born in a chemically activated state and can rearrange to 1,3-butadiene in competition with collisional deactivation to ground state **30**. Some time ago, Bauer proposed that the distribution of energy among the products of such a fragmentation reaction could be used as an operational criterion for discerning mechanism.[24] This criterion has been applied to the thermolysis of **14**, and using RRKM theory along with a multistep collisional deactivation scheme a quantitative estimate of energy distribution between **30** and N_2 has been obtained. It is found that most of the excess energy accumulates in **30**, providing strong evidence for a one-bond cleavage mechanism. On the basis of the RRKM calculations it was predicted that the replacement of the bridgehead hydrogens by methyl groups would greatly increase the number of vibrational modes of the activated species, thereby decreasing the probability of accumulation of energy into the reactive mode. This prediction has been experimentally confirmed as the thermolysis of **16** in the gas phase produces only 1,3-dimethylbicyclobutane (**31**) even at very low pressures.

References for Chapter I

1. *Diradicals*; Borden, W.T., Ed.; Wiley: New York, 1982.
2. Gajewski, J.J. *Hydrocarbon Thermal Isomerizations*; Academic: New York, 1981.
3. Wagner, P.J. In *Rearrangements in Ground and Excited States*; de Mayo, P., Ed.; Academic: New York, 1980; Vol. 1.
4. Berson, J.A. *Acc. Chem. Res.* **1978**, *11*, 446–453.
5. Benson, S.W. *J. Chem. Phys.* **1961**, *34*, 521–526.
6. Hay, P.J.; Hunt, W.J.; Goddard, W.A., III. *J. Am. Chem. Soc.* **1972**, *94*, 638–640.
7. For example: Berson, J.A.; Balquist, J.M. *J. Am. Chem. Soc.* **1968**, *90*, 7343–7344. Bergman, R.G.; Carter, W. *J. Am. Chem. Soc.* **1969**, *91*, 7411–7425. Crawford, R.J.; Lynch, T.R. *Can. J. Chem.* **1968**, *46*, 1457–1458. Doering, W. von E.; Sachdev, K. *J. Am. Chem. Soc.* **1974**, *96*, 1168–1187. Berson, J.A.; Pedersen, L.D.; Carpenter, B.K. *J. Am. Chem. Soc.* **1976**, *98*, 122–143.
8. Berson, J.A., see ref. 1, pp. 151-194.
9. Kelley, D.F.; Rentzepis, P.M.; Mazur, M.R.; Berson, J.A. *J. Am. Chem. Soc.* **1982**, *104*, 3764–3766.
10. Snyder, G.J.; Dougherty, D.A. *J. Am. Chem. Soc.* **1985**, *107*, 1774–1775. Snyder, G.J.; Dougherty, D.A. *J. Am. Chem. Soc.* **1986**, *108*, 299–300.
11. Dowd, P.; Paik, Y.H. *J. Am. Chem. Soc.* **1986**, *108*, 2788–2790.
12. Dowd, P. *Acc. Chem. Res.* **1972**, *5*, 242–248. Dowd, P.; Chow, M. *Tetrahedron* **1982**, *38*, 799–807.

13. Platz, M.S., see ref. 1, pp 195–222. Rule, M.; Matlin, A.R.; Seeger, D.E.; Hilinski, E.F.; Dougherty, D.A.; Berson, J.A. *Tetrahedron* **1982**, *38*, 787–798.

14. Platz, M.S., see ref. 1, pp. 222–255. Platz, M.S.; Carrol, G.; Pierrat, F.; Zayas, J.; Auster, S. *Tetrahedron* **1982**, *38*, 777–785.

15. Dowd, P. *J. Am. Chem. Soc.* **1970**, *92*, 1066–1068.

16. Roth, W.R.; Erker, G. *Angew. Chem., Intl. Ed. Engl.* **1973**, *12*, 503–504.

17. Buchwalter, S.L.; Closs, G.L. *J. Am. Chem. Soc.* **1979**, *101*, 4688–4694.

18. For a discussion of triplet ESR spectroscopy see: Wertz, J.E.; Bolton, J.R. *Electron Spin Resonance: Elementary Theory and Practical Applications*; McGraw Hill: New York, 1972; pp 223–257. Also Wasserman, E.; Snyder, L.C.; Yager, W.A. *J. Chem. Phys.* **1964**, *41*, 1763–1772. A short summary is also presented here in Chapter III.

19. Conrad, M.P.; Pitzer, R.M.; Schaefer, H.F., III *J. Am. Chem. Soc.* **1979**, *101*, 2245–2246.

20. Goldberg, A.H.; Dougherty, D.A. *J. Am. Chem. Soc.* **1983**, *105*, 284–290.

21. Chang, M.H.; Dougherty, D.A. *J. Am. Chem. Soc.* **1982**, *104*, 2333–2334.

22. Engel, P.S. *Chem. Rev.* **1980**, *80*, 99–150.

23. Adam, W.; DeLucchi, O. *Angew. Chem., Intl. Ed. Engl.* **1980**, *19*, 762–779.

24. Bauer, S.H. *J. Am. Chem. Soc.* **1969**, *91*, 3688–3689.

CHAPTER II

ONE-BOND CLEAVAGE IN A SYMMETRICAL BICYCLIC AZOALKANE

The versatility of azoalkanes in the synthesis of a variety of complex and unusual molecular frameworks is well known. In addition, thermal and photochemical deazetation from these compounds has also been utilized very effectively in the generation of a multitude of radicals and biradicals.[1,2] However, there still remains some doubt as to the nature of the initial mechanistic step involved in the thermal loss of nitrogen. Several interesting approaches have been used to address the key question of whether the two C–N bonds rupture simultaneously (mechanism **a** in Scheme II) with direct loss of N_2 or whether cleavage is sequential and produces a diazenyl radical as a short-lived intermediate (mechanism **b** in Scheme II).

Scheme II

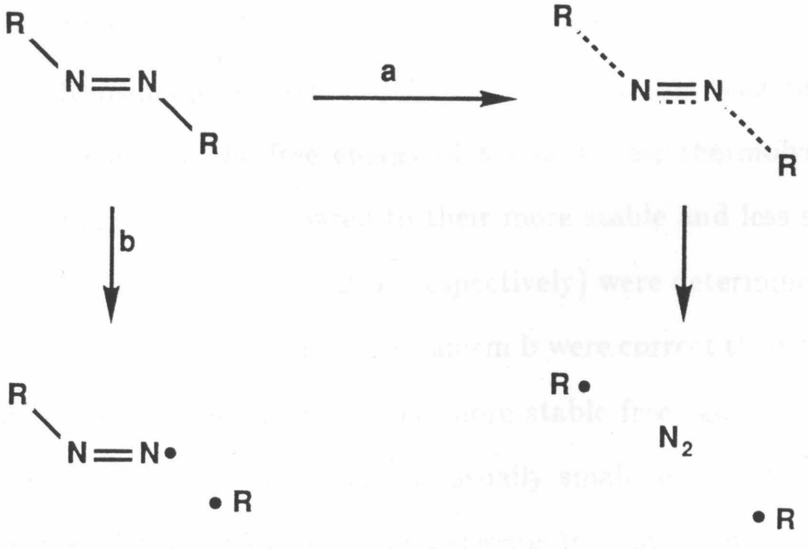

The earliest attempt to address this question was made by Ramsperger when he compared the E_a for decomposition of the azoalkanes **32**, **33**, and **34**.[3] Since the value for the unsymmetrical compound is very close to the average of the values for the symmetrical compounds, he concluded that both bonds must break at once. Unfortunately, later experiments showed that the E_a value that he used for **34** is incorrect, and the best current value[4] of 47.9 kcal mol^{-1} invalidates his conclusion.

32

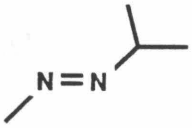

33

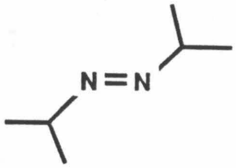

34

E_a (kcal mol^{-1})	51.2	47.5	40.9

Since then several other unsymmetrical azoalkanes have been synthesized and the Ramsperger criterion applied to their thermal deazetation. More explicitly, differences in the free energy of activation for thermolysis of some unsymmetrical azoalkanes compared to their more stable and less stable symmetrical analogues ($\Delta\Delta G_1^{\ddagger}$ and $\Delta\Delta G_2^{\ddagger}$ respectively) were determined. Some of the data are presented in Table I. If mechanism **b** were correct then $\Delta G^{\ddagger}$ should be dependent only on the nature of the more stable free radical, and $\Delta\Delta G_2^{\ddagger}$ should be zero. The fact that $\Delta\Delta G_2^{\ddagger}$ is usually small relative to $\Delta\Delta G_1^{\ddagger}$ was taken as good evidence for stepwise bond scission in unsymmetrical azoalkanes and simultaneous bond rupture in symmetrical azoalkanes.

Another approach which has been employed involves both thermochem-

Table I. Differences in Free Energy of Activation between Symmetrical and Unsymmetrical Azoalkanes[5]

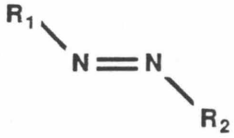

R_1	R_2	$\Delta\Delta G_1^{\ddagger}$	$\Delta\Delta G_2^{\ddagger}$
Me	*i*-Pr	3.5	0.7
Me	α-Phenethyl	13.7	3.8
Me	Allyl	14.0	1.0
t-Bu	Allyl	7.5	−2.4
Benzyl	α-Phenethyl	0.7	2.2
t-Bu	Cumyl	8.4	3.3

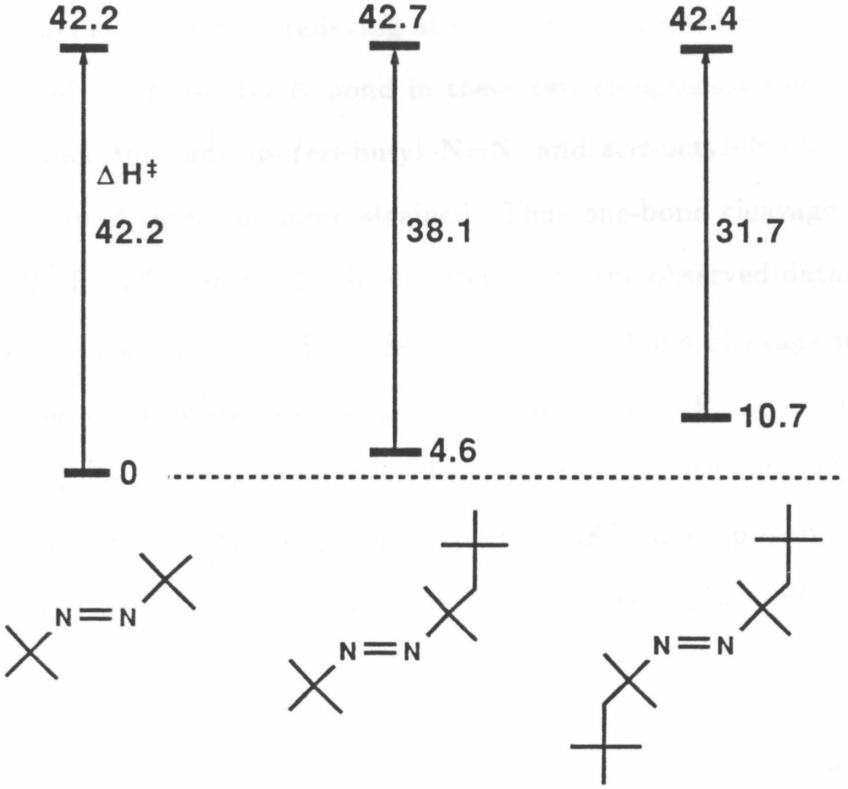

35 36 37

Figure 2. Relative ΔH_f° of ground state azoalkanes **35**, **36** and **37**, and the transition states for their deazetation.[6]

ical and kinetic data.[6] As shown in Figure 2, the relative heats of formation of azoalkanes **35**, **36**, and **37** are 0, 4.6, and 10.7 kcal mol^{-1} and addition of the experimental $\Delta H^{\ddagger}$ for thermolysis places all three transition states at about 42.5 kcal mol^{-1}. This strongly suggests that both C–N bonds are broken in the transition state thereby relieving all nonbonded interactions in **36** and **37**. If cleavage of the *tert*-octyl–N bond in these two compounds were stepwise it would produce the radicals *tert*-butyl–N=N· and *tert*-octyl–N=N· , of which the latter should surely be more strained. Thus one-bond cleavage predicts a higher $\Delta H^{\ddagger}$ for **37** than for **36**, inconsistent with the observed data.

Quite convincing evidence favoring the one-bond cleavage mechanism has also been put forward in a number of arylazoalkanes. Pryor[7] and Neuman[8] have studied the effect of pressure and solvent viscosity on rates of decomposition of compounds with the general structure **38**. Large, positive activation volumes have been obtained, consistent with the intermediacy of aryldiazenyl radicals.

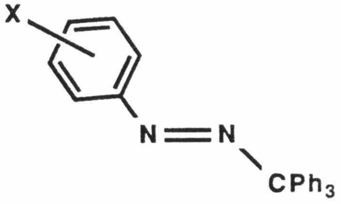

38

Chemically induced dynamic nuclear polarization techniques have also been used successfully in studies of azoalkane decomposition. Irradiation of **39t** at –125°C gives the *cis* isomer **39c**, which decomposes upon warming to –36°C. ^{15}N CIDNP reveals enhanced absorption in both *cis* and *trans* starting materials and emission of molecular nitrogen,[9] providing compelling evidence for a one-bond cleavage mechanism.

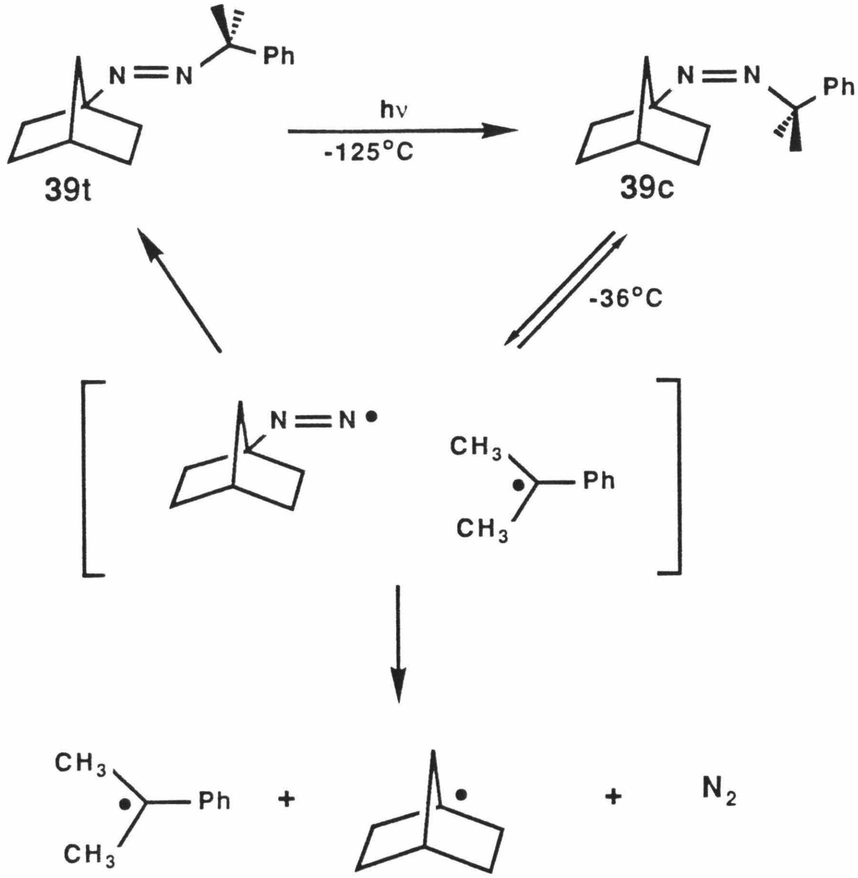

Engel has provided further evidence for formation of diazenyl radicals[10] upon photochemical decomposition of unsymmetrical azoalkanes containing the 1,1-dimethylallyl moiety. Thus, the product mixture obtained upon photolysis of **40** with a nitrogen laser contains the "turnaround" azoalkane **41** formed by the recombination of an alkyldiazenyl radical at the other end of the allyl radical.

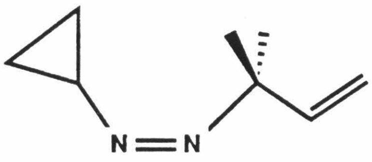

40

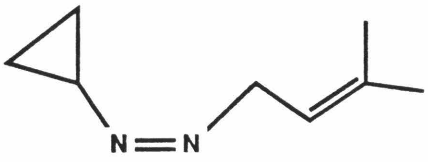

41

A few years ago, then, it seemed appropriate to summarize the mechanistic details as follows: "azoalkane thermolysis seems to proceed by a continuum of mechanisms between **a** and **b**; the more unsymmetrical the azo compound, the more unsymmetrically it cleaves".[1] However, some doubt was recently cast upon the simultaneous scission mechanism for nitrogen loss from symmetrical azoalkanes. Engel[11] has studied the thermolysis of bridgehead substituted 2,3-diazabicyclo[2.2.2]oct-2-enes (**42**) and found that although loss of N_2 is accelerated to the same degree as in acyclic azoalkanes by radical-delocalizing substituents the effect is much smaller with methyl groups. Either a concerted, asynchronous C–N bond scission mechanism or a reversible, stepwise mechanism can adequately explain these effects.

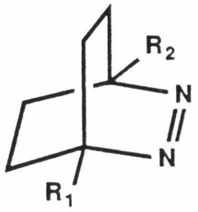

42

Calculations by Dannenberg[12] also point to one-bond cleavage in symmetrical azoalkanes. His MNDO studies favor a mechanism involving cleavage to a diazenyl radical which can then either recombine or further decompose to two alkyl radicals and a nitrogen molecule. We now provide the first experimental evidence for such a scheme in our present study.

Some time ago, Bauer proposed that the distribution of energy among the products of such a fragmentation reaction could be used as an operational criterion for discerning mechanism.[13] We have applied this criterion to the thermolysis of **14**, and using RRKM theory along with a multistep collisional deactivation scheme, a quantitative estimate of energy distribution between **30** and N_2 has been obtained. RRKM calculations also predicted that the replacement of the bridgehead hydrogens by methyl groups would greatly increase the number of vibrational modes of the activated species, thereby decreasing the probability of accumulation of energy into the reactive mode. Hence, 1,4-dimethyl-2,3-diazabicyclo[2.1.1]hex-2-ene (**16**) was synthesized and its thermal decomposition studied.

14

16

Synthesis

The key step in the synthetic strategy for **16** (Scheme III) involves the addition of 4-methyl- or 4-phenyl-1,2,4-triazoline-3,5-dione (MTAD or PTAD) to **31**. Earlier, Roth had observed that PTAD reacts with spirobicyclo[2.1.0]-pentane-5-cyclopropane (**43**) in acetone at 20°C to give adduct **44** in practically quantitative yield.[14]

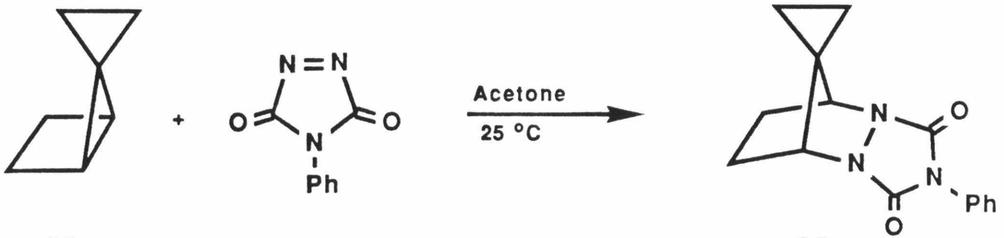

43

44

However, Amey and Smart studied the reactions between triazolinedione and 1-methyl-3-R-bicyclobutanes (R=CH_3, $CONH_2$, CO_2CH_3, and CN) in methylene chloride and found that for **31** only the "ene" product **45** was formed.[15] A surprising solvent effect was observed by Chang and Dougherty[16] for the addition of MTAD to **30**. The reaction takes place in *n*-hexane at 63°C and a 40% yield of the adduct **46** is obtained.

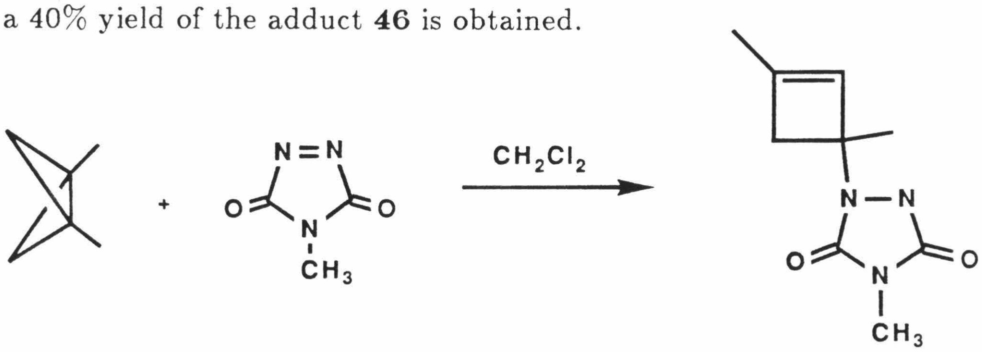

31 **45**

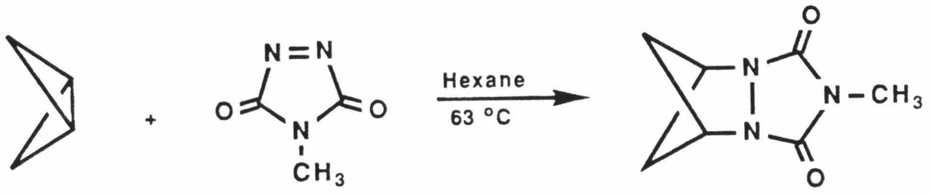

30 **46**

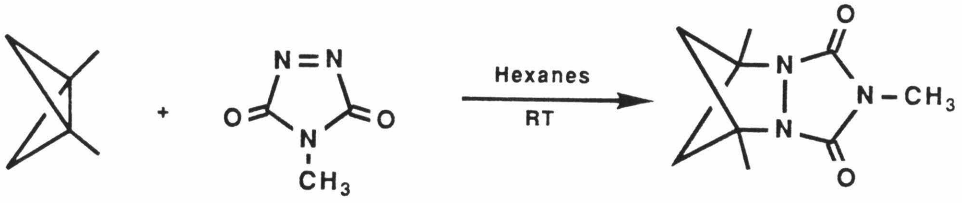

31 **47**

We have now found that the reaction between **31** and MTAD in hexanes also occurs smoothly at room temperature and adduct **47** can be easily isolated. Urazole **47** is then hydrolyzed using potassium hydroxide, and oxidized with cupric bromide. The copper complex thus obtained affords **16** upon treatment with ammonium hydroxide (Scheme III).

Scheme III

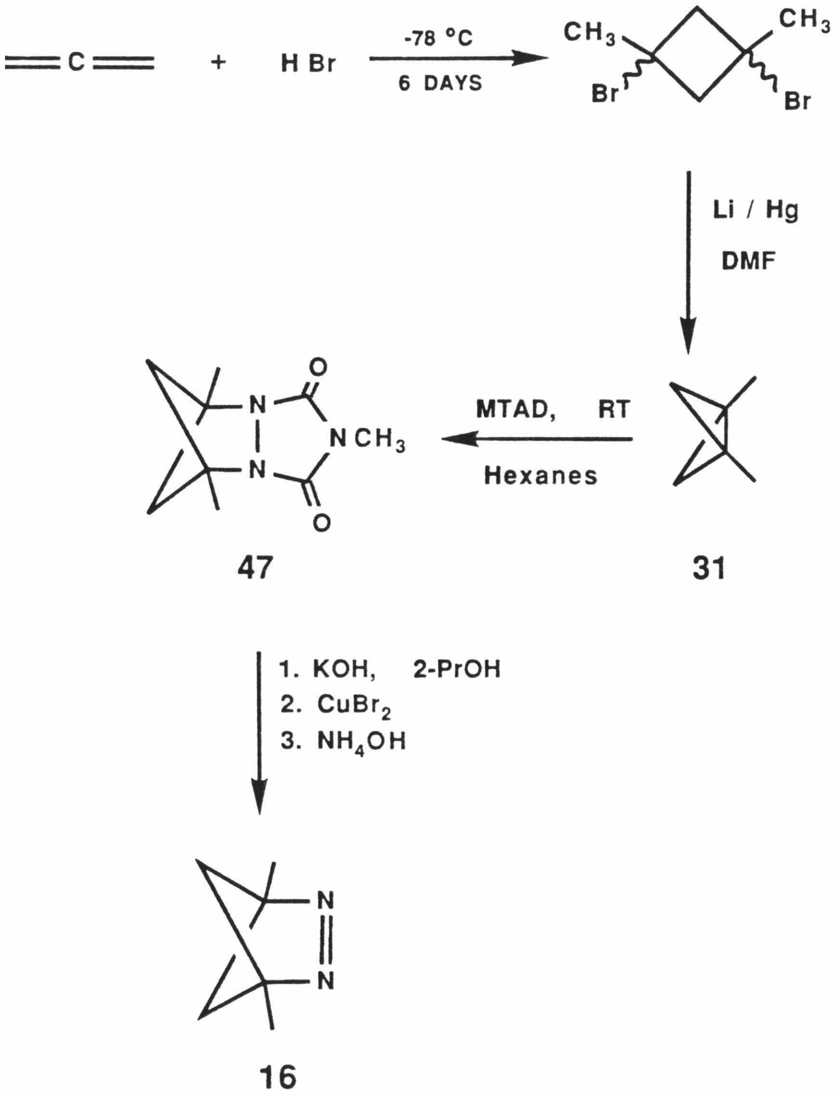
+
H Br
-78 °C
6 DAYS
CH3
CH3
Br
Br
Li / Hg
DMF
MTAD, RT
Hexanes
N
N
NCH3
O
O
47
31
1. KOH, 2-PrOH
2. CuBr2
3. NH4OH
N
N
16

Solution Phase Thermal Chemistry

Thermal decomposition of **16** in a benzene solution gives 1,3-dimethylbicyclobutane (**31**) as the sole detectable product. The rates for disappearance of **16** at several temperatures are given in Table II. The Arrhenius plot for these data yielded $E_a = 35.3 \pm 0.2$ kcal mol^{-1} and $\log A = 15.6 \pm 0.13$. Surprisingly, the thermolysis rate for **16** is lower than that for **14** by roughly a factor of three. The relevant activation parameters are given in Table III and it can be seen that the rate difference results from a roughly 1 kcal mol^{-1} difference in $\Delta H^{\ddagger}$.

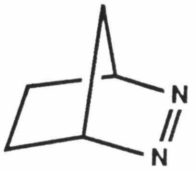

10

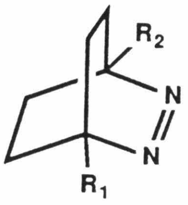

42a $R_1 = R_2 = H$
42b $R_1 = H, R_2 = CH_3$
42c $R_1 = R_2 = CH_3$

The closest analogy to the present case is the diazabicyclo[2.2.2]octyl system **42**.[11] Methyl substitution facilitates deazetation in that case and relative rates obtained for **42a**, **b** and **c** at 230°C are 1.0, 2.2 and 5.3, respectively. The rate enhancement, however, is quite small in **42** compared to acyclic azoalkanes. It is interesting to note that, using the empirical force field (EFF) of Kao,[17] **16** is calculated to be 3.4 kcal mol^{-1} less strained than **14**. The absolute accuracy of the EFF method as applied to azoalkanes remains to be determined, but there are other indications in the literature that bridgehead methyl substitution can stabilize strained rings.[11] Thus, it seems possible that a ground-state stabilization effect is responsible for the rate retardation in the decomposition of

16.[18] In fact, precisely such an effect was proposed to account for the unusually small rate acceleration due to methyl substitution in **42**.[11]

Also listed in Table III are activation parameters for thermolysis of two closely related azo compounds, **10** and **42a**. EFF calculations[17] indicate that **14** is 31 kcal mol^{-1} more strained than **10**. However, this substantial increase in strain on going from **10** to **14** is accompanied by only a modest decrease (<3 kcal mol^{-1}) in $\Delta H^{\ddagger}$ for N_2 loss. Clearly, most of the strain in **14** (and **16**) is still present in the transition state in the form of the four-membered ring. As discussed below, this result has significant implications for the gas phase thermal chemistry of **14**.

Gas Phase Thermal Chemistry

Thermolysis of **14** in the gas phase is remarkably different from that in solution. In benzene solution only bicyclobutane (**30**) is formed but in the gas phase both **30** and 1,3-butadiene are produced, and as shown in Figure 3 the product composition is strongly dependent on pressure.[19] At low pressures butadiene is the dominant and ultimately the exclusive product when N_2 is the bath gas. We have now determined that with benzene as the bath gas a much smaller, but still significant amount of butadiene is formed (Figure 3). Since it is known that bicyclobutane thermally rearranges to butadiene ($E_a = 40.6$ kcal mol^{-1}; $\log A = 14.23$),[20] the results of Figure 3 suggest that thermolysis of **14** produces highly vibrationally excited (chemically activated) bicyclobutane. It is well known that N_2 is much less efficient at collisionally deactivating vibrationally excited molecules than benzene. Thus, the difference between the two curves in Figure 3 is understandable. Similarly, 1,3-dimethylbicyclobutane (**31**) can rearrange to 2,3-dimethylbutadiene, with activation parameters quite similar to the unsubstituted system ($E_a = 43.3$ kcal mol^{-1}; $\log A = 14.45$).[21]

Table II. Rates for Thermolysis of **16** in Benzene

T^a, °C	$10^5\ k$, s^{-1}
100.83	0.866 ± 0.007
108.49	2.25 ± 0.01
112.93	3.765 ± 0.007
116.65	6.05 ± 0.05
120.38	9.31 ± 0.09
124.18	13.96 ± 0.09

---

[a] The errors in temperature are at most ± 0.03 °C.

Table III. Activation Parameters for Thermolysis of Bicyclic Azoalkanes

Compound	$\Delta H^{\ddagger}$ (kcal mol^{-1})	$\Delta S^{\ddagger}$ (eu)	k_{rel} [a]
14	33.7 ± 0.02[b]	10.0 ± 0.3[b]	1.0
16	34.5 ± 0.02	10.2 ± 0.5	0.396
10	36.2[c]	6.1[c]	0.0057
42a	44.3[c]	9.5[c]	10^{-6}

[a] Relative rates (s^{-1}) at 120 °C calculated from data of the previous two columns.

[b] From ref. 16.

[c] Average of values in ref. 1.

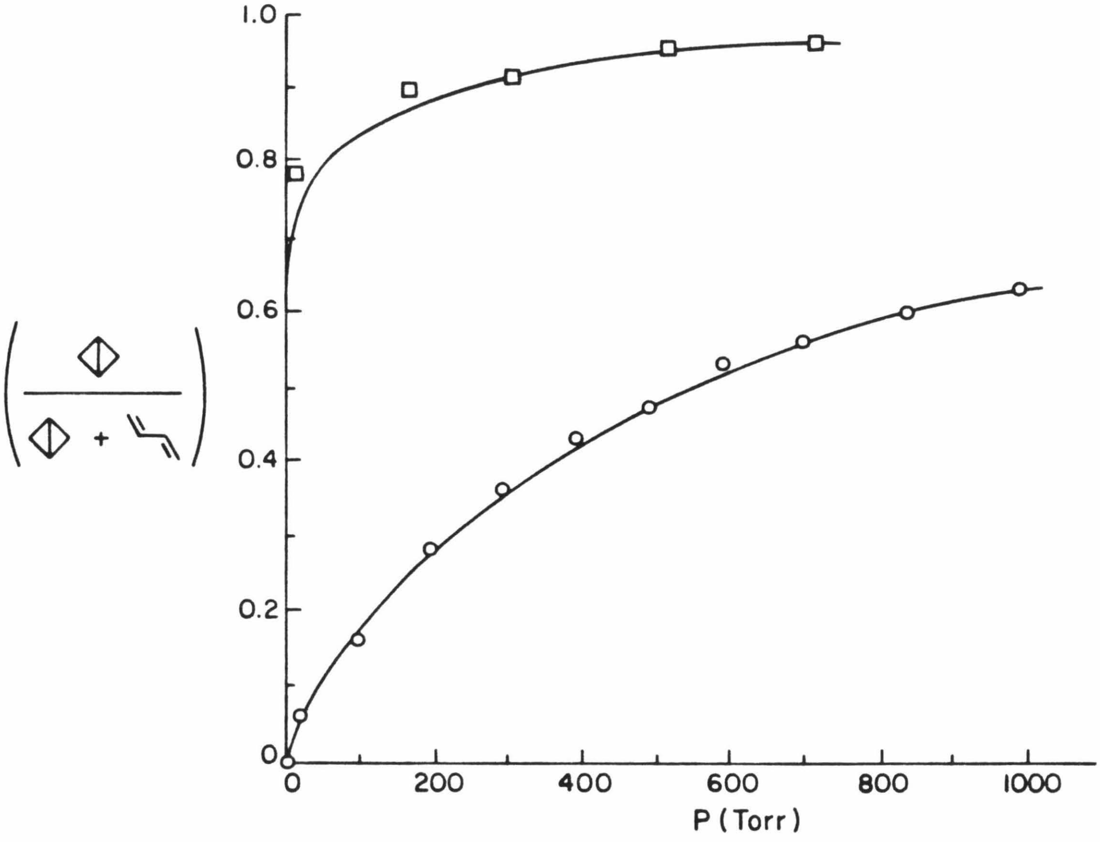

Figure 3. Product composition from gas phase thermolysis of **14** as a function of pressure. o: Nitrogen as bath gas; □: Benzene as bath gas.

However, in striking contrast to the results for **14**, gas phase thermolysis of **16** produces no butadiene — only **31** is produced even at very low pressures.

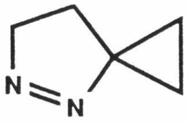

48

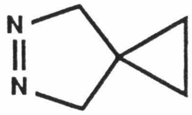

49

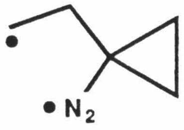

50

The apparent observation of a "hot molecule" effect from **14** is also remarkable in that only one other well-documented example of chemical activation has been reported. Bergman found that pyrolysis of pyrazoline **48** at 1 atm produced 98% spiropentane, but at 0.2 torr this value dropped to 81%, with the remainder being "hot molecule" products.[22] Interestingly, the isomeric, symmetrical pyrazoline **49** did not show a "hot molecule" effect. This result was rationalized with reference to earlier work by Bauer[13] in which it was proposed that the distribution of excess energy among the products of a reaction could be used as a probe of reaction mechanism. In the symmetrical diazene (**49**), the N_2 was presumed to be extruded in a symmetrical fashion. The N–N bond is much longer in the diazene than in N_2, and the N–N stretching mode is essentially perpendicular to and, therefore, weakly coupled to the reaction coordinate. Thus, the N_2 is expelled with a stretched N–N bond, i.e., in a highly vibrationally excited state. Most of the excess energy of the reaction is therefore carried off by the N_2, and the hydrocarbon is not chemically activated. In contrast, the unsymmetrical diazene (**48**) cleaves unsymmetrically to produce an intermediate diazenyl biradical (presumably **50**). Vibrational coupling between the N_2 and the hydrocarbon fragment can be efficient in the intermediate, and thus the hydrocarbon can be chemically activated.

Since labeling studies[19] have ruled out any other source of butadiene, the results of Figure 3 suggest that the *symmetrical* diazene **14** produces a much greater "hot molecule" effect than **48**, a seeming contradiction to the above analysis.

Thermochemistry and RRKM Calculations

Some qualitative insights into the reasons for the highly efficient chemical activation of bicyclobutane on its formation from **14** can be gained with reference to Figure 4. Included in Figure 4 are data for **14** and for azoalkane **10**, as an example of a well-characterized, fairly typical pyrazoline. The heats of formation are known for all structures shown[23] except **14**, for which the EFF[17] value was used. Transition state heats of formation were determined from the activation parameters.[24]

Both **14** and **10** decompose to hydrocarbons which have available to them a subsequent thermal rearrangement pathway. However, a major difference between **14** and **10** arises in the energy of the transition state for N_2 loss relative to that for hydrocarbon rearrangement. Because **14** is highly strained, and this strain is not relieved in the transition state for N_2 loss (see above), the deazetation transition state lies very high in energy. This leads to a substantial amount of excess energy in the products (**30** and N_2) beyond that required for the bicyclobutane-to-butadiene rearrangement. Even if the N_2 carries away a large amount of excess energy, as the Bergman/Bauer analysis would predict, there still could be enough energy left in the hydrocarbon fragment for rearrangement to occur. In contrast, the deazetation transition state for **10**

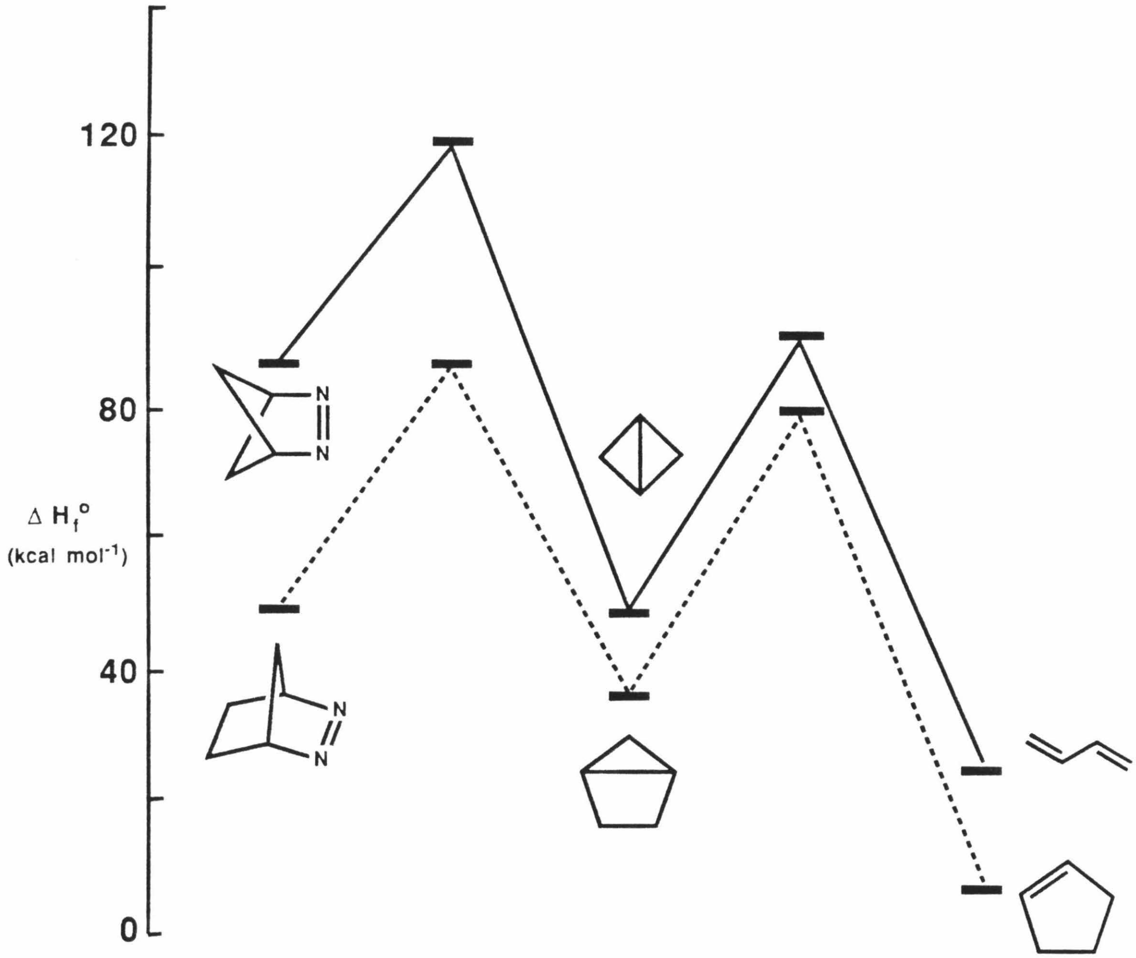

Figure 4. Energetics for the thermal decomposition of **10** and **14**.

is roughly equienergetic with the hydrocarbon rearrangement transition state, and therefore the hydrocarbon cannot be generated with an energy significantly above this barrier. Thus, the qualitative observation of chemical activation for **14** does not necessarily contradict the Bergman/Bauer analysis.

Another ambiguity in Figure 4 is the question of how much of the excess energy of the reaction E_{xs} is available to the N_2 fragment when it is expelled. If one considers the products to be bicyclobutane and N_2, then all of E_{xs} , which is equal to the ΔH_f° of the deazetation transition state minus ΔH_f° of bicyclobutane (since ΔH_f° of N_2 is zero), could end up as vibrational excitation in N_2. From Figure 4, E_{xs} is approximately 68 kcal mol^{-1}, and thus the N_2 could be very highly excited. However, the stereochemical scrambling observed on thermolysis of **51** suggests that the products are actually N_2 and 1,3-cyclobutanediyl (**13**).[19]

13

30

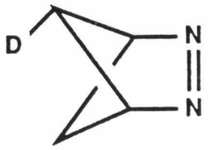

51

In such a case, not all of E_{xs} would be available to the N_2, because of the high energy content of **13**. The maximum vibrational energy available to the N_2 would be equal to $E_{xs} - \Delta H_f^\circ(\mathbf{13})$ and so quantitative analysis would require an evaluation of the ΔH_f° of biradical **13**. The uncertainties in evaluating ΔH_f° of biradicals are many, and in the case of **13** there is the additional problem of choosing a value for the ring strain energy. However, it seems likely that ΔH_f° of **13** is greater than ΔH_f° of the bicyclobutane-to-butadiene rearrangement transition state. Ring inversion (exo/endo isomerization) in **30** is not competitive with rearrangement to butadiene.[25] All recent results indicate that in the closely related bicyclo[2.1.0]pentane system, singlet biradical **11** is most likely a ring-inversion transition state or lies in a very shallow minimum.[26] If , by analogy the possibility of a very deep well for **13** is ruled out, then, like the ring-inversion transition state, it must lie above the rearrangement transition state. Using the most recent values for C–C bond dissociation energies[27] and assuming a reasonable ring strain energy,[28] thermochemical estimates[29] predict that **13** lies 6 kcal mol^{-1} above the transition state for rearrangement, consistent with this analysis.

The important consequence of this result is that even if *all* of the available excess energy is carried away by the N_2, leaving behind biradical **13** in its ground vibrational state and satisfying the Bergman/Bauer analysis of the results for **48** and **49**, the energy content of the bicyclobutane which is formed upon ring closure of **13** could still be above the rearrangement transition state. Thus, the chemical activation process being observed could actually be the ring closure of biradical **13**, not the deazetation of **14**.

The thermochemistry of Figure 4 allows one to conclude that there is potentially much more energy available to the products in the decomposition of **14** than in typical diazenes. This could provide a rationalization for the observation of chemical activation. However, from Figure 4 alone one cannot evaluate the distribution of E_{xs} between the fragmentation products. In order to apply the Bauer criterion to this system one must know how much of the available E_{xs} is carried away by the N_2 and how much by the hydrocarbon. In principle, one can solve this problem by using RRKM theory to evaluate the rate of rearrangement as a function of the energy content of the bicyclobutane, $k(E^*)$ where E^* is the energy content of the bicyclobutane *above* the threshold (activation) energy. Application of a multistep collisional deactivation scheme then allows one to determine which value of E^* is required to reproduce the data of Figure 3. In such a treatment all that matters is the value of E^* once the bicyclobutane is formed, regardless of whether it was formed directly from diazene **14** or from biradical **13**. The absolute amount of vibrational energy carried away by the N_2 could then be calculated by subtracting E^* and the hydrocarbon rearrangement threshold energy from E_{xs}.

RRKM theory calculates unimolecular rate constants by summing over each of the accessible quantum states of the transition complex.[30,31,32] It assumes that a molecule is comprised of oscillators which freely exchange vibrational energy. This statistical distribution of energy results in a finite probability that all the energy will accumulate in the reactive mode thereby forming products. Thus the predicted rate is

$$k_{uni} = \frac{N^{\ddagger}(E_{xs})}{h\rho(E^*)}$$

where

$N^{\ddagger}(E_{xs})$ is the total number of quantum states of the transition state with energy less than E_{xs}

$\rho(E)$ is the density of states of the reactant at energy E^*

The problem then boils down to calculation of N and ρ. For a system of s oscillators

$$N_s(\epsilon) = \frac{\epsilon^s}{s!\prod_i h\nu_i}$$

and

$$\rho_s(\epsilon) = \frac{\epsilon^{s-1}}{(s-1)!\prod_i h\nu_i}$$

The Hase–Bunker[33] computer program incorporates these equations and calculates rate constants. Input consists of s vibrational frequencies for the reactant and a reasonable approximation for the $s - 1$ vibrational frequencies of the transition state.

The application of RRKM theory to the rearrangement of bicyclobutane to butadiene is straightforward. A high-quality, completely analyzed vibrational spectrum of **30** is available,[34] thereby providing excellent vibrational frequencies for the ground state. The conversion of **30** to butadiene was considered to be a concerted, $[\sigma^2 s + \sigma^2 a]$ reaction.[35] Thus, for modeling the reaction transition state, symmetry coordinate S_{10} (frequency no. 11), in Wiberg's notation,[34] has been chosen as the reaction coordinate. This motion corresponds to the stretching of the two C–C bonds that are broken in the reaction, and a compression of the bonds that become double bonds. The reaction pathway was assigned a degeneracy of 2, as there are two equivalent sets of bonds that can cleave to give butadiene. The remaining vibrational frequencies for **30** were adjusted in the transition state so as to reproduce the high-pressure Arrhenius pre-exponential term for the rearrangement.

The results from the RRKM calculations are the unimolecular rate constants for the rearrangement of **30** for various values of the energy content. Computer printouts are given in Appendix A and a sampling of the data can be seen in Table IV. When one considers that at ca. 500 torr of N_2 as bath gas, where roughly equal amounts of **30** and butadiene are formed, the collision frequency[36] is ca. 2.4×10^{10} s^{-1}, it can immediately be seen that **30** must be formed with a substantial amount of excess energy in order for the rearrangement to compete with collisional deactivation.

Also shown in Table IV (and in Appendix A) are the results of a comparable RRKM calculation on the rearrangement of 1,3-dimethylbicyclobutane (**31**) to 2,3-dimethylbutadiene. Appropriate corrections (see experimental sec-

Table IV. Unimolecular Rate Constants for **30** and **31** from RRKM Calculations

E^*, kcal mol^{-1}	$k(E^*)$, s^{-1}	
	30	**31**
5.0	2.2×10^6	3.9×10^2
10.0	2.4×10^7	9.7×10^3
15.0	1.3×10^8	9.5×10^4
20.0	4.7×10^8	5.6×10^5
25.0	1.3×10^9	2.4×10^6
30.0	3.1×10^9	8.0×10^6
35.0	6.5×10^9	2.3×10^7
40.0	1.2×10^{10}	5.5×10^7
45.0	2.1×10^{10}	1.2×10^7
50.0	3.5×10^{10}	2.5×10^8
55.0	5.4×10^{10}	4.6×10^8

tion) were made to the list of ground state and transition state vibrational frequencies to account for the replacement of the bridgehead hydrogens of **30** by methyl groups. A dramatic decrease in $k(E^*)$ occurs upon methyl substitution. Such an effect has been observed previously and results from the greatly increased number of oscillators into which vibrational energy may flow, thus decreasing the probability of accumulation of energy into the reactive mode. The data presented in Table IV clearly show why no evidence of chemical activation is found in the thermal decomposition of diazene **16**. Quantitative modeling using the multistep collisional deactivation technique described below predicts <0.5% diene even at very low pressures.

In order to reproduce Figure 3, the collisional deactivation of vibrationally excited **30** must be considered explicitly. We have used the method developed by Hoare[37] and a brief summary is provided here. We assume that the energy region and the microscopic kinetic processes are as shown in Figure 5. We divide the active energy region into various levels (i, j, ...) and assume that the collisional transition probabilities in this region are independent of energy. Under steady state

$$\frac{dn_i}{dt} = \omega \sum_j P_{ij} n_j - n_i(k_i + \omega) + Rf_i = 0$$

where

n_i is the population of level i

ω is the collision frequency (number of collisions per molecule per unit time)

k_i is the reaction rate from level i

P_{ij} is the probability that a molecule in level j will undergo transition to level i during a random collision

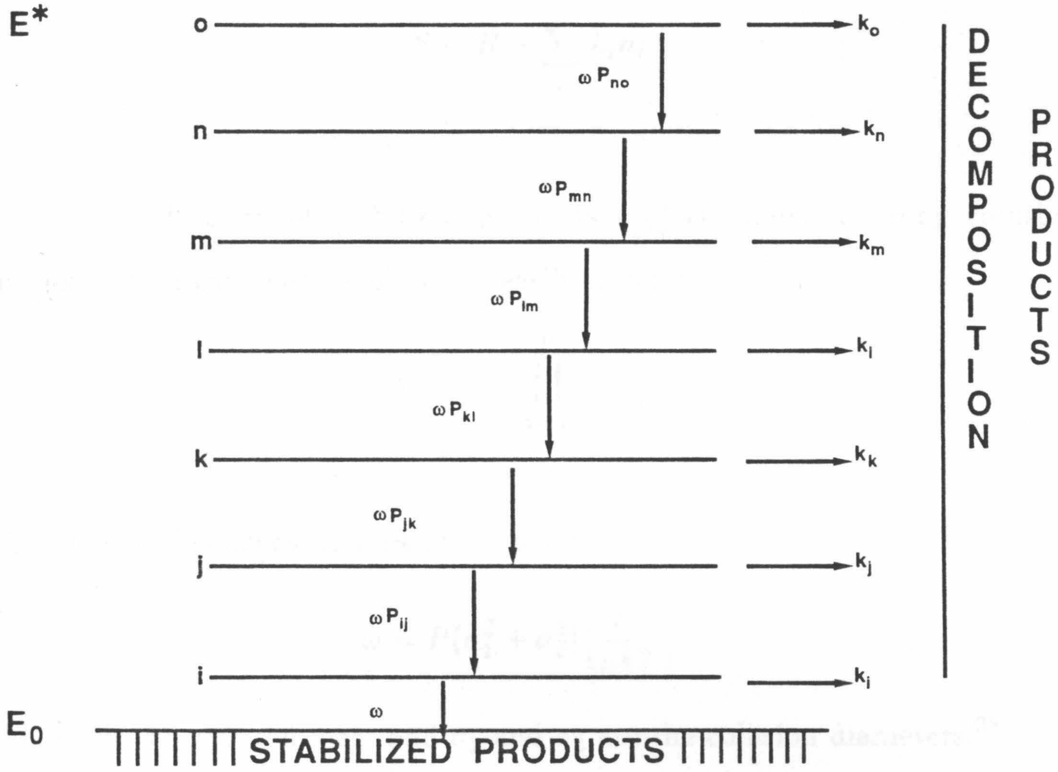

Figure 5. Energy region and microscopic kinetic processes for the deactivation scheme.

R is the total rate of chemical activation

f_i is the distribution function for the activation ($\sum_i f_i = 1$)

The rate of formation of decomposition product (D) is then given by

$$D = \sum_i k_i n_i$$

and the rate of formation of stabilization products (S) is

$$S = R - \sum_i k_i n_i$$

The fraction of stabilized products ($\frac{S}{D+S}$), under a strong collision approximation can then be obtained easily using[31]

$$\frac{S}{D+S} = \prod_{i=1}^{\nu} \frac{\omega}{\omega + k_i}$$

The collision frequency at pressure P is given by

$$\omega = P(\sigma_1^2 + \sigma_2^2)\left[\frac{8\pi}{\mu kT}\right]^{\frac{1}{2}}$$

where μ is the reduced mass and σ_1 and σ_2 are the collision diameters.[38]

The rate constants k_i are calculated from RRKM theory and depend upon the energy. Thus the stepladder deactivation scheme has two adjustable parameters. The first is the initial energy content of the bicyclobutane once it is formed from **14** (expressed as E^*). The second is the amount of vibrational energy removed by the bath gas per collision $\langle \Delta E \rangle$, i.e., the difference between the levels. It was initially assumed,[38] and subsequent modeling confirmed, that benzene is a strong collider in this system. That is, in a single collision with vibrationally excited bicyclobutane, a benzene molecule removes enough energy to drop the bicyclobutane down below the reaction threshold energy. We were unable to reproduce the data of Figure 3 without this assumption of benzene as a single-step, hard-collision deactivator. Thus, by using benzene as the bath gas, one of the adjustable parameters was eliminated and only one E^* remained.

As shown in Figure 6, the best fit to the benzene data of Figure 3 is obtained with a value of 25 kcal mol^{-1} for E^*. The highest possible value for E^*, i.e., the difference between the deazetation and rearrangement transition states (E^*_{max}) is 29 kcal mol^{-1} (Figure 4). Thus, *essentially all the excess energy from the deazetation of* **14** *is carried off by the bicyclobutane.*

Having established a value for E^*, one can now fit the N_2 deactivation data. It is established that N_2 is a relatively weak collider,[38] and the standard stepladder model[37] has been applied to evaluate its efficiency as a deactivator. As shown in Figure 6, the best fit to the data is obtained with a value of 0.35 kcal mol^{-1} (120 cm^{-1}) for $\langle \Delta E \rangle$ for N_2. The fit of the data is not precise, and it has often been noted that it is difficult to obtain one set of parameters that mimics both the high- and low-pressure regions.[39] Emphasis is placed on the high-pressure region, since it is felt that these data are more accurate.

The value of 0.35 kcal mol^{-1} for $\langle \Delta E \rangle$ for N_2 is relatively small compared to the values obtained from other studies using N_2.[38] It has been shown that for a given collider, $\langle \Delta E \rangle$ varies from system to system. A smaller value of $\langle \Delta E \rangle$ is obtained in those systems for which E^* is smaller, and in the present system, E^* is smaller than, for example, in the extensively studied[40] dimethylcyclopropane system. For the present system the important point is that any upward revision of $\langle \Delta E \rangle$ for N_2 will also require an increase in E^*. For example, with a $\langle \Delta E \rangle$ of 1.0 kcal mol^{-1}, a number more consistent with

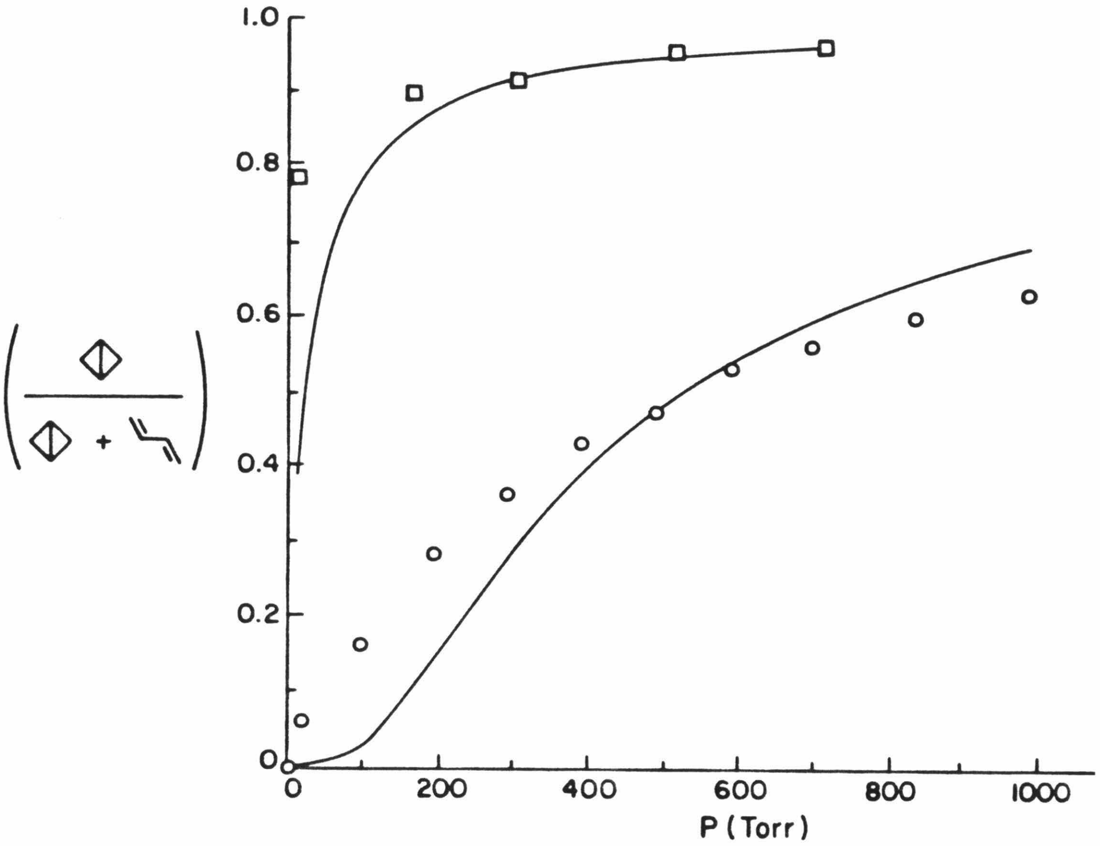

Figure 6. Theoretical fits to product composition data from gas phase thermolysis of **14**. Single points are experimental data. o: Nitrogen as bath gas; □: Benzene as bath gas. Solid lines are theoretical curves obtained as described in text.

other studies of N_2 as a collisional deactivator, a value for E^* of 29 kcal mol^{-1} gives a fit to the experimental data as good as that in Figure 6. Thus the N_2 data suggest that the 25 kcal mol^{-1} estimate of E^* from the benzene data should be viewed as a lower limit.

Mechanistic Implications

Before discussing the implication of our results on the mechanism of azoalkane decomposition, it is perhaps worthwhile to consider possible uncertainties in the above analysis. The three critical quantities are E^*_{max}, $k(E^*)$ and the efficiency of collisional deactivation as determined primarily by $\langle \Delta E \rangle$. The quantity E^*_{max} is derived from Figure 4, and the only value that could have a substantial uncertainty is ΔH_f° for **14**. The EFF method was parametrized[17] to precisely reproduce the ΔH_f° of **10**, and thus should be fairly reliable for **14**. Perhaps a value of 28 ± 3 kcal mol^{-1} would be appropriate for E^*_{max}. The unimolecular decomposition rate, $k(E^*)$ derives from RRKM theory. It would seem that the bicyclobutane-to-butadiene rearrangement is an ideal candidate for RRKM studies. The small size and well-understood vibrational spectrum of **30** along with the relatively constrained nature of the transition state would seem to diminish some of the uncertainties associated with the method. Concerning the collisional deactivation data, the fit for the benzene curve is fairly good, but the range in measured product ratios is relatively small. The fit for the N_2 data is poorer, but it does seem to provide a viable lower limit for E^*. From evaluation of the range of E^* values that can give an acceptable fit to the experimental curves, we can conclude that E^* is 25±2 kcal mol^{-1}.

We feel that the above-mentioned error bars are quite generous. For the present purposes, though, there is no need to fine tune the values any further. Since the amount of vibrational energy in the extruded N_2 equals

$E^*_{max} - E^*$, the qualitative result is clear-cut. The vast majority of the excess energy from the decomposition of **14** is absorbed by the hydrocarbon fragment **30**. Remembering that one quantum of vibrational energy in N_2 is worth ca. 6.7 kcal mol^{-1} (2345 cm^{-1}), any "hot" N_2 is at best in the $v = 1$ vibrational state, it seems quite possible that only a fraction of the ejected N_2 molecules are "hot" at all. Within the framework of the Bauer postulate,[13] then, *N_2 loss from* **14** *occurs in a stepwise fashion, via an intermediate diazenyl biradical.* The necessity of a diazenyl biradical as a true intermediate is brought about by the need to allow statistical redistribution of energy to occur prior to release of N_2.

Several recent studies have presented evidence for stepwise, one-bond cleavage in highly unsymmetrical *trans*, and certain symmetrical *cis*, acyclic diazenes and for 4-alkylidenepyrazolines.[41] However, the present work provides the first unambiguous experimental evidence favoring the one-bond cleavage mechanism in a simple pyrazoline, and the first time that the distribution of the excess energy between the products of such a reaction has been used as a mechanistic probe. Since our work, Engel[42] has studied the vibrational energy content of the *photo*fragments formed from azomethane. Using coherent anti-Stokes Raman spectroscopy (CARS) he finds that the population of nitrogen molecules in the $v = 0$, $v = 1$ and $v > 1$ levels are 84, 16 and <3% respectively in good agreement with our findings. However, no evidence was found for a diazenyl radical having a lifetime longer than 2 ns. In light of these results, the observation of a very small amount of chemical activation in the unsymmetrical structure **48**, but none in the symmetrical **49** does not justify the proposal of different mechanisms for the two. Perhaps the thermochemistries of **48** and **49** are slightly different, thereby providing the products from **48** with slightly more excess energy. Consistent with this interpretation is the fact that activation energy for decomposition of **48** is ca. 3-4 kcal mol^{-1} greater than that for **49**.[22]

EXPERIMENTAL SECTION

General. ^{1}H NMR spectra were recorded on a Varian EM–390 spectrometer. Fourier transform NMR spectra (^{1}H and ^{13}C) were recorded on a JEOL FX-90Q, and 500-MHz ^{1}H NMR spectra were recorded on a Bruker WM-500 spectrometer. UV spectra were recorded on a Beckman Model 25 spectrophotometer. IR spectra were recorded using a Perkin-Elmer 257 grating spectrometer. Elemental analyses and mass spectra were obtained by the Caltech Analytical Facility. Analytic gas chromatography was performed on a Hewlett-Packard 5840A chromatograph equipped with a flame ionization detector. Preparative gas chromatography was performed on a Varian Aerograph Model 920 chromatograph with a thermal conductivity detector.

1,3-Dimethylbicyclo[1.1.0]butane (31). A slight modification of the literature procedure[43] was adopted. 1,3-Dibromo-1,3-dimethylcyclobutane[44] (6.0 g, 25 mmol) in 10 mL DMF was added dropwise over a period of 1 h to a suspension of 2% lithium amalgam[45] (19.1 g, 54.6 mmol) in 15 mL DMF at room temperature. The reaction mixture was then stirred for another 2 h. The product was isolated by fractional distillation under reduced pressure to give 1.82 g (21.9 mmol, 88 % yield) of the product.

1,4,7-Trimethyl-2,4,6-triazatricyclo[5.1.1.0^{2,6}]nonane-3,5-dione (47).

In a 2-L , two-necked, round-bottomed flask fitted with a dry ice–acetone condenser and pressure-equalizing addition funnel was placed a solution of **31** (1.83 g, 21.9 mmol) in 1.5 L of hexanes. At room temperature and under a slow stream of nitrogen, a solution of MTAD[46] (2.75 g, 23.9 mmol) in 200 mL diethyl ether was added dropwise over a period of about 3 h. A white insoluble material was filtered off and the filtrate concentrated on a rotary evaporator. The resulting yellow oil was subjected to flash chromatography[47] on 70-230 mesh silica gel (5:1 methylene chloride, diethyl ether; $R_f = 0.55$). The product was isolated as a pale yellow oil (510 mg, 2.61 mmol, 12 % yield); ^{1}H NMR (C_6D_6) δ 0.98 (m, 2H), 1.36 (m, 2H), 1.51 (s, 6H), 2.58 (s, 3H); ^{13}C NMR (C_6D_6) δ 15.7 (CH_3), 25.0 ($N{-}CH_3$), 47.4 (CH_2), 69.9 (bridgehead), 160.3 (C=0); anal. C,H,N.

1,4-Dimethyl-2,3-diazabicyclo[2.1.1]hex-2-ene (16). An adaptation of the literature procedures[48] was used for the hydrolysis–oxidation of **47** to **16**. To a hot solution (40–45°C) of potassium hydroxide (1.2 g, 87 %, 19 mmol) in 20 mL 2-propanol (previously flushed with nitrogen for 15 min) was added **47** (468 mg, 2.4 mmol) and the mixture was refluxed under nitrogen for 2 h and subsequently cooled in an ice–water bath. The reaction mixture was acidified using 3 N hydrochloric acid, warmed to about 40°C for 10 min, cooled to room temperature and neutralized with 1 N ammonium hydroxide. A solution of cupric bromide (1.3 g, 6.0 mmol) in 15 mL water was added dropwise with gentle stirring. The pH was adjusted to about 6 using 1 N ammonium hydroxide and the reaction flask kept at room temperature for 1 h. Reddish-brown crystals of the copper complex appeared and were filtered, washed (with water, methanol and diethyl ether) and air dried. To a suspension of the complex in 30 mL of diethyl ether was added 25 mL of 1 N ammonium hydroxide at 0°C with vigorous stirring. The ethereal layer was separated and the aqueous layer extracted with ether. The combined organic phase was dried over magnesium sulfate. After filtration, the ether was distilled off through a 10 cm Vigreaux column. Care was taken not to heat the solution over 40°C. When about 1.5 mL of the solution remained, the distillation was stopped, and pure **16** was isolated by preparative gas chromatography. A 10 ft x 1/4 in. column of 10

% UCW-982 on Chromosorb WAW-DMCS mesh size 80/100 was used. At a column temperature of 55°C and a helium flow of 120 mL min^{-1}, the retention time for **16** was 13 min. A total of 114 mg (1.04 mmol, 41.7% yield) of the product was isolated; mp (sealed tube) 47–48°C; ^{1}H NMR (C_6D_6) δ 1.00 (m, 2H), 1.51 (s, 6H), 1.83 (m, 2H); ^{13}C NMR (C_6D_6) δ 15.57 (CH_3), 64.45 (CH_2), 83.48 (bridgehead); IR (CCl_4) 2995, 2980, 2940, 2875, 1445, 1422, 1380, 1285, 1150, 995 cm^{-1}; UV (*n*-hexane) λ_{max} 341 nm (ϵ=1320), 334 (ϵ=270), 330 (ϵ=226), 325 (ϵ=270); mass spectrum m/e 82 (30), 67 (60), 41 (67), 39 (60), 28 (100).

Kinetic Measurements. All kinetic experiments in the solution-phase thermal decomposition of **16** were conducted in sealed NMR tubes in a well-insulated silicone oil bath at temperatures between 100 and 125°C. A Bayley Model 253 proportional temperature controller was used. Accurate measurements of the temperature were made by using an iron–constantan thermocouple connected to a digital voltmeter. A stock solution of **16** (43 mg) in 5 mL benzene-d_6 was prepared. A number of NMR samples were then prepared using this solution by degassing (three freeze–pump–thaw cycles) and sealing the tubes under vacuum. Reactions were followed by 90-MHz ^{1}H NMR spectroscopy using multiple integrations. Because of the intense, well-separated NMR signals in **16** and the products, quite accurate quantitative analysis was possible. All rate plots and the Arrhenius and Eyring plots gave linear correlation coefficients of 0.9997 or better.

Gas-phase thermal studies were conducted in a specially-modified, 2-L Pyrex round-bottomed flask. A 5-mL test tube was glass-blown onto its bottom to serve as a reservoir. The flask was also fitted with a vacuum stopcock at the top. The vessel was treated with triethylamine for a day at 120°C and then evacuated. 1-2 mg samples of **14** and **16** were introduced into the reservoir. A bath gas was then transferred into the vessel. In the case of nitrogen, a known volume at atmospheric pressure was added into the vacuum system. Since the total volume of the system was known, the pressure of nitrogen in the reaction vessel could easily be calculated. In the case of benzene a known weight of the liquid was vacuum transferred into the vessel and its pressure at 120°C calculated using the ideal gas equation. The vessel was then heated at 120°C for 6–10 h. The products were condensed in the reservoir using liquid nitrogen, and solvent transferred into the vessel. Analyses were performed both by ^{1}H NMR spectroscopy and by gas chromatography on either a 20 in. x 1/4 in. UCW-982 column on Chromosorb WAW-DMCS or a 30 m x 1/4 mm DB-17 capillary column. Control experiments revealed that bicyclobutane and 1,3-dimethylbicyclobutane were stable under the reaction conditions. Addition of glass beads to increase the surface-to-volume ratio by a factor of 7 did not produce any significant change in the product ratios.

Calculations. The Hase–Bunker program[33] was used for RRKM studies on the decomposition of **30** to butadiene and **31** to 2,3-dimethylbutadiene. For **30**, the necessary vibrational frequencies were obtained as described in the text, and for **31**, they were obtained by appropriate adjustment of the frequencies for **30** in a manner similar to cyclopropane and 1,2-dimethylcyclopropane.[49] The Whitten–Rabinovitch algorithm[50] was used to calculate the sums and densities of states. All rates were obtained assuming harmonic oscillations. No internal rotors were considered, and contributions from external rotations were also ignored. The moments of inertia in the ground and transition states were taken to be the same, while the frequencies of the transition state were related to those of the ground state by the high-pressure Arrhenius pre-exponential term by

$$A = \frac{\prod_i^s \nu_i}{\prod_i^{s-1} \nu_i^{\ddagger}}$$

Here s is the total number of ground state oscillators and ‡ indicates the transition state, which has one less vibrational mode.

The multistep collisional deactivation scheme assumed a stepladder model.[37] Collisional diameters of 3.68 $\mathring{A}$ for nitrogen and 4.8 $\mathring{A}$ for benzene were used.[38] The values used for **30** (5.9 $\mathring{A}$) and **31** (7.0 $\mathring{A}$) were obtained by examining molecular models, and by comparison with literature values[40,51] for similar structures.

References for Chapter II

1. Engel, P.S. *Chem. Rev.* **1980**, *80*, 99–150.
2. Adam, W.; DeLucchi, O. *Angew. Chem., Intl. Ed. Engl.* **1980**, *19*, 762–779 and references therein.
3. Ramsperger, H.C. *J. Am. Chem. Soc.* **1929**, *51*, 2134–2143.
4. Perona, M.J.; Beadle, P.C.; Golden, D.M. *Int. J. Chem. Kinet.* **1973**, *5*, 495–512.
5. Engel, P.S.; Bishop, D.J. *J. Am. Chem. Soc.* **1975**, *97*, 6754–6762.
6. Garner, A.W.; Timberlake, J.W.; Engel, P.S.; Melaugh, R.A. *J. Am. Chem. Soc.* **1975**, *97*, 7377–7379.
7. Pryor, W.A.; Smith, K. *J. Am. Chem. Soc.* **1967**, *89*, 1741–1742. Pryor, W.A.; Smith, K. *J. Am. Chem. Soc.* **1970**, *92*, 5403–5412
8. Neuman, R.C., Jr.; Binegar, G.A. *J. Am. Chem. Soc.* **1983**, *105*, 134–135. Neuman, R.C., Jr.; Lockyer, G.D., Jr. *J. Am. Chem. Soc.* **1983**, *105*, 3982–3987.
9. Porter, N.A.; Dubay, G.R.; Green, J.G. *J. Am. Chem. Soc.* **1978**, *100*, 920–925. Green, J.G.; Dubay, G.R.; Porter, N.A. *J. Am. Chem. Soc.* **1977**, *99*, 1264–1265.
10. Engel, P.S.; Gerth, D.B. *J. Am. Chem. Soc.* **1983**, *105*, 6849–6851.
11. Engel, P.S.; Nalepa, C.J.; Horsey, D.W.; Keys, D.E.; Grow, R.T. *J. Am. Chem. Soc.* **1983**, *105*, 7102–7107.
12. Dannenberg, J.J.; Rocklin, D. *J. Org. Chem.* **1982**, *47*, 4529–4534. Dannenberg, J.J. *J. Org. Chem.* **1985**, *50*, 4963–4965.
13. Bauer, S.H. *J. Am. Chem. Soc.* **1969**, *91*, 3688–3689.
14. Roth, W.R.; Martin, M. *Tetrahedron Lett.* **1967**, 4695–4698.

15. Amey, R.L.; Smart, B.E. *J. Org. Chem.* **1981**, *46*, 4090–4092.
16. Chang, M.H.; Dougherty, D.A. *J. Org. Chem.* **1981**, *46*, 4092–4093.
17. Kao, J.; Huang, T.-N. *J. Am. Chem. Soc.* **1979**, *101*, 5546–5557.
18. There is precedent for methyl substitution slowing a pyrazoline decomposition. 3,3,5,5-Tetramethyl-4-isopropylidenepyrazoline decomposes much more slowly than 4-isopropylidenepyrazoline. This effect results from steric congestion in the transition state, as the development of a trimethylenemethane biradical-like structure leads to a more nearly planar carbon framework (see ref. 1). It is difficult to see any analogous interactions in **16**.
19. Chang, M.H.; Dougherty, D.A. *J. Am. Chem. Soc.* **1982**, *104*, 1131–1132.
20. Frey, M.H.; Stevens, I.D.R. *Trans. Faraday Soc.* **1965**, *61*, 90–94.
21. Chesick, J.P. *J. Phys. Chem.* **1964**, *68*, 2033–2034.
22. Shen, K.K.; Bergman, R.G. *J. Am. Chem. Soc.* **1977**, *99*, 1655–1657.
23. See ref. 1 and: Cox, J.D.; Pilcher, G. *Thermochemistry of Organic and Organometallic Compounds*; Academic: New York, 1970. Turner, R.B.; Goebel, P.; Mallon, B.J.; Doering, W. von, E.; Coburn, J.F., Jr.; Pomerantz, M. *J. Am. Chem. Soc.* **1968**, *90*, 4315–4322.
24. See ref. 1, 16 and: Willcott, M.R.; Cargill, R.L.; Sears, A.B. *Prog. Phys. Org. Chem.* **1972**, *9*, 25–98.
25. Wiberg, K.B.; Lavanish, J.M. *J. Am. Chem. Soc.* **1966**, *88*, 5272–5275.
26. Dervan, P.B.; Dougherty, D.A. In *Diradicals*; Borden, W.T., Ed.; Wiley: New York, 1982; pp 107–149.
27. Doering, W. von E. *Proc. Natl. Acad. Sci., USA* **1981**, *78*, 5279–5283.
28. We chose a ring-strain correction that is intermediate between those

proposed[29] for cyclobutane and cyclobutene. Biradical **13** should be more strained than cyclobutane because of the introduction of two sp^2 centers into the four-membered ring, but less strained than cyclobutene because of the diminished number of H–H eclipsing interactions.

29. Benson, S.W. *Thermochemical Kinetics*, 2nd. ed.; Wiley: New York, 1976.
30. Robinson, P.J.; Holbrook, K.A. *Unimolecular Reactions*; Wiley: New York, 1972; p 64.
31. Forst, W. *Theory of Unimolecular Reactions*; Academic: New York, 1973.
32. Callear, A.B. In *Comprehensive Chemical Kinetics*; Bamford, C.H.; Tipper, C.F.H., Eds.; Elsevier: New York, 1983; Vol. 24, pp 333–356.
33. Hase, W.L.; Bunker, D.L. *QCPE* **1973**, *11*, 234.
34. Wiberg, K.B.; Peters, K.S. *Spectrochimica Acta* **1977**, *33A*, 261–271.
35. Gajewski, J.J. *Hydrocarbon Thermal Isomerizations*; Academic: New York, 1981; pp 45–46.
36. See ref. 30; p 164.
37. Hoare, M. *J. Chem. Phys.* **1963**, *38*, 1630–1635.
38. Chan, S.C.; Rabinovitch, B.S.; Bryant, J.T.; Spicer, L.D.; Fujimoto, T.; Lin, Y.N.; Pavlou, S.P. *J. Phys. Chem.* **1970**, *74*, 3160–3176.
39. McCluskey, R.J.; Carr, R.W., Jr. *J. Phys. Chem.* **1976**, *80*, 1393–1398.
40. Rynbrandt, J.D.; Rabinovitch, B.S. *J. Phys. Chem.* **1970**, *74*, 1679–1685 and references therein.
41. Crawford, R.J.; Chang, M.H. *Tetrahedron* **1982**, *38*, 837–842.
42. Holt, P.L.; McCurdy, K.E.; Adams. J.S.; Burton, K.A.; Weisman, R.B.; Engel, P.S. *J. Am. Chem. Soc.* **1985**, *107*, 2180–2182.

43. Griesbaum, K.; Butler, P.E. *Angew. Chem., Intl. Ed. Engl.* **1967**, *6*, 444–445.

44. Griesbaum, K.; Naegele, W.; Wanless, G.G. *J. Am. Chem. Soc.* **1965**, *87*, 3151–3158.

45. Alexander, J.; Krishna Rao, G.S. *J. Chem. Educ.* **1970**, *47*, 277.

46. Cookson, R.C.; Gupte, S.S.; Stevens, I.D.R.; Watts, C.T. *Org. Syn.* **1971**, *51*, 121–127.

47. Still, W.C.; Kahn, M.; Mitra, A. *J. Org. Chem.* **1978**, *43*, 2923–2925.

48. Gassman, P.G.; Mansfield, K.T. *Org. Syn.* **1969**, *49*, 1–6. Adam, W.; DeLucchi, O.; Erden, I. *J. Am. Chem. Soc.* **1980**, *102*, 4806–4809. Jösel, R.; Schröder, G. *Liebigs Ann. Chem.* **1980**, 1428–1437.

49. Durig, J.R.; Nease, A.B.; Milani-Nejad, F. *J. Mol. Struct.* **1981**, *72*, 57–72.

50. Whitten, G.Z.; Rabinovitch, B.S.*J. Chem. Phys.* **1963**, *38*, 2466–2473.

51. Dorer, F.H. *J. Phys. Chem.* **1969**, *73*, 3109–311.

APPENDIX A

RESULTS OF RRKM CALCULATIONS

```
BICYCLOBUTANE TO 1,3-BUTADIENE
NO ROTORS, NO OVERALL ROTATION

EZERO =  40.60 KCAL/MOLE      ESTAR =  40.60 KCAL/MOLE      EINC =  1.00 KCAL/MOLE      REACTION PATH DEGENERACY = 2.0

 100  RATE CONSTANTS TO BE CALCULATED

NUMBER OF OSCILLATORS IN MOLECULE   NUMBER OF INTERNAL ROTORS IN MOLECULE

                 24                         0

FREQUENCIES IN MOLECULE

      3122.0      2926.0      2896.0      1302.0      1264.0      1242.0      1080.0       658.0
       422.0      1140.0      1090.0       912.0       650.0      2949.0      1268.0      1113.0
       983.0       736.0      3044.0      2971.0      1456.0      1149.0       940.0       861.0


EXTERNAL ROTATIONS TREATED AS INACTIVE


*****STRUCTURE OF THE CRITICAL CONFIGURATION IS SPECIFIED*****

NUMBER OF OSCILLATORS IN COMPLEX   NUMBER OF INTERNAL ROTORS IN COMPLEX

                 23                         0

FREQUENCIES IN COMPLEX

      3122.0      2925.0      2896.0      1302.0      1264.0      1242.0       624.0       658.0
       422.0      1140.0       912.0       650.0      2949.0      1268.0      1113.0       983.0
       425.0      3044.0      2971.0      1456.0      1149.0       940.0       491.0


SUM CAN NOT BE CALCULATED.  EDAG = ,    0.00 KCAL/MOLE
AN ATTEMPT WILL BE MADE TO CALCULATE A RATE CONSTANT AT      40.60 +  1.00 KCAL/MOLE


XXXXXXXXXXXXXXXXXXXXXXXXXXXXXXXXXXXXXXXXXXXXXXXXXXXXXXXXXXXXXXXXXXXXXXXXXXXXXXXXXXXXXXXXXXXXXXXXXXXXXXXXXXX

RATE CONSTANTS CALCULATED USING THESE OPTIONS:      KROT = -1  NANH = 0  NCRIT = 0  JDEN =  0  JSUM =  0


  ESTAR              EDAG           HARMONIC          HARMONIC            HARMONIC

KCAL/MOLE          KCAL/MOLE          DENSITY             SUM            RATE CONSTANT


  41.60               1.00        0.1150E+07        0.1606E+01         0.8376E+05
  42.60               2.00        0.1527E+07        0.6214E+01         0.2439E+06
  43.60               3.00        0.2020E+07        0.1922E+02         0.5705E+06
  44.60               4.00        0.2662E+07        0.5216E+02         0.1175E+07
  45.60               5.00        0.3494E+07        0.1291E+03         0.2215E+07
  46.60               6.00        0.4570E+07        0.2979E+03         0.3908E+07
  47.60               7.00        0.5956E+07        0.6499E+03         0.6542E+07
  48.60               8.00        0.7736E+07        0.1353E+04         0.1049E+08
```

```
  49.60             9.00      0.1001E+08      0.2709E+04        0.1621E+08
  50.60            10.00      0.1292E+08      0.5239E+04        0.2431E+08
  51.60            11.00      0.1662E+08      0.9833E+04        0.3547E+08
  52.60            12.00      0.2141E+08      0.1797E+05        0.5033E+08
  53.60            13.00      0.2739E+08      0.3207E+05        0.7020E+08
  54.60            14.00      0.3494E+08      0.5601E+05        0.9612E+08
  55.60            15.00      0.4444E+08      0.9593E+05        0.1294E+09
  56.60            16.00      0.5637E+08      0.1614E+06        0.1717E+09
  57.60            17.00      0.7130E+08      0.2670E+06        0.2245E+09
  58.60            18.00      0.8994E+08      0.4352E+06        0.2901E+09
  59.60            19.00      0.1132E+09      0.6993E+06        0.3704E+09
  60.60            20.00      0.1420E+09      0.1109E+07        0.4681E+09
  61.60            21.00      0.1778E+09      0.1737E+07        0.5857E+09
  62.60            22.00      0.2221E+09      0.2690E+07        0.7262E+09
  63.60            23.00      0.2768E+09      0.4121E+07        0.8928E+09
  64.60            24.00      0.3441E+09      0.6250E+07        0.1089E+10
  65.60            25.00      0.4268E+09      0.9387E+07        0.1319E+10
  66.60            26.00      0.5282E+09      0.1397E+08        0.1586E+10
  67.60            27.00      0.6523E+09      0.2061E+08        0.1895E+10
  68.60            28.00      0.8039E+09      0.3017E+08        0.2250E+10
  69.60            29.00      0.9887E+09      0.4381E+08        0.2657E+10
  70.60            30.00      0.1213E+10      0.6315E+08        0.3120E+10
  71.60            31.00      0.1486E+10      0.9039E+08        0.3646E+10
  72.60            32.00      0.1817E+10      0.1285E+09        0.4239E+10
  73.60            33.00      0.2218E+10      0.1815E+09        0.4906E+10
  74.60            34.00      0.2701E+10      0.2548E+09        0.5654E+10
  75.60            35.00      0.3284E+10      0.3555E+09        0.6489E+10
  76.60            36.00      0.3986E+10      0.4932E+09        0.7418E+10
  77.60            37.00      0.4829E+10      0.6805E+09        0.8448E+10
  78.60            38.00      0.5841E+10      0.9341E+09        0.9588E+10
  79.60            39.00      0.7052E+10      0.1276E+10        0.1084E+11
  80.60            40.00      0.8502E+10      0.1733E+10        0.1222E+11
  81.60            41.00      0.1023E+11      0.2344E+10        0.1374E+11
  82.60            42.00      0.1229E+11      0.3156E+10        0.1539E+11
  83.60            43.00      0.1475E+11      0.4231E+10        0.1720E+11
  84.60            44.00      0.1767E+11      0.5647E+10        0.1916E+11
  85.60            45.00      0.2113E+11      0.7506E+10        0.2129E+11
  86.60            46.00      0.2524E+11      0.9937E+10        0.2360E+11
  87.60            47.00      0.3010E+11      0.1310E+11        0.2610E+11
  88.60            48.00      0.3585E+11      0.1722E+11        0.2879E+11
  89.60            49.00      0.4263E+11      0.2254E+11        0.3169E+11
  90.60            50.00      0.5063E+11      0.2943E+11        0.3485E+11
  91.60            51.00      0.6005E+11      0.3830E+11        0.3823E+11
  92.60            52.00      0.7112E+11      0.4966E+11        0.4186E+11
  93.60            53.00      0.8413E+11      0.6419E+11        0.4574E+11
  94.60            54.00      0.9939E+11      0.8270E+11        0.4989E+11
  95.60            55.00      0.1173E+12      0.1062E+12        0.5430E+11
  96.60            56.00      0.1382E+12      0.1360E+12        0.5900E+11
  97.60            57.00      0.1626E+12      0.1736E+12        0.6400E+11
  98.60            58.00      0.1912E+12      0.2210E+12        0.6930E+11
  99.60            59.00      0.2245E+12      0.2805E+12        0.7492E+11
 100.60            60.00      0.2632E+12      0.3551E+12        0.8088E+11
 101.60            61.00      0.3083E+12      0.4484E+12        0.8717E+11
 102.60            62.00      0.3608E+12      0.5646E+12        0.9382E+11
 103.60            63.00      0.4217E+12      0.7091E+12        0.1008E+12
 104.60            64.00      0.4923E+12      0.8885E+12        0.1082E+12
 105.60            65.00      0.5741E+12      0.1111E+13        0.1160E+12
 106.60            66.00      0.6688E+12      0.1385E+13        0.1241E+12
 107.60            67.00      0.7783E+12      0.1723E+13        0.1327E+12
 108.60            68.00      0.9048E+12      0.2139E+13        0.1417E+12
 109.60            69.00      0.1051E+13      0.2649E+13        0.1511E+12
 110.60            70.00      0.1219E+13      0.3274E+13        0.1610E+12
 111.60            71.00      0.1413E+13      0.4037E+13        0.1713E+12
 112.60            72.00      0.1636E+13      0.4969E+13        0.1821E+12
 113.60            73.00      0.1892E+13      0.6103E+13        0.1934E+12
 114.60            74.00      0.2187E+13      0.7482E+13        0.2051E+12
```

```
 115.60          75.00      0.2525E+13      0.9153E+13      0.2174E+12
 116.60          76.00      0.2912E+13      0.1118E+14      0.2301E+12
 117.60          77.00      0.3356E+13      0.1363E+14      0.2434E+12
 118.60          78.00      0.3864E+13      0.1658E+14      0.2572E+12
 119.60          79.00      0.4445E+13      0.2013E+14      0.2716E+12
 120.60          80.00      0.5108E+13      0.2441E+14      0.2865E+12
 121.60          81.00      0.5866E+13      0.2954E+14      0.3019E+12
 122.60          82.00      0.6730E+13      0.3569E+14      0.3179E+12
 123.60          83.00      0.7715E+13      0.4305E+14      0.3345E+12
 124.60          84.00      0.8837E+13      0.5185E+14      0.3518E+12
 125.60          85.00      0.1011E+14      0.6234E+14      0.3696E+12
 126.60          86.00      0.1157E+14      0.7484E+14      0.3880E+12
 127.60          87.00      0.1321E+14      0.8971E+14      0.4070E+12
 128.60          88.00      0.1509E+14      0.1074E+15      0.4267E+12
 129.60          89.00      0.1721E+14      0.1283E+15      0.4470E+12
 130.60          90.00      0.1962E+14      0.1531E+15      0.4679E+12
 131.60          91.00      0.2235E+14      0.1825E+15      0.4895E+12
 132.60          92.00      0.2543E+14      0.2171E+15      0.5118E+12
 133.60          93.00      0.2893E+14      0.2580E+15      0.5348E+12
 134.60          94.00      0.3287E+14      0.3062E+15      0.5584E+12
 135.60          95.00      0.3733E+14      0.3629E+15      0.5827E+12
 136.60          96.00      0.4237E+14      0.4295E+15      0.6078E+12
 137.60          97.00      0.4805E+14      0.5077E+15      0.6335E+12
 138.60          98.00      0.5445E+14      0.5993E+15      0.6599E+12
 139.60          99.00      0.6166E+14      0.7066E+15      0.6871E+12
```

```
1,3-DIMETHYLBICYCLOBUTANE TO 2,3-DIMETHYL 1,3-BUTADIENE
NO ROTORS, NO OVERALL ROTATION

EZERO =  43.30 KCAL/MOLE      ESTAR =  43.30 KCAL/MOLE      EINC =  1.00 KCAL/MOLE      REACTION PATH DEGENERACY = 2.0

 100  RATE CONSTANTS TO BE CALCULATED


NUMBER OF OSCILLATORS IN MOLECULE   NUMBER OF INTERNAL ROTORS IN MOLECULE

                 42                             0

FREQUENCIES IN MOLECULE

      2925.0      2896.0      1264.0      1242.0      1080.0       658.0       422.0      1140.0
      1090.0       650.0      1268.0      1113.0       735.0      3044.0      2971.0      1456.0
       940.0       851.0      2962.0      2962.0      2948.0      2935.0      2918.0      2885.0
      1475.0      1462.0      1435.0      1435.0      1398.0      1380.0      1098.0      1070.0
      1035.0       978.0       877.0       767.0       488.0       413.0       305.0       258.0
       163.5       163.5


EXTERNAL ROTATIONS TREATED AS INACTIVE



*****STRUCTURE OF THE CRITICAL CONFIGURATION IS SPECIFIED*****

NUMBER OF OSCILLATORS IN COMPLEX   NUMBER OF INTERNAL ROTORS IN COMPLEX

                 41                             0

FREQUENCIES IN COMPLEX

      2925.0      2896.0      1264.0      1242.0       624.0       658.0       422.0      1140.0
       650.0      1268.0      1113.0       425.0      3044.0      2971.0      1456.0       940.0
       491.0      2962.0      2962.0      2948.0      2935.0      2918.0      2885.0      1475.0
      1462.0      1435.0      1435.0      1398.0      1380.0      1098.0      1070.0      1035.0
       978.0       877.0       767.0       488.0       413.0       305.0       258.0       163.5
       163.5


SUM CAN NOT BE CALCULATED.  EDAG = ,    0.00 KCAL/MOLE
AN ATTEMPT WILL BE MADE TO CALCULATE A RATE CONSTANT AT     43.30 +  1.00 KCAL/MOLE


XXXXXXXXXXXXXXXXXXXXXXXXXXXXXXXXXXXXXXXXXXXXXXXXXXXXXXXXXXXXXXXXXXXXXXXXXXXXXXXXXXXXXXXXXXXXXXXXXXXX


RATE CONSTANTS CALCULATED USING THESE OPTIONS:      KROT = -1  NANH = 0  NCRIT = 0  JDEN =  0  JSUM =  0



  ESTAR              EDAG              HARMONIC          HARMONIC            HARMONIC

KCAL/MOLE          KCAL/MOLE            DENSITY              SUM           RATE CONSTANT


  44.30               1.00        0.2987E+12        0.2021E+02          0.4058E+01
  45.30               2.00        0.4474E+12        0.1243E+03          0.1665E+02
```

```
  46.30           3.00      0.6669E+12      0.5658E+03      0.5087E+02
  47.30           4.00      0.9892E+12      0.2170E+04      0.1315E+03
  48.30           5.00      0.1460E+13      0.7393E+04      0.3035E+03
  49.30           6.00      0.2146E+13      0.2302E+05      0.6432E+03
  50.30           7.00      0.3139E+13      0.6671E+05      0.1274E+04
  51.30           8.00      0.4572E+13      0.1822E+06      0.2389E+04
  52.30           9.00      0.6630E+13      0.4729E+06      0.4276E+04
  53.30          10.00      0.9576E+13      0.1175E+07      0.7357E+04
  54.30          11.00      0.1377E+14      0.2810E+07      0.1223E+05
  55.30          12.00      0.1974E+14      0.6492E+07      0.1972E+05
  56.30          13.00      0.2817E+14      0.1454E+08      0.3095E+05
  57.30          14.00      0.4006E+14      0.3169E+08      0.4743E+05
  58.30          15.00      0.5676E+14      0.6733E+08      0.7112E+05
  59.30          16.00      0.8012E+14      0.1397E+09      0.1046E+06
  60.30          17.00      0.1127E+15      0.2839E+09      0.1510E+06
  61.30          18.00      0.1580E+15      0.5653E+09      0.2144E+06
  62.30          19.00      0.2209E+15      0.1105E+10      0.3000E+06
  63.30          20.00      0.3077E+15      0.2124E+10      0.4139E+06
  64.30          21.00      0.4271E+15      0.4017E+10      0.5637E+06
  65.30          22.00      0.5913E+15      0.7481E+10      0.7586E+06
  66.30          23.00      0.8159E+15      0.1374E+11      0.1009E+07
  67.30          24.00      0.1123E+16      0.2489E+11      0.1329E+07
  68.30          25.00      0.1540E+16      0.4452E+11      0.1733E+07
  69.30          26.00      0.2107E+16      0.7868E+11      0.2239E+07
  70.30          27.00      0.2874E+16      0.1375E+12      0.2868E+07
  71.30          28.00      0.3910E+16      0.2376E+12      0.3644E+07
  72.30          29.00      0.5305E+16      0.4065E+12      0.4594E+07
  73.30          30.00      0.7179E+16      0.6885E+12      0.5750E+07
  74.30          31.00      0.9689E+16      0.1155E+13      0.7148E+07
  75.30          32.00      0.1304E+17      0.1921E+13      0.8829E+07
  76.30          33.00      0.1752E+17      0.3167E+13      0.1084E+08
  77.30          34.00      0.2347E+17      0.5177E+13      0.1322E+08
  78.30          35.00      0.3137E+17      0.8396E+13      0.1605E+08
  79.30          36.00      0.4182E+17      0.1351E+14      0.1937E+08
  80.30          37.00      0.5564E+17      0.2159E+14      0.2326E+08
  81.30          38.00      0.7385E+17      0.3425E+14      0.2781E+08
  82.30          39.00      0.9780E+17      0.5396E+14      0.3308E+08
  83.30          40.00      0.1292E+18      0.8446E+14      0.3918E+08
  84.30          41.00      0.1704E+18      0.1314E+15      0.4621E+08
  85.30          42.00      0.2251E+18      0.2030E+15      0.5408E+08
  86.30          43.00      0.2958E+18      0.3120E+15      0.6322E+08
  87.30          44.00      0.3881E+18      0.4766E+15      0.7363E+08
  88.30          45.00      0.5080E+18      0.7240E+15      0.8545E+08
  89.30          46.00      0.6636E+18      0.1094E+16      0.9883E+08
  90.30          47.00      0.8652E+18      0.1644E+16      0.1139E+09
  91.30          48.00      0.1126E+19      0.2459E+16      0.1309E+09
  92.30          49.00      0.1462E+19      0.3659E+16      0.1500E+09
  93.30          50.00      0.1896E+19      0.5419E+16      0.1714E+09
  94.30          51.00      0.2453E+19      0.7988E+16      0.1952E+09
  95.30          52.00      0.3168E+19      0.1172E+17      0.2218E+09
  96.30          53.00      0.4084E+19      0.1712E+17      0.2513E+09
  97.30          54.00      0.5256E+19      0.2491E+17      0.2841E+09
  98.30          55.00      0.6752E+19      0.3608E+17      0.3203E+09
  99.30          56.00      0.8660E+19      0.5205E+17      0.3603E+09
 100.30          57.00      0.1109E+20      0.7479E+17      0.4044E+09
 101.30          58.00      0.1417E+20      0.1071E+18      0.4529E+09
 102.30          59.00      0.1809E+20      0.1527E+18      0.5060E+09
 103.30          60.00      0.2304E+20      0.2169E+18      0.5643E+09
 104.30          61.00      0.2931E+20      0.3070E+18      0.6280E+09
 105.30          62.00      0.3723E+20      0.4331E+18      0.6975E+09
 106.30          63.00      0.4721E+20      0.6089E+18      0.7732E+09
 107.30          64.00      0.5977E+20      0.8530E+18      0.8557E+09
 108.30          65.00      0.7556E+20      0.1191E+19      0.9451E+09
 109.30          66.00      0.9539E+20      0.1658E+19      0.1042E+10
 110.30          67.00      0.1202E+21      0.2301E+19      0.1147E+10
 111.30          68.00      0.1514E+21      0.3183E+19      0.1261E+10
```

```
 112.30          69.00     0.1902E+21     0.4391E+19      0.1384E+10
 113.30          70.00     0.2388E+21     0.6038E+19      0.1516E+10
 114.30          71.00     0.2993E+21     0.8279E+19      0.1658E+10
 115.30          72.00     0.3747E+21     0.1132E+20      0.1812E+10
 116.30          73.00     0.4684E+21     0.1544E+20      0.1976E+10
 117.30          74.00     0.5847E+21     0.2099E+20      0.2152E+10
 118.30          75.00     0.7290E+21     0.2847E+20      0.2341E+10
 119.30          76.00     0.9077E+21     0.3851E+20      0.2544E+10
 120.30          77.00     0.1129E+22     0.5196E+20      0.2760E+10
 121.30          78.00     0.1402E+22     0.6994E+20      0.2991E+10
 122.30          79.00     0.1739E+22     0.9389E+20      0.3237E+10
 123.30          80.00     0.2154E+22     0.1258E+21      0.3499E+10
 124.30          81.00     0.2666E+22     0.1680E+21      0.3779E+10
 125.30          82.00     0.3295E+22     0.2238E+21      0.4072E+10
 126.30          83.00     0.4068E+22     0.2980E+21      0.4392E+10
 127.30          84.00     0.5015E+22     0.3959E+21      0.4733E+10
 128.30          85.00     0.6177E+22     0.5249E+21      0.5094E+10
 129.30          86.00     0.7599E+22     0.6942E+21      0.5477E+10
 130.30          87.00     0.9338E+22     0.9162E+21      0.5882E+10
 131.30          88.00     0.1146E+23     0.1207E+22      0.6311E+10
 132.30          89.00     0.1405E+23     0.1586E+22      0.6765E+10
 133.30          90.00     0.1721E+23     0.2080E+22      0.7244E+10
 134.30          91.00     0.2106E+23     0.2721E+22      0.7749E+10
 135.30          92.00     0.2573E+23     0.3555E+22      0.8282E+10
 136.30          93.00     0.3142E+23     0.4634E+22      0.8843E+10
 137.30          94.00     0.3831E+23     0.6029E+22      0.9433E+10
 138.30          95.00     0.4668E+23     0.7828E+22      0.1005E+11
 139.30          96.00     0.5681E+23     0.1015E+23      0.1071E+11
 140.30          97.00     0.6907E+23     0.1313E+23      0.1139E+11
 141.30          98.00     0.8390E+23     0.1695E+23      0.1211E+11
 142.30          99.00     0.1018E+24     0.2185E+23      0.1287E+11
```

```
1,3-DIMETHYLBICYCLOBUTANE TO 2,3-DIMETHYL 1,3-BUTADIENE
NO ROTORS, NO OVERALL ROTATION

EZERO =  40.60 KCAL/MOLE     ESTAR =  40.60 KCAL/MOLE     EINC =  1.00 KCAL/MOLE     REACTION PATH DEGENERACY = 2.0

 100  RATE CONSTANTS TO BE CALCULATED


NUMBER OF OSCILLATORS IN MOLECULE   NUMBER OF INTERNAL ROTORS IN MOLECULE

                 42                         0

FREQUENCIES IN MOLECULE

      2925.0     2896.0     1264.0     1242.0     1080.0      658.0      422.0     1140.0
      1090.0      650.0     1268.0     1113.0      735.0     3044.0     2971.0     1456.0
       940.0      851.0     2962.0     2962.0     2948.0     2935.0     2918.0     2885.0
      1475.0     1462.0     1435.0     1435.0     1398.0     1380.0     1098.0     1070.0
      1035.0      978.0      877.0      767.0      488.0      413.0      305.0      258.0
       163.5      163.5


EXTERNAL ROTATIONS TREATED AS INACTIVE



*****STRUCTURE OF THE CRITICAL CONFIGURATION IS SPECIFIED*****

NUMBER OF OSCILLATORS IN COMPLEX   NUMBER OF INTERNAL ROTORS IN COMPLEX

                 41                         0

FREQUENCIES IN COMPLEX

      2925.0     2896.0     1264.0     1242.0      624.0      658.0      422.0     1140.0
       650.0     1268.0     1113.0      425.0     3044.0     2971.0     1456.0      940.0
       491.0     2962.0     2962.0     2948.0     2935.0     2918.0     2885.0     1475.0
      1462.0     1435.0     1435.0     1398.0     1380.0     1098.0     1070.0     1035.0
       978.0      877.0      767.0      488.0      413.0      305.0      258.0      163.5
       163.5


SUM CAN NOT BE CALCULATED.  EDAG = ,    0.00 KCAL/MOLE
AN ATTEMPT WILL BE MADE TO CALCULATE A RATE CONSTANT AT     40.60 +  1.00 KCAL/MOLE


XXXXXXXXXXXXXXXXXXXXXXXXXXXXXXXXXXXXXXXXXXXXXXXXXXXXXXXXXXXXXXXXXXXXXXXXXXXXXXXXXXXXXXXXXXXXXXXXXXXXXXXX

RATE CONSTANTS CALCULATED USING THESE OPTIONS:      KROT = -1  NANH = 0  NCRIT = 0  JDEN =  0  JSUM =  0


  ESTAR              EDAG             HARMONIC          HARMONIC             HARMONIC

KCAL/MOLE          KCAL/MOLE           DENSITY             SUM             RATE CONSTANT

  41.60              1.00         0.9766E+11        0.2021E+02          0.1241E+02
  42.60              2.00         0.1484E+12        0.1243E+03          0.5019E+02
```

```
  43.60           3.00      0.2244E+12      0.5658E+03      0.1512E+03
  44.60           4.00      0.3373E+12      0.2170E+04      0.3857E+03
  45.60           5.00      0.5046E+12      0.7393E+04      0.8784E+03
  46.60           6.00      0.7510E+12      0.2302E+05      0.1838E+04
  47.60           7.00      0.1112E+13      0.6671E+05      0.3596E+04
  48.60           8.00      0.1640E+13      0.1822E+06      0.6660E+04
  49.60           9.00      0.2406E+13      0.4729E+06      0.1178E+05
  50.60          10.00      0.3515E+13      0.1175E+07      0.2004E+05
  51.60          11.00      0.5114E+13      0.2810E+07      0.3294E+05
  52.60          12.00      0.7407E+13      0.6492E+07      0.5255E+05
  53.60          13.00      0.1068E+14      0.1454E+08      0.8162E+05
  54.60          14.00      0.1535E+14      0.3169E+08      0.1238E+06
  55.60          15.00      0.2197E+14      0.6733E+08      0.1837E+06
  56.60          16.00      0.3132E+14      0.1397E+09      0.2675E+06
  57.60          17.00      0.4449E+14      0.2839E+09      0.3825E+06
  58.60          18.00      0.6296E+14      0.5653E+09      0.5383E+06
  59.60          19.00      0.8879E+14      0.1105E+10      0.7463E+06
  60.60          20.00      0.1248E+15      0.2124E+10      0.1020E+07
  61.60          21.00      0.1748E+15      0.4017E+10      0.1378E+07
  62.60          22.00      0.2440E+15      0.7481E+10      0.1838E+07
  63.60          23.00      0.3396E+15      0.1374E+11      0.2425E+07
  64.60          24.00      0.4711E+15      0.2489E+11      0.3167E+07
  65.60          25.00      0.6515E+15      0.4452E+11      0.4097E+07
  66.60          26.00      0.8982E+15      0.7868E+11      0.5252E+07
  67.60          27.00      0.1235E+16      0.1375E+12      0.6675E+07
  68.60          28.00      0.1692E+16      0.2376E+12      0.8418E+07
  69.60          29.00      0.2313E+16      0.4065E+12      0.1054E+08
  70.60          30.00      0.3153E+16      0.6885E+12      0.1309E+08
  71.60          31.00      0.4286E+16      0.1155E+13      0.1616E+08
  72.60          32.00      0.5810E+16      0.1921E+13      0.1982E+08
  73.60          33.00      0.7856E+16      0.3167E+13      0.2417E+08
  74.60          34.00      0.1060E+17      0.5177E+13      0.2929E+08
  75.60          35.00      0.1425E+17      0.8396E+13      0.3531E+08
  76.60          36.00      0.1913E+17      0.1351E+14      0.4235E+08
  77.60          37.00      0.2561E+17      0.2159E+14      0.5054E+08
  78.60          38.00      0.3420E+17      0.3425E+14      0.6004E+08
  79.60          39.00      0.4557E+17      0.5396E+14      0.7099E+08
  80.60          40.00      0.6058E+17      0.8446E+14      0.8358E+08
  81.60          41.00      0.8036E+17      0.1314E+15      0.9800E+08
  82.60          42.00      0.1063E+18      0.2030E+15      0.1145E+09
  83.60          43.00      0.1404E+18      0.3120E+15      0.1332E+09
  84.60          44.00      0.1851E+18      0.4766E+15      0.1544E+09
  85.60          45.00      0.2444E+18      0.7240E+15      0.1776E+09
  86.60          46.00      0.3210E+18      0.1094E+16      0.2043E+09
  87.60          47.00      0.4208E+18      0.1644E+16      0.2343E+09
  88.60          48.00      0.5505E+18      0.2459E+16      0.2678E+09
  89.60          49.00      0.7188E+18      0.3659E+16      0.3052E+09
  90.60          50.00      0.9365E+18      0.5419E+16      0.3469E+09
  91.60          51.00      0.1218E+19      0.7988E+16      0.3932E+09
  92.60          52.00      0.1581E+19      0.1172E+17      0.4445E+09
  93.60          53.00      0.2048E+19      0.1712E+17      0.5012E+09
  94.60          54.00      0.2649E+19      0.2491E+17      0.5637E+09
  95.60          55.00      0.3419E+19      0.3608E+17      0.6325E+09
  96.60          56.00      0.4406E+19      0.5205E+17      0.7082E+09
  97.60          57.00      0.5667E+19      0.7479E+17      0.7912E+09
  98.60          58.00      0.7277E+19      0.1071E+18      0.8820E+09
  99.60          59.00      0.9328E+19      0.1527E+18      0.9811E+09
 100.60          60.00      0.1194E+20      0.2169E+18      0.1089E+10
 101.60          61.00      0.1525E+20      0.3070E+18      0.1207E+10
 102.60          62.00      0.1945E+20      0.4331E+18      0.1335E+10
 103.60          63.00      0.2477E+20      0.6089E+18      0.1474E+10
 104.60          64.00      0.3150E+20      0.8530E+18      0.1624E+10
 105.60          65.00      0.3998E+20      0.1191E+19      0.1786E+10
 106.60          66.00      0.5068E+20      0.1658E+19      0.1962E+10
 107.60          67.00      0.6414E+20      0.2301E+19      0.2151E+10
 108.60          68.00      0.8105E+20      0.3183E+19      0.2355E+10
```

```
109.60          69.00     0.1023E+21     0.4391E+19      0.2574E+10
110.60          70.00     0.1289E+21     0.6038E+19      0.2809E+10
111.60          71.00     0.1621E+21     0.8279E+19      0.3062E+10
112.60          72.00     0.2037E+21     0.1132E+20      0.3332E+10
113.60          73.00     0.2556E+21     0.1544E+20      0.3621E+10
114.60          74.00     0.3202E+21     0.2099E+20      0.3930E+10
115.60          75.00     0.4007E+21     0.2847E+20      0.4260E+10
116.60          76.00     0.5006E+21     0.3851E+20      0.4612E+10
117.60          77.00     0.6248E+21     0.5196E+20      0.4986E+10
118.60          78.00     0.7786E+21     0.6994E+20      0.5385E+10
119.60          79.00     0.9691E+21     0.9389E+20      0.5808E+10
120.60          80.00     0.1205E+22     0.1258E+21      0.6258E+10
121.60          81.00     0.1496E+22     0.1680E+21      0.6735E+10
122.60          82.00     0.1855E+22     0.2238E+21      0.7234E+10
123.60          83.00     0.2297E+22     0.2980E+21      0.7778E+10
124.60          84.00     0.2841E+22     0.3959E+21      0.8355E+10
125.60          85.00     0.3510E+22     0.5249E+21      0.8964E+10
126.60          86.00     0.4332E+22     0.6942E+21      0.9608E+10
127.60          87.00     0.5339E+22     0.9162E+21      0.1029E+11
128.60          88.00     0.6574E+22     0.1207E+22      0.1100E+11
129.60          89.00     0.8084E+22     0.1586E+22      0.1176E+11
130.60          90.00     0.9931E+22     0.2080E+22      0.1255E+11
131.60          91.00     0.1218E+23     0.2721E+22      0.1339E+11
132.60          92.00     0.1493E+23     0.3555E+22      0.1427E+11
133.60          93.00     0.1829E+23     0.4634E+22      0.1519E+11
134.60          94.00     0.2236E+23     0.6029E+22      0.1616E+11
135.60          95.00     0.2732E+23     0.7828E+22      0.1718E+11
136.60          96.00     0.3335E+23     0.1015E+23      0.1824E+11
137.60          97.00     0.4066E+23     0.1313E+23      0.1936E+11
138.60          98.00     0.4952E+23     0.1695E+23      0.2052E+11
139.60          99.00     0.6024E+23     0.2185E+23      0.2175E+11
```

```
1,3-DIMETHYLBICYCLOBUTANE TO 2,3-DIMETHYL 1,3-BUTADIENE
NO ROTORS, NO OVERALL ROTATION

EZERO =  43.30 KCAL/MOLE      ESTAR =  43.30 KCAL/MOLE      EINC =  1.00 KCAL/MOLE      REACTION PATH DEGENERACY = 2.0

 100  RATE CONSTANTS TO BE CALCULATED

NUMBER OF OSCILLATORS IN MOLECULE   NUMBER OF INTERNAL ROTORS IN MOLECULE

                 42                           0

FREQUENCIES IN MOLECULE

      2925.0      2896.0      1264.0      1242.0      1152.0       658.0       422.0      1140.0
      1141.0       650.0      1268.0      1113.0       773.0      3044.0      2971.0      1456.0
       940.0       881.0      2962.0      2962.0      2948.0      2935.0      2918.0      2885.0
      1475.0      1462.0      1435.0      1435.0      1398.0      1380.0      1098.0      1070.0
      1035.0       970.0       877.0       767.0       488.0       413.0       305.0       258.0
       163.5       163.5


EXTERNAL ROTATIONS TREATED AS INACTIVE


*****STRUCTURE OF THE CRITICAL CONFIGURATION IS SPECIFIED*****

NUMBER OF OSCILLATORS IN COMPLEX   NUMBER OF INTERNAL ROTORS IN COMPLEX

                 41                           0

FREQUENCIES IN COMPLEX

      2925.0      2896.0      1264.0      1242.0       575.0       658.0       422.0      1140.0
       650.0      1268.0      1113.0       400.0      3044.0      2971.0      1456.0       940.0
       421.0      2962.0      2962.0      2948.0      2935.0      2918.0      2885.0      1475.0
      1462.0      1435.0      1435.0      1398.0      1380.0      1098.0      1070.0      1035.0
       970.0       877.0       767.0       488.0       413.0       305.0       258.0       163.5
       163.5


SUM CAN NOT BE CALCULATED.  EDAG = ,   0.00 KCAL/MOLE
AN ATTEMPT WILL BE MADE TO CALCULATE A RATE CONSTANT AT     43.30 +  1.00 KCAL/MOLE


XXXXXXXXXXXXXXXXXXXXXXXXXXXXXXXXXXXXXXXXXXXXXXXXXXXXXXXXXXXXXXXXXXXXXXXXXXXXXXXXXXXXXXXXXXXXXXXXXXXXXXX

RATE CONSTANTS CALCULATED USING THESE OPTIONS:      KROT = -1  NANH = 0  NCRIT = 0  JDEN =  0  JSUM =  0


  ESTAR             EDAG             HARMONIC          HARMONIC             HARMONIC

 KCAL/MOLE        KCAL/MOLE          DENSITY             SUM             RATE CONSTANT

  44.30              1.00        0.2688E+12       0.2253E+02        0.5025E+01
  45.30              2.00        0.4024E+12       0.1400E+03        0.2086E+02
```

```
  46.30        3.00     0.5992E+12     0.6429E+03      0.6432E+02
  47.30        4.00     0.8881E+12     0.2483E+04      0.1676E+03
  48.30        5.00     0.1310E+13     0.8511E+04      0.3895E+03
  49.30        6.00     0.1923E+13     0.2664E+05      0.8306E+03
  50.30        7.00     0.2811E+13     0.7759E+05      0.1655E+04
  51.30        8.00     0.4091E+13     0.2128E+06      0.3118E+04
  52.30        9.00     0.5929E+13     0.5546E+06      0.5608E+04
  53.30       10.00     0.8557E+13     0.1383E+07      0.9691E+04
  54.30       11.00     0.1230E+14     0.3319E+07      0.1618E+05
  55.30       12.00     0.1761E+14     0.7692E+07      0.2618E+05
  56.30       13.00     0.2512E+14     0.1729E+08      0.4125E+05
  57.30       14.00     0.3570E+14     0.3777E+08      0.6343E+05
  58.30       15.00     0.5054E+14     0.8045E+08      0.9543E+05
  59.30       16.00     0.7130E+14     0.1674E+09      0.1407E+06
  60.30       17.00     0.1002E+15     0.3408E+09      0.2038E+06
  61.30       18.00     0.1405E+15     0.6803E+09      0.2903E+06
  62.30       19.00     0.1962E+15     0.1333E+10      0.4073E+06
  63.30       20.00     0.2731E+15     0.2566E+10      0.5634E+06
  64.30       21.00     0.3789E+15     0.4862E+10      0.7692E+06
  65.30       22.00     0.5242E+15     0.9072E+10      0.1038E+07
  66.30       23.00     0.7230E+15     0.1669E+11      0.1384E+07
  67.30       24.00     0.9942E+15     0.3028E+11      0.1826E+07
  68.30       25.00     0.1363E+16     0.5426E+11      0.2386E+07
  69.30       26.00     0.1864E+16     0.9605E+11      0.3090E+07
  70.30       27.00     0.2541E+16     0.1681E+12      0.3965E+07
  71.30       28.00     0.3455E+16     0.2909E+12      0.5048E+07
  72.30       29.00     0.4686E+16     0.4983E+12      0.6376E+07
  73.30       30.00     0.6337E+16     0.8452E+12      0.7996E+07
  74.30       31.00     0.8549E+16     0.1420E+13      0.9957E+07
  75.30       32.00     0.1150E+17     0.2364E+13      0.1232E+08
  76.30       33.00     0.1544E+17     0.3902E+13      0.1515E+08
  77.30       34.00     0.2068E+17     0.6386E+13      0.1851E+08
  78.30       35.00     0.2762E+17     0.1037E+14      0.2250E+08
  79.30       36.00     0.3682E+17     0.1671E+14      0.2721E+08
  80.30       37.00     0.4895E+17     0.2672E+14      0.3272E+08
  81.30       38.00     0.6494E+17     0.4243E+14      0.3917E+08
  82.30       39.00     0.8597E+17     0.6692E+14      0.4667E+08
  83.30       40.00     0.1136E+18     0.1048E+15      0.5535E+08
  84.30       41.00     0.1497E+18     0.1632E+15      0.6537E+08
  85.30       42.00     0.1969E+18     0.2525E+15      0.7689E+08
  86.30       43.00     0.2595E+18     0.3883E+15      0.8969E+08
  87.30       44.00     0.3403E+18     0.5937E+15      0.1046E+09
  88.30       45.00     0.4453E+18     0.9027E+15      0.1215E+09
  89.30       46.00     0.5815E+18     0.1365E+16      0.1407E+09
  90.30       47.00     0.7579E+18     0.2053E+16      0.1624E+09
  91.30       48.00     0.9859E+18     0.3073E+16      0.1869E+09
  92.30       49.00     0.1280E+19     0.4577E+16      0.2144E+09
  93.30       50.00     0.1658E+19     0.6783E+16      0.2452E+09
  94.30       51.00     0.2145E+19     0.1000E+17      0.2796E+09
  95.30       52.00     0.2770E+19     0.1469E+17      0.3180E+09
  96.30       53.00     0.3569E+19     0.2148E+17      0.3607E+09
  97.30       54.00     0.4592E+19     0.3126E+17      0.4082E+09
  98.30       55.00     0.5897E+19     0.4532E+17      0.4607E+09
  99.30       56.00     0.7560E+19     0.6542E+17      0.5187E+09
 100.30       57.00     0.9676E+19     0.9406E+17      0.5828E+09
 101.30       58.00     0.1236E+20     0.1347E+18      0.6532E+09
 102.30       59.00     0.1577E+20     0.1922E+18      0.7306E+09
 103.30       60.00     0.2009E+20     0.2733E+18      0.8154E+09
 104.30       61.00     0.2555E+20     0.3870E+18      0.9083E+09
 105.30       62.00     0.3243E+20     0.5463E+18      0.1010E+10
 106.30       63.00     0.4112E+20     0.7684E+18      0.1120E+10
 107.30       64.00     0.5204E+20     0.1077E+19      0.1241E+10
 108.30       65.00     0.6578E+20     0.1505E+19      0.1372E+10
 109.30       66.00     0.8301E+20     0.2096E+19      0.1514E+10
 110.30       67.00     0.1046E+21     0.2910E+19      0.1668E+10
 111.30       68.00     0.1316E+21     0.4028E+19      0.1835E+10
```

```
112.30          69.00     0.1654E+21     0.5558E+19     0.2015E+10
113.30          70.00     0.2075E+21     0.7647E+19     0.2209E+10
114.30          71.00     0.2601E+21     0.1049E+20     0.2419E+10
115.30          72.00     0.3255E+21     0.1435E+20     0.2644E+10
116.30          73.00     0.4067E+21     0.1958E+20     0.2886E+10
117.30          74.00     0.5076E+21     0.2664E+20     0.3146E+10
118.30          75.00     0.6327E+21     0.3614E+20     0.3425E+10
119.30          76.00     0.7876E+21     0.4891E+20     0.3724E+10
120.30          77.00     0.9792E+21     0.6603E+20     0.4043E+10
121.30          78.00     0.1216E+22     0.8890E+20     0.4384E+10
122.30          79.00     0.1508E+22     0.1194E+21     0.4748E+10
123.30          80.00     0.1867E+22     0.1600E+21     0.5136E+10
124.30          81.00     0.2310E+22     0.2139E+21     0.5550E+10
125.30          82.00     0.2854E+22     0.2850E+21     0.5986E+10
126.30          83.00     0.3523E+22     0.3797E+21     0.6461E+10
127.30          84.00     0.4343E+22     0.5047E+21     0.6967E+10
128.30          85.00     0.5347E+22     0.6693E+21     0.7504E+10
129.30          86.00     0.6577E+22     0.8855E+21     0.8072E+10
130.30          87.00     0.8079E+22     0.1169E+22     0.8676E+10
131.30          88.00     0.9914E+22     0.1540E+22     0.9313E+10
132.30          89.00     0.1215E+23     0.2025E+22     0.9988E+10
133.30          90.00     0.1488E+23     0.2656E+22     0.1070E+11
134.30          91.00     0.1820E+23     0.3478E+22     0.1145E+11
135.30          92.00     0.2224E+23     0.4544E+22     0.1225E+11
136.30          93.00     0.2714E+23     0.5925E+22     0.1309E+11
137.30          94.00     0.3309E+23     0.7711E+22     0.1397E+11
138.30          95.00     0.4031E+23     0.1002E+23     0.1490E+11
139.30          96.00     0.4905E+23     0.1299E+23     0.1587E+11
140.30          97.00     0.5963E+23     0.1681E+23     0.1690E+11
141.30          98.00     0.7241E+23     0.2171E+23     0.1798E+11
142.30          99.00     0.8784E+23     0.2800E+23     0.1911E+11
```

CHAPTER III

1,3-DIALKYL-1,3-CYCLOBUTANEDIYLS

Direct observation of biradicals has developed as an area of active research, and over the years several delocalized biradicals have been reported.[1] However, the only example of a localized biradical remained the landmark result of Buchwalter and Closs. In 1975, they photolyzed azoalkane **10** in a cyclohexane matrix at cryogenic temperatures and observed the ESR signal for 1,3-cyclopentanediyl (**11**). The zero-field splitting ($|D/hc| = 0.084\ \mathrm{cm}^{-1}$) was fully consistent with this structure and simple, semi-empirical calculations qualitatively reproduced it.[2] They also found that the triplet signal decayed when irradiation was discontinued. Thus, a Curie plot (signal intensity vs. temperature) could not be used to obtain the sign and magnitude of the S–T gap. Nevertheless, the signal can be observed at temperatures as low as 1.3 K where thermal population of the triplet state is highly unlikely, strongly suggesting that the triplet must be the ground state. This conclusion was also supported by their CIDNP studies at room temperature.

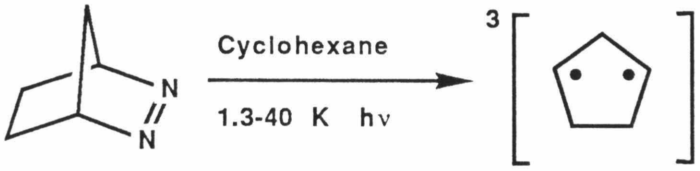

10 **11**

In an attempt to extend the Closs experiment, Chang and Dougherty synthesized 2,3-diazabicyclo[2.1.1]hex-2-ene (**14**).[3] However, when **14** was photolyzed in the cavity of an ESR spectrometer at 4 K, no signal was observed for triplet 1,3-cyclobutanediyl (**13**).[4] Based upon the room temperature chemistry of **14**, two possible explanations for the failure of the ESR experiment were suggested. First, biradical **13** might be kinetically unstable and readily convert to bicyclobutane. Second, **14** undergoes photochemistry which is quite different from most azoalkanes. In general, photochemical excitation of azoalkanes produces the singlet excited state from which intersystem crossing (isc) to the triplet excited state can occur in competition with (a) decay to the ground state and/or (b) a chemical reaction. Formation of a triplet biradical is considered to occur by nitrogen loss from the triplet excited azoalkane.

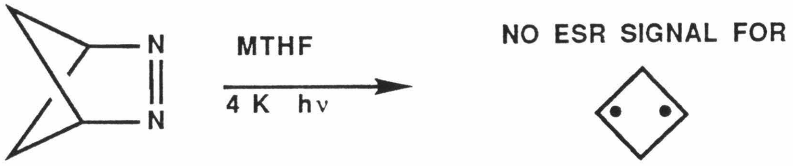

14 **13**

Unfortunately, the excited triplet state of **14** undergoes β C–C bond cleavage instead of nitrogen loss and a substantial amount of nitrogen-retained product (**15**) is formed.[4] Although this mode of reactivity was unusual, it was not unprecedented. Turro[5] had previously reported that sensitized photolysis of the strained azoalkane **52** leads to C–C bond cleavage.

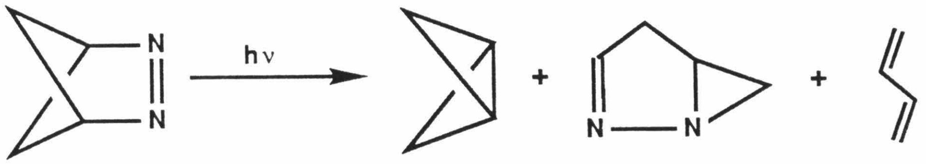

14 **30** **15**

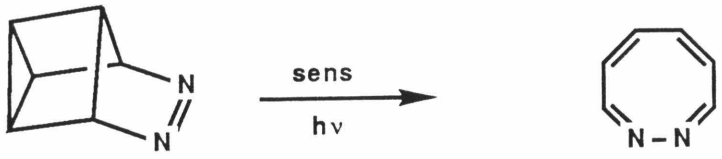

52

We have now found that this type of β C–C bond cleavage is general for 2,3-diazabicyclo[2.1.1]hex-2-enes. For example, either direct or sensitized photolysis of **16** in benzene at room temperature produces a mixture of 1,3-dimethylbicyclobutane (**31**) and 3,5-dimethyl-1,2-diazabicyclo[3.1.0]hex-2-ene **53**[6] in a ratio which is strongly dependent upon the spin multiplicity (Table V).

16 **31** **53**

Surprisingly, however, photolysis of **16** in an MTHF matrix at 4 K does produce an ESR signal for triplet biradical **20** (see below). Since **14** and **16** show very similar photochemical behavior, detection of **20** and failure to detect **13** suggest that reactivity of the biradicals rather than precursor photochemistry is responsible for the observations. Thus, it seems that introduction of alkyl substituents at the potential radical centers increases the biradical lifetime.

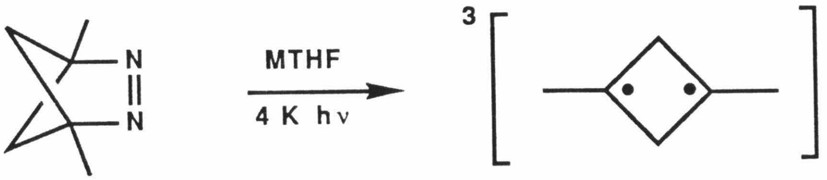

16 **20**

Hence, we also decided to synthesize the closely related compounds 1,4-

bis(trideuteriomethyl)-, 1,4-diethyl- and 1,4-dipropyl-2,3-diaza-bicyclo[2.1.1]hex-2-enes (**17**, **18**, and **19** respectively) and study their low-temperature photolyses in order to systematically investigate substituent effects on 1,3-cyclobutanediyls.

17 R = CD_3

18 R = C_2H5

19 R = *n*- C_3H_7

Synthesis

The first step in the synthesis of **18** and **19** (Scheme IV) involves the reduction of the ester functionalities in urazole **54**[7] (obtained by the photochemical addition of MTAD to 1,3-dicarbomethoxybicyclobutane[8]) to give the diol **55**. We originally used lithium borohydride for this purpose but now prefer the milder conditions employing sodium borohydride in methanol.[9] Treatment of the diol with mesyl chloride (to give dimesylate **56**) followed by reflux with sodium iodide in 2-butanone afforded the diiodide **57**. Lithium dimethylcopper was used to convert **57** to the diethyl urazole **58**.[10] Another route to **58** involved the oxidation of **55** in a two-step process[11,12] involving formation of the dipyruvate ester **59** followed by its photolysis to the dialdehyde **60**.[7] Treatment of **60** in situ with Wittig reagent followed by catalytic hydrogenation afforded **58**. The dipropyl urazole **61** was prepared similarly using the appropriate Wittig reagent. Finally, standard hydrolysis–oxidation (see Chapter II) of urazoles **58** and **61** afforded the azoalkanes **18** and **19**, respectively.

Synthesis of **17** (Scheme V) involved the reduction of **54** using sodium borodeuteride to the tetradeuteriodiol **62** followed by mesylation to **63**. Treat-

Table V. Product Yields[a] from Photolysis of **16** at Room Temperature

Conditions	**31**	**53**
Direct	88	12
Thioxanthone Sensitized	15	85

[a] As determined by ^{1}H NMR.

Scheme IV

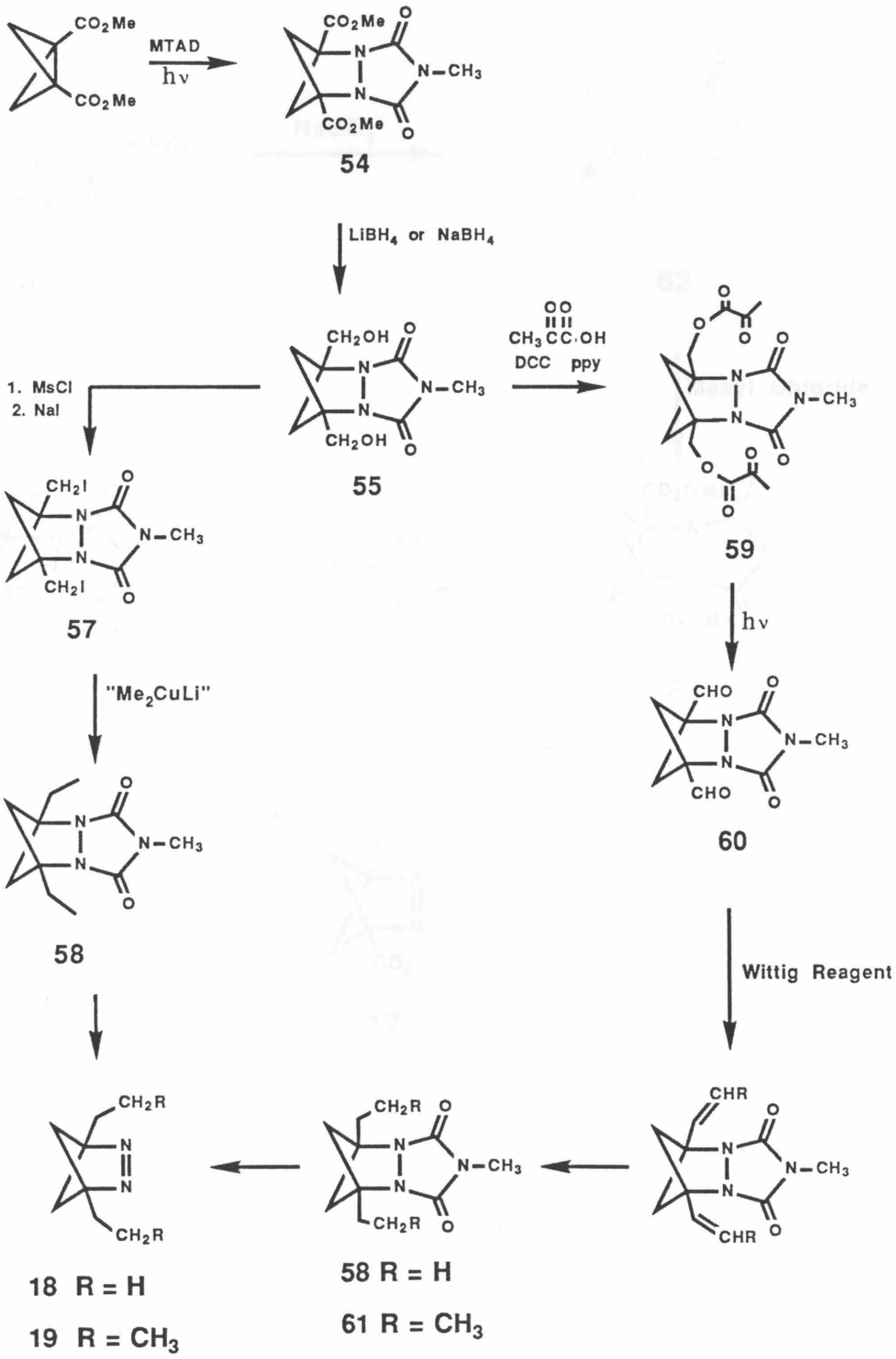

CO₂Me
CO₂Me
MTAD
hν
CO₂Me
N
N
N–CH₃
CO₂Me
O
O
54
LiBH₄ or NaBH₄
CH₂OH
CH₂OH
N–CH₃
55
1. MsCl
2. NaI
O O
CH₃CC·OH
DCC ppy
59
hν
CHO
CHO
60
CH₂I
CH₂I
57
"Me₂CuLi"
58
Wittig Reagent
CHR
CHR
CH₂R
CH₂R
58 R = H
61 R = CH₃
N
N
18 R = H
19 R = CH₃

Scheme V

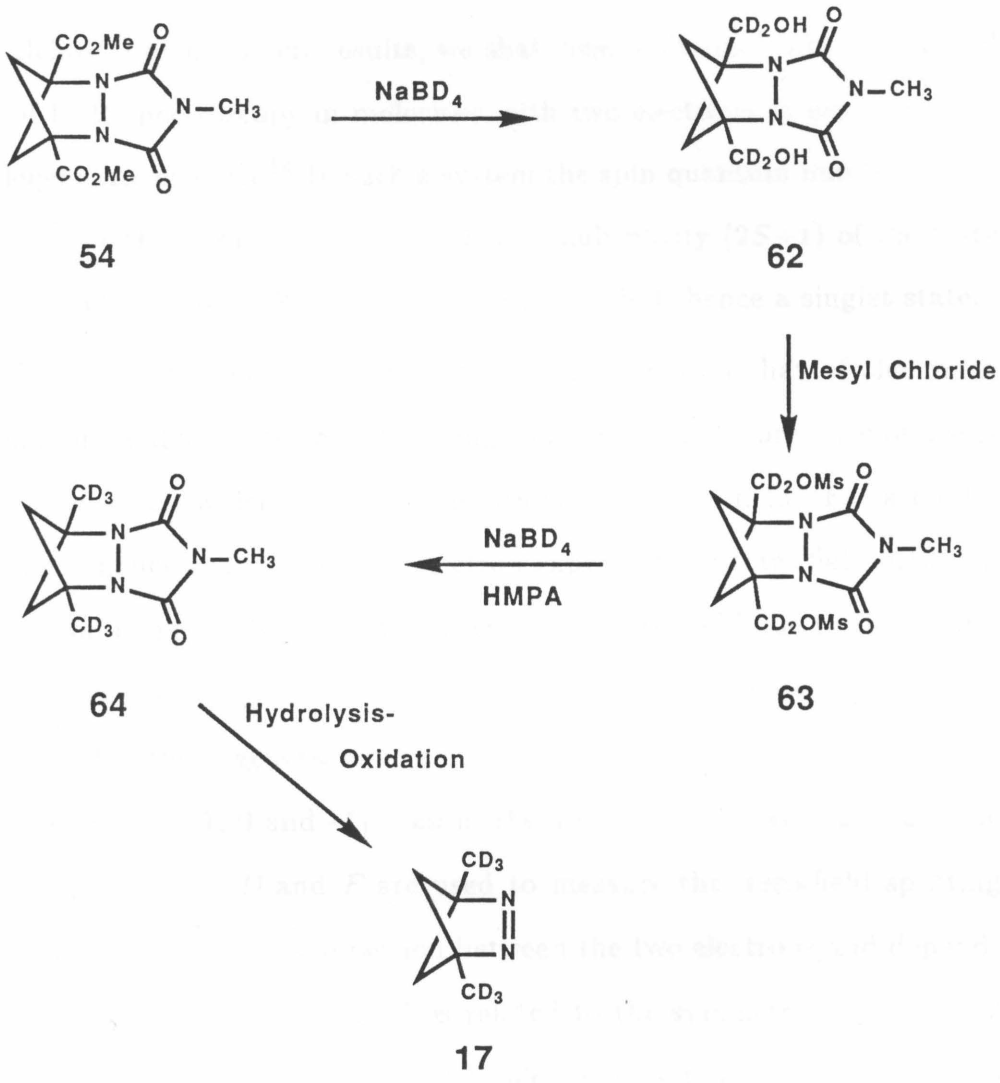
CO2Me
CO2Me
N-CH3
54
NaBD4
CD2OH
CD2OH
N-CH3
62
Mesyl Chloride
CD2OMs
CD2OMs
N-CH3
63
NaBD4
HMPA
CD3
CD3
N-CH3
64
Hydrolysis-
Oxidation
CD3
CD3
17

ment of **63** with sodium borodeuteride in hexamethylphosphoric triamide[13] then afforded the hexadeuterated dimethyl urazole **64** from which **17** can be easily obtained by hydrolysis–oxidation.

Electron Spin Resonance Studies

Before presenting our results, we shall briefly discuss some theoretical aspects of ESR spectroscopy in molecules with two electrons in degenerate or nearly degenerate orbitals.[14] In such a system the spin quantum number S can take values of either 1 or 0. When $S = 1$, the multiplicity $(2S+1)$ of the state is 3; hence a triplet state. When $S=0$, multiplicity is 1; hence a singlet state.

ESR spectroscopy of the triplet state differs from that of the much more common doublet state ($S = 1/2$, single electron) in the presence of a second nearby electron which creates an additional magnetic field. For a triplet molecule, resonance occurs when an electron experiences a total field made up of the external magnetic field and the internal magnetic field due to the second electron. Thus, the dipole-dipole interaction between the two electrons results in the removal of the degeneracy of the three triplet sublevels (with spin quantum number $m_s = +1$, 0 and –1) even in the absence of an external magnetic field. Two parameters D and E are used to measure this zero-field splitting (zfs). D is a measure of the interaction between the two electrons and depends upon the interelectronic distance. E is related to the symmetry properties of the magnetic system such that if the molecule has threefold or greater symmetry, E will be zero. If this system is placed in an external magnetic field the energy of the three magnetic sublevels changes as a function of H (e.g., Figure 7a). Clearly there are two transitions which are allowed by the selection rule $\Delta m_s = 1$. However, at low fields, this selection rule breaks down due to state-mixing and a third, "forbidden" $\Delta m_s = 2$ transition can be observed. Hence

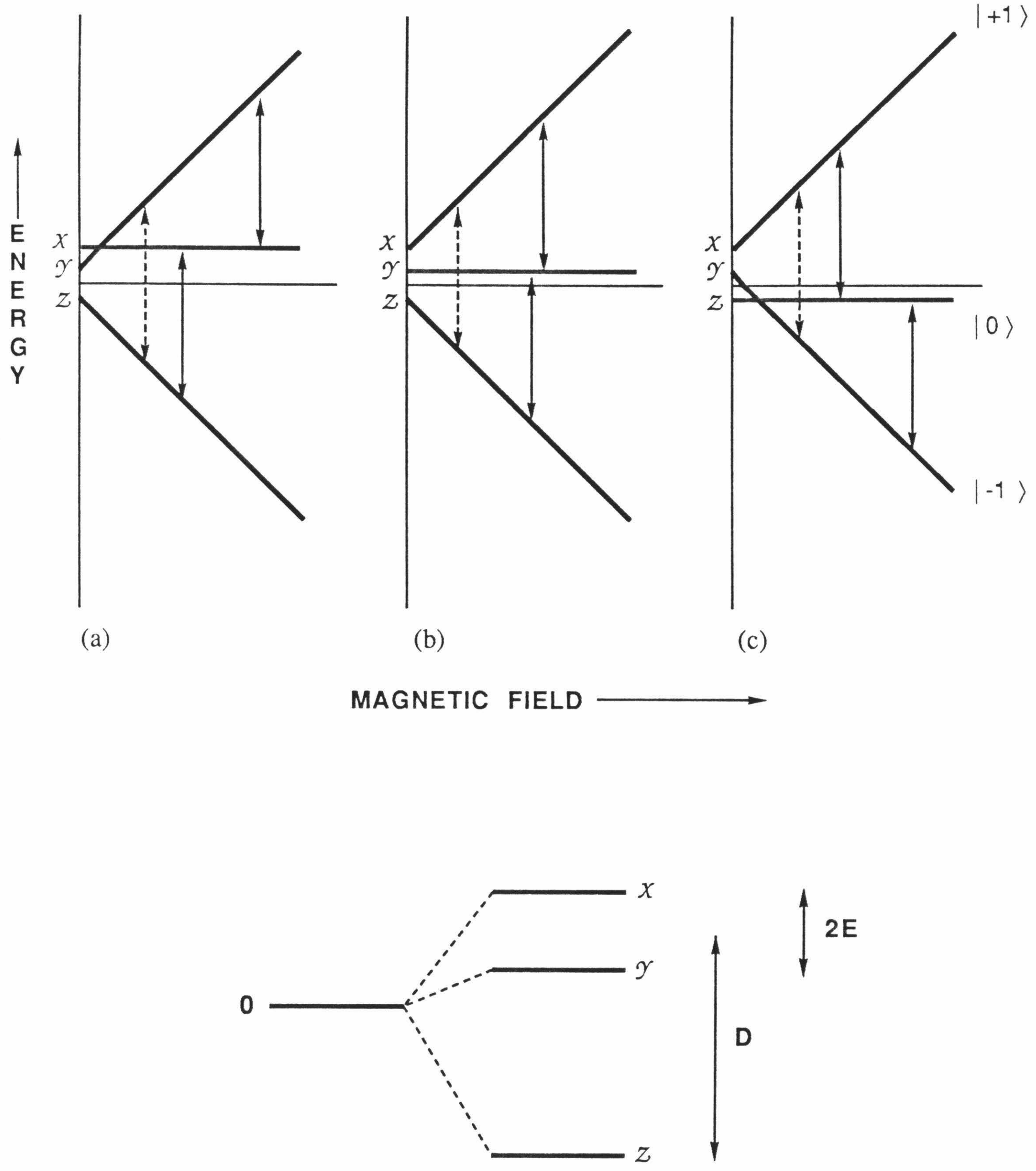

Figure 7. Triplet energy levels as a function of magnetic field strength. (a) $H \| X$, (b) $H \| Y$, and (c) $H \| Z$.

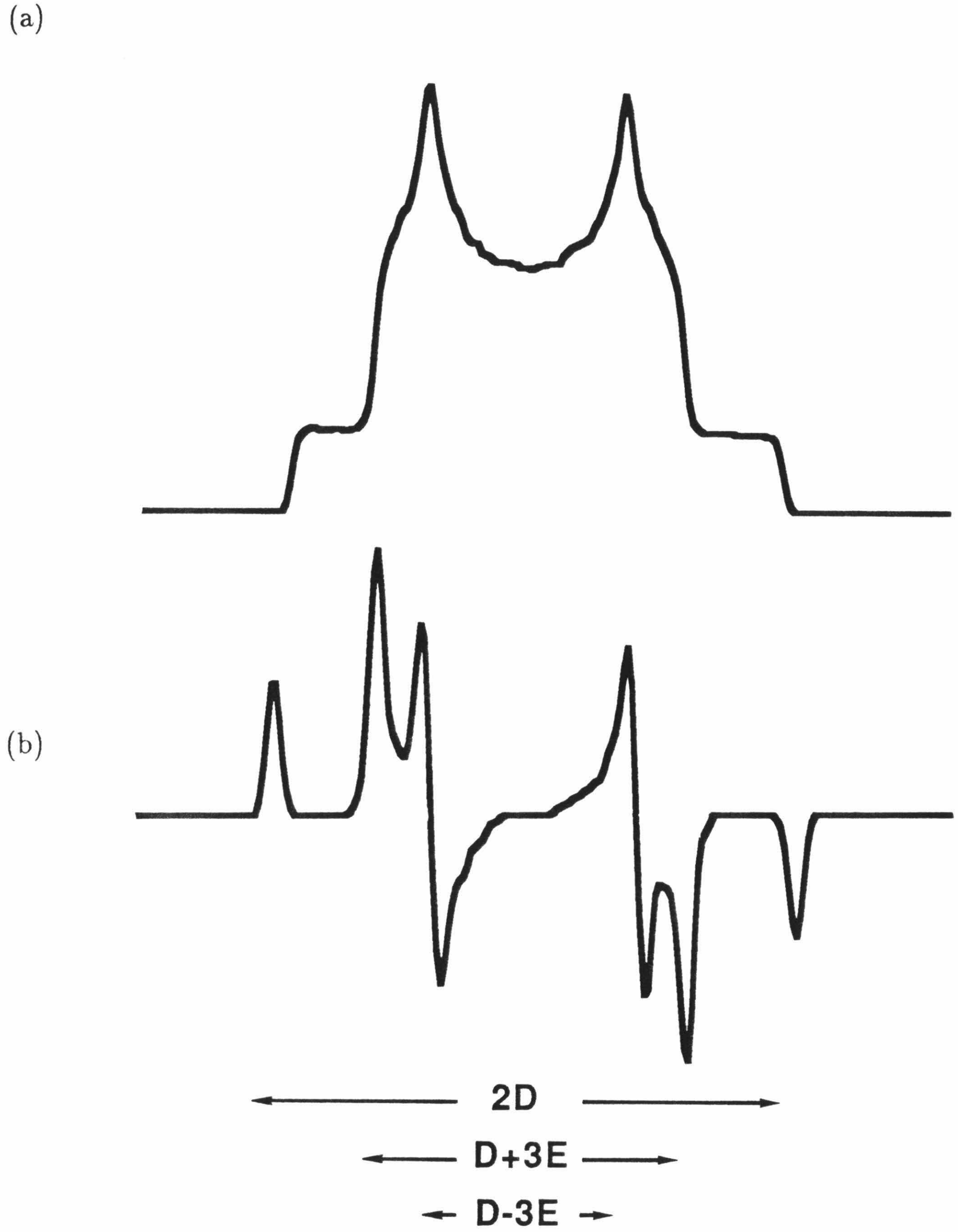

Figure 8. Theoretical (a) absorption and (b) derivative ESR spectra for a randomly oriented triplet system.

an oriented triplet spin system should show three transitions at field strengths governed by the zfs parameters. Since it is usually convenient to use randomly oriented samples, one observes a superposition of transitions obtained from all possible orientations of the molecule with respect to the magnetic field. The theoretical absorption and first-derivative spectra for such a system (see discussion below) are shown in Figure 8. Six peaks can be observed and their positions are related to D and E as indicated. In addition there can be up to four resonant fields at which the "forbidden" ($\Delta m_s = 2$) transitions are observed. As we shall see in the mathematical discussion later, their positions are given by H_{min} (corresponding to the lowest limit of absorption) and H_x, H_y, H_z (corresponding to the orientations in which the external magnetic field is along one of the three principal axes of the electron spin-spin coupling tensor). These four turning points are directly related to the zfs parameters and can be calculated quite easily.

The Spin Hamiltonian

When an electron ($S = 1/2$) is placed in an external magnetic field, the two magnetic sublevels ($m_s = 1/2, -1/2$) are split. This Zeeman interaction can be described by the Hamiltonian

$$\hat{\mathcal{H}}_{Zeeman} = g\beta H \cdot \hat{S}$$

where

g is the electronic g-factor

β is the Bohr magneton

H is the external magnetic field

$\hat{S}$ is the spin operator

The resulting energy separation between the two sublevels is

$$\Delta W = g\beta H$$

and the selection rule $\Delta m_s = 1$ allows one transition for this doublet state.

Mathematically, the difference between a doublet and a triplet state arises mainly from a dipole-dipole (or spin-spin) interaction between the two unpaired electrons. Generally, this is considered as a perturbation on the total Hamiltonian, and an additional term representing this dipolar interaction can be written as

$$\hat{\mathcal{H}}_{ss} = g^2\beta^2 \left[\frac{\hat{S}_1 \cdot \hat{S}_2}{r^3} - \frac{3(\hat{S}_1 \cdot \vec{r})(\hat{S}_2 \cdot \vec{r})}{r^5} \right]$$

where

$\vec{r}$ is the interelectronic vector

$\hat{S}_1, \hat{S}_2$ are spin operators such that the total spin operator is given by

$$\hat{S} = \hat{S}_1 + \hat{S}_2$$

Using Cartesian coordinates, $\hat{\mathcal{H}}_{ss}$ can be expressed as

$$\hat{\mathcal{H}}_{ss} = \frac{g^2\beta^2}{2r^5} \begin{pmatrix} \hat{S}_x & \hat{S}_y & \hat{S}_z \end{pmatrix} \begin{pmatrix} r^2 - 3x^2 & -3xy & -3xz \\ -3xy & r^2 - 3y^2 & -3yz \\ -3xz & -3yz & r^2 - 3z^2 \end{pmatrix} \begin{pmatrix} \hat{S}_x \\ \hat{S}_y \\ \hat{S}_z \end{pmatrix}$$

or

$$\hat{\mathcal{H}}_{ss} = \hat{S} \cdot D \cdot \hat{S}$$

D is a traceless second-rank tensor and can be diagonalized to give a set of principal axes X, Y, Z such that

$$\hat{\mathcal{H}}_{ss} = D_{XX}\hat{S}_x^2 + D_{YY}\hat{S}_y^2 + D_{ZZ}\hat{S}_z^2$$

Substituting $\mathcal{X} = -D_{XX}$, $\mathcal{Y} = -D_{YY}$ and $\mathcal{Z} = -D_{ZZ}$ we can write the total Hamiltonian as

$$\hat{\mathcal{H}} = g\beta H.\hat{S} - \mathcal{X}\hat{S}_x^2 - \mathcal{Y}\hat{S}_y^2 - \mathcal{Z}\hat{S}_z^2$$

Here $\mathcal{X}$, $\mathcal{Y}$, and $\mathcal{Z}$ represent the energies of this system in the absence of an external magnetic field and can be obtained by operating with the above Hamiltonian on the following triplet spin functions

$$|T_+\rangle = |\alpha_1\alpha_2\rangle$$

$$|T_0\rangle = \frac{1}{\sqrt{2}}|\alpha_1\beta_2 + \beta_1\alpha_2\rangle$$

$$|T_-\rangle = |\beta_1\beta_2\rangle$$

In matrix form the solution is given by

$$\hat{\mathcal{H}} = \begin{array}{c} \\ |T_+\rangle \\ |T_0\rangle \\ |T_-\rangle \end{array} \begin{array}{c} \begin{array}{ccc} |T_+\rangle & |T_0\rangle & |T_-\rangle \end{array} \\ \begin{pmatrix} g\beta H_Z - \frac{1}{2}(\mathcal{X} + \mathcal{Y}) - \mathcal{Z} & \frac{1}{\sqrt{2}}g\beta(H_X - iH_Y) & -\frac{1}{2}(\mathcal{X} - \mathcal{Y}) \\ \frac{1}{\sqrt{2}}g\beta(H_X + iH_Y) & -(\mathcal{X} + \mathcal{Y}) & \frac{1}{\sqrt{2}}g\beta(H_X - iH_Y) \\ -\frac{1}{2}(\mathcal{X} - \mathcal{Y}) & \frac{1}{\sqrt{2}}g\beta(H_X + iH_Y) & -g\beta H_Z - \frac{1}{2}(\mathcal{X} + \mathcal{Y}) - \mathcal{Z} \end{pmatrix} \end{array}$$

where H_X, H_Y, and H_Z, are components of H. We can easily solve for the energy levels when $H \| \mathrm{Z}$ ($\mathrm{H}_X = \mathrm{H}_Y = 0$). Using $\mathcal{X} + \mathcal{Y} + \mathcal{Z} = 0$, the secular determinant in this case becomes

$$\begin{vmatrix} g\beta H_Z - \frac{1}{2}\mathcal{Z} - W & 0 & -\frac{1}{2}(\mathcal{X} - \mathcal{Y}) \\ 0 & \mathcal{Z} - W & 0 \\ -\frac{1}{2}(\mathcal{X} - \mathcal{Y}) & 0 & -g\beta H_Z - \frac{1}{2}\mathcal{Z} - W \end{vmatrix} = 0$$

and the three solutions are given by

$$W_Z = \mathcal{Z}$$

and

$$W_{X,Y} = -\frac{\mathcal{Z}}{2} \pm \frac{1}{2}\sqrt{4g^2\beta^2H_Z^2 + (\mathcal{X} - \mathcal{Y})^2}$$

Thus, in zero magnetic field the triplet energy levels are given by

$$W_X = \mathcal{X}$$

$$W_Y = \mathcal{Y}$$

$$W_Z = \mathcal{Z}$$

Since $\mathcal{X} + \mathcal{Y} + \mathcal{Z} = 0$, we only need two independent parameters. These zfs parameters are usually denoted by D and E and are related to $\mathcal{X}$, $\mathcal{Y}$, and $\mathcal{Z}$ as follows

$$D = -\frac{3\mathcal{Z}}{2}$$

$$E = -\frac{1}{2}(\mathcal{X} - \mathcal{Y})$$

Thus, in terms of the zfs parameters the three triplet levels at zero field become

$$W_X = \frac{1}{3}D - E$$

$$W_Y = \frac{1}{3}D + E$$

$$W_Z = -\frac{2}{3}D$$

Figure 7 shows how these energy levels change as a function of the external magnetic field in the three cases $H\|$X, $H\|$Y, and $H\|$Z. Also shown in Figure 7 are the allowed $\Delta m_s = 1$ and the "forbidden" $\Delta m_s = 2$ transitions. The positions of these transitions can be calculated quite easily (see below) from the zfs parameters. Several theoretical methods have also been devised to obtain D and E.[15] For example, Higuchi[16] has shown that both D and E are related to the average distance between the two electrons as follows

$$D = \frac{3}{4} g^2 \beta^2 \langle \frac{r^2 - 3Z^2}{r^5} \rangle$$

$$E = \frac{3}{4} g^2 \beta^2 \langle \frac{Y^2 - X^2}{r^5} \rangle$$

where $\langle\ \rangle$ denotes an average over the electronic wave function and X, Y, and Z are the principal axes.

Another way to obtain a general solution for the Hamiltonian describing a triplet spin system has been developed by Kottis and Lefebvre.[17] Using the spin wavefunctions

$$T_X = \frac{1}{\sqrt{2}} |\beta_1 \beta_2 - \alpha_1 \alpha_2\rangle$$

$$T_Y = \frac{i}{\sqrt{2}} |\beta_1 \beta_2 + \alpha_1 \alpha_2\rangle$$

$$T_Z = \frac{1}{\sqrt{2}} |\alpha_1 \beta_2 - \beta_1 \alpha_2\rangle$$

they have shown that for each orientation of the molecule with respect to the external magnetic field, the secular equation giving its three energy levels is

$$W^3 - W\ [\ (g\beta H)^2 - (\mathcal{X}\mathcal{Y} + \mathcal{X}\mathcal{Z} + \mathcal{Y}\mathcal{Z})] +$$

$$(g\beta H)^2\ [\ \mathcal{X} \sin^2\theta \cos^2\phi + \mathcal{Y} \sin^2\theta \sin^2\phi + \mathcal{Z} \cos^2\theta] - \mathcal{X}\mathcal{Y}\mathcal{Z} = 0$$

Here θ and ϕ are the Euler angles as shown below for $H \| Z$. In order for two roots of this equation to be separated by $\delta = h\nu$ of microwave energy, the following condition must be satisfied:

$$\mathcal{X}\sin^2\theta\cos^2\phi + \mathcal{Y}\sin^2\theta\sin^2\phi + \mathcal{Z}\cos^2\theta = \frac{\mathcal{X}\mathcal{Y}\mathcal{Z}}{(g\beta H)^2}\pm$$

$$3^{-3/2}\left[\frac{(\delta^2+\mathcal{X}\mathcal{Y}+\mathcal{X}\mathcal{Z}+\mathcal{Y}\mathcal{Z})}{(g\beta H)^2}-1\right]\left[(2g\beta H)^2-\delta^2-4(\mathcal{X}\mathcal{Y}+\mathcal{X}\mathcal{Z}+\mathcal{Y}\mathcal{Z})\right]^{1/2}$$

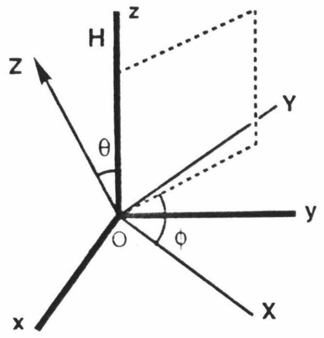

If we denote this as

$$f(\theta,\phi) = F(H,\delta)$$

the resonance field for fixed δ and a given orientation can be represented graphically as in Figure 9. Here the function $F(H,\delta)$ is plotted with H as the variable. If a line is drawn parallel to the H axis at an energy value of $f(\theta,\phi)$, the abscissas of intersection give the resonance fields for that orientation. Since $f(\frac{\pi}{2},0) = \mathcal{X}$, $f(\frac{\pi}{2},\frac{\pi}{2}) = \mathcal{Y}$, and $f(0,0) = \mathcal{Z}$, lines drawn for values $\mathcal{X}$, $\mathcal{Y}$, and $\mathcal{Z}$ will give all nine resonant fields. In addition there will be resonance at the value of H where $F(H,\delta)$ ceases to be a real function. This is given by

$$H_{min} = \frac{1}{2g\beta}\left[\delta^2+4(\mathcal{X}\mathcal{Y}+\mathcal{X}\mathcal{Z}+\mathcal{Y}\mathcal{Z})\right]^{1/2}$$

or

$$H_{min} = \frac{1}{2g\beta}\left[\delta^2-4\left(\frac{D^2}{3}+E^2\right)\right]^{1/2}$$

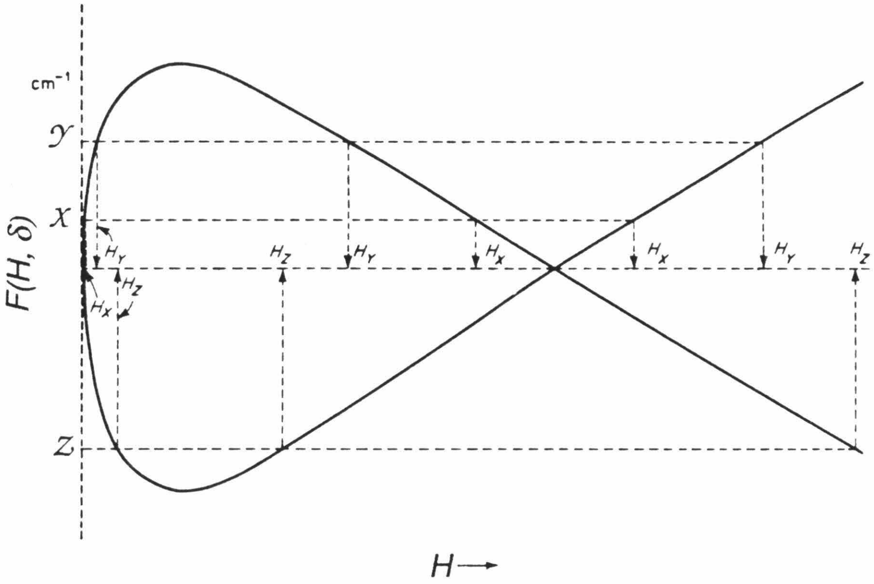

Figure 9. The value of the function $F(H, \delta)$ for a particular orientation plotted against magnetic field strength.

Simulation of Triplet ESR Spectra

The first step towards spectral simulation involves solving the equation $f(\theta,\phi) = F(H,\delta)$ for H. For convenience if we set

$$y = (g\beta H)^2$$

$$N = \mathcal{X}\sin^2\theta\cos^2\phi + \mathcal{Y}\sin^2\theta\sin^2\phi + \mathcal{Z}\cos^2\theta$$

$$O = \mathcal{X}\mathcal{Y}\mathcal{Z}$$

$$P1 = \mathcal{X}\mathcal{Y} + \mathcal{X}\mathcal{Z} + \mathcal{Y}\mathcal{Z}$$

we can write

$$N = \frac{O}{y} \pm 3^{-3/2}\left[\frac{\delta^2 + P1}{y} - 1\right]\left[4y - (\delta^2 + 4P1)\right]^{1/2}$$

which can be expanded to

$$\frac{27}{4}\left[N^2 + \frac{O^2}{y^2} - \frac{2NO}{y}\right]y^2 = (\delta^2 + P1)^2 y + y^3 - 2y^2(\delta^2 + P1) - \frac{(\delta^2 + 4P1)}{4}y^2$$

$$-\frac{(\delta^2 + P1)^2(\delta^2 + 4P1)}{4} + \frac{(\delta^2 + P1)(\delta^2 + 4P1)}{2}y$$

This equation is of the form

$$y^3 + Py^2 + Qy + R = 0$$

for

$$P = -\left[2(\delta^2 + P1) + \frac{(\delta^2 + 4P1)}{4}\right] - \frac{27}{4}N^2$$

$$Q = (\delta^2 + P1)^2 - \frac{(\delta^2 + P1)(\delta^2 + 4P1)}{2} + \frac{27}{2}NO$$

$$R = -\frac{1}{4}\left[(\delta^2 + P1)^2(\delta^2 + 4P1) + 27O^2 \right]$$

A change of variable will further reduce this equation to the form[18]

$$x^3 + Ax + B = 0$$

where

$$x = y + \frac{P}{3}$$

$$A = Q - \frac{P^2}{3}$$

$$B = \frac{2P^3}{27} - \frac{PQ}{3} + R$$

The three solutions to this equation are

$$x_1 = -2r\cos(\frac{\gamma}{3})$$

$$x_2 = 2r\cos(120^\circ + \frac{\gamma}{3})$$

$$x_3 = 2r\cos(240^\circ + \frac{\gamma}{3})$$

where

$$r = \sqrt{|A/3|}$$

$$\cos\gamma = \frac{B}{2r^3}$$

Thus, for each orientation, (i.e., each set of θ and ϕ) we will obtain three resonant fields. We have used a computer program[19] (Appendix B, TRIPLET1) to calculate the resonant fields for a large number of orientations. Assuming that each transition is equally probable, part two of the program (TRIPLET2) then adds up the number of times resonance occurs at a particular field strength to give intensities. In part three (TRIPLET3), a linewidth is assigned to each peak and an absroption spectrum is produced by smoothing the data. The derivative spectrum is calculated in part four (TRIPLET4).

We have also developed a program whereby isotropic hyperfine coupling (hfc) can be incorporated (Appendix B, HFC). Instead of introducing a new term into the Hamiltonian, we have taken the much easier route of splitting each resonance line into the appropriate number of lines with specified intensities (following Pascal's triangle). Addition of resonance intensities at various field strengths, addition of linewidth, and smoothing then gives an absorption spectrum in the usual way. Multiple coupling constants can be introduced by repeating the program HFC the required number of times. We must point out here that our approach does not in any way represent a rigorous treatment of hfc in rigid media. We have used it as a tool to aid in the reproduction of observed spectra by overlap of simple hfc patterns.

Results

Photolysis of frozen solutions of azoalkanes **16–19** in 2-methyltetrahydrofuran (MTHF) or acetone between 4–25 K produces ESR spectra for the corresponding triplet 1,3-dialkyl-1,3-cyclobutanediyls **20–23** (Figures 10–12).

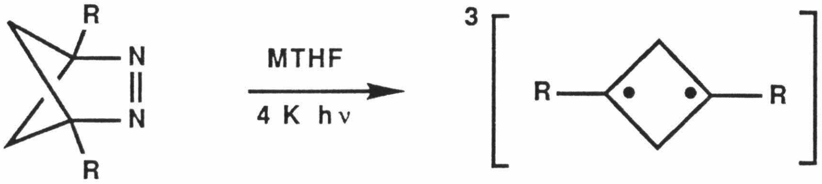

16	R = CH_3	**20**
17	R = CD_3	**21**
18	R = C_2H_5	**22**
19	R = n-C_3H_7	**23**

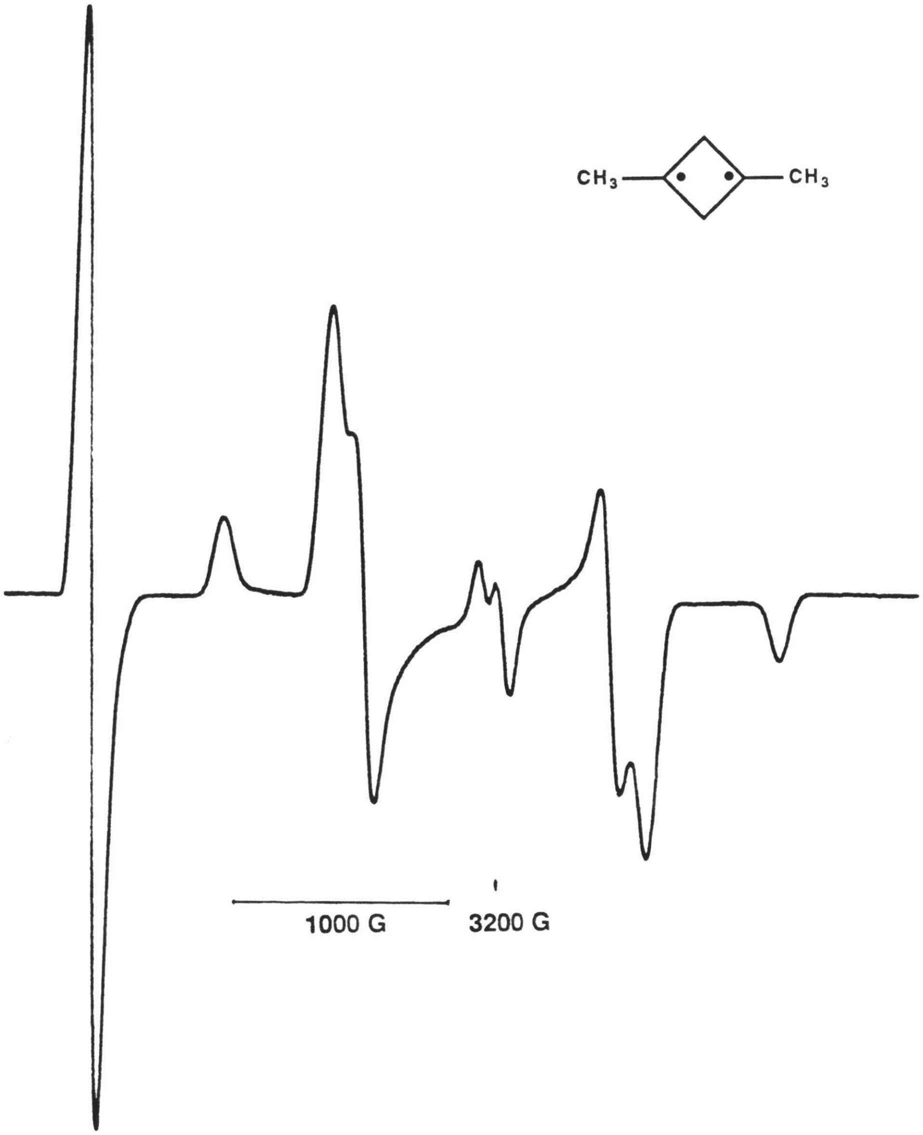

Figure 10. ESR spectrum for **20** obtained upon photolysis of an MTHF matrix containing **16** at 4 K.

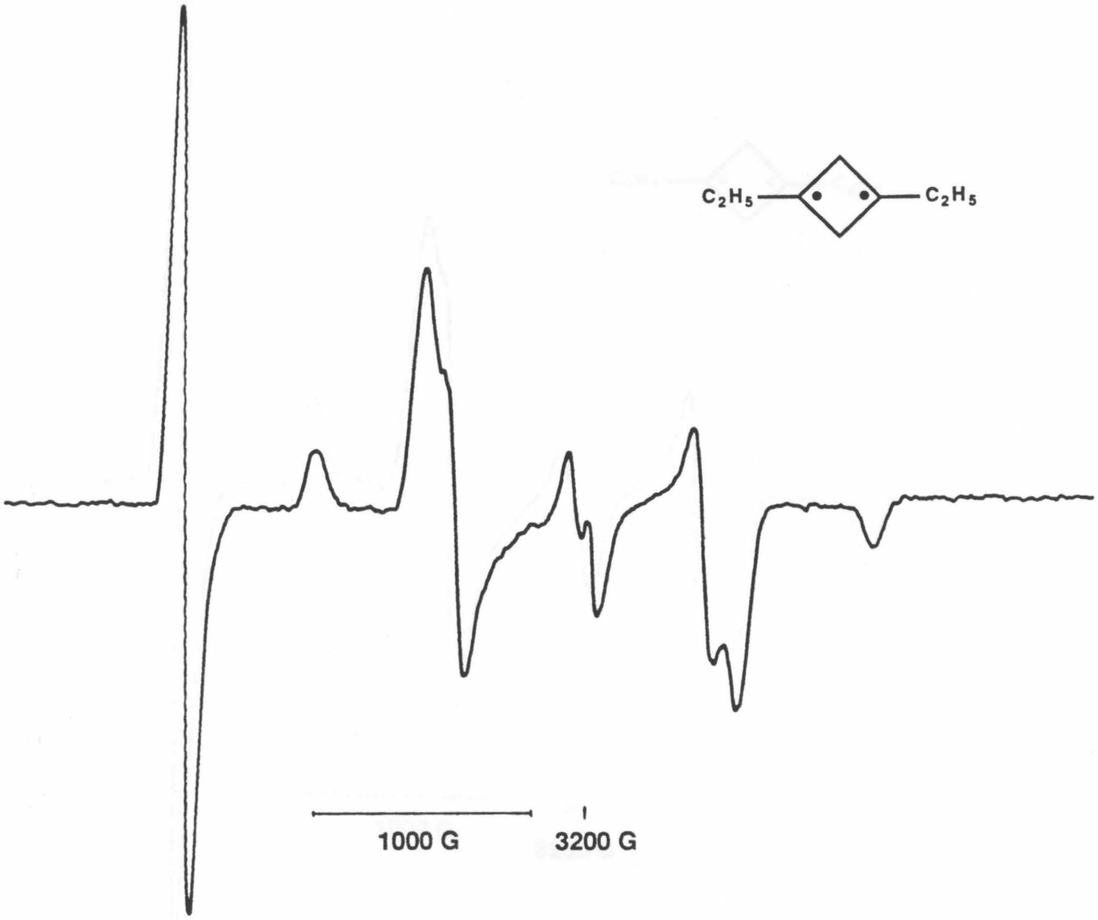

Figure 11. ESR spectrum for **22** obtained upon photolysis of an MTHF matrix containing **18** at 4 K.

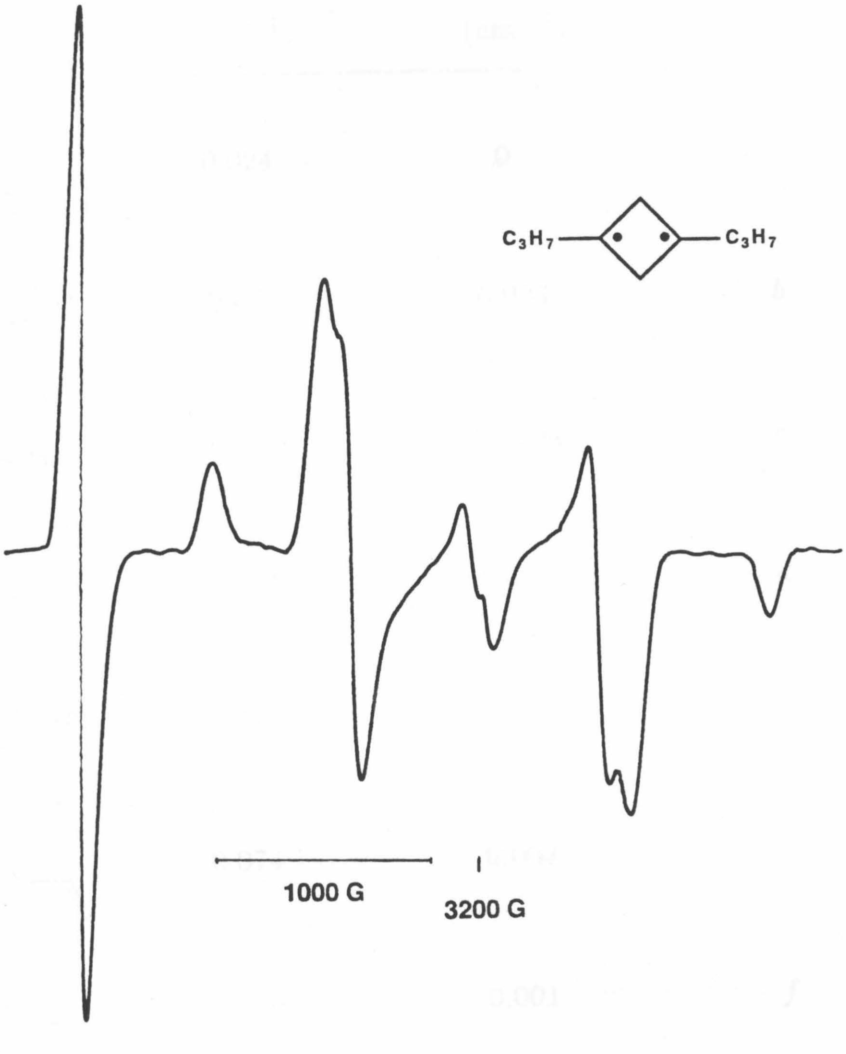

Figure 12. ESR spectrum for **23** obtained upon photolysis of an MTHF matrix containing **19** at 4 K.

Table VI. ZFS Parameters for Selected Biradicals

Biradical	$\lvert D/hc \rvert$ (cm^{-1})	$\lvert E/hc \rvert$ (cm^{-1})	Reference
	0.024	0	*a*
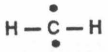	0.69	0.003	*b*
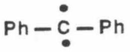	0.4055	0.0194	*c*
	0.084	0.002	*d*
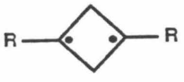 R = Me, Et, n-Pr	0.112	0.005	*e*
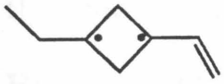	0.074	0.003	*f*
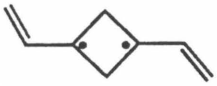	0.050	0.001	*f*
	0.060	0.002	*g*

---

[a] See ref. 1a. [b] Bernheim, R.A.; Bernard, H.W.; Wang, P.S.; Wood, L.S.; Skell, P.S. *J. Chem. Phys.* **1970**, *53*, 1280–1281. [c] Wasserman, E.; Trozzolo, A.M.; Yager, W.A.; Murray, R.W. *J. Chem. Phys.* **1964**, *40*, 2408–2410. [d] See ref. 2. [e] This work. [f] See ref. 7. [g] See ref. 21.

Each spectrum shows transitions in both the $\Delta m_s = 1$ and $\Delta m_s = 2$ regions and, as expected, they are all essentially identical ($|D/hc| = 0.112$ cm^{-1} and $|E/hc| = 0.005$ cm^{-1}). A comparison of zfs parameters with some other triplet biradicals is presented in Table VI. Clearly, the observed D-value is much too small for a carbene and much too large for a delocalized biradical. In comparison to **11** the observed D-value is larger, consistent with the expectation that the four-membered ring brings the radical centers closer together than the five-membered ring, resulting in greater interaction between the electrons. High-quality theoretical studies (valence double-ς basis set, ab-initio Hartree-Fock) have shown that the radical centers are 2.10 Å[7] and 2.37 Å[20] apart in **13** and **11** respectively. Using these distances and the point-charge approximation for integral evaluation, the D-values for the two biradicals have been calculated. When the calculated D-value for **11** is scaled to match the experimental value and the same scaling factor is applied to **20** a D-value of 0.114 cm^{-1} is obtained. This remarkable agreement between calculated and experimental values, indeed fortuitous to some extent, confirms our assignment of **20**–**23** as the carriers of the ESR signals.

Hyperfine Coupling

Careful examination of the $\Delta m_s = 2$ region of the ESR spectrum for **21** reveals that hyperfine coupling (hfc) is quite well resolved (Figure 13). Recently, $\Delta m_s = 2$ transitions in the ESR spectra for biradicals **65**[7], **66**[21], **3**[22], and **67**[23] have also been found to show considerable hfc (Figure 14). These results were quite surprising because even though hfc for a variety of triplet species in single crystals has been investigated,[24] very few previous observations of hfc in randomly oriented triplet samples have been made. The main reason for this seems to be the complex patterns obtained due to the inherent anisotropy of the spectra, especially in the $\Delta m_s = 1$ region. The $\Delta m_s = 2$ transition is much more isotropic but even for this region very few examples of resolved hfc structure can be found in the literature.[22,23,25]

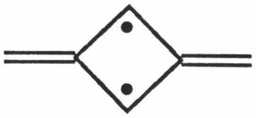

3

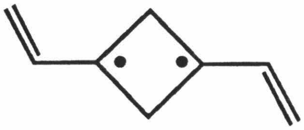

65

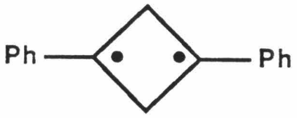

66

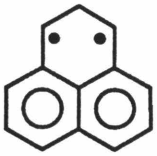

67

The observed spectra for **3** and **66** are simple seven- and five-line patterns and tentative assignments can be made. Thus, the six protons in **3** must have similar hfc constants of 6–7 G. Similarly in **66** the measured coupling of 22.5 G can be associated with the four equivalent ring protons. However, the spectra for **21** and **65** appear to be much more complex and visual analysis alone is not enough for assignment of coupling to various protons. Since **65** has four ring protons, four allylic protons, and two vinylic protons it is easy to understand why an intricate hfc pattern is observed. If the three sets exhibit different coupling, overlap of peaks can result in considerable complexity. But in **21** there is only one set of four equivalent protons and a simple five-line spectrum should result (the deuterium couplings are about six times smaller and should only contribute to line broadening).

A simple explanation for the complexity of the spectra for **21** becomes clear when the four turning points in the $\Delta m_s = 2$ region are calculated.[17] Table

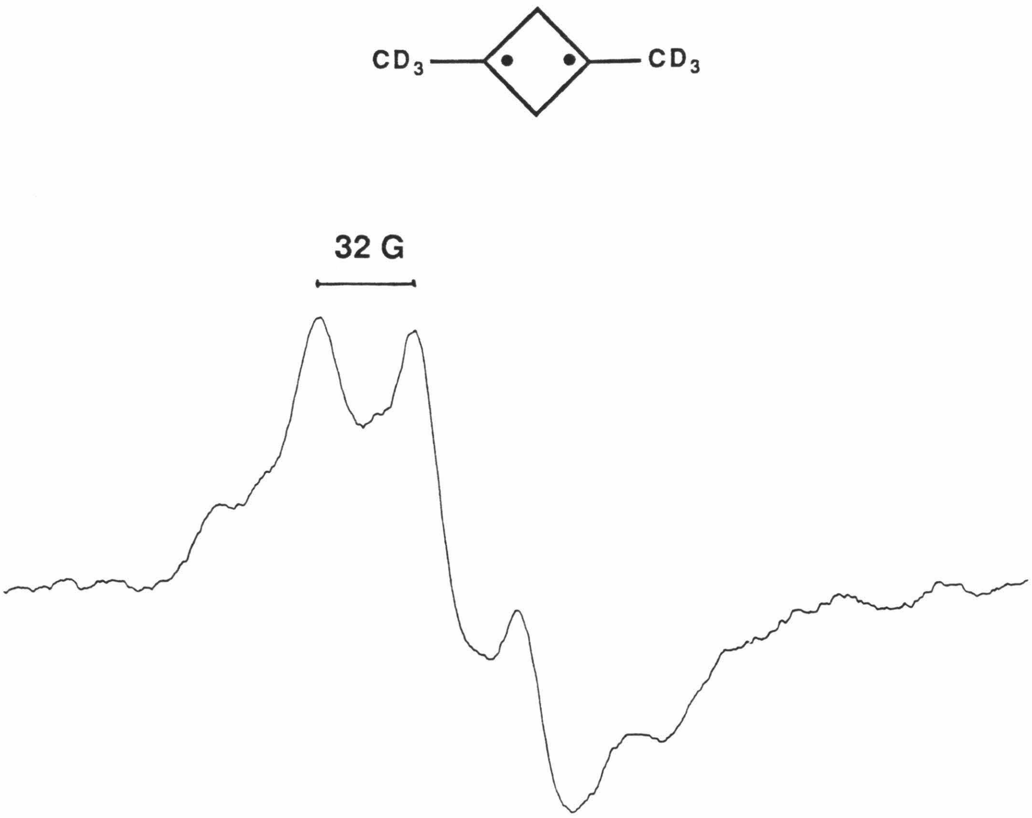

Figure 13. The $\Delta m_s = 2$ region of the ESR spectrum for **21**.

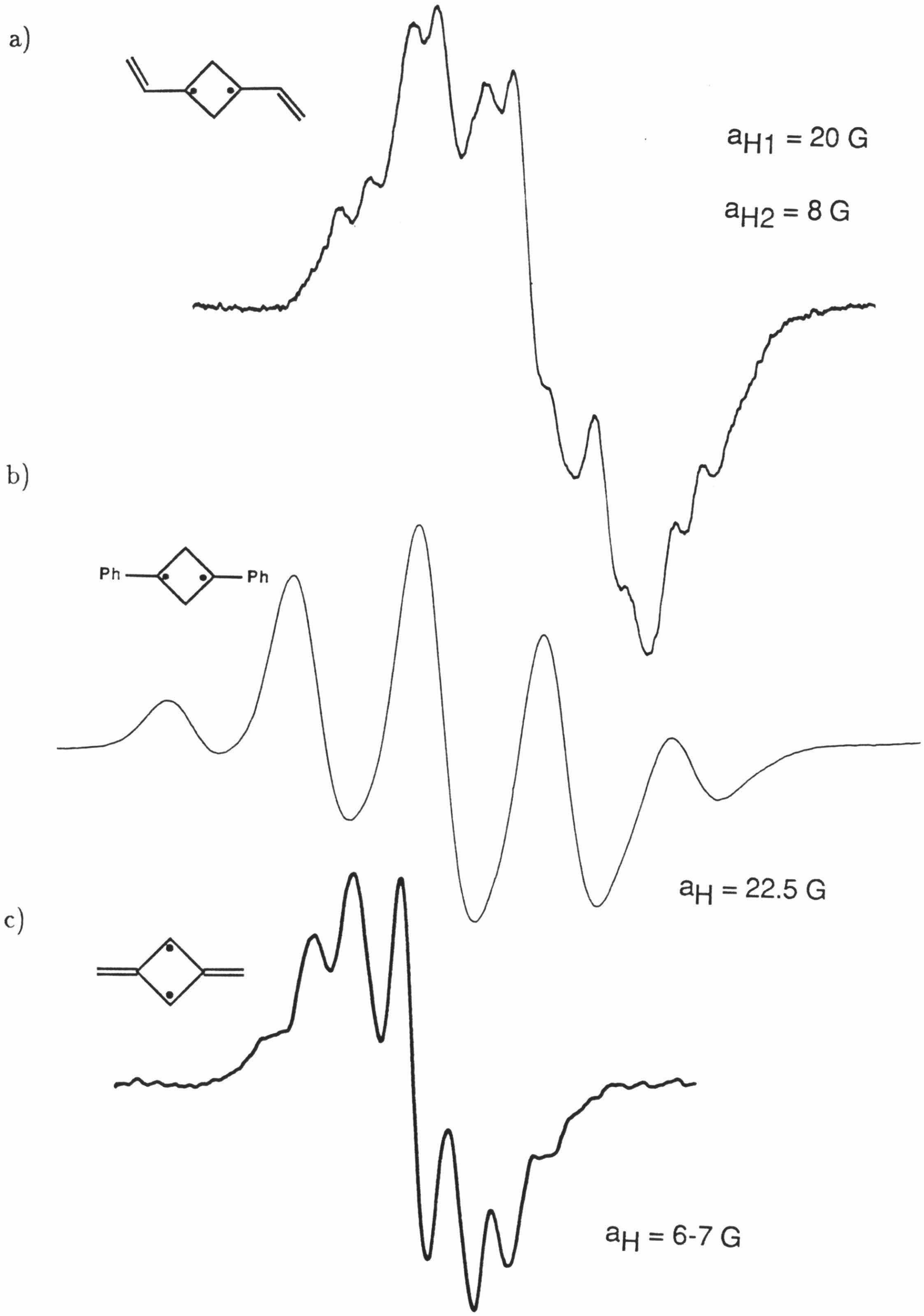

Figure 14. The $\Delta m_s = 2$ regions of the ESR spectra for (a) **65**, (b) **66**, and (c) **3**.

Table VII. Positions of Turning Points for ESR Spectra for Triplet Biradicals in the $\Delta m_s = 2$ Region[a]

Biradical	$\vert D/hc\vert$ (cm^{-1})	$\vert E/hc\vert$ (cm^{-1})	H_{min} (G)	H_x (G)	H_y (G)	H_z (G)
21	0.112	0.005	1502	1532	1553	1654
65	0.074	0.003	1590	1603	1611	1655
66	0.0598	0.0017	1613	1622	1626	1655
3	0.0205	0.0028	1650	1650	1652	1655

[a] For microwave frequency of 9.27 GHz.

VII shows the results of such a calculation for the biradicals under consideration. It must be kept in mind that the number of orientations for which resonance occurs at these fields decreases in going along the series H_{min}, H_x, H_y, H_z, and hence the largest contributions to the lineshape come from resonances at H_{min} and H_x. From Table VII it is clear that for biradicals with small D-values (e.g., **3** and **66**) the separation between H_{min} and H_x is small compared to spectral linewidth. On the other hand, in biradicals with large D-values (e.g., **21**) this separation is quite large, and as a result the lineshape for the $\Delta m_s = 2$ transition should be broad and unsymmetrical.

To support this analysis we have simulated the $\Delta m_s = 2$ spectra for the biradicals **21** and **65** using the computer programs described earlier (Figures 15a and b). Even though we have considered all transition probabilities to be unity and we have assumed isotropic hfc throughout the spectrum, the simulated spectra are in remarkable agreement with experiment, and we can assign hfc constants of 20 and 32 G for the ring protons in **65** and **21**, respectively. The four olefinic protons in **65** can also be assigned apparent hfc constants of 8 G. We must point out that hfc constants of less than 4–5 G can be easily lost in the linewidth and will not produce any visible splitting. We believe this explains why hfc due to the two vinylic protons in **65** cannot be discerned.

Our work represents the first time that hfc has been assigned to protons in randomly oriented samples of a closely related series of triplet structures. Specifically, hfc constants of 32, 20, and 22.5 G have been observed for the ring protons in **21**, **65**, and **66**, respectively. For comparison, the solid state β-H hfc for the biradical **67** is 26 G[23] and the solution phase β-H hfc for cyclobutyl radical (**68**) is 36.66 G.[26]

The β-H hfc in free radicals (rigid medium) is usually isotropic, and its

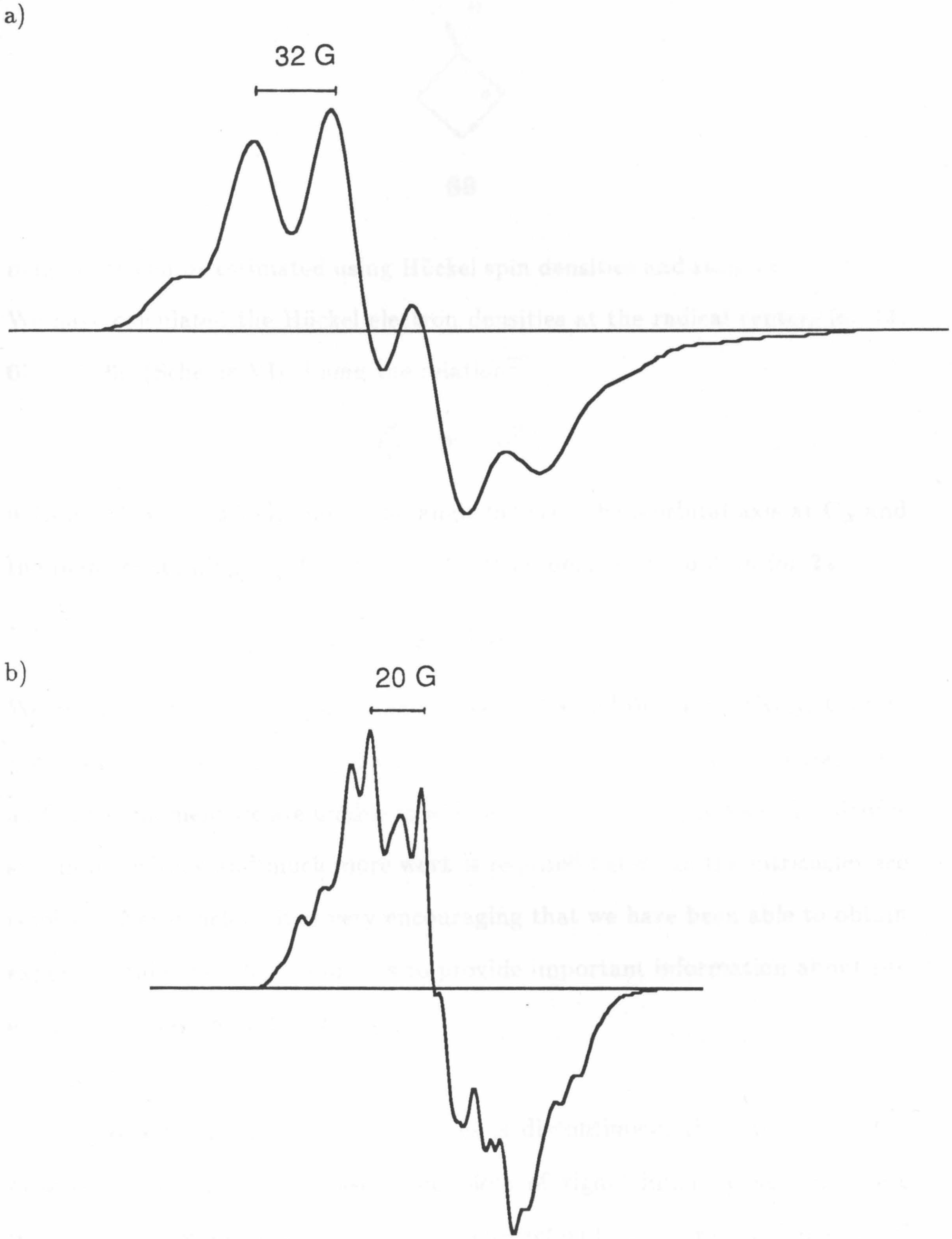

Figure 15. Simulated $\Delta m_s = 2$ regions of the ESR spectra for (a) **21**, (b) **65**.

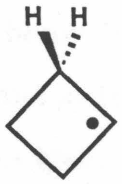

68

magnitude can be estimated using Hückel spin densities and standard relations. We have calculated the Hückel electron densities at the radical centers for **21**, **65**, and **66** (Scheme VI). Using the relation[27]

$$a_H^\beta = \rho C \cos^2 \theta$$

with $\rho = 1$, C = 42.5 G, and θ (the angle between the *p*-orbital axis at C_α and the plane containing C_α, C_β and H_β) to be 30 degrees, we obtain for **21**

$$a_H^\beta = 31.75$$

We can also predict values of 16 and 20 G for **65** and **66**, respectively. Clearly there is considerable disparity between these values and the experimental data, and at the moment we are unable to offer an explanation. However, this field is still in its infancy and much more work is required before all the intricacies are resolved. Nevertheless, it is very encouraging that we have been able to obtain experimental data which promises to provide important information about the electronic structure of biradicals.

Decay Kinetics

When irradiation of the samples is discontinued, the intensity of the observed ESR signals decreases, and plots of signal intensity vs. time are markedly nonexponential. Such decay characteristics are well precedented[28] for reactions in rigid media and have been ascribed to the static orientation of reactive species relative to the matrix. It is reasoned that molecules in different

Scheme VI

Hückel electron densities at the radical centers for various biradicals.

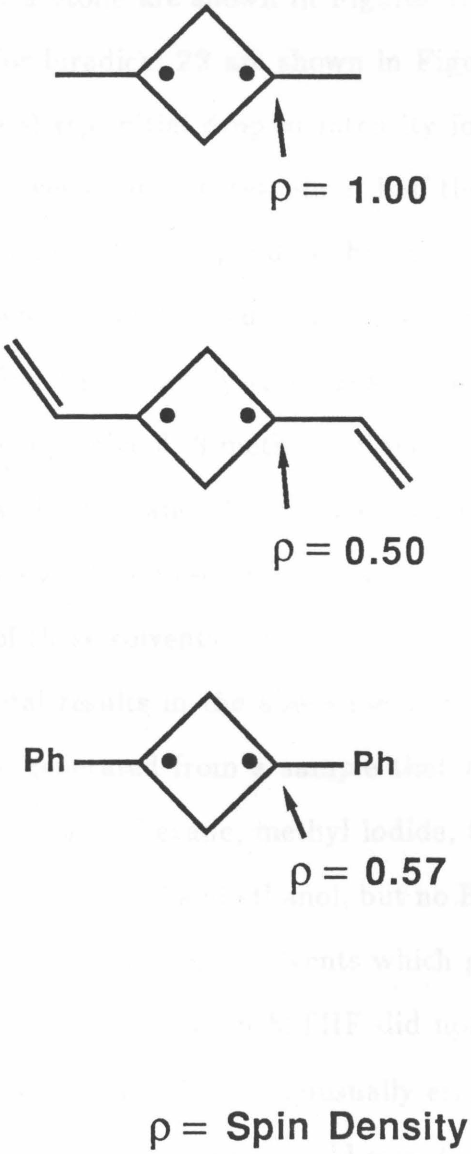

sites face different degrees of hindrance (or freedom) towards reactivity, and a distribution of unimolecular rate constants arises. Superposition of all the rates gives the decay curve its nonexponential appearance, and quite complex kinetics are obtained.

Typical decay curves for biradical **20** (obtained by the photolysis of **16** for 10 s) in MTHF and acetone are shown in Figures 16 and 17, respectively. Similar kinetic curves for biradical **22** are shown in Figures 18 and 19. Characteristically, there is a sharp initial drop in intensity followed by a region of much slower decay. At lower temperatures, about half the initial concentration of biradicals persists even after an hour, and further decrease in intensity occurs only very slowly. We have also attempted to generate ESR signals in a variety of other solvents and find that photolyses of azoalkanes **16** or **18** in diethyl ether, 2-propanol, propylene glycol, 3-methylpentane, cyclohexane, and a 1:1 mixture of 1-propanol and 2-propanol do produce triplet 1,3-cyclobutanediyls. However, extremely low signal-to-noise ratios make it impractical to follow the decay behavior in any of these solvents. Furthermore, it is not always possible to reproduce experimental results in the above-mentioned solvents, and often no visible signal can be generated from a sample that had previously shown a signal. We also tried pentane, hexane, methyl iodide, tetrahydrofuran, benzene, and a 1:1 mixture of methanol and ethanol, but no ESR signals were seen. Thus, MTHF and acetone were the only solvents which provided adequate intensities for kinetic work. However, even MTHF did not turn out to be very useful since it produced signals which were unusually erratic in their behavior. For example, a rise in the signal intensity could sometimes be seen (for both **20** and **22**) after the light was shuttered (Figure 20). It is extremely difficult to pinpoint the source of this problem due to the large number of experimental

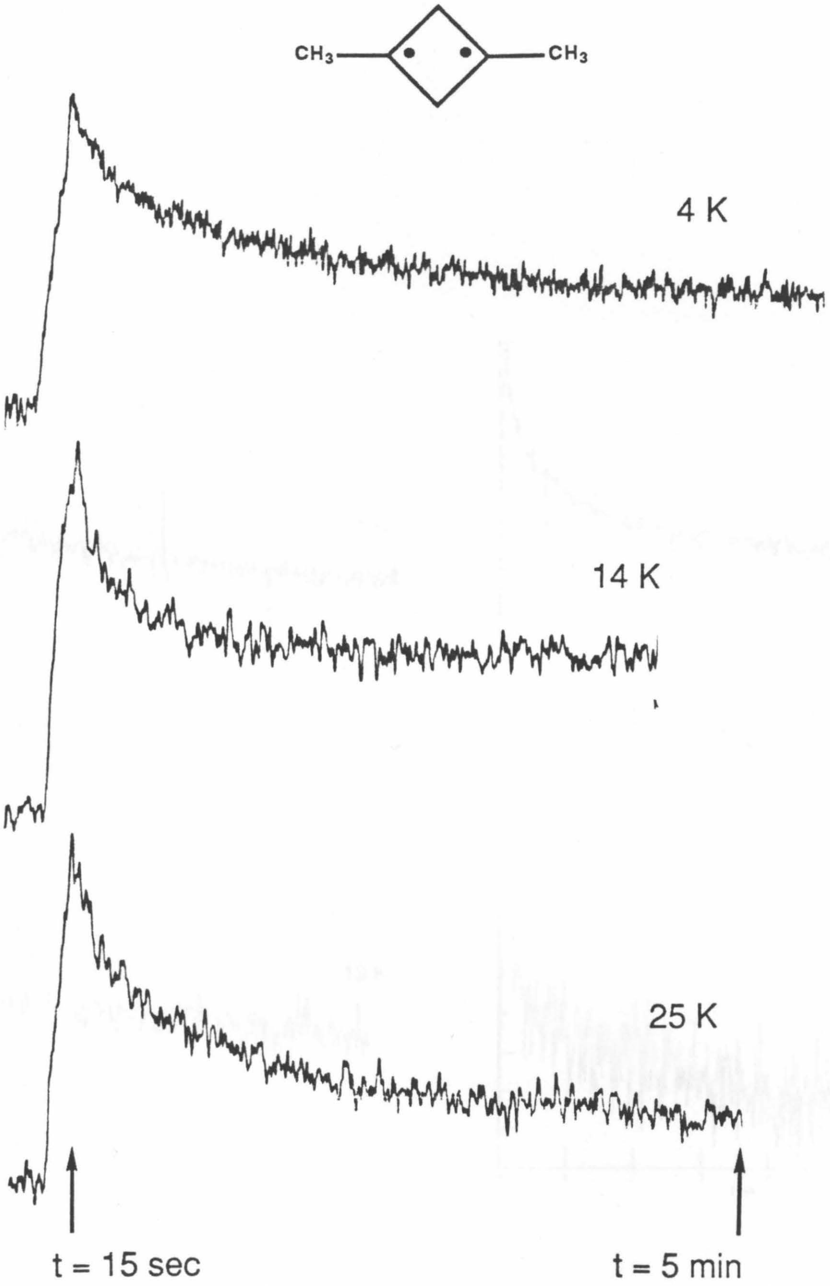

Figure 16. Intensity of the ESR signal vs. time plots for the generation and decay of **20** in MTHF at various temperatures.

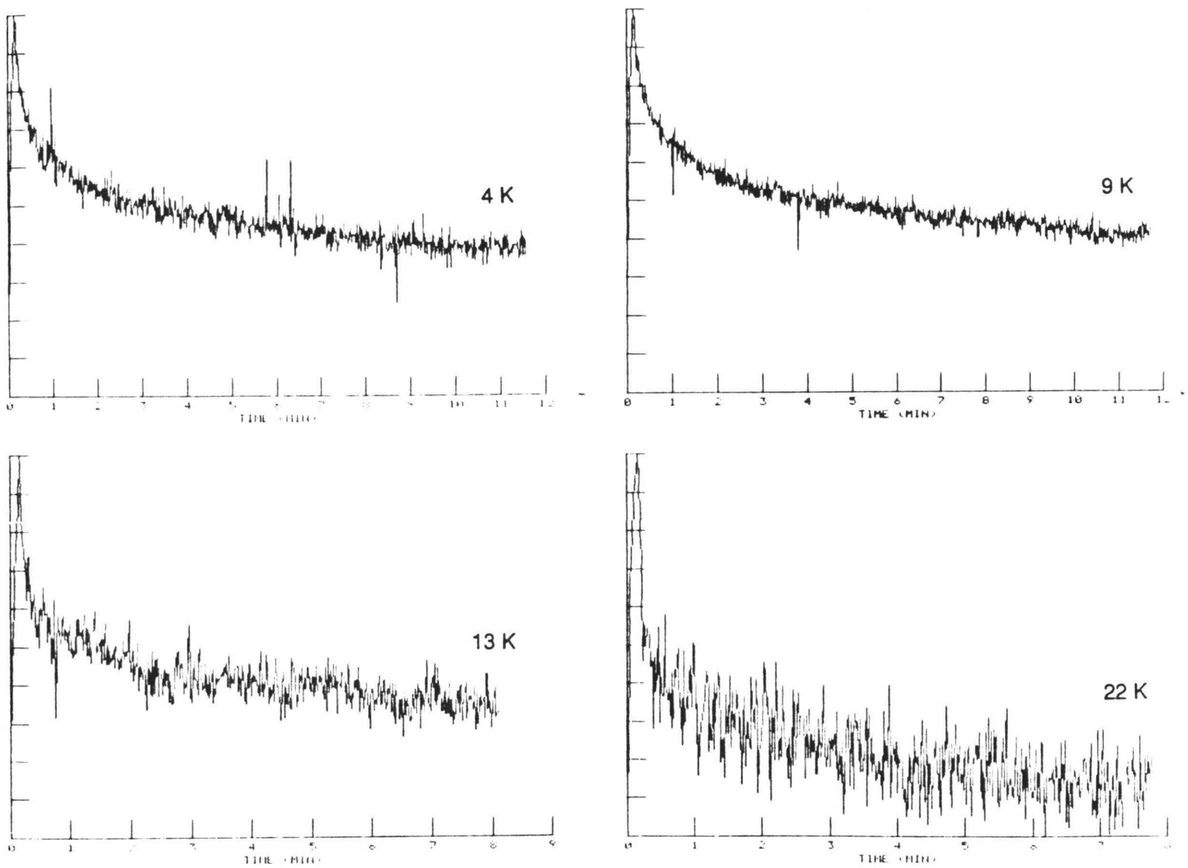

Figure 17. Intensity of the ESR signal vs. time plots for the generation and decay of **20** in acetone at various temperatures.

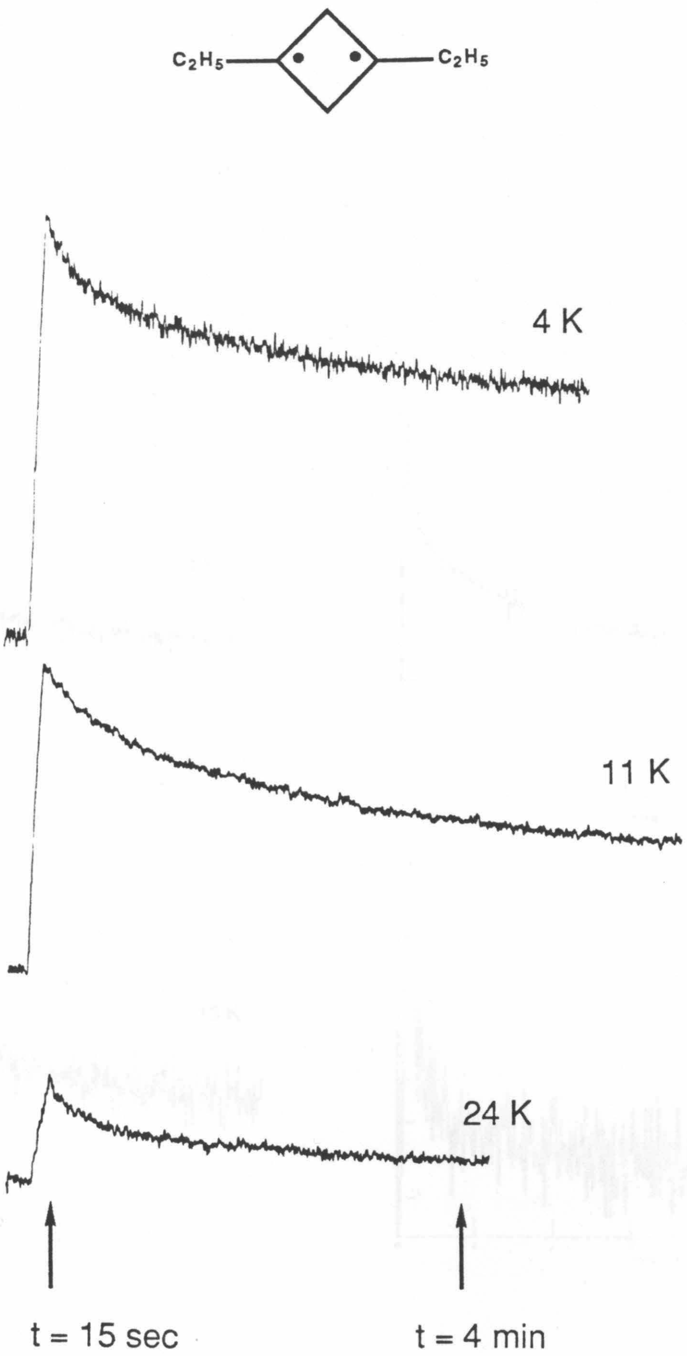

Figure 18. Intensity of the ESR signal vs. time plots for the generation and decay of **22** in MTHF at various temperatures.

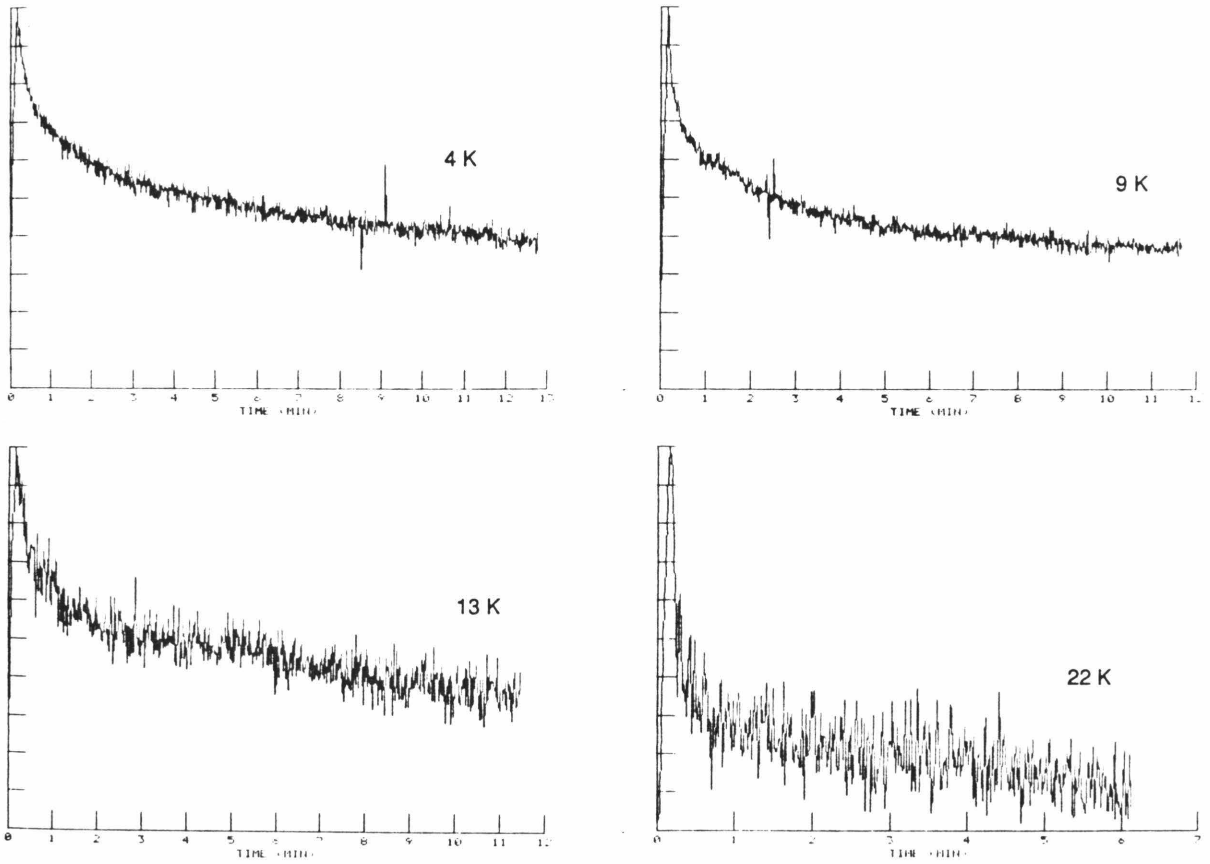

Figure 19. Intensity of the ESR signal vs. time plots for the generation and decay of **22** in acetone at various temperatures.

variables involved but we can rule out certain possibilities.

First, a gradual cooling of the matrix following initial heating (due to the intense light beam) could, in principle, give rise to the observed effect. However, the Curie law (signal intensity $\propto 1/T$) would require that the temperature, in some cases, be at least twice as high as the set temperature. We have tested this hypothesis by irradiating a sample tube containing a calibrated carbon-glass resistor which acts as a low-temperature thermometer. We do observe a small rise in temperature during irradiation but once the lamp is turned off the temperature drops down to its original value in less than two seconds.

Second, the formation of diazenyl biradicals (e.g., **69**) during photolysis, followed by slow loss of nitrogen to produce triplet 1,3-cyclobutanediyls could explain the strange effects we observe. Since this process would have to be thermally activated, even a small energy barrier of about 1 kcal mol^{-1} would result in an extremely slow reaction at 4 K. If this were the case, we would be able to detect the diazenyl biradicals. However, there is no direct evidence for the involvement of long-lived diazenyl biradicals in the triplet chemistry of these systems, and we consider this possibility extremely unlikely.

Since our attempts at accurate determination of kinetic parameters were hampered by low signal-to-noise ratios and irreproducibility, we opted to undertake a comparative study of the biradical **11** versus **20** and **22** in order to obtain qualitative information about the reaction. As mentioned earlier, **11** was the only localized biradical to be directly observed before our work, and in that study Closs had also found similar behavior for biradical decay.[2] We have repeated some of his experimental work and applied our new approach for the inclusion of matrix-site effects in analyzing the data. Intensity vs. time plots for **11** (obtained by photolysis of **10** for 60 s) over a range of temperatures are

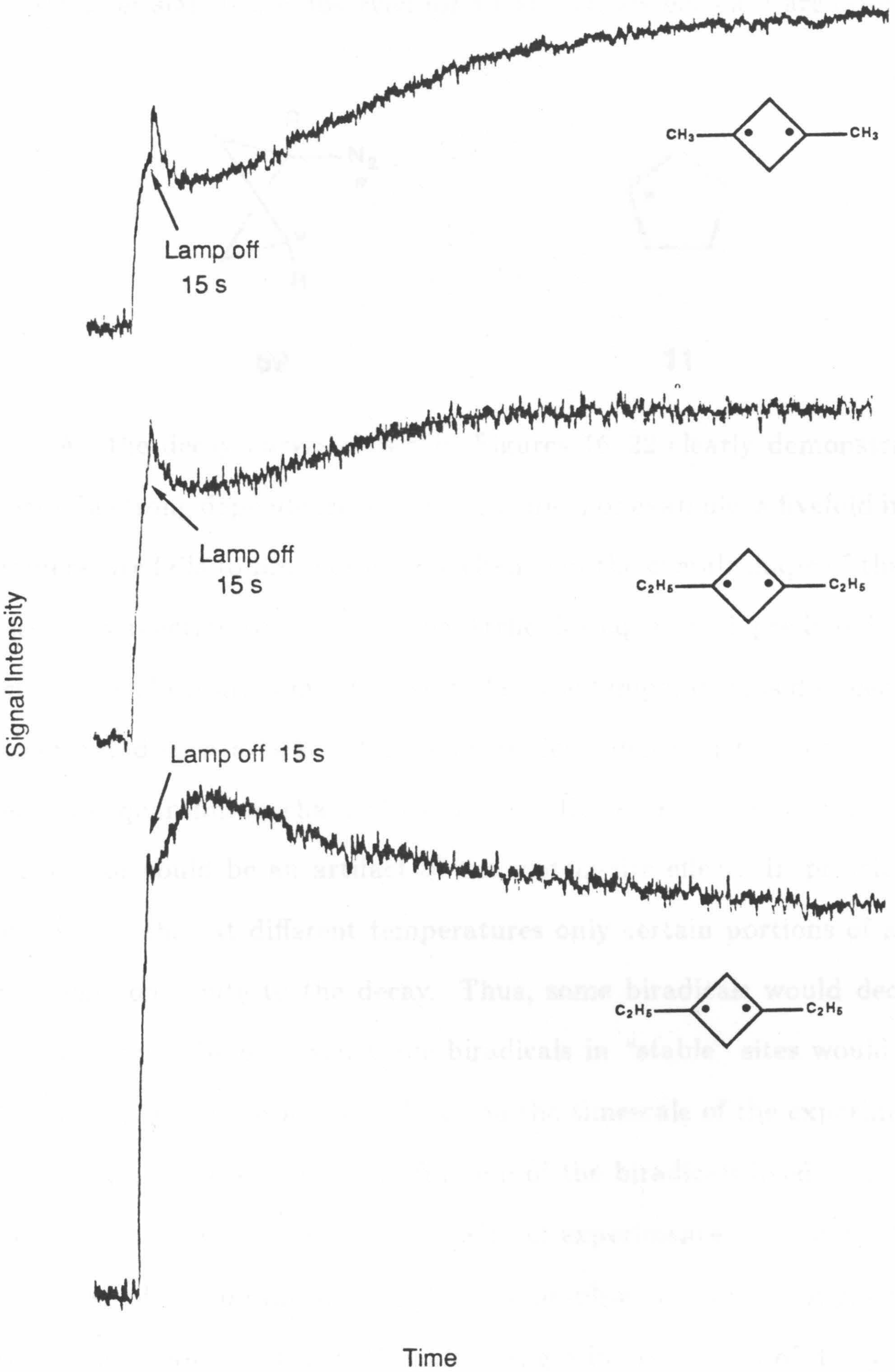

Figure 20. Examples of erratic behavior of intensity of the ESR signal for biradicals **20** and **22** in MTHF.

shown in Figures 21 and 22 for two different solvents, MTHF and cyclohexane. Much stronger signals are observed for **11** and consistent data are obtained.

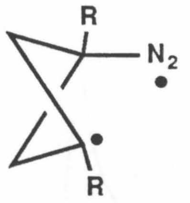

69

11

All the decay curves shown in Figures 16–22 clearly demonstrate the absence of a strong dependence on temperature. For example, a fivefold increase in temperature fails to produce a large change in the overall shape of the decay profiles. Any reaction which obeys the Arrhenius equation is predicted to show an astronomical variation in rates even when the temperature is doubled. Closs has interpreted such a lack of temperature dependence in the decay of **11** as evidence for quantum-mechanical tunneling.[2] However, it is not clear whether such behavior could be an artifact of the matrix-site effect. In principle, one could imagine that at different temperatures only certain portions of a broad distribution contribute to the decay. Thus, some biradicals would decay too rapidly and never be observed while biradicals in "stable" sites would be extremely long lived and would not decay on the timescale of the experiment. In an extreme case where only a tiny fraction of the biradicals lived long enough to allow detection, we would be at the edge of experimental capability. In such a case, most of the biradicals would never be observed, and changes in temperature might not result in noticeable changes in the shapes of decay curves. Therefore, matrix-site effects must be explicitly incorporated into any analysis which attempts to determine kinetic parameters from studies in rigid media.

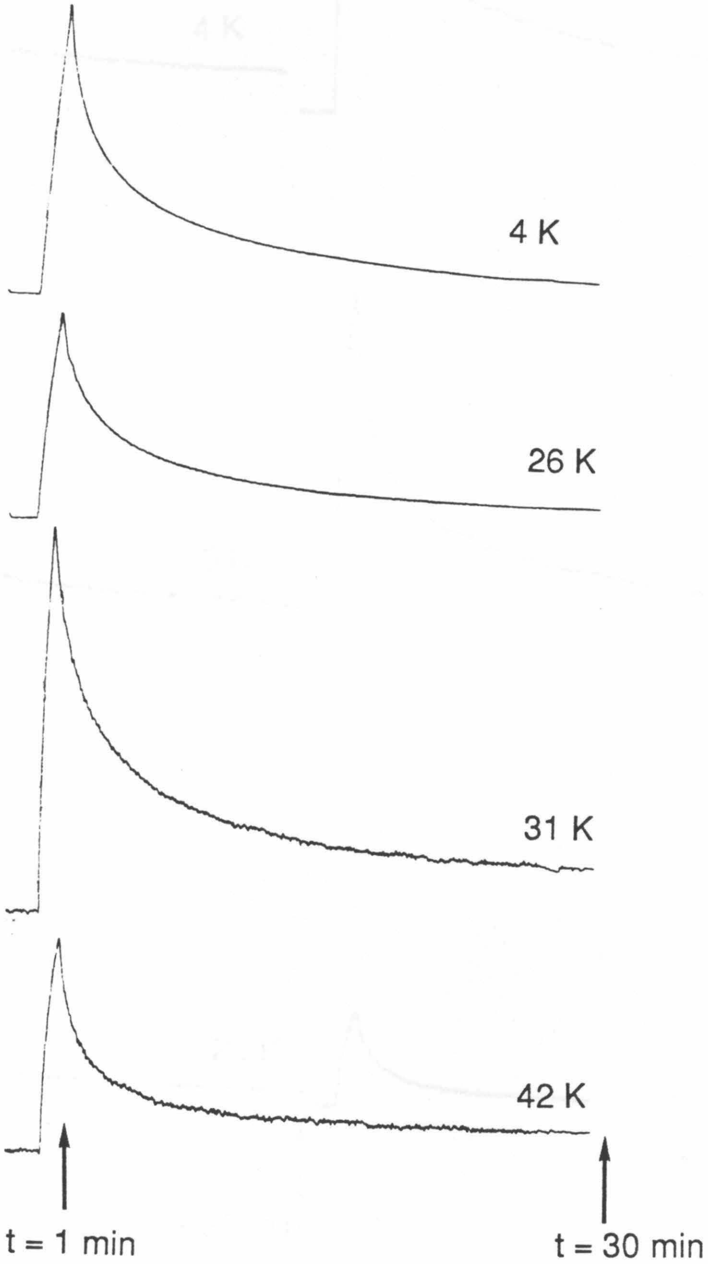

Figure 21. Intensity of the ESR signal vs. time plots for the generation and decay of **11** in MTHF at various temperatures.

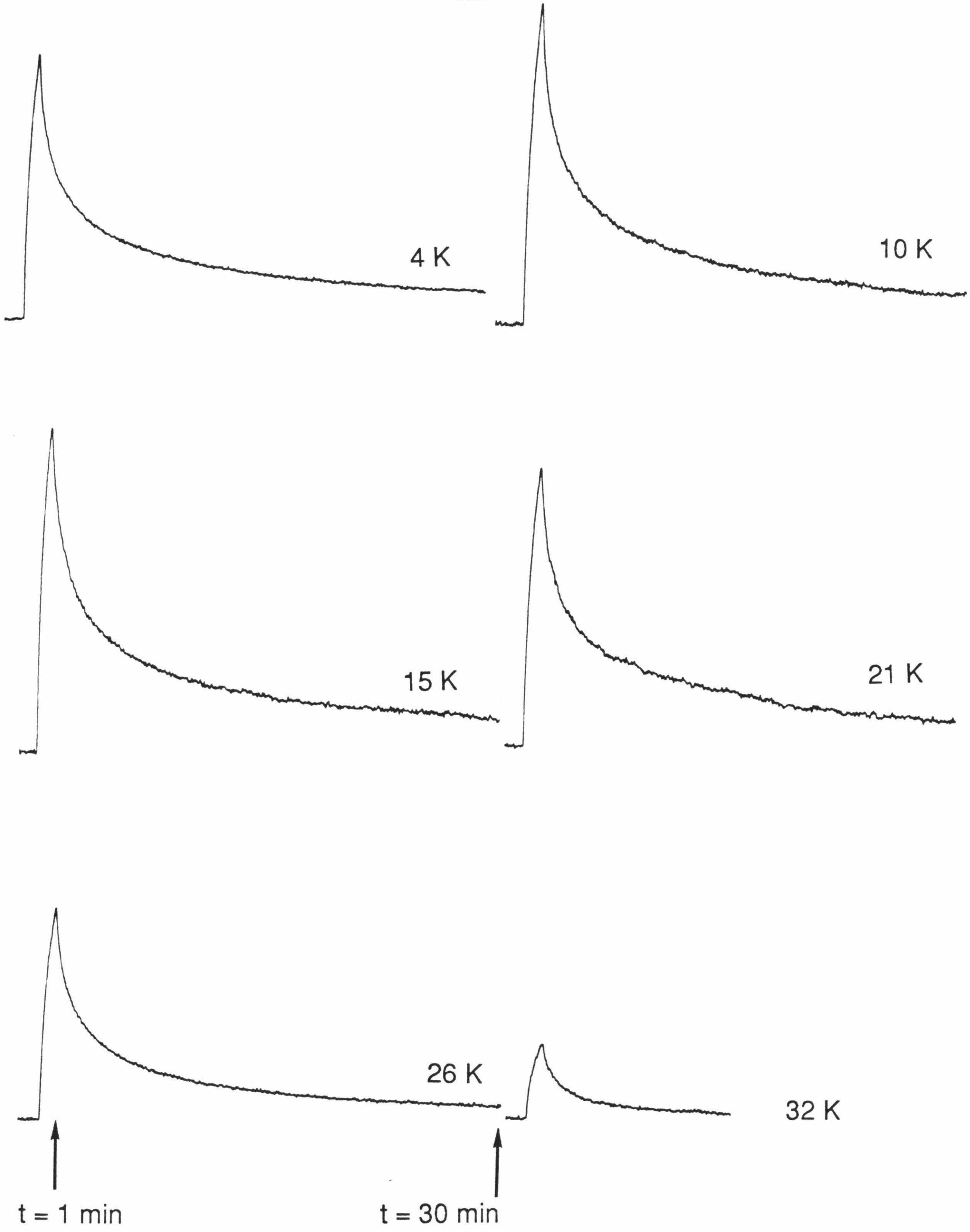

Figure 22. Intensity of the ESR signal vs. time plots for the generation and decay of **11** in cyclohexane at various temperatures.

Several approaches to this general problem have appeared in the literature[29,30] and some important features are briefly discussed next.

Suppose at time t there are $N_k(t)$ sites which decay exponentially at a rate between k and $k + dk$. This distribution can be written as

$$F(k,t) = \frac{N_k(t)}{\sum_k N_k(0)} = \frac{N_k(0)e^{-kt}}{\sum_k N_k(0)}$$

The decay profile will then be given by

$$f(t) = \int_0^\infty F(k,t)dk = \int_0^\infty F(k,0)e^{-kt}dk$$

Thus

$$f(t) = \mathcal{L}\{F(k,0)\}$$

or

$$F(k,0) = \mathcal{L}^{-1}\{f(t)\}$$

where $\mathcal{L}$ denotes a Laplace transformation,[31] $\mathcal{L}^{-1}$ an inverse Laplace transformation, and $F(k,0)$ is the initial distribution of rate constants.

In principle, if one knows an analytic expression for the function $f(t)$, one can obtain $F(k,0)$ by taking an inverse Laplace transform. For example, Austin et al.[29] have shown that for

$$f(t) = (1 + t/t_0)^{-n}$$

one can obtain

$$F(k,0) = \frac{n(kt_0)^n}{\kappa T\Gamma(n+1)}\exp(-kt_0)$$

where n and t_0 are parameters which depend on temperature and are determined experimentally, κ is Boltzmann's constant, and Γ represents the Gamma function. This distribution then gives a most probable rate constant

$$k_0 = \frac{n}{t_0}$$

Similarly, Doba et al.[30] have shown that by using

$$f(t) = \exp(-ct^{1/2})$$

one can obtain

$$F(k,0) = \frac{c}{\sqrt{4\pi k^3}} \exp(-c^2/4k)$$

a distribution which reaches a maximum for

$$k_0 = \frac{c^2}{6}$$

We have found that we cannot fit our experimental decay curves using either of these analytical approaches and a numerical method of obtaining the inverse Laplace transform is needed. However, this is extremely difficult to do since minute changes in $f(t)$ produce very large, and sometimes random variations in $F(k,0)$. We have therefore decided to conduct our analysis in a somewhat different manner wherein we start by assuming an initial distribution and calculate the function $f(t)$. The shape and position of $F(k,0)$ are then varied until a good fit between the experimental and theoretical decay curves is obtained. We initially assumed, and our results confirmed, that a Gaussian function over $\ln k$ is a good representation of the distribution. This is especially convenient since this distribution is directly related to a distribution over energy of activation. Thus, we used

$$F(k,0) = \exp\{-w(\ln \frac{k}{k_0})^2\}$$

in most of our attempts to obtain theoretical fits to our kinetic data. The width of this distribution depends upon w, and k_0 represents the most probable rate constant. Sponsler[7] has recently developed a computer program which also treats the decay of the biradical during photolysis of its precursor azoalkane, and both the rise and fall of signal intensity can be modeled. The output from this program gives the initial distribution which best reproduces the experimental decay data, and for a series of curves at different temperatures we can obtain a set of initial distributions over $\ln k$. As mentioned earlier, these can then be converted to distributions over energy of activation, E, such that

$$F(E,0) = \exp\{-\frac{w}{R^2T^2}(E - E_0)^2\}$$

where E_0 is the most probable energy of activation. The distribution $F(E,0)$ is still Gaussian in character but its width is now determined by w/R^2T^2. It is also easy to see that the standard deviation can be expressed as[32]

$$\sigma = \sqrt{\frac{R^2T^2}{2w}}$$

and the width at half-height follows from the relation

$$F.W.H.M. = 2.354\sigma$$

Since the initial distribution over E should be the same for all kinetic runs for the same biradical, σ should be a constant. Then, if the values of σ obtained from fittings for different temperatures are similar, an average σ can be used for further analysis. Recently this method has been used successfully for the first time by Sponsler in his study of the decay kinetics of the delocalized biradical **65**.[7] He obtains quite good fits to experimental data using a fixed distribution ($\sigma = 0.425$ kcal mol^{-1}). Further, he uses the most probable rate constants to obtain a linear Arrhenius plot from which he can extract $E_0 = 1.2$ kcal mol^{-1} and $\log A = 3.8$.

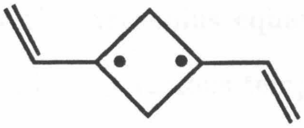

65

Theoretical fits to our experimental data using a Gaussian initial distribution are presented in Figures 23 and 24 for biradical **11** in MTHF and in cyclohexane, respectively. Figures 25 and 26 show similar data for biradicals **20** and **22**, respectively, in acetone. We have chosen to emphasize the acetone data for **20** and **22** because these are much more well-behaved and reproducible. The parameters k_0, w, and σ for the best fits at several temperatures are presented in Table VIII. Examination of the values of σ reveals that a significant increase in the width of the energy of activation distribution is required to fit the data at higher temperatures, and we cannot obtain a good fit for all the decay traces using the same distribution over E. However, closer inspection of the data in Table VIII shows that the width of the distribution over ln k does remain relatively constant and very small changes in w are observed. In addition, the change in k_0 is much smaller than expected for a more than fivefold increase in temperature.

Since all our samples are prepared identically, it is hard to imagine that a change in temperature brings about the drastic changes in the initial energy of activation distribution indicated by Table VIII. This suggests that the conversion of the distribution over ln k to a distribution over E using the Arrhenius equation (see above) is inappropriate. One implication of these findings is that we cannot use this analytical method in the same way as Sponsler did to obtain E_0 and log A.[7]

We can see how far from Arrhenius behavior our observations deviate by modeling the temperature dependence of the curves. Using a fixed distribution over E which is forced to obey the Arrhenius equation we can calculate the shapes of the intensity vs. time plots at various temperatures. The results are shown in Figure 27 and it is clear that quite different shapes are observed for

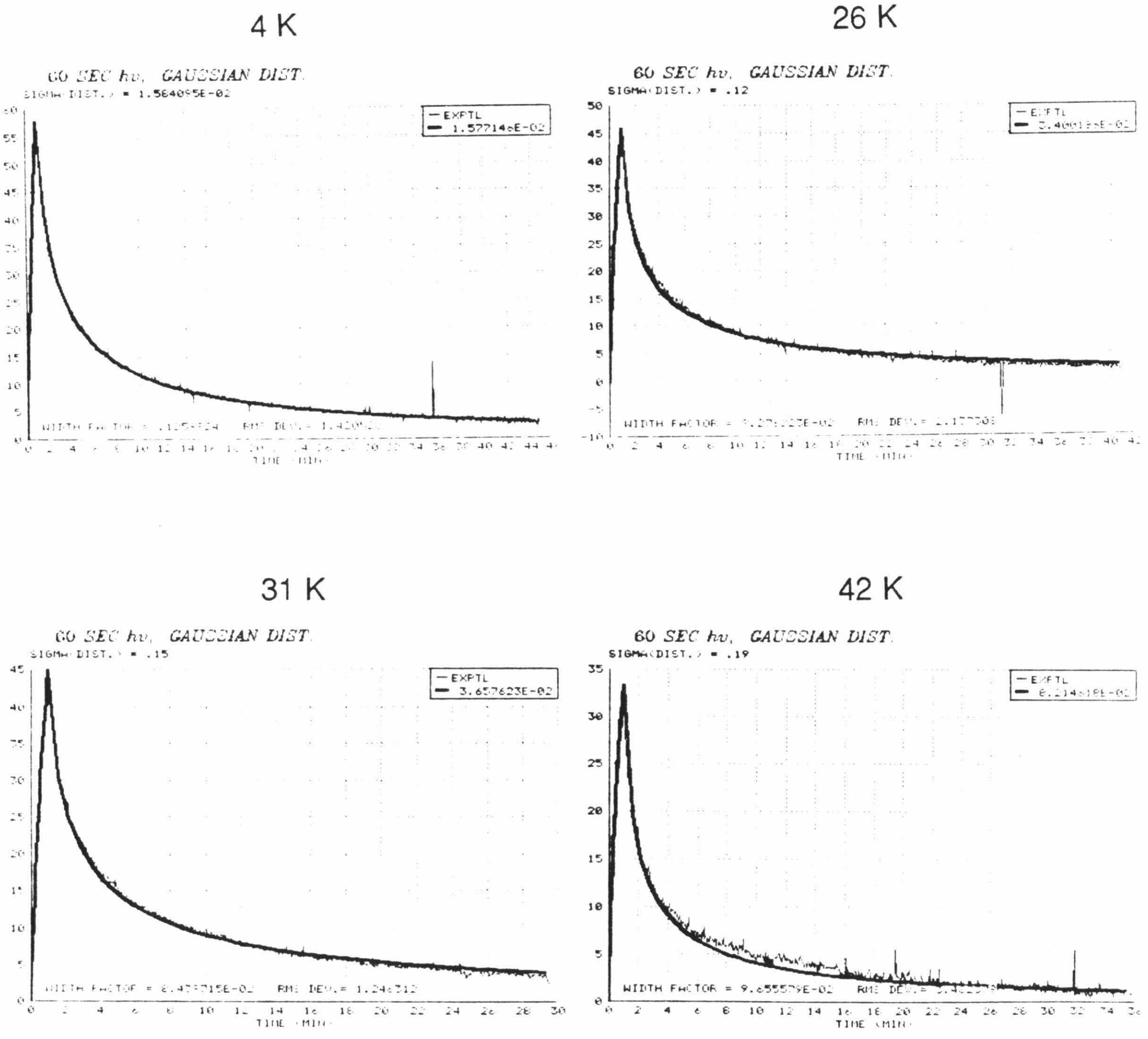

Figure 23. Fits to the decay data for **11** in MTHF at various temperatures.

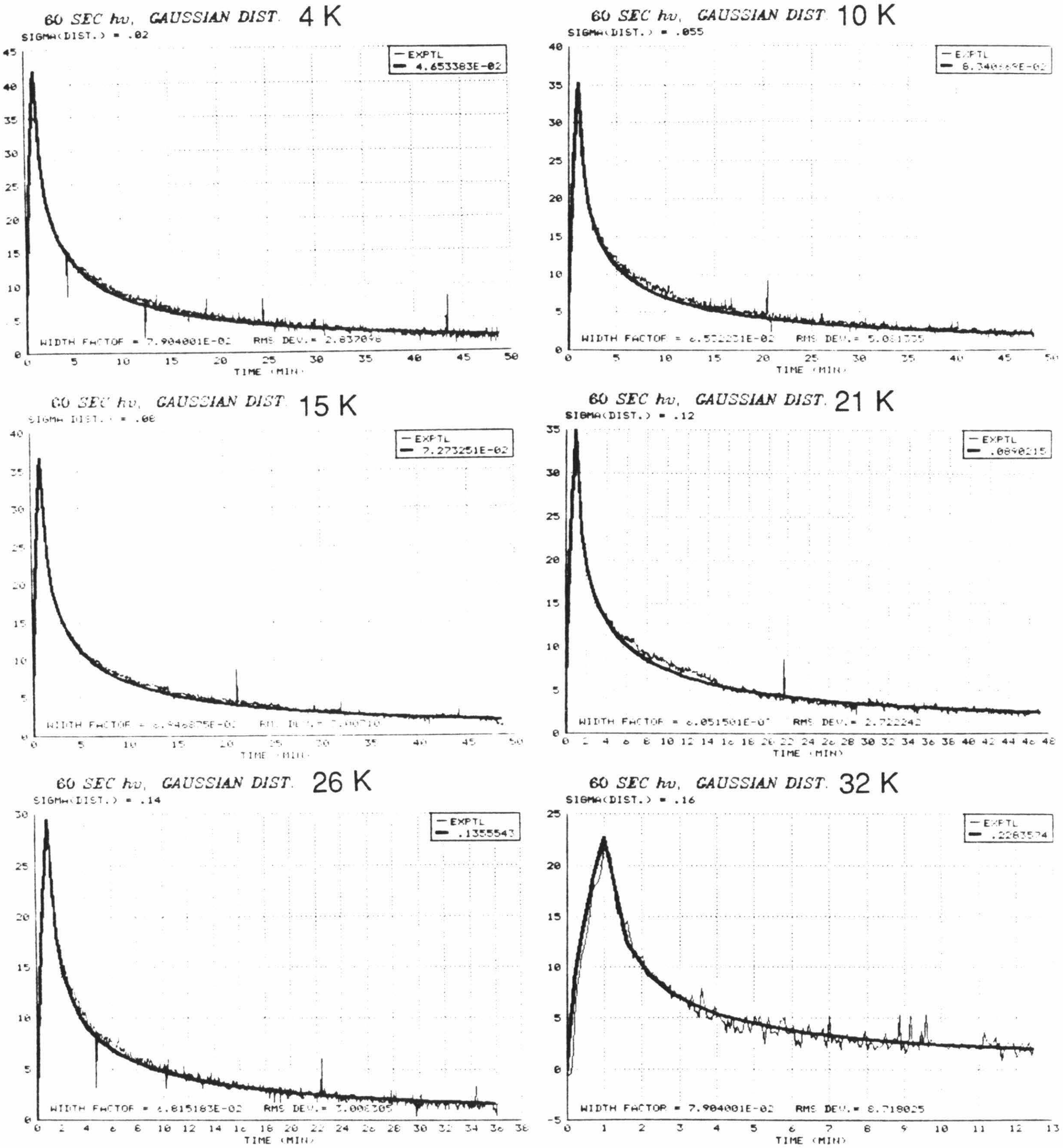

Figure 24. Fits to the decay data for **11** in cyclohexane at various temperatures.

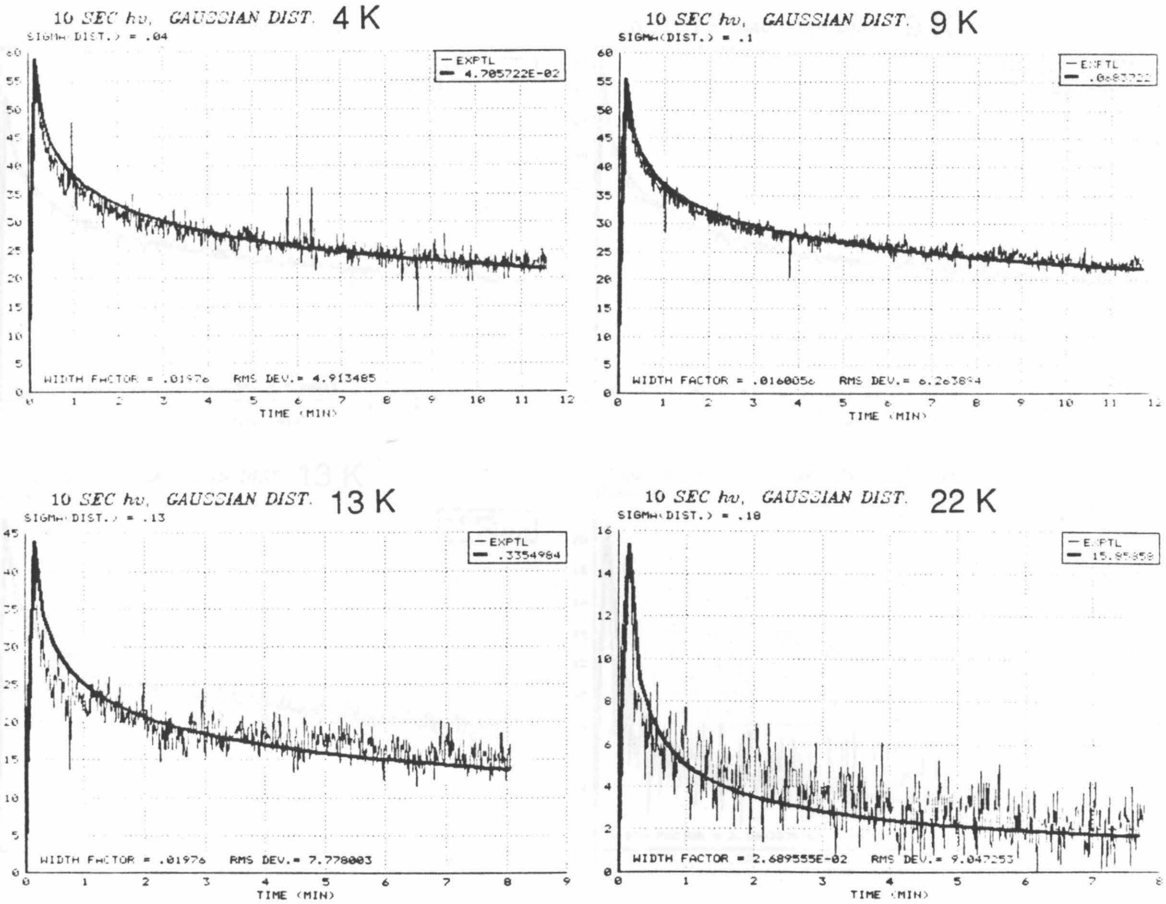

Figure 25. Fits to the decay data for **20** in acetone at various temperatures.

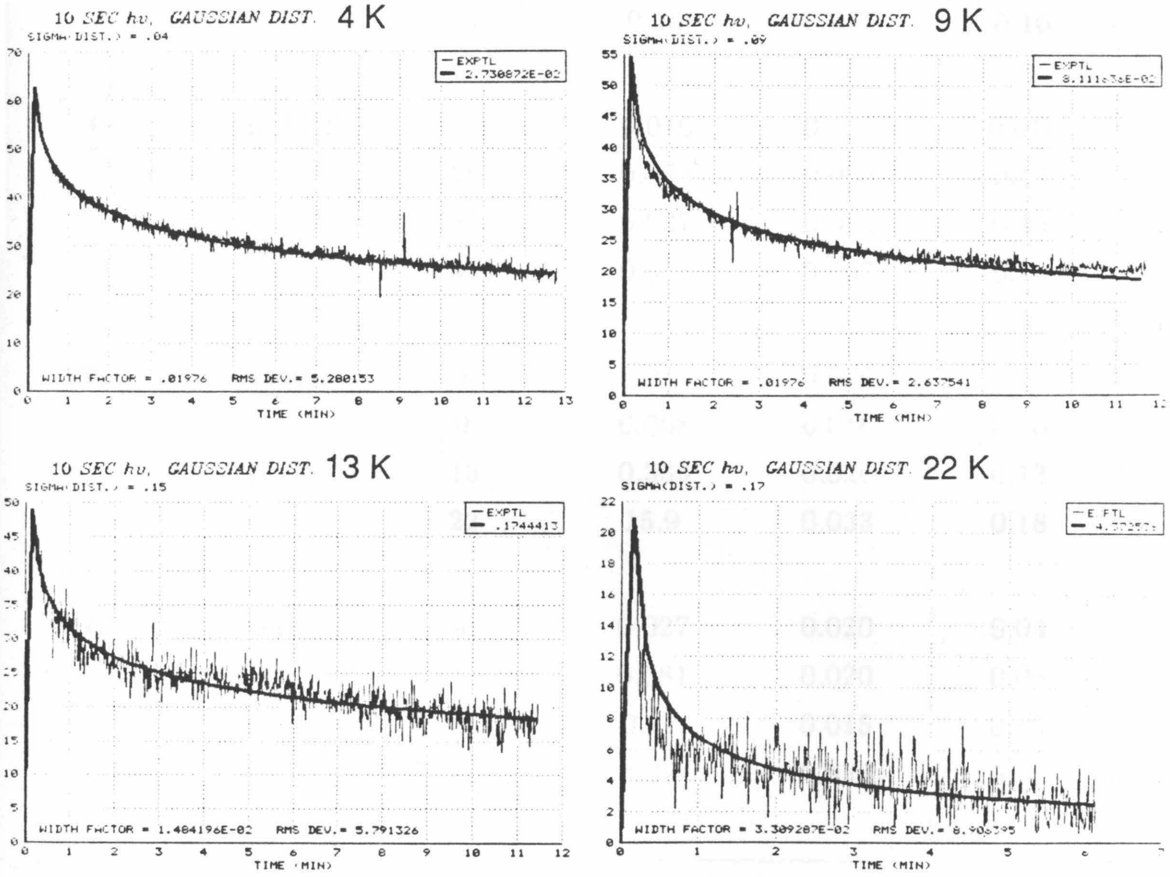

Figure 26. Fits to the decay data for **22** in acetone at various temperatures.

Table VIII. Characteristic Parameters of the Distributions Giving the Best Fits to Decay Data

Biradical	Solvent	Temperture[a]	k_0	w	σ^b
11	Cyclohexane	4	0.046	0.079	0.02
		10	0.083	0.065	0.055
		15	0.073	0.069	0.08
		21	0.089	0.060	0.12
		26	0.13	0.068	0.14
		32	0.23	0.079	0.16
11	MTHF	4	0.016	0.126	0.016
		26	0.034	0.093	0.12
		31	0.037	0.084	0.15
		42	0.082	0.097	0.19
20	Acetone	4	0.047	0.020	0.04
		9	0.068	0.016	0.10
		13	0.335	0.020	0.13
		22	15.9	0.033	0.18
22	Acetone	4	0.027	0.020	0.04
		9	0.081	0.020	0.09
		13	0.17	0.015	0.15
		22	4.37	0.033	0.17

[a] ± 0.3 K. [b] In kcal mol^{-1}

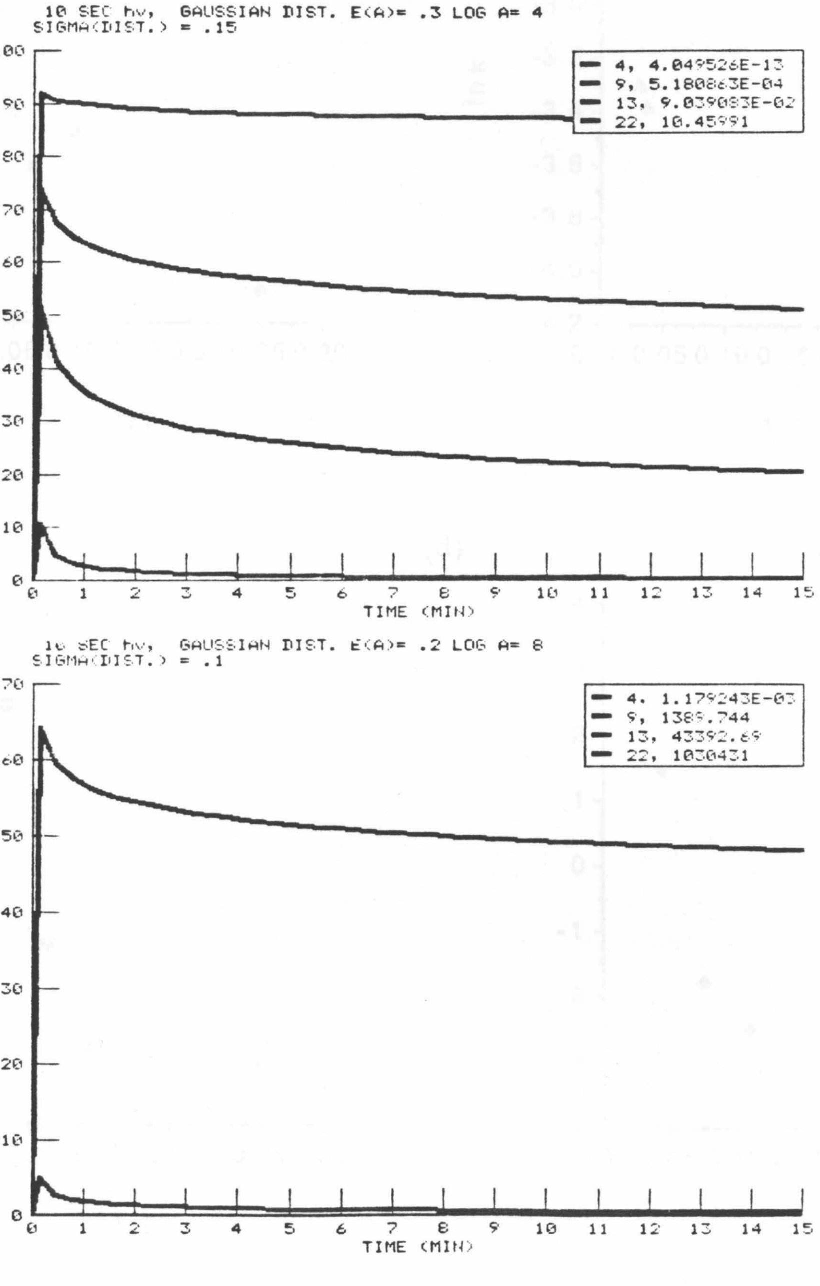

Figure 27. Theoretical decay curves calculated assuming Arrhenius behavior.

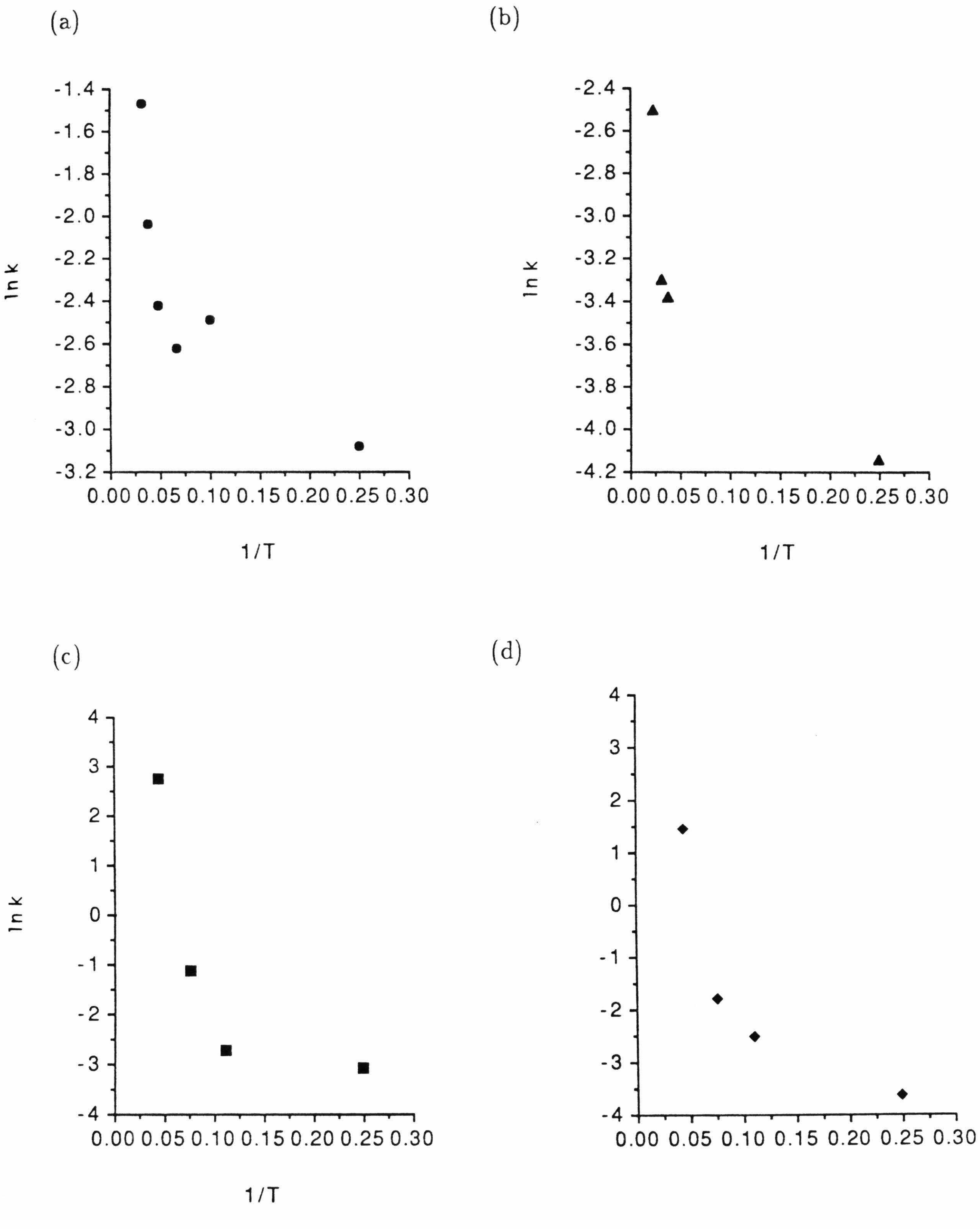

Figure 28. Arrhenius plot of the most probable rate constant for (a) **11** in cyclohexane, (b) **11** in MTHF, (c) **20** in acetone and (d) **22** in acetone.

the decay traces at different temperatures. For example, if we reproduce our experimental shape for decay at 22 K we notice that at 4 K there is almost no decay at all, and the biradical is indefinitely stable (Figure 27a). If, on the other hand, we reproduce the shape of our decay trace at 4 K, simulation shows that we should not see any signal for the biradical even at 13 K (Figure 27b). Thus, it is clear that not only are the shapes of the curves very different, they are quite sensitive to changes in temperature. We have repeated this procedure for several different distributions with identical results, and we conclude that *the same distribution over E obeying the Arrhenius equation cannot produce the observed shapes of the decay traces.*

Clearly, the decay behavior we have seen for **11**, **20** and **22** does not respond to temperature in the conventional way. This is also evident from clearly nonlinear Arrhenius plots (Figure 28) obtained using the most probable rate constants given in Table VIII. Closs had seen a similar deviation from linearity when he used the initial rate of decay for **11** at various temperatures to obtain an Arrhenius plot. We believe that k_0 better represents the information in the decay curves than the initial rate because the matrix-site effect is directly included in the form of a distribution over $\ln k$.

Nonlinearity in Arrhenius plots is generally interpreted as evidence for the intervention of quantum-mechanical tunneling, and several examples can be found in the literature.[2,33] Thus, we must include a tunneling correction factor, Q, in the rate constant

$$k = QAe^{-E/RT}$$

To apply this equation, we first need to estimate the magnitude of A. Since we are observing the decay of a triplet species, A must be smaller than the normal preexponential factor for unimolecular reactions. In similar calculations, Closs[2] used log $A = 8$ for the decay of triplet **11**. Very few experimental determinations of A have been made for such processes. Dowd[1a] has estimated that log A for the decay of triplet TMM (**4**) is between 6 and 8, and Barton et al.[34] have determined log $A = 7.10 \pm 0.50$ for the decay of the triplet biradical **70**.

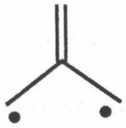

4

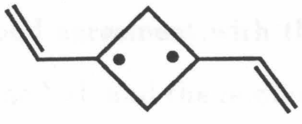

65

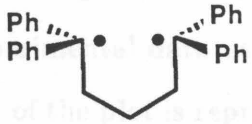

70

However, in **65**, a system very closely related to ours, Sponsler has determined that log A could be as low as 4.[7] Thus, we decided to evaluate tunneling parameters using both log $A = 4$ and log $A = 8$. We have used the Bell tunneling model for a parabolic barrier of width $2a$ and height E.[35] This model predicts the tunneling factor to be

$$Q = \frac{e^{\alpha}}{\beta - \alpha}(\beta e^{-\alpha} - \alpha e^{-\beta})$$

where

$$\alpha = \frac{E}{RT}$$

$$\beta = \frac{2a\pi^2(2mE)^{1/2}}{h}$$

In his analysis of the decay of triplet **11**, Closs[7] calculated tunneling rates using this method to match his experimental initial rate data, and we will do the same with our most probable rates. For **11** we will assume that the mass of the tunneling particle is 68 dalton. One could say that the nuclear motions required for the reaction may not involve the whole molecule and a smaller value should be used. Indeed, Closs analyzed all his data using a mass of 14 dalton. However, such a decrease in mass only results in a corresponding increase in the width of the barrier, and the values of E and k are not affected.

The results of the calculations of rate constants including the tunneling contribution for **11** are shown in the form of Arrhenius plots in Figure 29. Thus, we get extremely good agreement with the experimental data using the parameters shown in Scheme VII, and the nonlinearity of the plot is reproduced quite well.

In Scheme VII we have also shown the parameters used by Closs to fit his data. If we use a mass of 68 rather than 14 dalton which he used, we obtain values for both the barrier height and barrier width which are quite similar to what we have found. This amazing agreement highlights the qualitative similarity in our approaches to the problem. Even though the initial rates used by Closs in his Arrhenius plots are two orders of magnitude smaller than our values of k_0, the shapes of the Arrhenius plots appear to be alike. It seems that Closs' observation that the onset of curvature in these plots determines the height and width of the barrier is correct, and values of $E = 1$–2 kcal mol^{-1} and $2a = 0.15$–0.30 Å seem quite sufficient to explain the decay data.

In summary, we have shown that a matrix-site effect alone does not explain the temperature independence of the decay curves. Additionally, we have shown that a pronounced curvature in the Arrhenius plots obtained using k_0 from an analysis specifically incorporating matrix effects implies a substantial tunneling component. Thus, even though we can obtain very limited data for biradicals **20** and **22**, Figure 28 clearly indicates tunneling in their decay. In these cases very small energy barriers are involved. For example, the data for

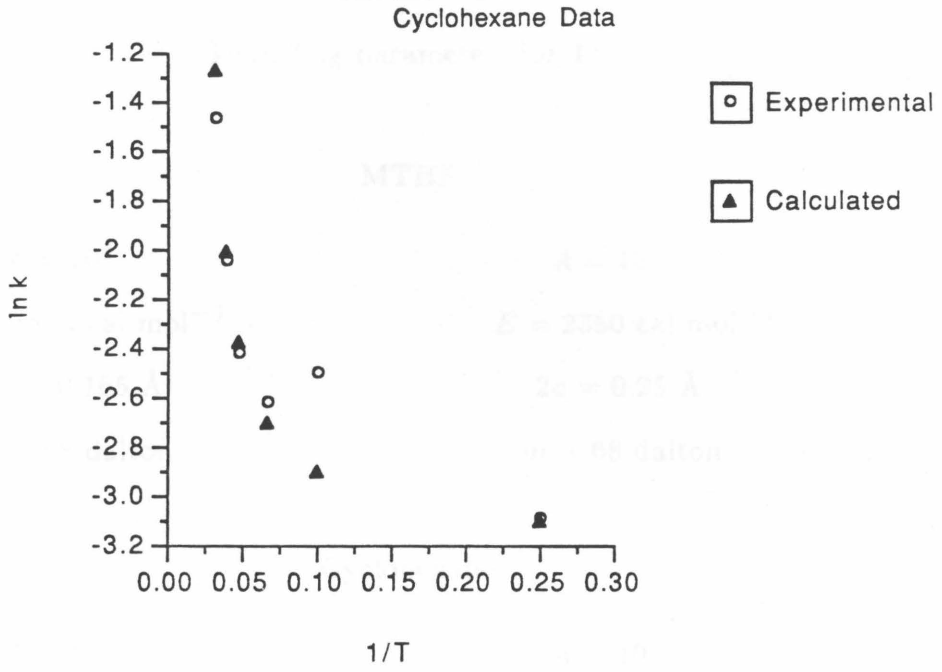

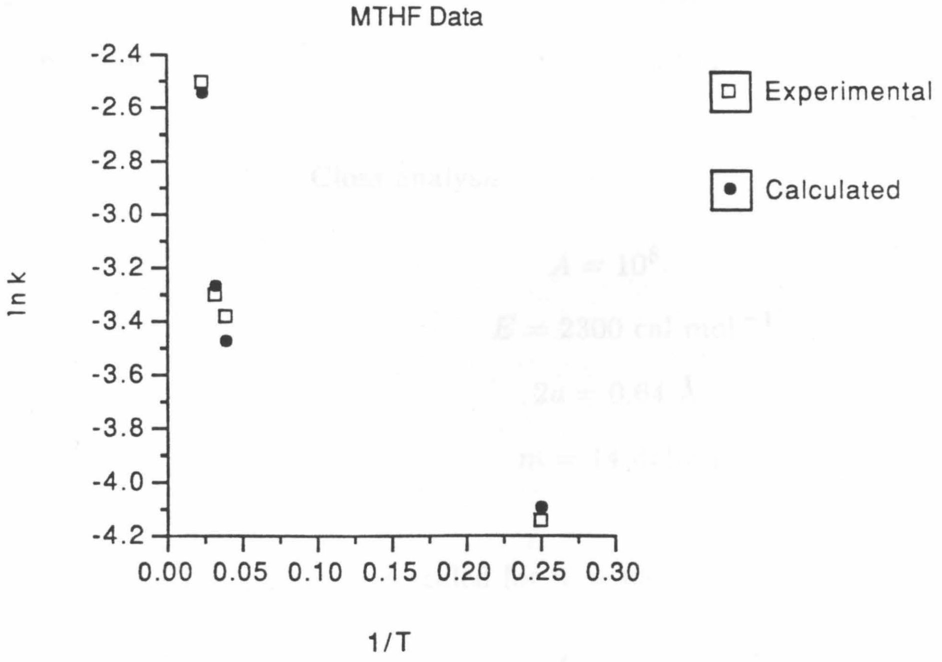

Figure 29. Calculated rates including tunneling component for **11** along with experimental data.

Scheme VII

Tunneling parameters for **11**.

MTHF

$A = 10^4$

$E = 1850$ cal mol^{-1}

$2a = 0.165$ Å

$m = 68$ dalton

$A = 10^8$

$E = 2350$ cal mol^{-1}

$2a = 0.25$ Å

$m = 68$ dalton

Cyclohexane

$A = 10^4$

$E = 850$ cal mol^{-1}

$2a = 0.23$ Å

$m = 68$ dalton

$A = 10^8$

$E = 1600$ cal mol^{-1}

$2a = 0.29$ Å

$m = 68$ dalton

Closs analysis

$A = 10^8$

$E = 2300$ cal mol^{-1}

$2a = 0.64$ Å

$m = 14$ dalton

Closs parameters scaled for $m = 68$

$A = 10^8$

$E = 2300$ cal mol^{-1}

$2a = 0.29$ Å

$m = 68$ dalton

20 can be fitted quite well for $E = 750$ cal mol^{-1}, $2a = 0.39$ Å, $m = 82$ dalton and $A = 10^8$. Small changes can be very significant when we are dealing with energy barriers of this size and can result in large rate variations, especially when tunneling is important. Perhaps this is why we get such irreproducible behavior upon changing solvents.

High-quality theoretical studies[7] have predicted an S–T gap of about 1.5 kcal mol^{-1} for **20**. Using these values we can construct a partial potential energy diagram for the reaction, highlighting the region where tunneling occurs (Figure 30). The important area must be where the singlet and triplet surfaces cross and tunneling must occur through the narrow barrier marked **a**. Small changes in the geometry of the biradicals can have a significant effect on the relative positions of the singlet and triplet energy surfaces. Therefore, we can expect the barrier width and the barrier height to be slightly different for biradicals in different matrix sites. Tunneling rates are especially sensitive to changes in the width of the barrier, and a spread in its values could be partly responsible for the width of the distribution over ln k (i.e., w). Since this contribution to w does not change significantly with temperature, our observation of a relatively constant value for w is quite consistent with this analysis.

Reaction Pathway

Having provided good evidence for the involvement of quantum-mechanical tunneling in the decay of triplet 1,3-cyclobutanediyls, we will now discuss the reaction process itself. One can envision three pathways for biradical decay: (a) abstraction of a hydrogen atom from the surrounding matrix, (b) 1,2-H shift producing a substituted cyclobutene, or (c) closure to form a 1,3-dialkylbicyclobutane.

Abstraction from the matrix has precedent in the chemistry of carbenes.

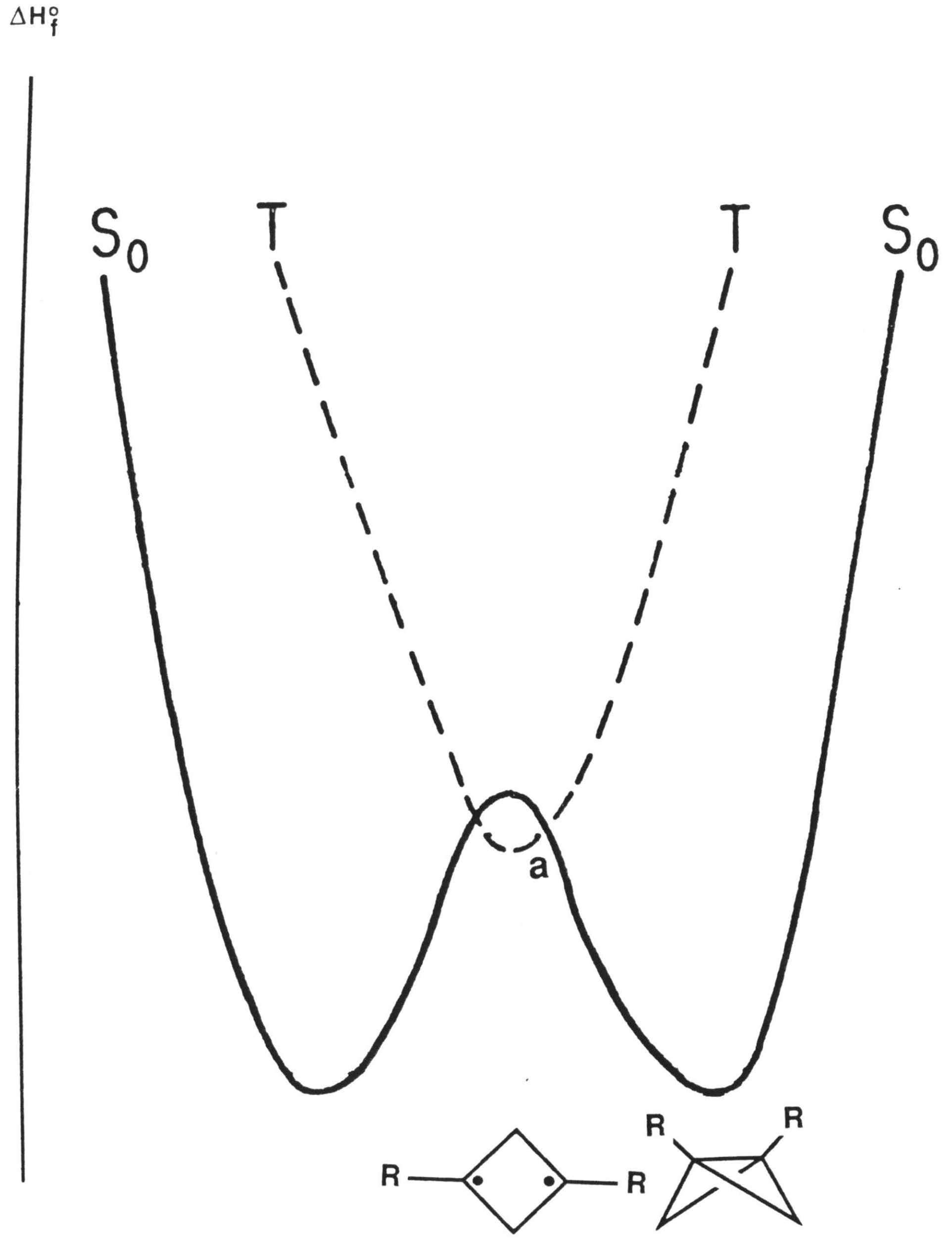

Figure 30. General energy diagram for the reactivity of biradicals.

Platz[36] has observed that triplet diphenylcarbene abstracts hydrogen atoms from matrix materials. Large kinetic isotope effects were seen, implying that tunneling was important. However, the highest rate for H-atom abstraction was $6.3 \times 10^{-2}\ s^{-1}$ at 98 K and extrapolation suggests an extremely low rate at 4 K. Furthermore, we do not see the rise in the intensity of a doublet signal which should accompany hydrogen abstraction, although the resulting free radicals should be quite stable at the low temperatures and should be easily detectable. We have also followed the decay of biradical **20** in both acetone and acetone-d_6 and find no visible difference in the two decay traces (Figure 31), strongly indicating that the decay process is not the abstraction of a hydrogen atom from the matrix host.

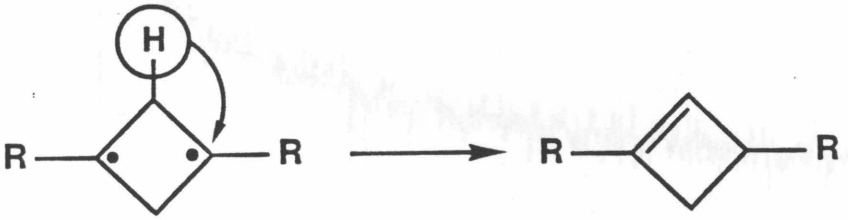

We have never seen any evidence for 1,2-H shift in our extensive thermal and photochemical decomposition studies of the 2,3-diazabicyclo[2.1.1]hex-2-ene ring system at room temperature. In order to see if this is also true at cryogenic temperatures, we photolyzed a sample of **16** in acetone-d_6 to generate an ESR signal for biradical **20**. The sample was then brought up to

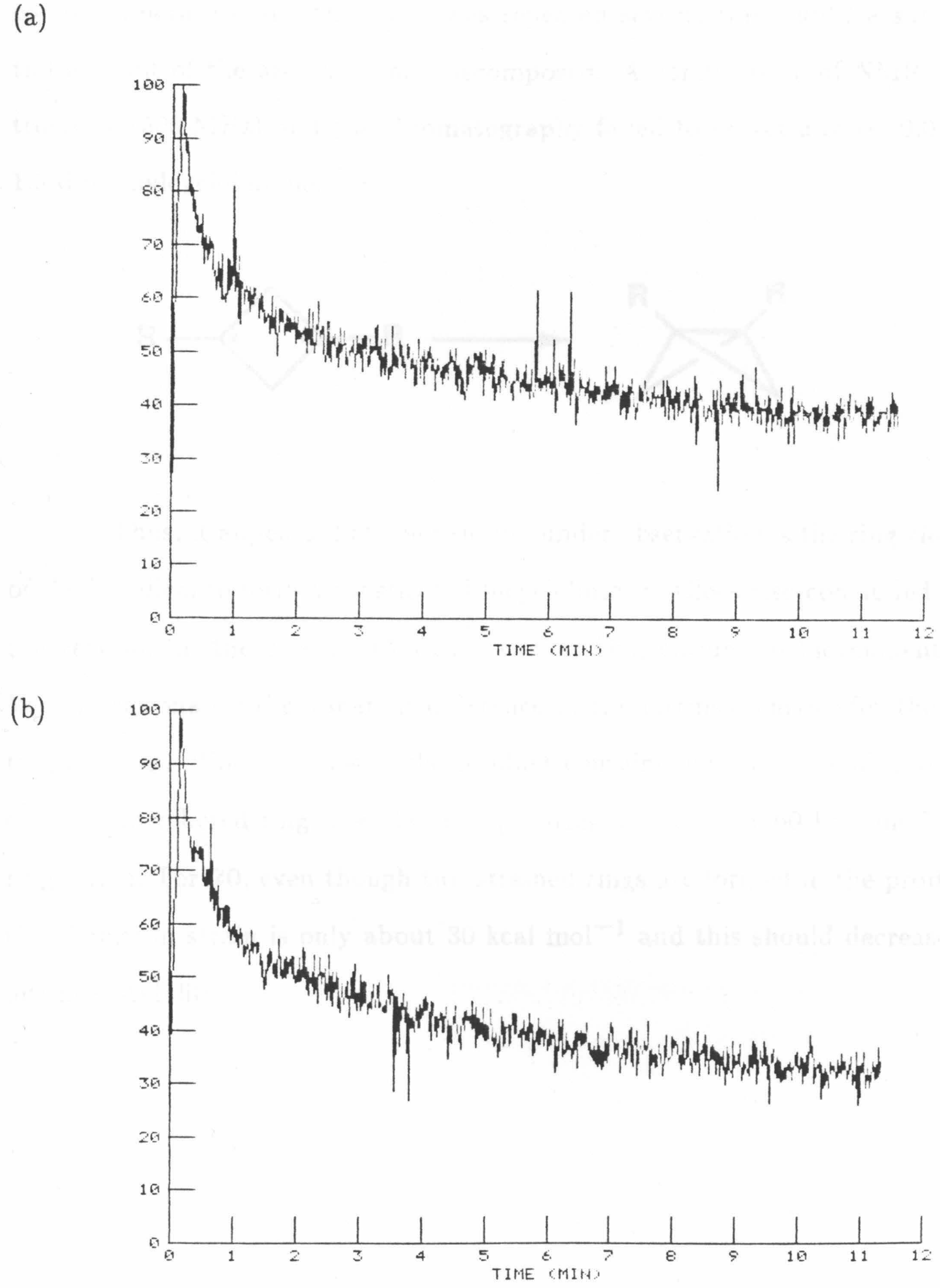

Figure 31. Intensity vs. time plots for the decay of **20** in (a) acetone and (b) acetone-d_6 at 4 K.

room temperature and this cycle was repeated several times until a substantial amount of the azoalkane had decomposed. A combination of NMR spectroscopy (500-MHz) and gas chromatography failed to detect any (< 0.05 %) 1,3-dimethylcyclobutene.[37]

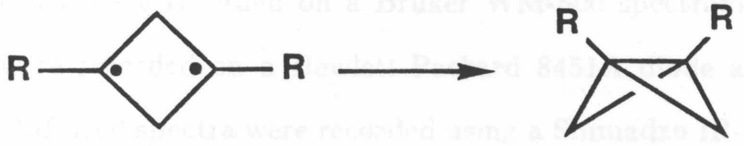

Thus, it appears that the reaction under observation is the ring closure of the biradical to form a substituted bicyclobutane. Closs also concluded that the reaction in the case of **11** was a similar ring closure to bicyclopentane. We can rationalize the apparent difference in the intrinsic barrier for the two ring systems. When **11** closes, the product contains one three-membered and one four-membered ring, thereby incorporating an extra 55–60 kcal mol^{-1} in ring strain. For **20**, even though two strained rings are formed in the product, the change in strain is only about 30 kcal mol^{-1} and this should decrease its intrinsic stability.

EXPERIMENTAL SECTION

General. ^{1}H NMR spectra were recorded on a Varian EM–390 spectrometer. Fourier transform NMR spectra (^{1}H and ^{13}C) were recorded on a JEOL FX-90Q or GX-400 spectrometer, or a Varian XL-200 spectrometer, and 500-MHz ^{1}H NMR spectra were recorded on a Bruker WM-500 spectrometer. Ultraviolet spectra were recorded on a Hewlett-Packard 8451A diode array spectrophotometer. Infrared spectra were recorded using a Shimadzu IR-435 or a Mattson Instruments Sirius 100 FT-IR spectrometer fitted with a Starlab minicomputer. Mass spectra were obtained by the Caltech Analytical Facility. Analytic gas chromatography was performed on a Hewlett-Packard 5840A chromatograph equipped with a flame-ionization detector. Preparative gas chromatography was performed on a Varian Aerograph Model 920 chromatograph with a thermal conductivity detector.

1,7-Dicarbomethoxy-4-methyl-2,4,6-triazatricyclo[5.1.1.0^{2,6}]nonane-3,5-dione (54). A methylene chloride solution of 1,3-dicarbomethoxybicyclobutane (3.29 g, 19.4 mmol) and MTAD (2.74 g, 24.3 mmol) was photolyzed with a Hanovia 450-W medium-pressure, mercury arc lamp and a Pyrex filter. Filtration and recrystallization from ethyl acetate afforded 3.28 g (11.6 mmol, 60%) of **54** as a white solid; mp 176.5–177.5°C; ^{1}H NMR (CDCl$_3$) δ 2.26 (m, 2H), 2.69 (m, 2H), 3.03 (s, 3H), 3.85 (s, 6H); ^{13}C NMR (CDCl$_3$) δ 26.0 (NCH$_3$), 45.0 (CH$_2$), 53.2 (OCH$_3$), 68.9 (bridgehead), 159.7 (NCO), 164.4 (OCO); IR (CHCl$_3$) 3037, 2956, 1793, 1750 (sh), 1719, 1442, 1397, 1322, 1237, 1163, 1066 cm^{-1}; UV (CH$_2$Cl$_2$) λ_{max} 246 nm (ϵ=270); mass spectrum (EI) m/e 283, 251, 224, 194, 168, 167 (100), 166, 152, 139, 135; anal. C,H,N.

1,7-Bis(hydroxymethyl)-4-methyl-2,4,6-triazatricyclo[5.1.1.0^{2,6}]non-

ane-3,5-dione (55). Sodium borohydride (2.85 g, 75.3 mmol) was added carefully to a stirred suspension of **54** (2.13 g, 7.53 mmol) in 50 mL methanol. The resulting solution was refluxed under nitrogen for 2 h. After cooling to room temperature, 3N hydrochloric acid (ca. 20 mL) was added to neutralize the solution. The methanol was removed by rotary evaporation and the resulting aqueous solution freeze-dried. Extraction with ethanol and flash chromatography[38] (9:1 methylene chloride, ethanol; $R_f = 0.35$) gave 1.31 g (5.77 mmol, 77%) of **55** as a colorless oil; ^{1}H NMR ($CDCl_3$) δ 1.92 (m, 4H), 2.98 (s, 3H), 3.72 (t, 2H), 4.03 (d, 4H); ^{13}C NMR ($CDCl_3$) δ 26.1 (NCH_3), 42.8 (CH_2), 60.2 (CH_2O), 73.6 (bridgehead), 160.8 (CO); IR ($CDCl_3$) 3440, 2930, 1760, 1692, 1550, 1265 cm^{-1}; exact mass calcd 227.0906, found 227.0907.

1,7-Bis((methylsulfonyloxy)methyl)-4-methyl-2,4,6-triazatricyclo-[5.1.1.0^{2,6}]nonane-3,5-dione (56). A mixture of diol **55** (370 mg, 1.63 mmol) and triethylamine (0.68 mL, 495 mg, 4.89 mmol) in 25 mL methylene chloride was cooled in an ice–water bath. Under an atmosphere of nitrogen, mesyl chloride (0.28 mL, 411 mg, 3.58 mmol) was then added dropwise over a period of 5 min. After stirring for 0.5 h the heterogeneous reaction mixture was washed with 10 mL each of cold water, cold 10% hydrochloric acid, cold saturated sodium bicarbonate solution and cold saturated sodium chloride solution. The methylene chloride layer was separated and dried over magnesium sulfate, filtered and rotovapped to give 602 mg (1.57 mmol, 94%) of a white solid; ^{1}H NMR ($CDCl_3$) δ 1.93 (m, 2H), 2.39 (m, 2H), 3.03 (s, 3H), 3.08 (s, 6H), 4.80 (s, 4H).

1,7-Bis(iodomethyl)-4-methyl-2,4,6-triazatricyclo[5.1.1.0^{2,6}]nonane-3,5-dione (57). A mixture of **56** (601 mg, 1.57 mmol) and sodium iodide (1.18 g, 7.85 mmol) in 50 mL of 2-butanone was brought to reflux under a nitrogen atmosphere. After 1 h the heterogeneous mixture was rotovapped and the yellow solid was extracted with 50 mL ether. The solution was then washed with 25 mL of water and 25 mL of a 10% solution of sodium thiosulfate, dried over magnesium sulfate, filtered and rotovapped to obtain 609 mg (1.36 mmol, 85%) of the product as a white solid; ^{1}H NMR ($CDCl_3$) δ 1.88 (m, 2H), 2.26 (m, 2H), 3.03 (s, 3H), 3.82 (s, 4H); UV ($CDCl_3$) λ_{max} 265 nm.

1,7-Diethyl-4-methyl-2,4,6-triazatricyclo[5.1.1.0^{2,6}]nonane-3,5-dione (58). To a 500-mL flask charged with copper(I) bromide–dimethyl sulfide complex (9.11 g, 44.3 mmol) and 90 mL diethyl ether, and maintained at 0°C under a nitrogen atmosphere, 56 mL of a 1.6 M solution of methyllithium in diethyl ether (88.0 mmol) was added slowly. A yellow precipitate first appeared and then disappeared. Diiodide **57** (990 mg, 2.21 mmol) in 50 mL ether and 10 mL methylene chloride (for solubility) was then added dropwise over a period of 15 min. The reaction was stopped after another 15 min when all the starting material and the monoiodide were gone (TLC). After quenching with 75 mL of a saturated solution of ammonium chloride and warming to room temperature, the organic layer was separated, washed with water and dried over magnesium sulfate. Filtration, removal of solvent and flash chromatography[38] (1:1 ether, petroleum ether; R_f=0.35) gave 117 mg (0.5 mmol, 26%) of **58** as a colorless oil; ^{1}H NMR ($CDCl_3$) δ 1.00 (t, 6H), 1.62 (m, 2H), 1.75 (m, 2H), 2.09 (q, 4H), 2.96 (s, 3H); ^{13}C NMR ($CDCl_3$) δ 9.3 (CH_3), 22.2 (CH_2), 25.5 (NCH_3), 43.6 (CH_2), 74.5 (bridgehead), 159.8 (CO); exact mass calcd 223.1321, found 223.1319.

1,7-Bis(pyruvoyloxymethyl)-4-methyl-2,4,6-triazatricyclo[5.1.1.0^{2,6}]-nonane-3,5-dione (59).[7] To a solution of diol **55** (1.54 g, 6.8 mmol) in 10 mL methylene chloride was added pyruvic acid (1.74 g, 19.8 mmol) and 4-

pyrrolidinopyridine (ppy, 200 mg, 1.3 mmol). 1,3-Dicyclohexylcarbodiimide (DCC, 4.08 g, 19.8 mmol) was then added carefully to this solution.[11] The reaction was extremely vigorous and was stopped after 20 min. Filtration, removal of solvent and flash chromatography[38] over carefully dried (overnight in oven) silica (1:1 ethyl acetate, methylene chloride; $R_f = 0.36$) gave 2.44 g (6.6 mmol, 98%) of **59** in the form of a yellow oil (98%); ^{1}H NMR ($CDCl_3$) δ 1.85 (m, 2H), 2.3 (m, 2H), 2.4 (s, 4H), 2.98 (s, 3H), 4.85 (s, 6H); ^{13}C NMR ($CDCl_3$) δ 26.5 (NCH_3), 33.3 (CH_3), 42.7 (CH_2), 61.2 (OCH_2), 70.3 (bridgehead), 159.6 and 159.8 (CO_2 and CON) , 190.7 (CO).

1,7-Diethyl-4-methyl-2,4,6-triazatricyclo[5.1.1.0^{2,6}]nonane-3,5-dione (58). A solution of dipyruvate **59** (100 mg, 0.27 mmol) in 250 mL benzene (freshly distilled from calcium hydride under nitrogen) was photolyzed for 3 h with a Hanovia 450-W medium-pressure, mercury arc lamp and a Pyrex filter.[11b] The solution was poured into a 500 mL flask and the solvent was removed until only about 40 mL remained. This dialdehyde solution was degassed and kept under a nitrogen atmosphere to be used later on.

To a degassed suspension of methyltriphenylphosphonium bromide (486 mg, 1.36 mmol) in 40 mL benzene (freshly distilled from calcium hydride under nitrogen) was added a 1.47 M solution of *n*-butyllithium (0.83 mL, 1.23 mmol) and the yellow reaction mixture allowed to stir for 1 h. The dialdehyde solution prepared previously was then added to the stirred ylide solution via cannula. The reaction mixture turned an orange-rust color. After 20 min, 25 mL of 5% aqueous hydrochloric acid was added and the color disappeared. The layers were separated and the aqueous layer was extracted with diethyl ether (2 x 50 mL). The combined organic layer was washed with 20 mL each of 5% hydrochloric acid, a saturated solution of sodium bicarbonate, and water. This solution was then dried over magnesium sulfate, filtered, rotovapped and flash chromatographed[38] to obtain 31.2 mg (0.14 mmol, 52%) of the diene as a colorless oil; ^{1}H NMR ($CDCl_3$) δ 2.05 (m, 2H), 2.19 (m, 2H), 3.02 (s, 3H), 5.40 (m, 4H), 6.45 (m, 2H). The oil was dissolved in 10 mL ethyl acetate and a pinch of palladium on carbon catalyst was added. Hydrogenation on a Parr shaker (45 psi, 1 h), filtration through Celite and removal of solvent gave clean urazole **58** as a colorless oil.

1,4-Diethyl-2,3-diazabicyclo[2.1.1]hex-2-ene (18). To a hot solution (40–45°C) of potassium hydroxide (50 mg, 86%, 0.75 mmol) in 1 mL 2-propanol (previously flushed with nitrogen for 15 min) was added **58** (25 mg, 0.1 mmol) and the mixture was refluxed under nitrogen for 2 h and subsequently cooled in an ice–water bath. The reaction mixture was acidified using 3 N hydrochloric acid, warmed to about 40°C for 10 min, cooled to room temperature, and neutralized with 1 N ammonium hydroxide. A solution of cupric bromide (56 mg, 0.25 mmol) in 1 mL water was added dropwise with gentle stirring. The pH was adjusted to about 6 using 1 N ammonium hydroxide and the reaction flask was kept at room temperature for 1 h. Reddish-brown crystals of the copper complex separated and were filtered, washed (with water and diethyl ether) and air dried. To a suspension of the complex in 30 mL of diethyl ether was added 25 mL of 1 N ammonium hydroxide at 0°C with vigorous stirring. The ethereal layer was separated and the aqueous layer was extracted with ether. The combined organic phase was dried over magnesium sulfate. After filtration, the ether was distilled off through a 10 cm Vigreaux column. Care was taken not to heat the solution over 40°C. When about 1.5 mL of the solution remained, the distillation was stopped, and pure **18** was isolated by preparative gas chromatography. A 10 ft x 1/4 in. column of 10 % UCW-

982 on Chromosorb WAW-DMCS mesh size 80/100 was used. At a column temperature of 85°C and a helium flow of 120 mL min^{-1}, the retention time for **18** was 14 min and the product was isolated as a colorless oil; ^{1}H NMR (acetone-d_6) δ 1.07 (t, 6H), 1.77 (m, 2H), 1.98 (m, 2H), 2.13 (q, 4H); ^{13}C NMR ($CDCl_3$) δ 10.7 (CH_3), 23.0 (CH_2), 60.5 (CH_2), 88.9 (bridgehead); UV (ether) λ_{max} 344 nm.

1,7-Dipropyl-4-methyl-2,4,6-triazatricyclo[5.1.1.0^{2,6}]nonane-3,5-dione (60). A solution of dipyruvate **59** (105 mg, 0.29 mmol) in 250 mL benzene (freshly distilled from calcium hydride under nitrogen) was photolyzed for 3 h with a Hanovia 450-W medium-pressure, mercury arc lamp and a Pyrex filter.[11b] The solution was poured into a 500 mL flask and the solvent was removed until only about 40 mL remained. This dialdehyde solution was degassed and kept under a nitrogen atmosphere.

To a degassed suspension of ethyltriphenylphosphonium bromide (456 mg, 1.23 mmol) in 40 mL benzene (freshly distilled from calcium hydride under nitrogen) was added a 1.47 M solution of *n*-butyllithium (0.72 mL, 1.06 mmol) and the yellow reaction mixture allowed to stir for 1 h. The dialdehyde solution was then added to the stirred ylide solution via cannula. The reaction mixture turned an orange-rust color. After 20 min, 25 mL of 5% aqueous hydrochloric acid was added and the color disappeared. The layers were separated and the aqueous layer extracted with diethyl ether (2 x 50 mL). The combined organic layer was washed with 20 mL each of 5% hydrochloric acid, saturated sodium bicarbonate solution, and water. The solution was dried over magnesium sulfate, filtered and rotovapped to obtain 43 mg of crude diene. The oil was dissolved in 10 mL ethyl acetate and a pinch of palladium on carbon catalyst was added. Hydrogenation on a Parr shaker (45 psi, 1 h), filtration through

Celite and removal of solvent gave 41.1 mg (0.16 mmol, 56%) of clean urazole **60** as a colorless oil; ^{1}H NMR ($CDCl_3$) δ 0.95 (t, 6H), 1.49 (m, 4H), 1.67 (m, 2H), 1.86 (m, 2H), 2.05 (m, 4H), 2.98 (s, 3H); ^{13}C NMR ($CDCl_3$) δ 14.4 (CH_3), 18.8 (CH_2), 25.7 (NCH_3), 31.3 (CH_2), 44.9 (bridging CH_2), 73.8 (bridgehead), 159.3 (CO).

1,4-Dipropyl-2,3-diazabicyclo[2.1.1]hex-2-ene (19). To a hot solution (40–45°C) of potassium hydroxide (80 mg, 86%, mmol) in 0.5 mL 2-propanol (previously flushed with nitrogen for 15 min) was added **60** (41 mg, 0.16 mmol) and the mixture was refluxed under nitrogen for 2 h and subsequently cooled in an ice–water bath. The reaction mixture was acidified using 3 N hydrochloric acid, warmed to about 40°C for 10 min, cooled to room temperature, and neutralized with 1 N ammonium hydroxide. A solution of cupric bromide (91 mg, 0.41 mmol) in 0.5 mL water was added dropwise with gentle stirring. The pH was adjusted to about 6 using 1 N ammonium hydroxide and the reaction flask was kept at room temperature for 1 h. Reddish-brown crystals of the copper complex separated and were filtered, washed (with water and diethyl ether) and air dried. To a suspension of the complex in 30 mL of diethyl ether was added 25 mL of 1 N ammonium hydroxide at 0°C with vigorous stirring. The ethereal layer was separated and the aqueous layer was extracted with ether. The combined organic phase was dried over magnesium sulfate. After filtration, the ether was distilled off through a 10 cm Vigreaux column. Care was taken not to heat the solution over 40°C. When about 1.5 mL of the solution remained, the distillation was stopped, and pure **19** was isolated by low temperature recrystallization although the crystals melted when brought up to room temperature; ^{1}H NMR (C_6D_6) δ 0.90 (t, 6H), 1.11 (m, 2H), 1.41 (app sextet, 4H), 1.84 (m, 4H), 1.93 (app t, 4H); ^{13}C NMR (C_6D_6) δ 15.1 (CH_3), 20.3 (CH_2), 32.7 (CH_2), 61.5 (CH_2), 87.9 (bridgehead); UV (ether) λ_{max} 346 nm.

1,7-Bis(hydroxydideuteriomethyl)-4-methyl-2,4,6-triazatricyclo-[5.1.1.0^{2,6}]nonane-3,5-dione (62). Sodium borodeuteride was used in the procedure for the synthesis of **55** to obtain **62**.

1,7-Bis((methylsulfonyloxy)dideuteriomethyl)-4-methyl-2,4,6-triazatricyclo[5.1.1.0^{2,6}]nonane-3,5-dione (63). The tetradeuteriodiol **62** was used in the procedure for the synthesis of **56** to obtain **63**.

1,7-Bis(trideuteriomethyl)-4-methyl-2,4,6-triazatricyclo[5.1.1.0^{2,6}]-nonane-3,5-dione (64). To a solution of **63** (106 mg, 0.27 mmol) in 6 mL hexamethylphosphoric triamide was added sodium borodeuteride (67 mg, 1.62 mmol) and the mixture stirred at room temperature for 32 h. After quenching with 10 mL of a saturated solution of sodium chloride, the reaction mixture was extracted with diethyl ether (3 x 15 mL). The organic layer was dried over magnesium sulfate, filtered, rotovapped and flash chromatographed[38] to obtain 51 mg (0.25 mmol, 91%) of **64** as a colorless oil. The ^1H NMR spectrum showed that deuterium incorporation was about 95%.

1,4-Bis(trideuteriomethyl)-2,3-diazabicyclo[2.1.1]hex-2-ene(17). The urazole **64** was used in the procedure for synthesis of **16** (see Chapter II) to obtain **17**.

ESR Experiments. A Varian E-line Century Series X-band spectrometer equipped with an Oxford Instruments ESR-900 continuous liquid-helium flow cryostat was used to obtain ESR spectra at low temperatures. The temperature at the sample was measured before and after each experiment using a calibrated carbon-glass thermistor (Lakeshore Cryotronics) placed inside a sample tube. During each experiment the temperature was monitored continuously by a gold-chromel thermocouple fixed 1 cm below the sample in the quartz dewar. Temperature was varied using either the helium flow rate or the automatic DTC2 temperature controller.

An Oriel 1000-W mercury-xenon arc lamp was focussed into the microwave cavity for photolysis. Various optical filters (Schott, Corning, Oriel) or a grating monochromator (Oriel model 77250) were used to obtain narrow bands of light of the desired wavelength range.

Samples were prepared from solutions of 2–3 mg of azoalkanes in 300 μL of solvent (MTHF used was freshly distilled from benzophenone-ketyl). The solution was placed in 4 mm o.d. quartz ESR tubes equipped with high-vacuum stopcocks. Tubes were then degassed (three freeze–pump–thaw cycles), frozen in liquid nitrogen and inserted into the ESR cavity.

Decay curves were obtained by irradiating for a short time (10–60 s) while holding the magnetic field constant at the top of the first derivative peak of the $\Delta m_s = 2$ transition and scanning over time. Similar curves were obtained when the magnetic field was held constant at a value corresponding to one of the peaks in the $\Delta m_s = 1$ region.

Detection limits on 1,3-dimethylcyclobutene. ESR allows detection of extremely small amounts of material and our signals correspond to about 10^{-7} moles.[39] However, we accumulated at least 10^{-5} moles of product by repeated photolysis of the sample which originally contained ca. 3 mg of azoalkane. By gas chromatography we were able to detect 1 mg of an authentic sample of 1,3-dimethylcyclobutene in 400 mL of solvent. Thus, we could have detected 0.05 % of the substituted cyclobutene in the ESR sample.

References for Chapter III

1. (a) Trimethylenemethane: Dowd, P. *Acc. Chem. Res.* **1972**, *5*, 242–248. Dowd, P.; Chow, M. *Tetrahedron* **1982**, *38*, 799–807. (b) 2-Alkylidene-1,3-cyclopentanediyls: Berson, J.A. *Acc. Chem. Res.* **1978**, *11*, 446–453. (c) *m*-Xylylene and *m*-Quinomethane: Rule, M.; Matlin, A.R.; Seeger, D.E.; Hilinski, E.F.; Dougherty, D.A.; Berson, J.A. *Tetrahedron* **1982**, *38*, 787–798. (d) 1,8-Naphthoquinomethane and related structures: Platz, M.S.; Carrol, G.; Pierrat, F.; Zayas, J.; Auster, S. *Tetrahedron* **1982**, *38*, 777–785. (e) Tetramethyleneethanes: Dowd, P. *J. Am. Chem. Soc.* **1970**, *92*, 1066–1068. Roth, W.R.; Erker, G. *Angew. Chem., Intl. Ed. Engl.* **1973**, *12*, 503–504.
2. Buchwalter, S.L.; Closs, G.L. *J. Am. Chem. Soc.* **1979**, *101*, 4688–4694.
3. Chang, M.H.; Dougherty, D.A. *J. Org. Chem.* **1981**, *46*, 4092–4093.
4. Chang, M.H.; Dougherty, D.A. *J. Am. Chem. Soc.* **1982**, *104*, 2333–2334.
5. Turro, N.J.; Renner, C.A.; Waddell, W.H.; Katz, T.J. *J. Am. Chem. Soc.* **1976**, *98*, 4320–4322. Turro, N.J. *Modern Molecular Photochemistry*; Benjamin/Cummings: Menlo Park, CA, 1978; pp 548–549.
6. Compound **53** was identified on the basis of spectral data and its comparison with the parent **15**.[4]
7. Sponsler, M.B. Ph.D. Dissertation, California Institute of Technology, 1987.
8. Coffey, C.E. U.S. Patent 3 657 317, 1972.
9. Brown, M.S.; Rapoport, H. *J. Org. Chem.* **1963**, *28*, 3261–3263.
10. Ireland, R.E.; Daub, J.P. *J. Org. Chem.* **1981**, **46**, 479–485.

11. Hassner, A.; Alexanian, V. *Tetrahedron Lett.* **1978**, *46*, 4475–4478.

12. Binkley, R.W. *J. Org. Chem.* **1976**, *41*, 3030–3031. Leermakers, P.A.; Warren, P.C.; Vesley, G.F. *J. Am. Chem. Soc.* **1964**, *86*, 1768–1771.

13. Hutchins, R.O.; Kandasamy, D.; Dux, F., III; Maryanoff, C.A.; Rotstein, D.; Goldsmith, B.; Burgoyne, W.; Cistone, F.; Dalessandro, J.; Puglis, J. *J. Org. Chem.* **1978, 43**, 2259–2267.

14. Wertz, J.E.; Bolton, J.R. *Electron Spin Resonance: Elementary Theory and Practical Applications*; McGraw Hill: New York, 1972; pp 223–257. Also Wasserman, E.; Snyder, L.C.; Yager, W.A. *J. Chem. Phys.* **1964**, *41*, 1763–1772.

15. Rule, M.; Matlin, A.R.; Seeger, D.E.; Hilinski, E.F.; Dougherty, D.A.; Berson, J.A. *Tetrahedron* **1982**, *38*, 787–798.

16. Higuchi, J. *J. Chem. Phys.* **1963**, *38*, 1237–1245. Higuchi, J. *J. Chem. Phys.* **1964**, *39*, 1847–1852.

17. Kottis, P.; Lefebvre, R. *J. Chem. Phys.* **1963**, *39*, 393–403. Kottis, P.; Lefebvre, R. *J. Chem. Phys.* **1964**, *41*, 379–393.

18. Fischbeck, H.J.; Fischbeck, K.H. *Formulas, Facts and Constants*; Springer Verlag: New York, 1982; pp 34–35.

19. The computer program was a FORTRAN version of the original BASIC program written by Dr. J.M. McBride (Yale University) and made available by Dr. E.F. Hilinski (Florida State University) which was modified to run on an IBM PC.

20. Conrad, M.P.; Pitzer, R.M.; Schaefer, H.F., III *J. Am. Chem. Soc.* **1979**, *101*, 2245–2246.

21. Coms, F.D., unpublished results.

22. Snyder, G.J.; Dougherty, D.A. *J. Am. Chem. Soc.* **1985**, *107*, 1774–

1775.

23. Muller, J.-F.; Muller, D.; Dewey, H.J.; Michl, J. *J. Am. Chem. Soc.* **1978**, *100*, 1629–1630.

24. Hirota, N.; Hutchison, C.A., Jr.; Palmer, P. *J. Chem. Phys.* **1964**, *40*, 3717–3725. Dowd, P.; Gold, A.; Sachdev, K. *J. Am. Chem. Soc.* **1968**, *90*, 2715–2716. Claesson, O.; Lund, A.; Gillbro, T.; Ichikawa, T.; Edlund, O.; Yoshida, H. *J. Chem. Phys.* **1980**, *72*, 1463–1470.

25. Grivet, J.-Ph. *Mol. Phys.* **1970**, *19*, 389–398. de Groot, M.S.; Van der Waals, J.H. *Mol. Phys.* **1960**, *3*, 190–200. de Groot, M.S.; Van der Waals, J.H. *Mol. Phys.* **1959**, *2*, 333–340.

26. Fessenden, R.W.; Schuler, R.H. *J. Chem. Phys.* **1963**, *39*, 2147–2195.

27. Fischer, H. In *Free Radicals*; Kochi, J.K., Ed.; Wiley: New York, 1973; Vol. II, pp 446–448.

28. French, W.G.; Willard, J.E.; *J. Phys. Chem.* **1968**, *72*, 4604–4608. Sprague, E.D. *J. Phys. Chem.* **1973**, *77*, 2066–2070. Neiss, M.A.; Willard, J.E. *J. Phys. Chem.* **1975**, *79*, 783–791. Hudson, R.L.; Shiotan, M.; Williams, F. *Chem. Phys. Lett.* **1977**, *48*, 193–195.

29. Austin, R.H.; Beeson, K.; Eisenstein, L.; Frauenfelder, H.; Gunsalus, I.C.; Marshall, V.P. *Phys. Rev. Lett.* **1974**, *32*, 403–405.

30. Doba, T.; Ingold, K.U.; Siebrand, W. *Chem. Phys. Lett* **1984**, *103*, 339–342. Doba, T.; Ingold, K.U.; Siebrand, W.; Wildman, T.A. *Faraday Discuss. Chem. Soc.* **1984**, *78*, 175–191. Doba, T.; Ingold, K.U.; Siebrand, W.; Wildman, T.A. *J. Phys. Chem.* **1984**, *88*, 3165–3167.

31. Margenau, H.; Murphy, G.M. *The Mathematics of Physics and Chemistry*; D Van Nostrand: New Jersey, 1964.

32. Bevington, P.R. *Data Reduction and Error Analysis for Physical Sci-*

ences; McGraw Hill: New York, 1969; pp 43–49.

33. Goldanskii, V.I. *Ann. Rev. Phys. Chem.* **1976**, *27*, 85–126. Le Roy, R.J.; Murai, H.; Williams, F. *J. Am. Chem. Soc.* **1980**, *102*, 2325–2334. Eisenstein, L. *Int. J. Quantum Chem.* **1976**, 21–27.

34. Barton, D.H.R.; Charpiot, B.; Ingold, K.U.; Johnston, L.J.; Motherwell, W.B.; Scaiano, J.C.; Stanforth, S. *J. Am. Chem. Soc.* **1985**, *107*, 3607–3611.

35. Bell, R.P. *The Tunnel Effect in Chemistry*; Chapman and Hall: New York, 1980. Bell, R.P. *Trans. Faraday Soc.* **1959**, *55*, 1–4. Caldin, E.F. *Chem. Rev.* **1969**, *69*, 135–156.

36. Platz, M.S.; Senthilnathan, V.P.; Wright, B.B.; McCurdy, C.W., Jr. *J. Am. Chem. Soc.* **1982**, *104*, 6494–6501.

37. Authentic samples of 1,3-dimethylcyclobutene were prepared using the procedure of Crowley, K.J. *Tetrahedron* **1965**, *12*, 1001–1014.

38. Still, W.C.; Kahn, M.; Mitra, A. *J. Org. Chem.* **1978**, *43*, 2923–2925.

39. Determined for **3** by direct spin-counting technique. Snyder, G.J.; Dougherty, D.A., unpublished results.

APPENDIX B

SOURCE LISTING OF COMPUTER PROGRAMS

```
C     ++++++++++++++++++++++++++++++++++++++++++++++++++++++++++++++++
C
C            TRIPLET ESR POWDER SPECTRUM SIMULATION PART I
C
C     Originally written in BASIC by J.M. McBride (Yale University).
C     Obtained from E.F. Hilinski (Florida State University).
C     Adapted for use on IBM PC/AT by Rakesh Jain.
C     Based on the method developed by P. Kottis and R. Lefebvre in
C     J. Chem. Phys. 39, 393 (1963); 41, 379 (1964).
C     See also E. Wasserman, L.C. Snyder, and W.A. Yager in
C     J. Chem. Phys. 41, 1763 (1964).
C
C     This part calculates resonance fields for a number of different
C     orientations of the molecule with respect to the magnetic field.
C
C     ++++++++++++++++++++++++++++++++++++++++++++++++++++++++++++++++
C
      DIMENSION FIELD(250),COUNT(250),H(10000,3)
      REAL N
      INTEGER T5
      PI=3.141592654
C
C     ++++++++++++++++++++++++++++++++++++++++++++++++++++++++++++++++
C
C     INPUT is from data file TRIPLET1.IN
C     The first line contains D and E values (in 1/cm)
C     The second line contains the frequency of the spectrometer in MHz.
C     The third line contains values for the step size for changing the
C     angles THETA and PHI (in deg). Values of 2.00 work well for both.
C     CMSTEP is used to generate a number of values of PHI according to
C     the cos(THETA) dependence.
C     OUTPUT is to data file TRIPLET1.OUT
C
C     ++++++++++++++++++++++++++++++++++++++++++++++++++++++++++++++++
C
      OPEN (3,FILE='TRIPLET1.IN',STATUS='OLD')
      OPEN (1,FILE='TRIPLET1.OUT',STATUS='UNKNOWN')
      READ (3,100) D,E
      WRITE (1,145)
      WRITE (1,100) D,E
      D=D*29979.
      E=E*29979.
      X=D/3.+E
      Y=D/3.-E
      Z=-2.*D/3.
```

```
      READ (3,101) DEL
      WRITE (1,146)
      WRITE (1,101) DEL
      WRITE (1,147)
      READ (3,100) TSTEP,CMSTEP
      WRITE (1,100) TSTEP,CMSTEP
      READ (3,99) GX,GY,GZ
      WRITE (1,98)
      WRITE (1,99) GX,GY,GZ
      READ (3,5) HMIN,HMAX
      WRITE (1,4)
    4 FORMAT ( ' HMIN    HMAX')
      WRITE (1,5) HMIN,HMAX
    5 FORMAT (2F8.2)
      O=X*Y*Z
      P1=X*Y+X*Z+Y*Z
      WRITE (1,102)
  102 FORMAT( '  THETA    PHI      T5   H(T5,1)  H(T5,2)  H(T5,3)')
      T5=1
      C1=90./CMSTEP
      T=0.0
      CSTEP=22.5
      DO 41 T=0.,90.,TSTEP
      IF(T.EQ.0.0) GO TO 39
      CSTEP=90.0/(COS((90.-T)*PI/180.)*C1)
   39 DO 40 C=0.,90.-CSTEP,CSTEP
      N=X*(SIN(T*PI/180.)*COS(C*PI/180.))**2
     &+Y*(SIN(T*PI/180.)*SIN(C*PI/180.))**2
     &+Z*(COS(T*PI/180.))**2
      P= -(2*(DEL**2+P1)+(DEL**2+4.*P1)/4.)-(27./4.)*N**2
      Q= (DEL**2+P1)**2+((DEL**2+4.*P1)*(DEL**2+P1))/2.+(27./2.)*O*N
      R= -((DEL**2+4.*P1)*(DEL**2+P1)**2+27.*O**2)/4.
C
C     ++++++++++++++++++++++++++++++++++++++++++++++++++++++++++++++++++++
C
C     We have converted the equation representing the resonance fields
C     into the form Y**3 + P*Y**2 + Q*Y + R = 0
C     We shall now convert this into an equation of the form
C     Y**3 + A*Y + B = 0 whose solutions are known. For details see
C     H.J. Fischbeck and K.H. Fischbeck in " Formulas, Facts and
C     Constants" Springer Verlag: New York 1982.
C
C     ++++++++++++++++++++++++++++++++++++++++++++++++++++++++++++++++++++
C
```

```
      A=Q-P**2/3.
      B=P**3/13.5-P*Q/3.+R
      A1=(180./PI)*ACOS(-B/(2*((-A)**1.5/(SQRT(27.)))))/3.
      E=2.*SQRT(-A/3.)
      GTC=GX*(SIN(T*PI/180.)*COS(C*PI/180.))**2
     &+GY*(SIN(T*PI/180.)*SIN(C*PI/180.))**2
     &+GZ*(COS(T*PI/180.))**2
      B1=1.39968*GTC
      H(T5,1)=(SQRT(E*COS(PI/180.*(A1))-P/3.))/B1
      H(T5,2)=(SQRT(E*COS(PI/180.*(120.+A1))-P/3.))/B1
      H(T5,3)=(SQRT(E*COS(PI/180.*(240.+A1))-P/3.))/B1
      WRITE (1,103)T,C,T5,H(T5,1),H(T5,2),H(T5,3)
      T5=T5+1
      IF (T.LT.0.5) GO TO 41
   40 CONTINUE
   41 CONTINUE
      WRITE (1,150)
  150 FORMAT(25X,'-1.0')
   98 FORMAT( '   G(XX)     G(YY)     G(ZZ) ')
   99 FORMAT(3F10.7)
  100 FORMAT(F8.6,1X,F8.6)
  101 FORMAT(F8.2)
  145 FORMAT( ' D(1/cm) E(1/cm)')
  146 FORMAT( ' hnu(MHz)')
  147 FORMAT( '   TSTEP   CMSTEP')
  500 FORMAT(1X,F8.2)
  700 FORMAT(1X,2F8.2)
  103 FORMAT(1X,F7.2,1X,F7.2,1X,I7,3(1X,F8.2))
      END
```

```
C     ++++++++++++++++++++++++++++++++++++++++++++++++++++++++++++++++++
C             TRIPLET ESR POWDER SPECTRUM SIMULATION PART II
C
C     This part of the program adds the number of times that each
C     resonance field occurs (as calculated by part I of the simulation
C     program POWFIELD).
C     Originally written in BASIC by J.M. McBride (Yale University).
C     Obtained from E.F. Hilinski (Florida State University).
C     Adapted for use on IBM PC/AT by Rakesh Jain.
C
C     ++++++++++++++++++++++++++++++++++++++++++++++++++++++++++++++++++
C
      DIMENSION FIELD(250),COUNT(250),H(10000,3)
      REAL N
      INTEGER T5,T6
      PI=3.141592654
C
C     ++++++++++++++++++++++++++++++++++++++++++++++++++++++++++++++++++
C
C     INPUT from the file generated by TRIPLET1 i.e., TRIPLET1.OUT
C     Generates an OUTPUT file called TRIPLET2.OUT
C     The output consists of: D,E,DEL,TSTEP,CMSTEP,GX,GY,GZ,HMIN,HMAX
C     and a list of data point number (I), the correspoding magnetic
C     field strength given by HMIN+(I-1.0)*HSTEP, and the number of
C     times resonance occurs at that field strength given by COUNT(I).
C
C     ++++++++++++++++++++++++++++++++++++++++++++++++++++++++++++++++++
C
      OPEN (1,FILE='TRIPLET1.OUT',STATUS='OLD')
      OPEN (4,FILE='TRIPLET2.OUT',STATUS='UNKNOWN')
      READ (1,3)
    3 FORMAT(A70)
      READ (1,4) D,E
      WRITE (4,4) D,E
      READ (1,3)
      READ (1,8) DEL
      WRITE (4,8) DEL
      READ (1,3)
      READ (1,4) TSTEP,CMSTEP
      WRITE (4,4) TSTEP,CMSTEP
    4 FORMAT (F8.6,1X,F8.6)
    8 FORMAT (F8.2)
      READ (1,3)
      READ (1,6) GX,GY,GZ
      WRITE (4,6) GX,GY,GZ
```

```
    6 FORMAT(3F10.7)
      READ (1,3)
      READ (1,5) HMIN,HMAX
      WRITE (4,5) HMIN,HMAX
    5 FORMAT (2F8.2)
      READ (1,3)
      DO 10 I=1,10000
      READ (1,103)H(I,1),H(I,2),H(I,3)
  103 FORMAT (24X,3(1X,F8.2))
      IF (H(I,1).LT.0) GO TO 11
   10 CONTINUE
   11 HSTEP=(HMAX-HMIN)/249.
      SUM=0.0
      T6=I-1
C
C     ++++++++++++++++++++++++++++++++++++++++++++++++++++++++++++++++++
C
C     In this loop unit intensities of each calculated resonance field
C     are added up at each of 250 points chosen by the scaling factor
C     HSTEP.
C
C     ++++++++++++++++++++++++++++++++++++++++++++++++++++++++++++++++++
C
      DO 70 I=1,250
      FIELD(I)=0.0
   70 COUNT(I)=0.0
      T5=1
      DO 60 T5=1,T6
      I=INT((H(T5,1)-HMIN+(1.5*HSTEP))/HSTEP)
      IF (I.GT.250) GO TO 50
      IF (I.LT.1) GO TO 50
      COUNT(I)=COUNT(I)+1.
   50 I=INT((H(T5,2)-HMIN+(1.5*HSTEP))/HSTEP)
      IF (I.GT.250) GO TO 55
      IF (I.LT.1) GO TO 55
      COUNT(I)=COUNT(I)+1.
   55 I=INT((H(T5,3)-HMIN+(1.5*HSTEP))/HSTEP)
      IF (I.GT.250) GO TO 60
      IF (I.LT.1) GO TO 60
      COUNT(I)=COUNT(I)+1.
   60 CONTINUE
      DO 200 I=1,250
  200 WRITE(4,300)HMIN+(I-1)*HSTEP,COUNT(I)
  300 FORMAT(2(1X,F10.3))
      END
```

```
C     ++++++++++++++++++++++++++++++++++++++++++++++++++++++++++++++++
C
C             TRIPLET ESR POWDER SPECTRUM SIMULATION PART III
C
C     This part of the program assigns a Gaussian linewidth to each
C     field intensity calculated by the first two parts of the program.
C     These intensities can then be summed thereby broadening and
C     smoothing the lineshape.
C     T is the value of the linewidth and K is the sum distance and
C     these parameters can be input in free format via the keyboard
C     when prompted by the display screen.
C     Originally written in BASIC by J.M. McBride (Yale UNiversity).
C     Obtained from E.F. Hilinski (Florida State University).
C     Adapted for use on IBM PC/AT by Rakesh Jain.
C
C     ++++++++++++++++++++++++++++++++++++++++++++++++++++++++++++++++
C
      DIMENSION FIELD(250),COUNT(250),COUNT1(250),S(10000)
      REAL N
      INTEGER T5,T6
C
C     ++++++++++++++++++++++++++++++++++++++++++++++++++++++++++++++++
C
C     Input is from file TRIPLET2.OUT which is generated by part II of
C     this program. File HFC.OUT generated by FORTRAN program HFC is
C     also in a format which can directly be used as input for TRIPLET3
C     by renaming it TRIPLET2.OUT
C     The output is generated as X-Y data in a file TRIPLET3.OUT which
C     can be used directly in the plotting program or in the program
C     TRIPLET4 which then calculates the derivative spectrum.
C
C     ++++++++++++++++++++++++++++++++++++++++++++++++++++++++++++++++
C
      OPEN (4,FILE='TRIPLET2.OUT',STATUS='OLD')
      OPEN (2,FILE='TRIPLET3.OUT',STATUS='UNKNOWN')
      DO 1 I=1,250
      COUNT(I)=0.0
      COUNT1(I)=0.0
    1 FIELD(I)=0.0
      READ (4,6)D,E
      WRITE (2,6)D,E
      READ (4,4)DEL
    4 FORMAT (F8.2)
      READ (4,6)TSTEP,CMSTEP
      READ (4,11) GX,GY,GZ
      READ (4,5) HMIN,HMAX
```

```
    5 FORMAT (2F8.2)
    6 FORMAT(F8.6,1X,F8.6)
   11 FORMAT(3F10.7)
      DO 10 I=1,250
   10 READ (4,600) FIELD(I),COUNT(I)
  600 FORMAT(2(1X,F10.3))
      WRITE(6,899)
  899 FORMAT(' ENTER LINEWIDTH(R) AND SUM DISTANCE(I) (EG. 10.0,20):')
      READ(5,*) T,K
      WRITE(2,898) DEL,TSTEP,CMSTEP,T,K
  898 FORMAT(F8.2,1X,F8.2,1X,F8.2,1X,F8.2,1X,I4)
      WRITE (2,43)
   43 FORMAT ('H')
      WRITE (2,44)
   44 FORMAT ('I')
      WRITE (2,46)
   46 FORMAT ('1')
      WRITE (2,47)
   47 FORMAT('250')
C
C     ++++++++++++++++++++++++++++++++++++++++++++++++++++++++++++++++++
C
C     This part of the program assigns a linewidth (T) to each point and
C     sums up the intensities over a number of points to give a spectrum
C     which represents an absorption ESR for the given ZFS parameters.
C
C     ++++++++++++++++++++++++++++++++++++++++++++++++++++++++++++++++++
C
      H3=(HMAX-HMIN)/249.
      T=(T/H3)**2
      K=INT(K/H3)+1
      A1=-LOG(2.)/T
      IF (K.LT.20) GO TO 50
      K=20
   50 DO 70 I=1,K
   70 S(I)=EXP(A1*I**2)
      B=0.0
      DO 75 I=1,250
   75 COUNT1(I)=COUNT(I)
      I=K
      DO 100 J=1+I,250-I
      DO 90 L=1,I
      COUNT1(J)=COUNT1(J)+S(L)*(COUNT(J-L)+COUNT(J+L))
   90 CONTINUE
  100 CONTINUE
      DO 200 I=1,250
  200 WRITE(2,700) FIELD(I), COUNT1(I)
  700 FORMAT(2(1X,F10.3))
      END
```

```
C
C     +++++++++++++++++++++++++++++++++++++++++++++++++++++++++++++++++++
C              TRIPLET ESR POWDER SPECTRUM SIMULATION PART IV
C
C     This program reads data from a data file generated by TRIPLET3
C     smoothes the data by a quatratic/cubic least squares procedure,
C     and differentiates the data using a quadratic filter.
C     The smoothing and differentiation procedures are described in:
C     A.Savitzky,M.J.E.Golay, AnalChem, 36, 1627-1639 (1964), and
C     R.R.Ernst, AdvMagRes, 2, 1-135 (1966), esp. p. 45.
C    The program is patterned after QEPR by Jeff Gelles (and Craig
C     Martin).
C
C
C     Input data file                         --- for004
C     Input parameter file                    --- for005
C     Deriv. data dI/dH output                --- for008
C
C     The program is designed to produce an ESR derivative spectrum
C     from an ESR absorption spectrum -- dI/dH.
C
C                   NBL      -- baseline
C                   NSM, NDV -- number of adjacent points to be used
C                               for smoothing and differentiation,
C                               respectively.  These must be ODD
C                               integral values between 3 and 35.
C                               For deriv. only, enter 01 for NSM;
C                   format(I2,1X,I2)
C     +++++++++++++++++++++++++++++++++++++++++++++++++++++++++++++++++++
C
      DIMENSION PAR(23), CFIL(35), DFIL(35)
      REAL A(250), B(250), C(250), X(250)
      CHARACTER XAXIS,YAXIS
C
C     +++++++++++++++++++++++++++++++++++++++++++++++++++++++++++++++++++
C
C      Read data from input file TRIPLET3.OUT
C
C     +++++++++++++++++++++++++++++++++++++++++++++++++++++++++++++++++++
C
```

```
      OPEN(UNIT=4, FILE='TRIPLET3.OUT', STATUS='OLD')
      OPEN(UNIT=8, FILE='TRIPLET4.OUT', STATUS='UNKNOWN')
      READ(4,3) D,E
    3 FORMAT(F8.6,1X,F8.6)
      WRITE(8,3) D,E
      READ(4,4) DEL,TSTEP,CMSTEP,T,K
      WRITE(8,4)DEL,TSTEP,CMSTEP,T,K
    4 FORMAT(F8.2,1X,F8.2,1X,F8.2,1X,F8.2,1X,I4)
      READ(4,5) XAXIS
      WRITE(8,5)XAXIS
      READ(4,5) YAXIS
      WRITE(8,5)YAXIS
    5 FORMAT(A1)
      READ(4,6) NLINES
      WRITE(8,6)NLINES
      READ(4,*) NPTS
      WRITE(8,*)NPTS
    6 FORMAT(I3)
      DO 1 I=1,NPTS
    1 READ(4,412) X(I),A(I)
      NBL=0
      NSM=5
      NDV=5
C
C     ++++++++++++++++++++++++++++++++++++++++++++++++++++++++++++++++++++
C
C     Determination of convolution functions
C
C     ++++++++++++++++++++++++++++++++++++++++++++++++++++++++++++++++++++
C
    7 MSM=(NSM-1)/2
      MDV=(NDV-1)/2
      CNORM=0
      DNORM=0
      DO 1017 I=1,NSM
      J=I-MSM-1
      CFIL(I) = 3*MSM**2 + 3*MSM - 1 - 5*J**2
      CNORM=CNORM + CFIL(I)
 1017 CONTINUE
      DO 9743 I=1,NDV
      J=I-MDV-1
      DFIL(I) = J
      DNORM=DNORM + J**2
 9743 CONTINUE
C
C     ++++++++++++++++++++++++++++++++++++++++++++++++++++++++++++++++++++
C
C      Quadratic/Cubic Smoothing in NSM window
```

```
      DO 88 K=1+MSM,NPTS-MSM
      B(K)=0
      M=0
      DO 119 L=K-MSM,K+MSM
      M=M+1
      B(K) = B(K) + A(L)*CFIL(M)
  119 CONTINUE
      B(K) = B(K)/CNORM
   88 CONTINUE
      DO 741 N=1,MSM
  741 B(N)=0
C
C     ++++++++++++++++++++++++++++++++++++++++++++++++++++++++++++++++++++
C
C      Quadratic Filter and Derivative in NDV window
C
C     ++++++++++++++++++++++++++++++++++++++++++++++++++++++++++++++++++++
C
      DO 417 K=1+MDV+MSM,NPTS-MDV-MSM
      C(K)=0
      M=0
      DO 428 L=K-MDV,K+MDV
      M=M+1
      C(K) = C(K) + B(L)*DFIL(M)
  428 CONTINUE
      C(K) = C(K)/DNORM
  417 CONTINUE
C
C     ++++++++++++++++++++++++++++++++++++++++++++++++++++++++++++++++++++
C
C      Write data to output files
C
C     ++++++++++++++++++++++++++++++++++++++++++++++++++++++++++++++++++++
C
      DO 443 N=1,NPTS
      WRITE(8,412)X(N),C(N)
  412 FORMAT(2(1X,F10.3))
  443 CONTINUE
  441 STOP
      END
```

```
      DIMENSION H(250),HINT(250),BINT(250)
      INTEGER PASCAL(25),PASCAL1(25)
C
C     ++++++++++++++++++++++++++++++++++++++++++++++++++++++++++++++++
C
C     INPUT from the file generated by TRIPLET2 i.e., TRIPLET2.OUT
C     Generates an OUTPUT file called HFC.OUT
C     the program splits the intensity at each value of H into NNUC+1
C     peaks according to the input pattern of relative intensities.
C     The output consists of: D,E,DEL,TSTEP,CMSTEP,GX,GY,GZ,HMIN,HMAX
C     and a list of peak intensities at various values of the magnetic
C     field.
C
C     ++++++++++++++++++++++++++++++++++++++++++++++++++++++++++++++++
C
      OPEN (1,FILE='TRIPLET2.OUT',STATUS='OLD')
      OPEN (4,FILE='HFC.OUT',STATUS='UNKNOWN')
      READ (1,4) D,E
      WRITE (4,4) D,E
      READ (1,8) DEL
      WRITE (4,8) DEL
      READ (1,4) TSTEP,CMSTEP
      WRITE (4,4) TSTEP,CMSTEP
    4 FORMAT (F8.6,1X,F8.6)
    8 FORMAT (F8.2)
      READ (1,6) GX,GY,GZ
      WRITE (4,6) GX,GY,GZ
    6 FORMAT(3F10.7)
      READ (1,5) HMIN,HMAX
      WRITE (4,5) HMIN,HMAX
    5 FORMAT (2F8.2)
      DO 1 I=1,250
    1 READ (1,412)H(I),HINT(I)
  412 FORMAT(2(1X,F10.3))
      WRITE (6,999)
  999 FORMAT(' ENTER NUMBER OF EQUIVALENT NUCLEII (FORMAT I2)')
      READ(5,998)NNUC
  998 FORMAT(I2)
      WRITE (6,997)
  997 FORMAT(' ENTER COUPLING CONSTANT IN GAUSS (FORMAT F4.2)')
      READ (5,141)HFC
  141 FORMAT(F4.2)
      WRITE (6,990)
  990 FORMAT(' GIVE PASCAL INTENSITIES (FREE FORMAT, ONE ON EACH LINE)')
```

```
      DO 989 J=1,NNUC+1
989   READ(5,*)PASCAL1(J)
      NPEAKS=NNUC+1
      NSTEP=NINT(HFC*249./(HMAX-HMIN))
      DO 400 I=1,250
400   BINT(I)=0
      PEAKS=FLOAT(NPEAKS)
      P=PEAKS/2.
      R=MOD(P,AINT(P))
      IF (R.NE.0.) GOTO 101
      IF (R.EQ.0.) GOTO 167
167   K=NPEAKS+1
      PASCAL(1)=0.
      DO 102 J=2,K
102   PASCAL(J)=PASCAL1(J-1)
      L=NPEAKS/2
131   DO 996 I=25,225
      DO 995 J=-L,L
      BINT(I+(J-1)*NSTEP)=BINT(I+(J-1)*NSTEP) + HINT(I)*PASCAL(J+L+1)
995   CONTINUE
996   CONTINUE
      GOTO 24
101   K=(NPEAKS-1)/2
      DO 886 I=25,225
      DO 885 J=-K,K
      BINT(I+J*NSTEP)=BINT(I+J*NSTEP)+HINT(I)*PASCAL1(J+K+1)
885   CONTINUE
886   CONTINUE
 24   DO 993 I=1,250
993     WRITE (4,994)H(I),BINT(I)
994   FORMAT(2(1X,F10.3))
      END
```

CHAPTER IV

BIRADICAL REARRANGEMENTS AT 4 K

Reactions performed under cryogenic conditions have resulted in the successful isolation and characterization of numerous high-energy species. The strategy in such experiments is to cool the reactants to a temperature at which their thermal energy is lower than the energy barrier for reaction. In other words, this procedure effectively "traps" the reactive species in its potential well. We have applied this technique to study the effects of the matrix and the low temperature on reactions with very small energies of activation. Our observations indicate that chemical activation becomes extremely important in such processes due to the ineffectiveness of the environment at energy transfer. Thus, reactions which are insignificant under normal conditions can become extremely important under cryogenic conditions.

Results

Photolysis (304–388 nm or monochromatic 334±2 nm light) of 2,3-diazabicyclo[2.2.1]hept-2-ene-7-spirocyclopropane (**24**)[1] in a glassy or polycrystalline matrix (generally MTHF but also acetone, propylene glycol or heptane) at 4–35 K in the cavity of an ESR spectrometer produces the spectrum shown in Figure 32a.

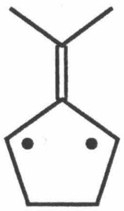

2

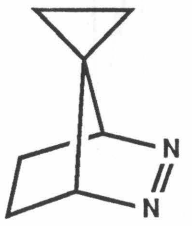

24

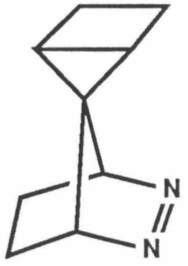

25

A qualitatively similar spectrum is seen from diazene **25**[2] (Figure 33a). The zero-field splitting (zfs) parameters[3] observed are remarkably similar to those reported for the TMM derivative 2-isopropylidene-1,3-cyclopentanediyl (**2**) and

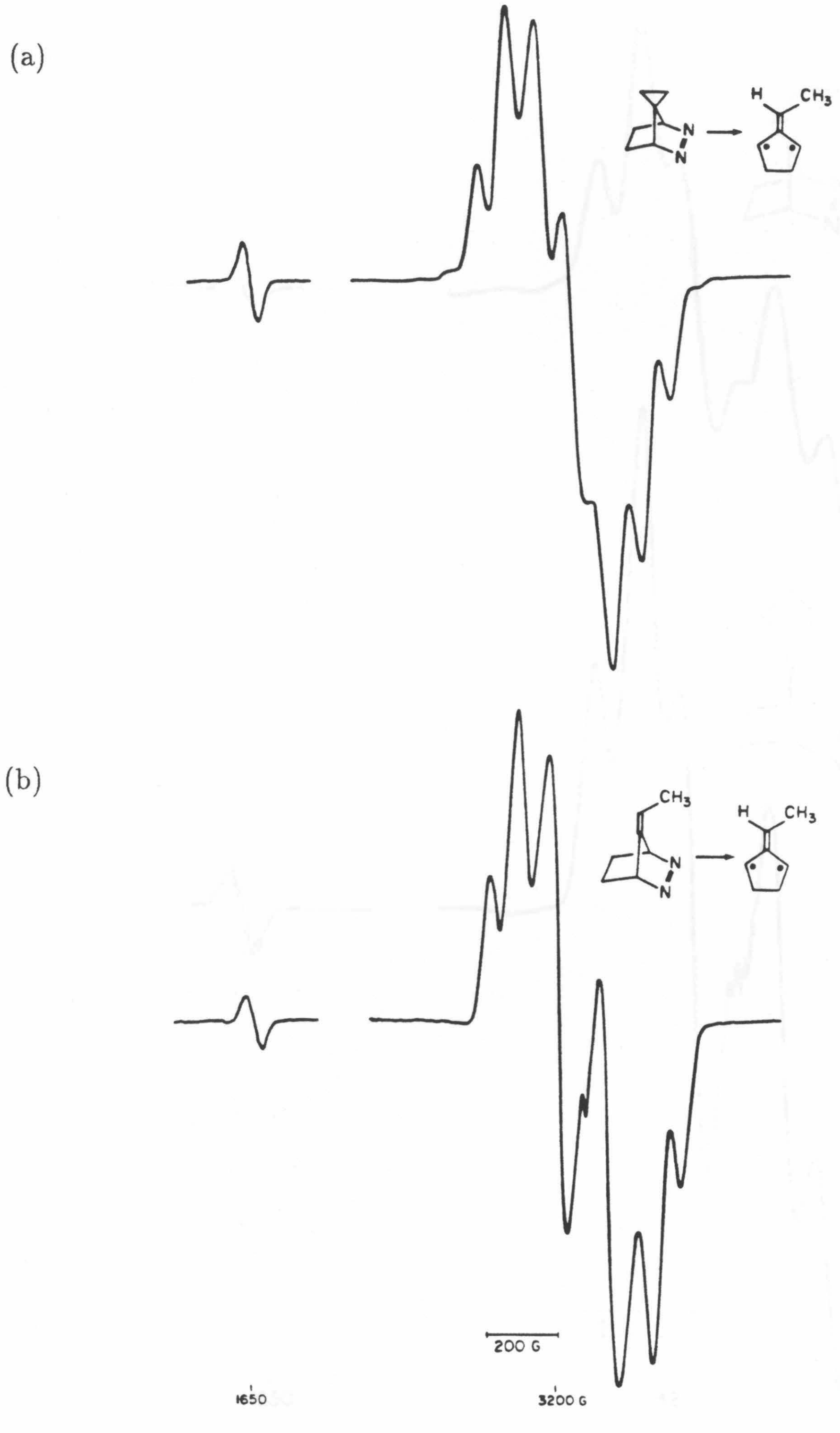

Figure 32. ESR spectrum obtained upon irradiation of an MTHF matrix containing (a) **24** and (b) **71**.

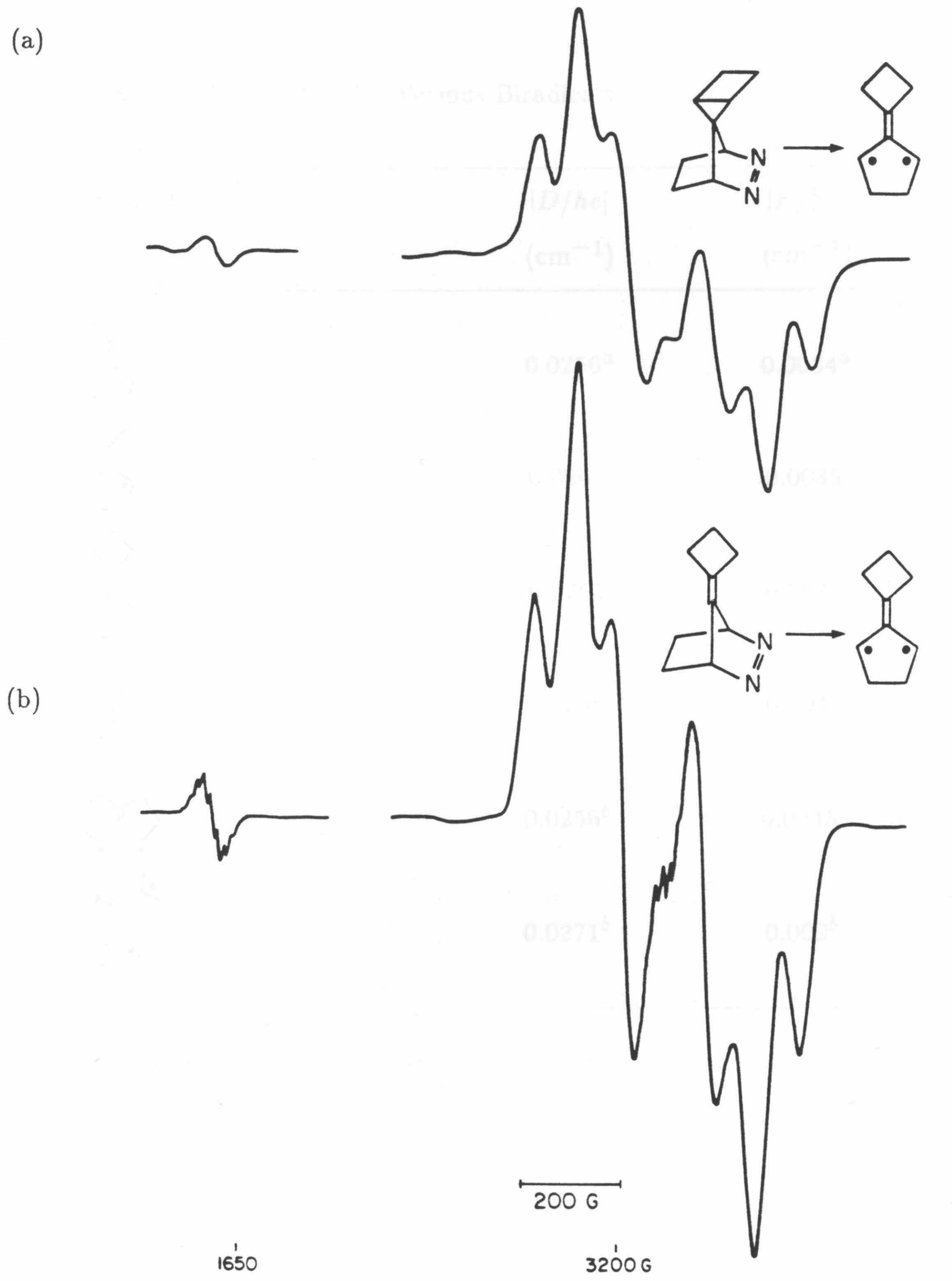

Figure 33. ESR spectrum obtained upon irradiation of an MTHF matrix containing (a) **25** and (b) **72**.

Table IX. ZFS Parameters for Various Biradicals

Biradical	$\lvert D/hc \rvert$ (cm^{-1})	$\lvert E/hc \rvert$ (cm^{-1})
	0.0256[a]	0.0034[a]
	0.0264	0.0035
	0.0255	0.0030
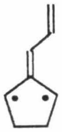	0.025[b]	0.004[b]
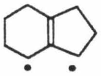	0.0256[b]	0.0045[b]
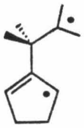	0.0271[b]	0.009[b]

[a] See ref. 4. [b] Tentative assignment.

Scheme VIII

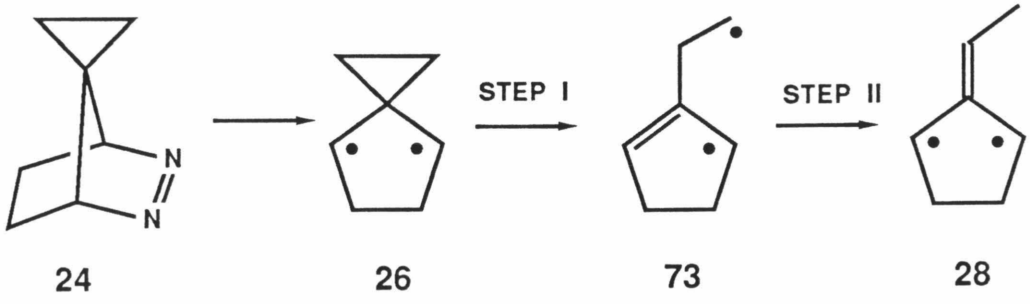

related structures[4] (Table IX). The ESR signals obtained from **24** and **25** give linear Curie plots over a broad temperature range, indicating the species being observed have triplet ground states.[5] In addition, these triplet signals were quite stable thermally, that derived from **24** being stable to at least 146 K in propylene glycol.

As discussed below, consideration of the above data suggests that the carriers of the ESR signals are TMM's that arise, at least conceptually, as shown in Scheme VIII. In Scheme VIII, and throughout this work, all biradicals shown are in their triplet states unless denoted otherwise. The precise conversions this scheme implies are **24** to **28** and **25** to **29**. We therefore set out to prepare authentic samples of **28** and **29** by photolysis of diazenes **71**[6] and **72**, respectively.

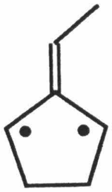
28

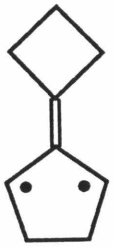
29

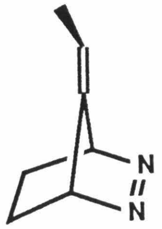

71

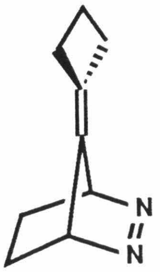

72

These diazenes were synthesized in a straightforward manner, the key steps being the syntheses of the appropriate fulvenes using the method developed recently by Little[7] (Scheme IX) in which cyclopentadiene is reacted with an aldehyde or ketone in the presence of pyrrolidine. Addition of diethylazodicarboxylate to the fulvene, followed by selective reduction of the endocyclic double bond and hydrolysis–oxidation then affords the azoalkane.

Photolysis of **71** and **72** at 4–77 K does indeed produce thermally stable triplet ESR signals with zfs parameters completely in accord with expectation. Based upon substantial precedent,[4] one can assert with confidence that the triplet species arising from **71** and **72** are the TMM's **28** and **29**. As shown in Figures 32 and 33, the spectra from **71** and **72** are essentially identical to those from **24** and **25**, respectively. The spectra from the authentic precursors (**71**/**72**) are always more intense and accompanied by fewer radical impurities, which accounts for the minor differences in the central regions of the spectra. There is one important difference between the authentic precursors **71** and **72**, and the diazenes **24** and **25**. When photolysis is conducted at 77 K, only **71** and **72** give TMM's. No triplet signal is seen when **24** or **25** is photolyzed at 77 K even though photolysis at 4–35 K produces a biradical that is quite stable when warmed to 77 K or higher (see above).

While the results of Figures 32 and 33 support the general route of Scheme VIII, they can hardly be considered compelling. One can imagine a wide range of biradical structures having zfs parameters in the range observed. An especially attractive alternative is an "allyl + p" biradical (e.g., **73**). Fortunately, in many of the spectra we have observed, there is much more information than just the zfs parameters.

Scheme IX

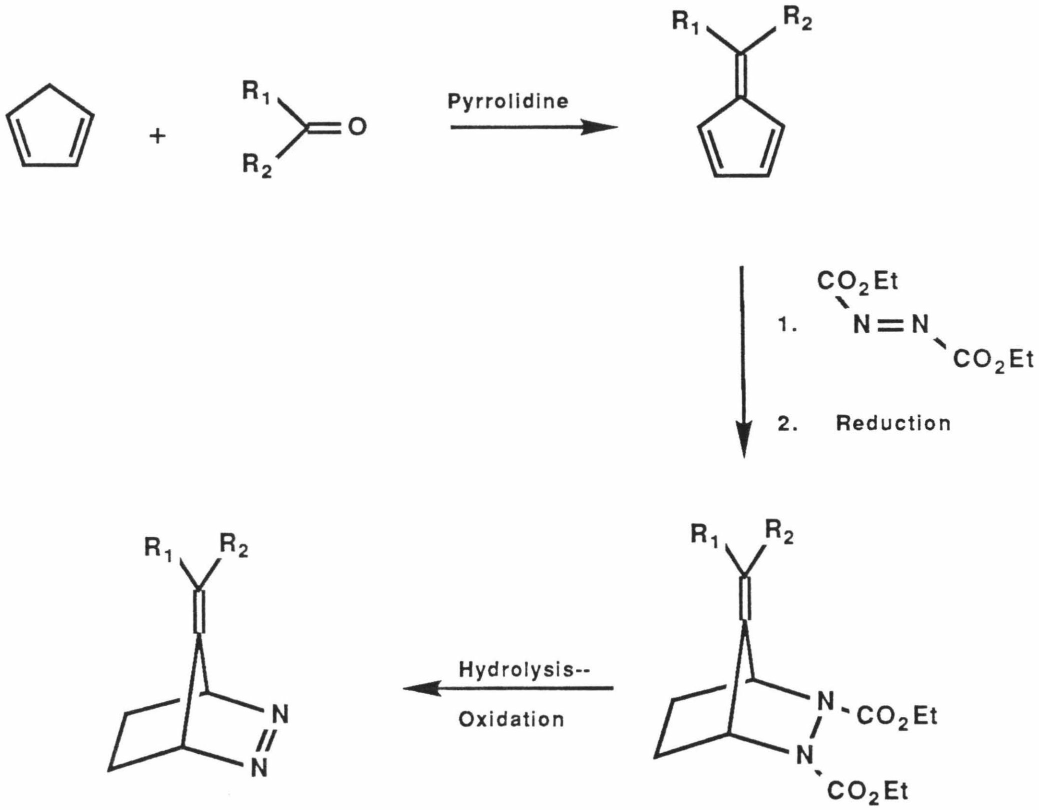

R_1
R_2
O
+
Pyrrolidine
1.
CO_2Et
N=N
2. Reduction
Hydrolysis--
Oxidation
N
$N-CO_2Et$

Hyperfine Coupling

All the spectra that we have recorded clearly show the half-field ($\Delta m_s = 2$) transition that is diagnostic of a triplet spectrum. Distinctive hyperfine patterns are observable on these transitions. Figure 34 shows the $\Delta m_s = 2$ transitions in the spectra from diazenes **24** and **71**. The pattern is complex, but it is clear that the two spectra are essentially superimposable.

More importantly, diazenes **25** and **72** give well-defined, ***interpretable*** hyperfine patterns that are, again, identical as shown in Figure 35. Nine evenly spaced lines separated by ca. 13.5 G are clearly visible. The intensity pattern, combined with further results described below, indicate that we are observing the inner nine lines of an eleven-line spectrum. With this assignment the intensities follow the binomial expansion remarkably well.[8] The two outermost lines should be ten times weaker than their nearest neighbors, and thus difficult to detect. Such an eleven-line pattern indicates coupling to ten equivalent protons. These must be the eight protons that are β to the radical centers in **29** and the two protons that are α (i.e., on the radical centers). Coincidentally, the apparent hyperfine coupling (hfc) constant, a_H, is approximately the same for all these protons.

Obtaining identical spectra from different precursors again provides further support for our structural assignment. However, the fact that the hyperfine patterns of Figure 35 can be related to a specific structural feature of the biradicals involved provides a much more powerful tool. In particular, we can observe the changes in hfc patterns that result when precursor **25** is specifically deuterated to give **74** and **75**.[2] According to Scheme VIII, diazene **74** should produce biradical **76** with two deuteria in β positions. Since $a_D = a_H/6.514$, this substitution should reduce the number of hfc lines by two. The spectrum

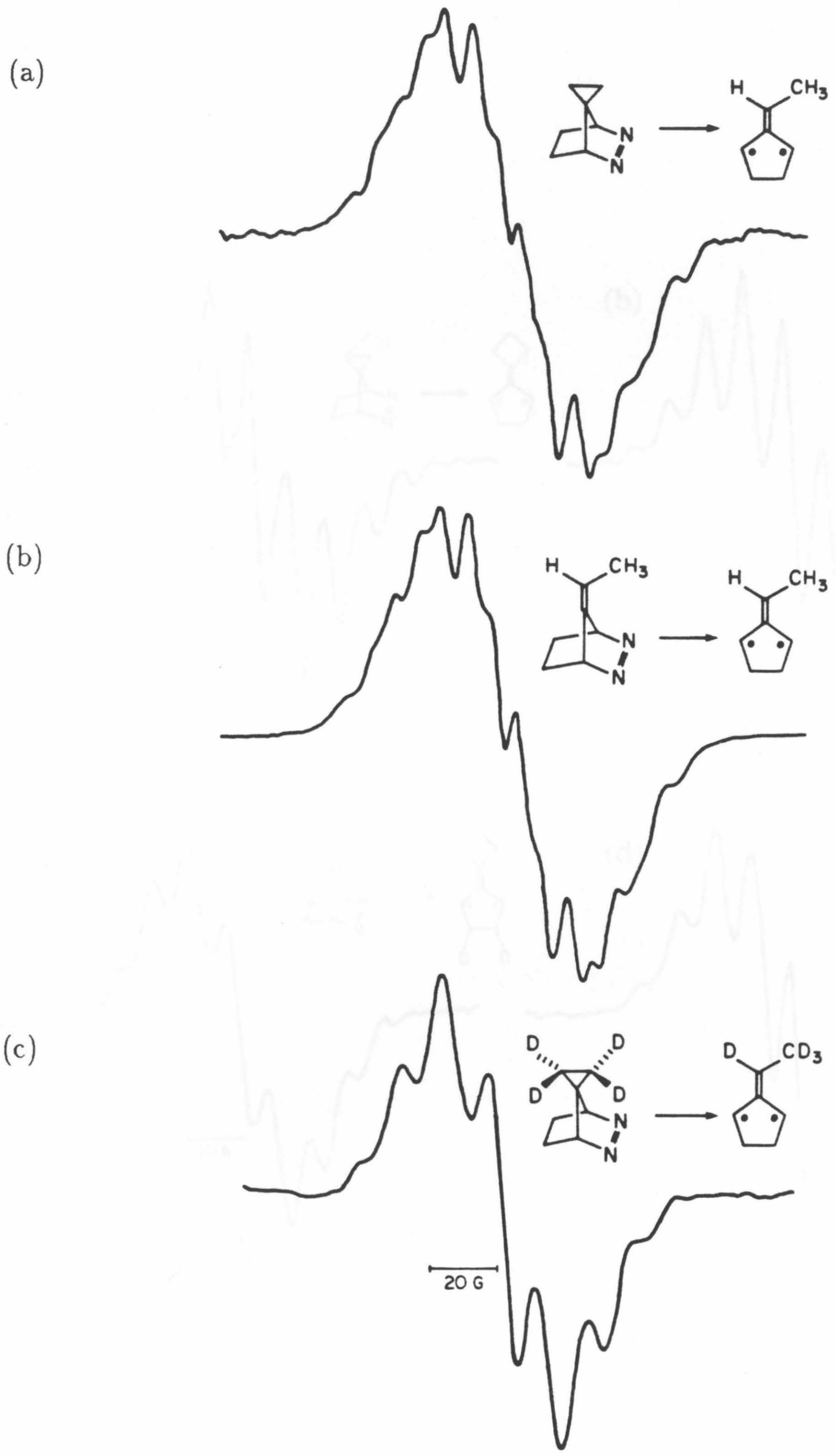

Figure 34. Half-field ($\Delta m_s = 2$) transitions in the ESR spectra obtained from (a) **24**, (b) **71**, and (c) **78**.

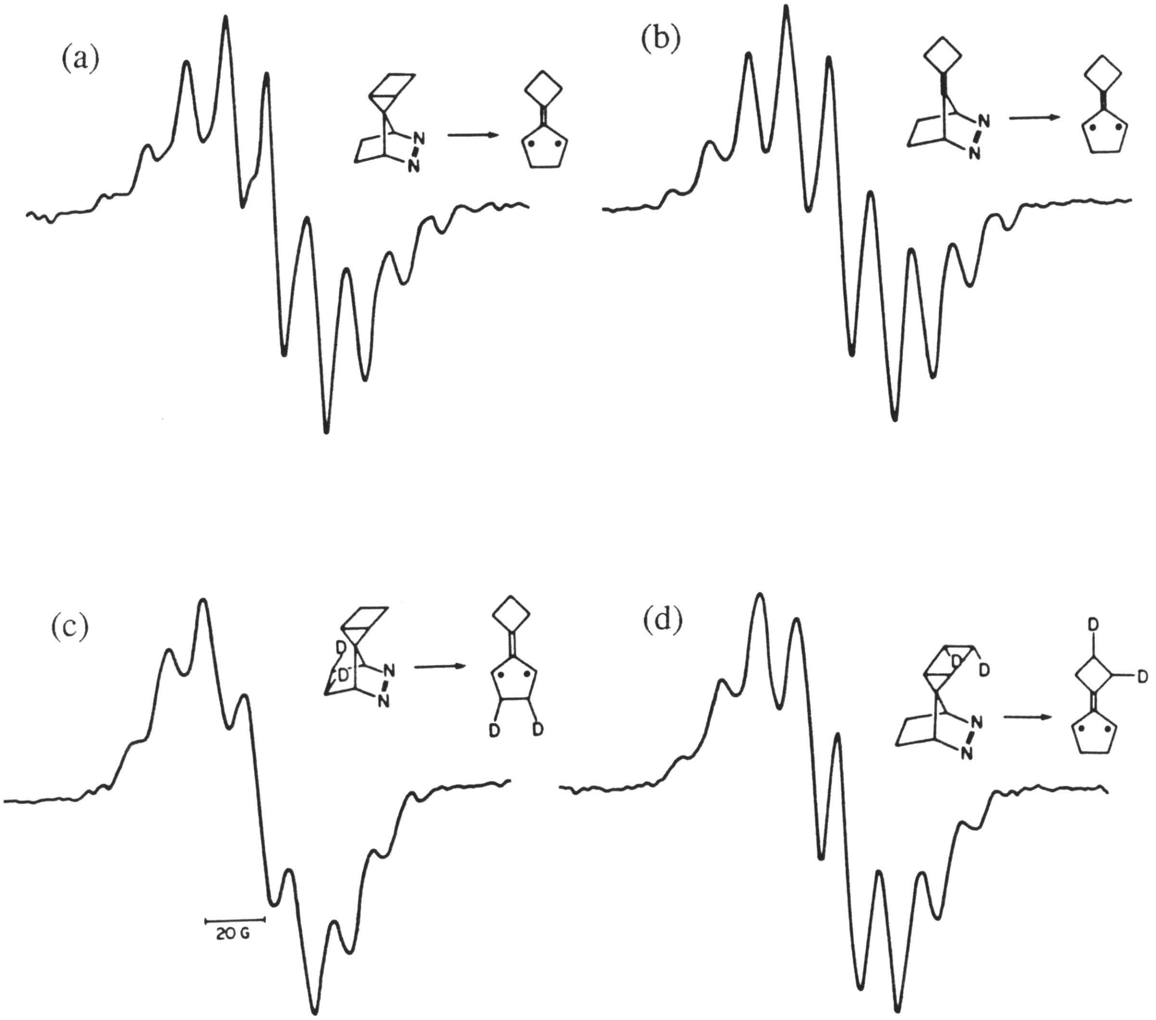

Figure 35. Half-field ($\Delta m_s = 2$) transitions in the ESR spectra obtained from (a) **25**, (b) **72**, (c) **74**, and (d) **75**.

shown in Figure 35c is completely in accord with expectation. Although the lines are broadened by deuterium coupling, the basic pattern is unchanged and there are two fewer lines.

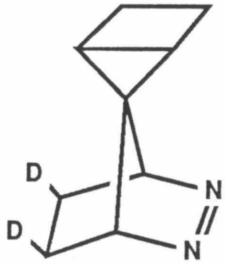

74

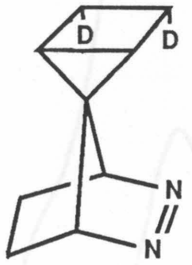

75

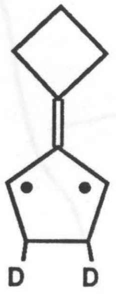

76

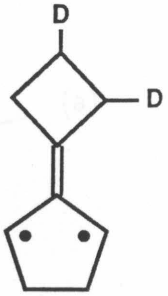

77

The more convincing case is provided by diazene **75**. Scheme VIII predicts that **75** should produce **77**, in which only one of the two deuteria ends up in a position that can show hfc. Figure 35d clearly bears out this expectation. There is an important difference between Figure 35d, and all the other hyperfine patterns we have shown. In Figure 35d, when the signal crosses the baseline in the center of the spectrum, it is going from lower left to upper right. This indicates that the true spectrum (i.e., not the first derivative) has a minimum in the center. The actual absorption spectrum, obtained by integration, confirms this (Figure 36). This requires an even number of lines in the spectrum and thus coupling to an odd number of protons. In Figure 35a–c, the crossing is upper left to lower right indicating a maximum (see Figure 36). This requires an odd number of lines and thus an even number of protons. The fact that Scheme VIII predicted that this sort of parity change would result from incorporation of deuteria that are quite remote from where one might have expected radical character provides compelling support for the scheme.

Our analysis is further supported by the fact that spectral simulation (see Chapter III for details) using an isotropic 13.5 G hfc produces almost

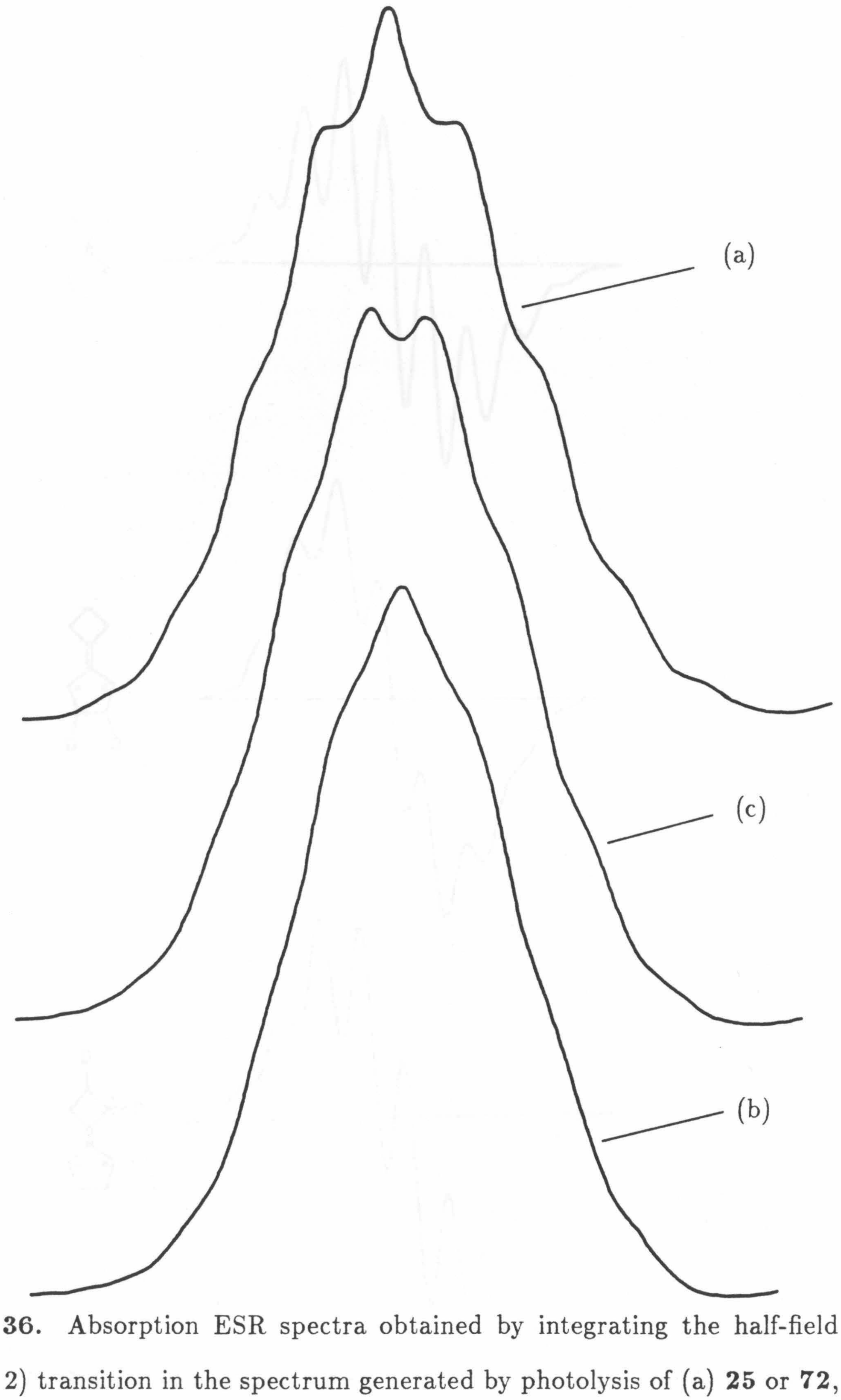

Figure 36. Absorption ESR spectra obtained by integrating the half-field ($\Delta m_s = 2$) transition in the spectrum generated by photolysis of (a) **25** or **72**, (b) **74**, and (c) **75**.

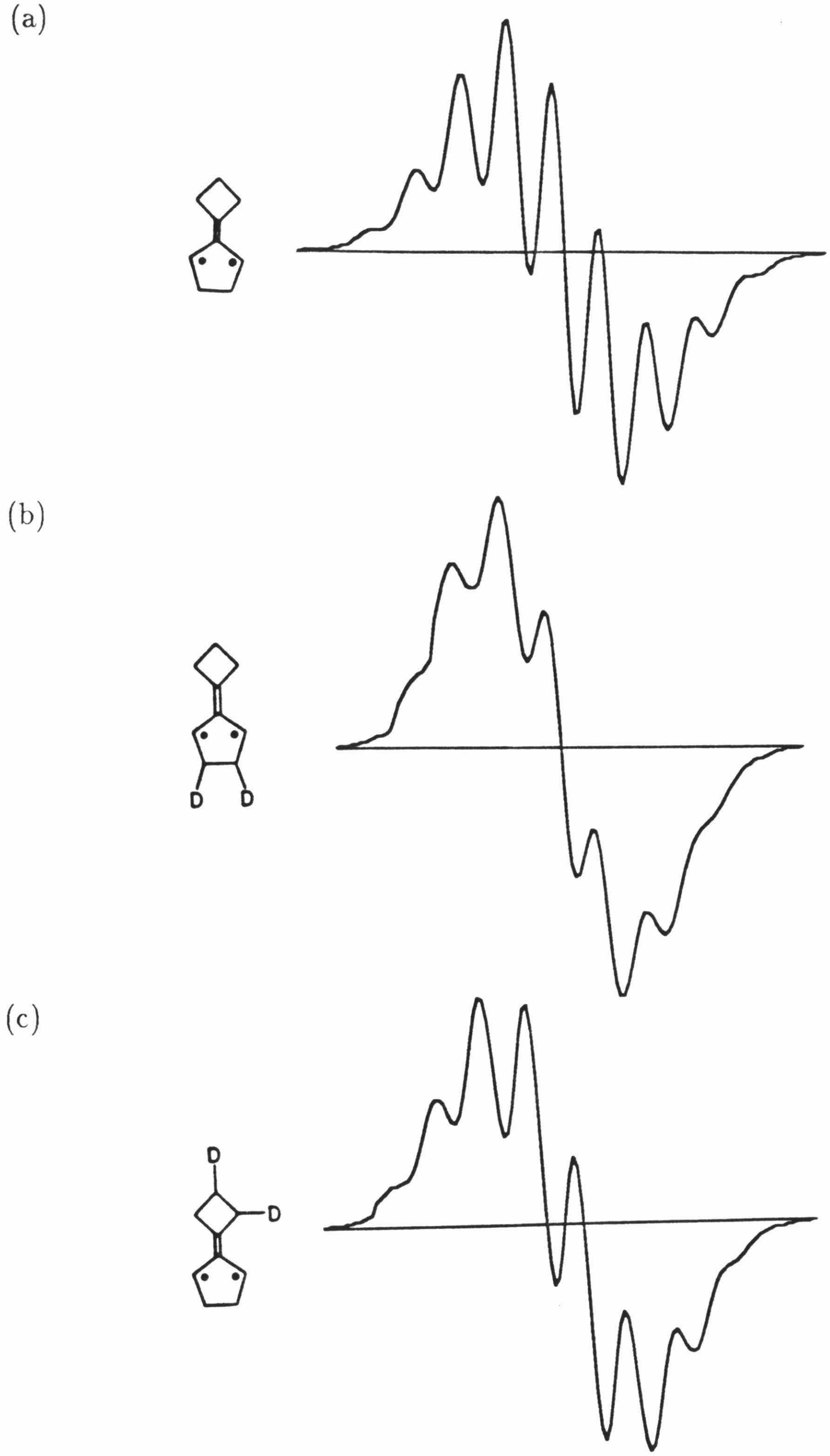

Figure 37. Simulated half-field ($\Delta m_s = 2$) transitions for the ESR spectra obtained from (a) **25** or **72**, (b) **74**, and (c) **75**.

superimposable patterns (Figure 37). To get a good match, different linewidths must be used in the three simulations. This is, of course, due to the unresolved deuterium hfc which broadens the lines in the spectra of **76** and **77**.

It is fortunate that the apparent hfc constants for all the protons in **29** are identical. Had a_H^α and a_H^β been different, the complexity of the spectrum along with the intrinsic broadness of the lines in rigid media would probably have made a straightforward analysis extremely difficult. We reasoned that the complex hfc pattern for **28** arose from the protons of the methyl group. Due to their different orientation, these protons could have hfc constants that are not the same as those for the ring β protons. To circumvent this problem we prepared the tetradeuterio diazene **78** as a precursor to biradical **79**. As shown in Figure 34c, the $\Delta m_s = 2$ pattern is now an easily interpretable seven line spectrum with $a_H = 13.5$ G. The six protons that couple must be two α and four β. Once again, spectral simulation using an isotropic 13.5 G hfc constant for six equivalent protons produces an almost identical spectrum (Figure 38). This supports the above argument that the α and β protons in these systems have nearly identical apparent hfc constants, and the spectra for **29** (Figures 35a and b) have in fact eleven lines.

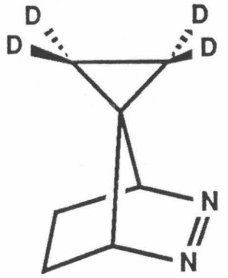

78

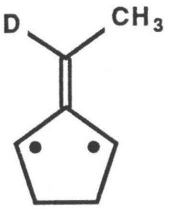

79

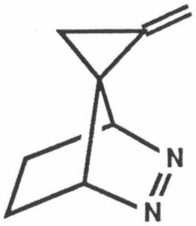

80

81

We consider the above data as irrefutable proof that diazenes **24** and **25** give rise to the TMM's **28** and **29**, respectively, upon photolysis in a matrix

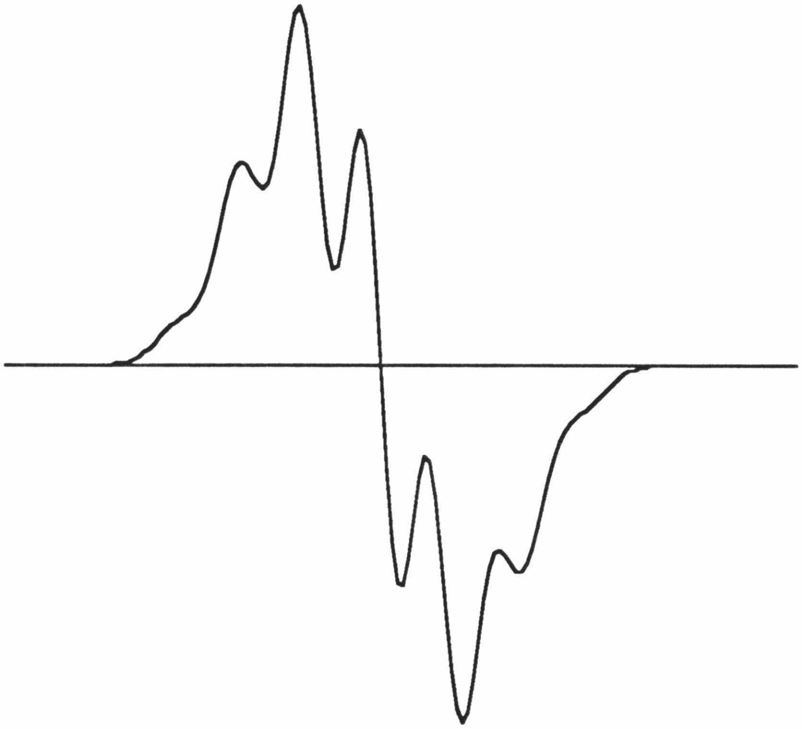

Figure 38. Simulated half-field ($\Delta m_s = 2$) transitions for the ESR spectra obtained from **78**.

at 4–35 K. The observation of two examples suggests that this remarkable rearrangement could be general. In support of this possibility Berson et al. have found that diazene **80**[9] also gives rise to a thermally stable triplet ESR spectrum upon photolysis at 4–83 K.[10] The zfs parameters (Table IX) are completely consistent with the structure **81** that would be expected on the basis of Scheme VIII. Neither interpretable hyperfine nor generation from an authentic precursor is available in this case, so assignment must be considered tentative. If correct, however, this would represent another example of "wrong bond" cleavage.[9] One would expect biradical **82** to cleave bond *a* to give the doubly allylic biradical **83**, instead of the presumably stronger bond *b* to give **84** as required by Scheme VIII. Cleavage of bond *b* is apparently also involved in the chemistry of such structures under conventional conditions.[9]

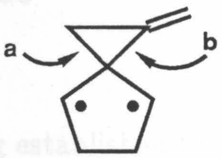

82

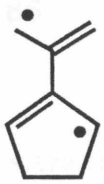

83

84

The results for **24** and **25** also suggest that attempts to prepare "allyl + p" biradicals from the appropriate precursors should lead to TMM's. Diazene **85**[2] is such a precursor, in that loss of nitrogen should produce "allyl + p" biradical **86**. It was observed by McElwee-White[11] that direct photolysis of **85** under matrix-isolation conditions produces no ESR signal. However, when benzophenone is included as a sensitizer, a triplet signal is seen.[12] Again the zfs parameters (Table IX) are completely in accord with a TMM structure.

Additionally, the ESR signal is thermally stable up to at least 100 K in propylene glycol.[5,11] These attributes seem to be more consistent with TMM **87** than with **86**. It should be recognized, however, that the ring closure pathway that has been suggested as the thermal decomposition path for other "allyl + p" systems (see below) is much less viable for **86** due to ring strain. In fact the preferred decomposition path for **86** is presumably C–C bond cleavage to give 2,3-divinylcyclopentene.[2] Thus it is difficult to predict the thermal stability of **86**.

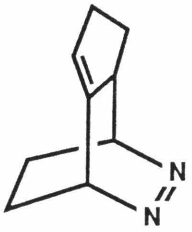

85

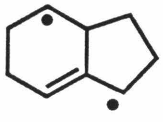

86

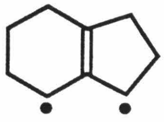

87

Having established that TMM's are the carriers of the ESR signals, we wished to evaluate whether Scheme VIII is the actual route to these structures. In particular, we wished to probe the intermediacy of biradicals **26** and **73**. We therefore prepared tetramethyl diazene **88**. Our goal was to supress the hydrogen migration (step II of Scheme VIII) and perhaps directly observe the "allyl + p" biradical. Photolysis of **88** in MTHF at 4–35 K produces the ESR spectrum shown in Figure 39. The D-value is similar to the TMM's we have observed, but the E-value is very much different (Table IX). The fact that $D \approx 3E$ gives the spectrum its unusual appearance.

Unlike all the other spectra we have described, the signal of Figure 39 is not thermally stable over a broad temperature range. It decays at temperatures as low as 35 K, although it is almost indefinitely stable at 4 K. The thermal instability combined with the large E-value establishes that the carrier of the signal of Figure 39 is not an alkylidenecyclopentanediyl (TMM) of the sort we have observed previously.

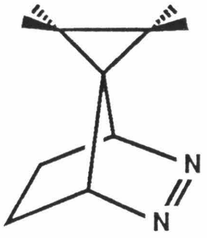

88

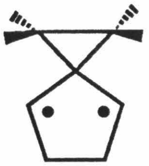

89

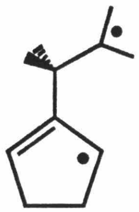

90

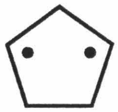

11

The two most likely carriers of the signal are biradicals **89** and **90**. The cyclopropyl-1,1-dicarbinyl type structure **89** can be ruled out on the basis of its D-value. The parent 1,3-cyclopentanediyl (**11**) displays[13] a value for $|D/hc| = 0.084\ \text{cm}^{-1}$, much larger than the $0.027\ \text{cm}^{-1}$ seen here. One could argue that delocalization through the Walsh orbitals of the cyclopropane could substantially diminish the D-value. However, this effect has been previously evaluated computationally using ab-initio wavefunctions and a complete numerical evaluation of the zfs integrals.[5] The calculations predict a decrease of less than 20% upon the incorporation of a spirocyclopropane ring. Consistent with this finding, Roth has concluded from thermal rearrangement studies that the spirocyclopropyl ring in structure **26** does not measurably stabilize the biradical.[1]

Further, we have found that irradiation of the ESR signal between 350–420 nm and below 300 nm results in an irreversible decrease of the intensity. This, implies that the biradical absorbs light in this region.[14] The UV-vis spectrum for matrix-isolated allyl radical has been observed previously and consists of a weak transition between 350–410 nm and a strong transition at 213 nm which tails out above 300 nm.[15] The striking similarity is good evidence for the

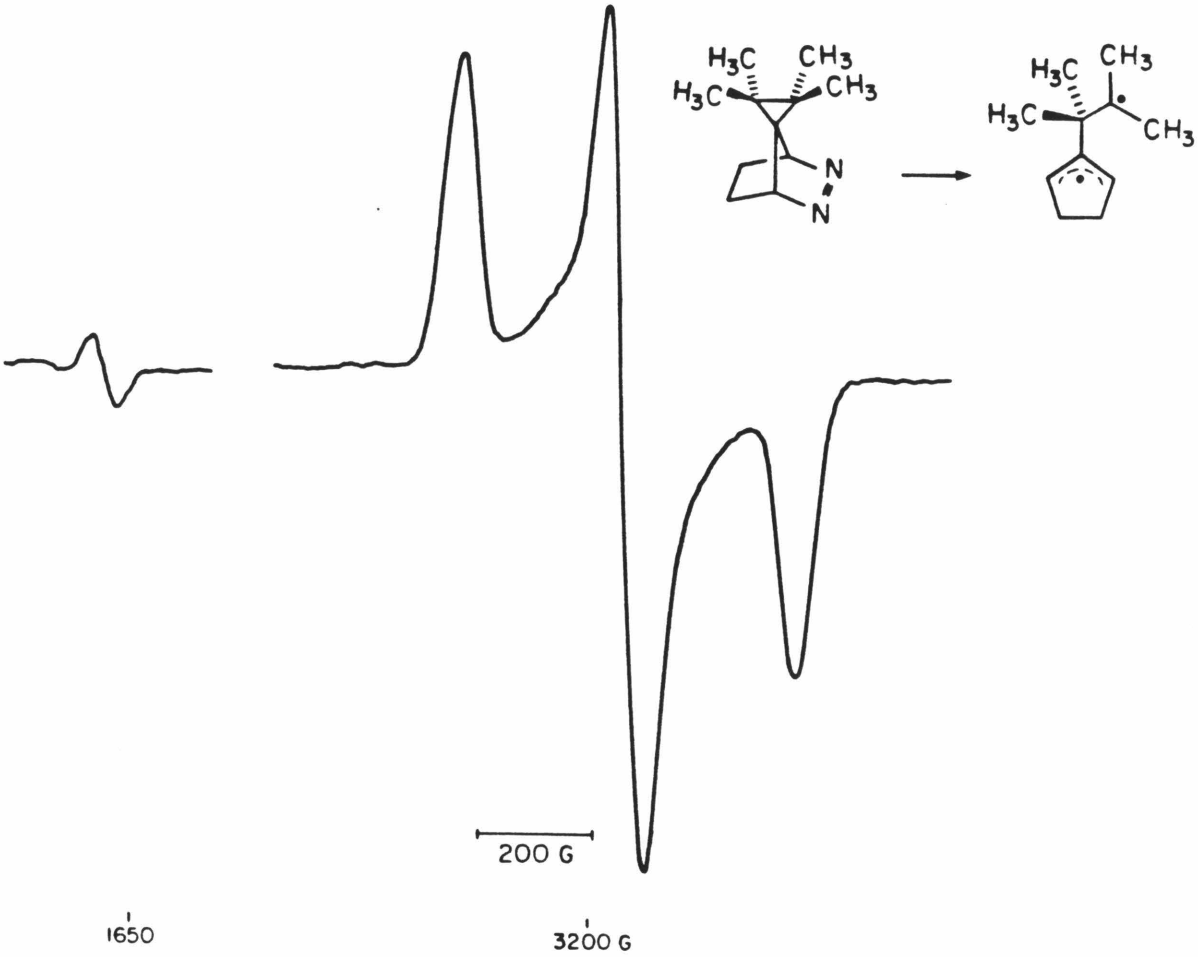

Figure 39. ESR spectrum obtained upon irradiation of an MTHF matrix containing **88**.

presence of an allyl moiety in **90**.[16]

We therefore tentatively assign biradical **90** as the carrier of the signal in Figure 39. The *D*-value is quite consistent with a delocalized 1,4-biradical. The thermal instability presumably indicates a relatively facile ring closure to bicyclo[3.2.0]hept-1-ene (**91**), a well-precedented process for biradicals of this type.[1,17]

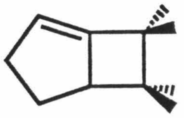

91

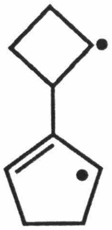

92

We have occasionally seen shoulders on the outer lines of the spectra generated when diazenes **25**, **74** and **75** are photolyzed at 4 K. Because they are shoulders it is not possible to determine their separation accurately. We estimate it as 600–625 G, implying a value for $|D/hc| = 0.028\text{–}0.029\ \mathrm{cm}^{-1}$, if the shoulders are indeed the outer lines of a triplet spectrum. On warming to 8 K these lines decay irreversibly over a period of ca. 20 min. We tentatively ascribe these signals to "allyl + p" structure **92**.

Discussion

Before discussing the results of our matrix-isolation experiments, we will briefly review the chemistry of these diazenes under conventional conditions. For the parent system, **24**, it has been shown[1] that both thermolysis (140°C) and photolysis (20°C) give predominantly the spiropentane derivative **43**. Sensitized photolysis, however, gives predominantly olefin **93**. These results can be rationalized by invoking the cyclopropyl-1,1-dicarbinyl biradical

26. In the triplet state (sensitized photolysis), **26** cannot ring close to **43**, but instead undergoes ring cleavage to biradical **73**. Diazene **25** also shows the same general reactivity pattern,[2] although its sensitized photolysis is more complex and involves pathways in addition to the cleavage route displayed by **24**.

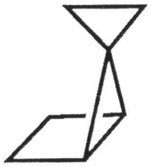

43

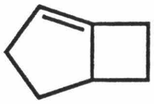

93

Another useful reference point for our discussion is the thermochemistry of the processes involved. There is a significant amount of relevant experimental data which can be combined with standard group increments and strain energies[18] to arrive at the overall scheme of Figure 40. This scheme can only be considered semi-quantitatively accurate, but it does lead to several important conclusions. We assume that after excitation from S_0 to S_1 of the diazene, intersystem crossing (ISC) to T_1 occurs. Loss of singlet nitrogen then produces a triplet hydrocarbon directly. While such ISC in diazenes is relatively rare under conventional conditions, there is precedent for it becoming more important at lower temperatures.[19] This is because there are small thermal barriers to nitrogen loss on S_1. As the temperature is lowered, such barriers become more difficult to cross, and ISC, the rate of which is generally considered to be independent of temperature, becomes competitive. Indeed we have found that both direct and sensitized low-temperature photolysis of **24** produce a greater fraction of **26** than observed at room temperature (Table X).

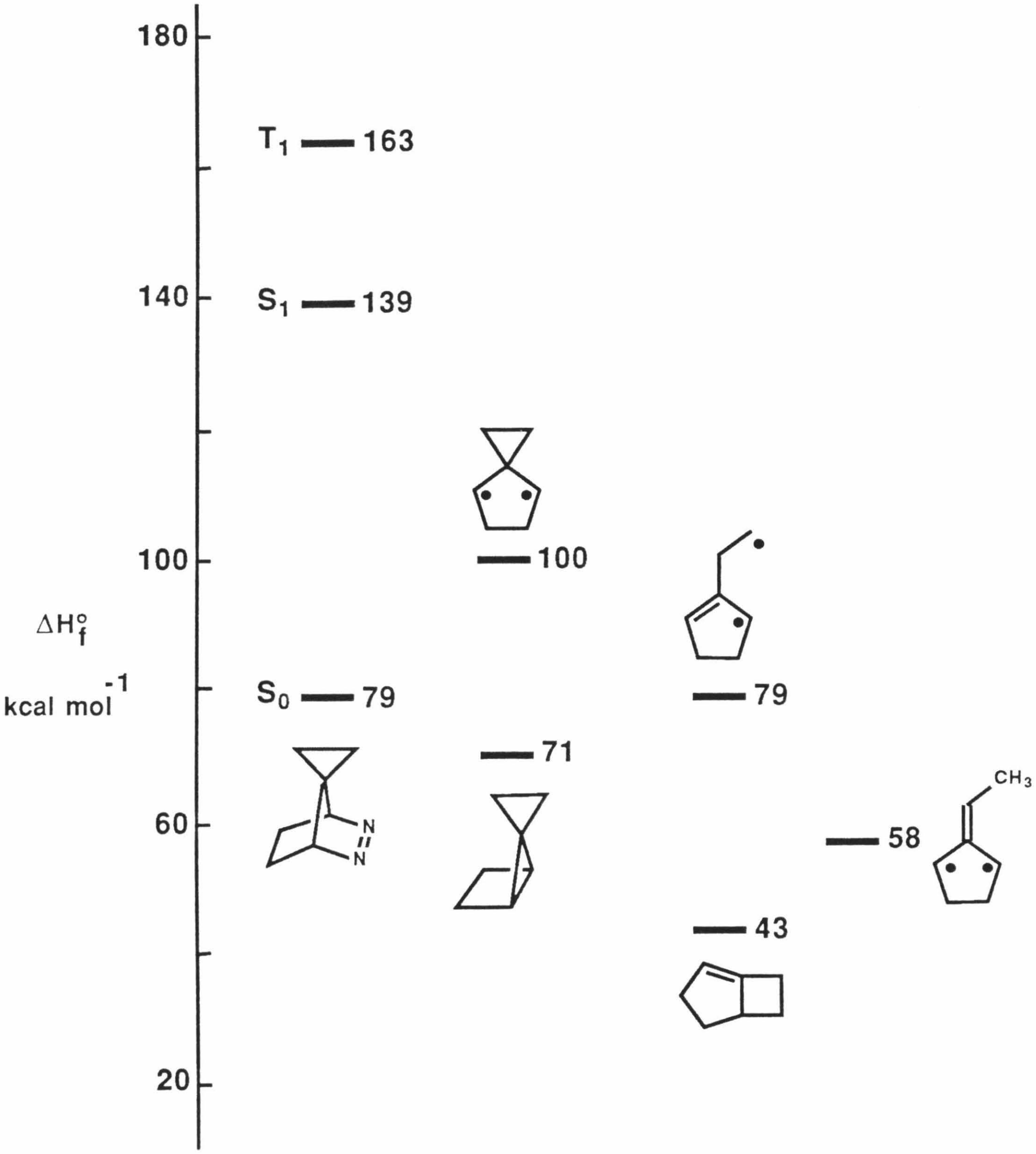

Figure 40. Thermochemistry for the decomposition of **24**.

Table X. Composition of the product mixture obtained upon photolysis of **24** at various temperatures

Solvent	Fluid/Matrix	Temperature	**43**	**93**
Ether	Fluid	25 °C	90[a]	10[a]
Acetone-d_6	Fluid	25 °C	89	11
Acetone-d_6	Fluid	–78 °C	87	13
Acetone-d_6	Matrix	–125 °C	50	50
Acetone-d_6	Matrix	–196 °C	4	96

[a] See ref. 1.

Given this analysis, Figure 40 leads to an important conclusion concerning the viability of the stepwise mechanism of Scheme VIII as the actual path to the TMM products. All the reactions proposed, i.e., **24**(T_1) to **26** to **73** to **28** are substantially exothermic and, of course, spin-allowed. All alternative reactions are spin-forbidden, a factor that should significantly slow their rates.

The Stepwise Mechanism

Step I, the Cyclopropylcarbinyl Cleavage. We shall now consider whether Scheme VIII is a viable mechanistic route to TMM's such as **28**. As discussed above, the first step (**26** to **73**) is the observed path in solution at room temperature.[1] It has also long been considered as an important component of the rearrangement of spiropentanes to methylenecyclobutanes, and has been observed in a number of other systems.[17] Thus, it is perhaps not surprising that it should occur in a matrix at low temperatures. However, it is surprising that the cleavage is so rapid ($k > 1\ \mathrm{s}^{-1}$) at 4 K that **26** never accumulates to an extent sufficient for ESR detection.

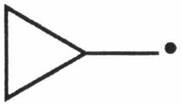

94

95

The reaction is the biradical version of the intensely studied cyclopropylcarbinyl-to-3-butenyl rearrangement (**94** to **95**).[20] The activation parameters for this monoradical process (log $A = 12.5$; $E_a = 5.9$ kcal mol^{-1}; $k(25^\circ\mathrm{C}) = 1.3 \times 10^8\ \mathrm{s}^{-1}$) show that such a reaction would be expected to be extremely slow at 4 K. In the biradical version there is a greater thermodynamic driving force for the rearrangement due to the development of allylic resonance, and this should lead to a decrease in E_a. Product studies show[1] that in triplet biradical **26**, the rate of cleavage to **73** is ca. 10 times faster that the rate of closure to **43** at room temperature. Closure to **43** is a spin-forbidden process in a hydrocarbon with a constrained geometry and would be expected to have a rate not greater than 10^9 s^{-1}.[21] Thus, the upper limit to the cleavage rate is ca. 10^{10} s^{-1}. If $\log A = 12.5$ this implies a barrier of 3.4 kcal mol^{-1}, which would be completely insurmountable at 4 K. Only barriers on the order of 0.2 kcal mol^{-1} or less can be overcome rapidly by thermal activation at 4 K. It seems unlikely that the developing allylic resonance could almost completely eliminate E_a. In addition, such a small barrier would require an anomalously low $\log A$ (ca. 10) in order for the cleavage rate to be 10^{10} s^{-1} at room temperature. It is hard to imagine why a spin-allowed, unimolecular, bond-cleavage reaction would have such a low $\log A$. We do note that the stereoelectronics for cleavage may not be particularly favorable in this case, since the optimal arrangement appears to be one in which a cyclopropyl C–C bond is aligned with a radical *p*-orbital.[20] We, of course, cannot rule out the possibility that the monoradical cleavage is simply a poor model for the biradical cleavage, and a combination of stereoelectronics, allylic stabilization and perhaps other effects conspire to give the reaction of **26** going to **73** remarkably low $\log A$ and E_a values.

There are, however, alternatives to thermal activation. One is quantum-mechanical tunneling.[22] In fact, the closely related biradical **11** is believed to undergo ring closure (to bicyclo[2.1.0]pentane) via heavy-atom tunneling.[13] The key to achieving tunneling when heavy-atom (i.e., non-hydrogen) motions are involved (as in **26** to **73**) is to have a small, *narrow* barrier.[23] It is possible that the ring opening (**26** to **73**) has such a narrow barrier through which tunneling can occur at 4 K. However, it is difficult to imagine that the cleavage barrier is very much smaller and narrower than that for the closure of **11**.[13] The ring closure of **11** is more exothermic than the conversion **26** to **73**. Additionally, it appears that more substantial heavy-atom motions are involved in the cleavage of **26**. Yet, the tunneling of **11** is slow enough that the biradical can be detected easily by ESR under the same conditions as the present work. Based on these observations we cannot rule out tunneling, but we consider it to be highly unlikely.

Another way to get over an "insurmountable" barrier is chemical activation ("hot molecule" effects). Figure 40 shows that ca. 39 kcal mol^{-1} of excess energy is available after nitrogen loss from T_1 of **24**. In *thermal* deazetations of this type, most of the excess energy is localized within the hydrocarbon fragment, rather than the nitrogen.[24] If this is also true (or even nearly so) in the present case, the initial energy of **26** is well above the small ($<$ 3 kcal mol^{-1}) barrier for its rearrangement to **73**. Chemical activation is well known in the gas phase, where collisional deactivation of hot molecules can be quite slow. It has been proposed in condensed media when the chemically activated process has a relatively small barrier ($<$ 25 kcal mol^{-1}).[25] It is not certain how effective an MTHF matrix would be at collisional deactivation, but there is no reason to expect it to be more effective than a liquid phase.[26] In fact, one might expect that vibronic coupling would be less effective under the present conditions than in fluid media. This could mean that chemical activation would be more likely in a matrix than in a liquid. In any case, deactivation in a matrix should depend mainly on the exchange of energy during vibrations, and in order to compete effectively with such a process, ring opening of **26** must occur on a similar timescale. To estimate the unimolecular rate constant, we have modeled this reaction using RRKM theory.[27] The vibrational spectrum of bicyclo[2.1.0]pentane[28] was used as a starting point to obtain the frequencies for **26** and some low-frequency modes were incorporated for the biradical. Since the reaction is spin allowed but may face some stereoelectronic constraints, we have used $A = 4.4 \times 10^{11}$. Computer printouts of the results are given in Appendix C and a sample of the data is presented in Table XI. It is evident that for small barriers, the reaction is essentially controlled by the Arrhenius preexponential factor. It must be noted that an extremely rapid reaction can occur even when there is < 10 kcal mol^{-1} of excess energy, i.e., even if the matrix withdraws a substantial part of the energy. In contrast, for reactions with energy barriers of 20–40 kcal mol^{-1}, even excess energies of 50 kcal mol^{-1} result in very slow reactions. Qualitatively, then, the calculations indicate that it is quite possible for the reaction to compete favorably with deactivation of "hot" **26**. Biradical **26** reacts faster than it can be cooled by the medium, and thus never accumulates to an extent that would allow detection. It is tempting to conclude that "hot" **26** preferentially cleaves to **73** rather than closes to **43** because of the spin-allowed nature of the cleavage, or perhaps because of some dynamic effect. However, we cannot rule out the possibility that ring closure is also an important reactive mode for "hot" **26** because extremely small amounts of material are formed in ESR experiments and quantitative analysis is not possible.

Step II, the Hydrogen Shift. Unlike step I, the hydrogen shift reaction **73** to **28** is, to our knowledge, completely unprecedented. It is formally a 1,2-H shift in a free radical, a reaction that is completely unknown in solution.[20] Such shifts are important in certain biradical systems (see below), but extensive

Table XI. Unimolecular Rate Constants for **26** from RRKM Calculations

E_a	k_2 [a]	k_4 [a]	k_{10} [a]	k_{50} [a]
4.0	1.8×10^{10}	3.5×10^{10}	9.2×10^{10}	3.5×10^{10}
6.0	2.18×10^{9}	5.2×10^{9}	2.0×10^{10}	1.6×10^{10}
10.0	5.5×10^{7}	1.8×10^{8}	1.2×10^{9}	3.6×10^{10}
20.0	3.7×10^{4}	1.7×10^{4}	2.8×10^{6}	1.1×10^{9}
40.0	8.0×10^{-1}	5.68×10^{0}	2.2×10^{2}	2.1×10^{6}

[a] k_E = Rate constant when E kcal mol^{-1} excess energy is present.

studies of a variety of reactions thought to involve "allyl + p" biradicals such as **73** have failed to uncover any involvement of TMM's.[1,17] It thus appears that the present reaction conditions have opened up a completely new reaction pathway.

For this observation we feel that quantum-mechanical tunneling provides an especially suitable explanation. Note that chemical activation provides an attractive way to achieve conventional chemistry at low temperatures but it is not apparent how chemical activation can open new reaction channels. Tunneling, however, seems quite feasible for the conversion of **73** to **28**. Tunneling is often involved in hydrogen-atom and proton transfers at low temperatures. One common aspect of such reactions is very large kinetic isotope effects (KIE), such that ^{2}H tunnels much more slowly than ^{1}H, or perhaps not at all.[29] This reasoning prompted our synthesis of tetradeuterio analog **78**. However, no perceptible change in the chemistry occurred. If tunneling is involved it must be quite efficient, since ^{2}H tunnels rapidly. Two factors could be involved in making tunneling especially effective in the conversion of **73** to **28**.

The first effect is the very short distance the hydrogen must move. Most H (and H^+) transfers that involve tunneling are not 1,2 shifts and therefore involve longer migration distances. The shorter distance in the present case implies a narrower barrier, and thus much faster tunneling. The second effect is the possibility that biradical **73**, like **26**, is born in a vibrationally excited state. The thermochemistry (Figure 40) is certainly consistent with this possibility. If so, the conversion **73** to **28** could be an example of vibrationally assisted tunneling (VAT), a notion that is implicit in most tunneling models and that has been explicitly developed recently.[23b]

Tunneling also nicely explains the unusual effect in which photolysis of

24 and **25** at 77 K does not produce TMM's. The expected decay path for a biradical like **73** is ring closure to **93**. This reaction is apparently slow at 4 K and so a new process involving tunneling can compete. As the temperature is raised the rate of the ring closure should increase substantially, but the tunneling rate should increase only slightly. Thus, the ring closure should overtake the H shift at higher temperatures. This would explain why no TMM is seen at 77 K from **24** and **25**.

96

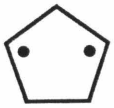

11

13

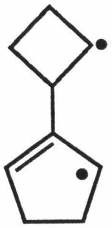

92

Although deuteration did not measurably slow the hydrogen-shift, apparently the incorporation of the ethano bridge in **92** (relative to **73**) does to some extent, if the assignment of **92** as the carrier of the outer wings in the spectra derived from **25** is correct. While this may at first seem surprising, it does have precedent. A similar 1,2-H shift is often invoked to explain the presence of olefinic products in reactions thought to involve simple 1,3-biradicals. Examples include the conversion of trimethylene (**96**) to propene, and **11** to cyclopentene. In contrast, reactions that involve 1,3-cyclobutanediyl (**13**) do not produce cyclobutene.[18,24a,30] A stereoelectronic effect has been invoked to explain this result.[24a] The smaller C–C–C angle at the CH_2 group of **13** moves the radical center away from the hydrogens that must migrate. Additionally the ring constraints make it more difficult to achieve an arrangement in which a C–H bond is aligned with a radical *p*-orbital. Analogous effects are present in **92**. One might expect that a tunneling reaction would be especially sensitive to stereoelectronic effects. Small changes in barrier height and, more importantly, barrier width can have substantial effects on tunneling rates. Another possible explanation of this result would be that VAT is important. The larger size of **92** vs. **73** would make such a "chemically activated" process less efficient. Thus, it seems plausible that the hydrogen-shift reaction could be slower in **92** than **73**.

The possibility of the second step in Scheme VIII being photochemical was also considered. In order to rule out such a secondary photochemical process, we measured the intensity of the ESR signal as a function of the amount of light incident upon the sample. For a process involving a single photochemical step, a linear dependence is expected; whereas for a two-photon process, signal intensity should be proportional to the square of the incident light intensity. Figure 41 shows plots of the data along with least-squares fits to a straight line and a parabola. Despite substantial scatter in the data, we observe a much better correlation with the straight line, suggesting that only one photochemical step is involved.

Alternative Mechanisms

In order to consider Scheme VIII as a viable mechanistic path to the TMM's we observe, some unusual effects must be invoked. However, it is quite difficult to develop alternatives. As always one could say that diazenyl biradicals such as **97** are involved. However, conversion of **97** to **98** is even less likely than **26** to **73** since allylic resonance is not developed. Furthermore, there is no direct evidence for the involvement of diazenyl biradicals in the triplet chemistry of this or any related system.

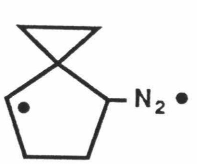

97

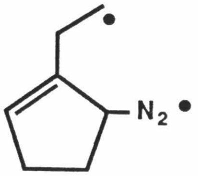

98

We have considered a direct, one-step conversion of **26** to **28**. The motions involved are quite unlike anything previously described in the thermal rearrangement literature. It should be recognized, however, that once "hot molecule" effects are considered, the notion of a stepwise mechanism becomes fuzzy. One can envision a scenario in which **26** is formed in a vibrationally excited state and is never relaxed but goes on directly to **73**. Similarly, **73** is vibrationally excited and never relaxes but goes on directly (VAT ?) to **28** which finally "cools down". In such a process **26** and **73** can hardly be considered intermediates. Rather, the reaction involves exploration of the high energy regions of the triplet C_7H_{10} surface. As it is deactivated, the molecule falls into the deepest well — the thermodynamic sink **28**.

Magnitude of hfc constants

As pointed out earlier, these studies provide the first determination of hfc constants at the α and β positions of an alkylidenecyclopentanediyl. The observation of interpretable hfc in the $\Delta m_s = 2$ transition in a sample of randomly oriented triplet species is extremely rare. Usually complications arise due to the inherent anisotropy of the systems, in that there are four stationary resonant fields (turning points) in this region of the spectrum.[32] As discussed in Chapter III their positions are given by H_{min} (corresponding to the lowest limit

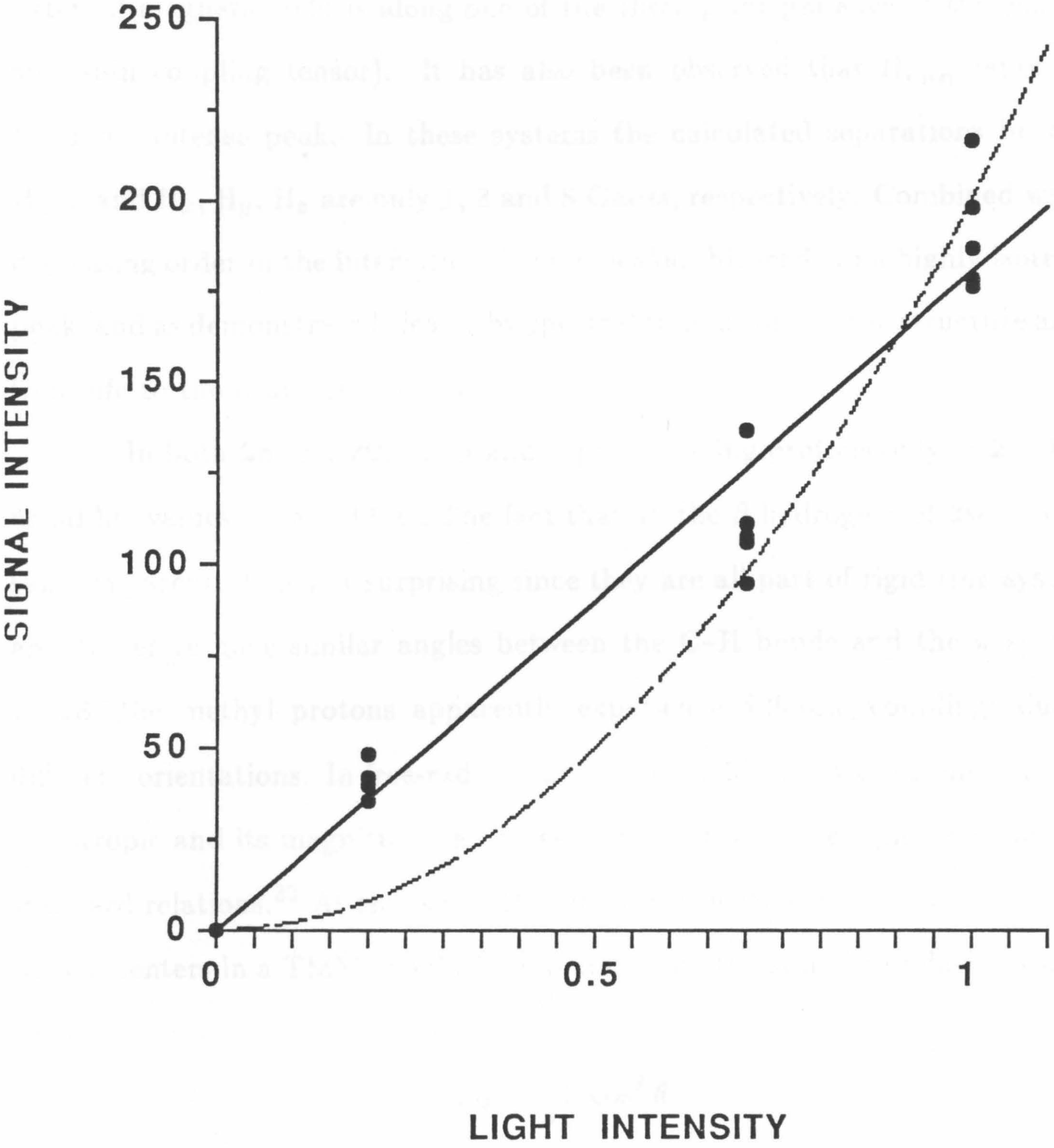

Figure 41. Dependence of signal intensity on light intensity.

of absorption) and H_x, H_y, and H_z (corresponding to orientations in which the external magnetic field is along one of the three principal axes of the electron spin-spin coupling tensor). It has also been observed that H_{min} represents the most intense peak. In these systems the calculated separations between H_{min} and H_x, H_y, H_z are only 1, 3 and 8 Gauss, respectively. Combined with a decreasing order in the intensities of these peaks, this leads to a highly isotropic peak, and as demonstrated clearly by spectral simulation, all the structure arises from hfc to the α and β protons.

In both **28** and **29**, the α and β protons (ring protons only in **28**) have equal hfc values of ca. 13.5 G. The fact that all the β hydrogens of **29** have the same apparent hfc is not surprising since they are all part of rigid ring systems and therefore have similar angles between the C–H bonds and the π system. In **28**, the methyl protons apparently experience different couplings due to different orientations. In free-radical samples in rigid media the β hfc constant is isotropic and its magnitude can be esimated using Hückel spin densities and standard relations.[33] At this level, the electron density (ρ) at each of the three radical centers in a TMM should be 1/3 and using the standard relation we can write

$$a_H^\beta = \frac{1}{3} C \cos^2\theta$$

If we assume C to be 42.5 G and θ (the angle between the *p*-orbital axis at C_α and the plane containing C_α, C_β and H_β) to be 30 degrees, we obtain

$$a_H^\beta = 10.6$$

In TMM-like structures, however, we must also take into account a spin polarization effect arising from the negative spin density at the central carbon atom.[34] For example, in the parent TMM (**4**), Hückel calculations alone predict a_H^α to be 7.1 G whereas the experimental value obtained from single-crystal studies is 8.9 G.[35] If we scale the calculated value for a_H^β in our systems by the same factor (8.9/7.1), a value of 13.3 G is obtained, in close agreement with our observations.

99

Another useful reference is cyclopentenyl, **99**, for which $a_H^\alpha = 14$ G and $a_H^\beta = 22$ G.[36] For cyclopentenyl we are not concerned with the absolute magnitude of the hfc, but only the relative values of a_H^α and a_H^β. The α coupling in **28** and **29** is significantly larger than the parent TMM. In addition, based on the data for **99**, one might have expected a_H^β in **28** and **29** to be significantly larger than a_H^α, but it is not. It is tempting to conclude that these two effects are related and perhaps reflect the role of the ethano bridge in the spin polarization mechanism.[34] However, the same spin polarization effect is operative in allyl and it is difficult to develop some influence of the ethano bridge that is important for **28** vs. TMM but not in **99** vs. allyl. It must be pointed out that α hfc constants are anisotropic, and oriented samples are required for determination of the principal values of the hfc tensor.[35] Since we have only used randomly oriented samples, the apparent a_H^α might correspond to just one tensor component. In any case, more work is required before a complete understanding of hfc in biradicals can be achieved. We consider it quite encouraging that we have been able to obtain experimental data which promises to provide important information about the electronic structure of biradicals.

EXPERIMENTAL SECTION

General. ^{1}H NMR were obtained on a Varian EM-390 spectrometer. Fourier-transform ^{1}H NMR were obtained on a JEOL GX-400 spectrometer. Ultraviolet spectroscopy was performed on a Hewlett-Packard 8451A diode array spectrometer. Synthetic photolyses were carried out using a 450-W Hanovia medium-pressure mercury arc lamp. Elemental analyses and mass spectra were obtained by the Caltech Analytic Facility.

ESR experiments. A Varian E-line Century Series X-band spectrometer equipped with an Oxford Instruments ESR-900 continuous liquid helium flow cryostat was used to obtain ESR spectra at low temperatures. The temperature at the sample was measured before and after each experiment using a calibrated carbon-glass thermistor (Lakeshore Cryotronics) placed inside a sample tube and is accurate to within ± 0.3 K. During each experiment the temperature was monitored continuously by a gold-chromel thermocouple fixed 1 cm below the sample in the quartz dewar. Temperature was varied using either the helium flow rate or the automatic DTC2 temperature controller.

An Oriel 1000-W mercury-xenon lamp was focussed into the microwave cavity for photolysis. Various optical filters or an Oriel monochromator were used to obtain narrow bands of light of the desired wavelength range.

Samples were prepared from solutions of about 2–3 mg of azoalkanes in 300 μL of solvent (MTHF used was freshly distilled over benzophenone-ketyl). The solution was placed in 4 mm o.d. quartz ESR tubes equipped with high-vacuum stopcocks. Tubes were then degassed (three freeze–pump–thaw cycles), frozen in liquid nitrogen and inserted into the ESR cavity.

Photochemical studies. The photolysis of azoalkane **24** at room temperature and low temperatures was carried out in 4 mm o.d. quartz tubes fitted with high-vacuum stopcocks. A stock solution of **24** in acetone-d_6 (0.35 M) was used and samples were degassed by three freeze–pump–thaw cycles. A 1000-W mercury–xenon arc lamp (Oriel) was used along with optical filters (Schott). Direct irradiation was carried out between 323–345 nm and benzophenone sensitized photolysis at $\lambda > 358$ nm. A pentane–liquid nitrogen bath was used to maintain a temperature of –125 °C.

Dependence of signal intensity on light intensity. These studies were performed by measuring the growth of the ESR signal for biradical **28** at 4 K upon photolysis of diazene **24** in an MTHF matrix for 1 min. The intensity of the incident light was varied using optical filters. A mercury interference filter and a KG-4 or a KG-5 filter (Schott) were used to obtain three different intensities as shown below. The transmittance was measured both by a UV-vis spectrophotometer and a thermopile detector.

Interference filter Transmittance = 1.00
Interference filter + KG-4 Transmittance = 0.70
Interference filter + KG-5 Transmittance = 0.21

Synthesis.

2,3-Dicarboethoxy-7-cyclobutylidene-2,3-diazabicyclo[2.2.1]heptane (100). To a sample of 6,6-trimethylenefulvene[7,37] (0.71 g, 6.1 mmol, 1.0 eq) in 35 mL dry ether was added diethylazodicarboxylate (1.15 g, 6.6 mmol, 1.1 eq). The mixture was stirred under nitrogen for 1 h. Filtration through basic alumina and removal of solvent gave 1.7 g of a pale yellow oil which was characterized by NMR spectroscopy; ^{1}H NMR (CDCl$_3$) δ 1.04 (t, 6H), 1.93 (quintet, 2H), 2.62 (br t, 4H), 4.20 (quartet, 4H), 5.18 (br s, 2H), 6.65 (br s, 2H). Since attempts at purification resulted in decomposition, the oil was immediately subjected to catalytic hydrogenation[38] (ethyl acetate, 10% palladium on charcoal). Filtration through Celite, removal of the solvent and flash chromatography[39] (3:1 ether, petroleum ether; R_f=0.35) afforded **100** (1.11 g) in the form of a colorless oil; ^{1}H NMR ($CDCl_3$) δ 1.03 (t, 6H), 1.64–1.81 (br m, 4H), 1.94 (quintet, 2H), 2.62 (br t, 4H), 4.20 (quartet, 4H), 4.56 (br s, 2H); ^{13}C NMR ($CDCl_3$) δ 14.8, 17.3, 27.5, 29.6, 58.6, 62.1, 127.7, 128.3, 156.9.

7-Cyclobutylidene-2,3-diazabicyclo[2.2.1]hept-2-ene (72). A solution of potassium hydroxide (3.02 g, 87%, 46.9 mmol, 12.5 eq) in 3 mL 2-propanol (previously purged with nitrogen for 15 min) was brought to reflux. Degassed 2-propanol (3 mL) containing carbamate **100** (1.11 g, 3.7 mmol, 1.0 eq) was added dropwise. Reflux was maintained for 2 h after which the reaction mixture was cooled to room temperature and sodium bicarbonate (2.0 g) added. After stirring for 0.5 h, the suspension was filtered, yellow mercuric oxide (4.0 g) was added to the filtrate, and the heterogeneous mixture was stirred at 0°C for 2 h.[40] Filtration through Celite, extraction of the brown solution with pentane, removal of solvent, and flash chromatography[39] (1:1 ethyl acetate, petroleum ether; R_f=0.45) gave 274 mg of **72** in the form of a white solid; ^{1}H NMR ($CDCl_3$) δ 1.04 (m, 2H), 1.58 (m, 2H), 1.92 (quintet, 2H), 2.58 (t, 4H), 5.15 (s, 2H); ^{13}C NMR ($CDCl_3$) δ 17.4, 21.6, 29.5, 73.6, 127.6, 133.6; UV (pentane) λ_{max} 336 nm (ϵ =73), 341 nm (ϵ =80).

2,3-Dicarboethoxy-7-ethylidene-2,3-diazabicyclo[2.2.1]heptane (101). 6-Methylfulvene[7,37] (0.95 g, 10.3 mmol, 1.0 eq) in 40 mL dry ether was stirred at room temperature with diethylazodicarboxylate (2.0 g, 11.4 mmol, 1.1 eq) for 1 h. Filtration through basic alumina and removal of solvent yielded 2.5 g of a pale yellow oil which was characterized by NMR spectroscopy; ^{1}H NMR

($CDCl_3$) δ 1.03 (t, 6H), 1.59 (d, 3H), 4.21 (quartet, 4H), 4.61–4.97 (m, 3H), 6.7–6.9 (br s, 2H). Without further purification this oil was taken up in 25 mL ethanol and about 2 mL hydrazine was added.[41] Air was bubbled through the solution for 14 h. Solvent was then removed from the solution and the residue was taken up in 50 mL of diethyl ether. This solution was washed repeatedly with water until the aqueous layer was neutral by pH paper. The ethereal layer was dried over magnesium sulfate, filtered through Celite, and the solvent was removed. Flash chromatography[39] (3:1 ether, pentane; R_f=0.35) gave 1.04 g of **101** as a colorless oil ; ^{1}H NMR ($CDCl_3$) δ 1.10 (t, 6H), 1.62 (d, 3H), 1.75–1.91 (m, 4H), 4.21 (quartet, 4H), 5.12 (br s, 2H), 6.55 (m, 1H); ^{13}C NMR ($CDCl_3$) δ 12.9, 14.6, 28.0, 58.8, 61.9, 128.1, 138.7, 157.3; anal. C,H,N.

7-Ethylidene-2,3-diazabicyclo[2.2.1]hept-2-ene (71). A solution of potassium hydroxide (0.26 g, 87%, 4.0 mmol, 12.0 eq) in 1 mL 2-propanol (previously purged with nitrogen for 15 min) was brought to reflux. Degassed 2-propanol (1 mL) containing carbamate **101** (0.09 g, 0.3 mmol, 1.0 eq) was added and the mixture heated at reflux for 2 h. Solvent was then removed and the yellow paste obtained was taken up in 5 mL of a saturated solution of sodium bicarbonate. This solution was extracted with methylene chloride (5 x 10 mL). The organic layer was dried over magnesium sulfate and filtered. Yellow mercuric oxide (1.0 g) was then added and the mixture stirred at 0°C for 3 h. Filtration through Celite, removal of solvent and recrystallization from pentane yielded 12 mg of **71** in the form of white crystals. ^{1}H NMR was identical to that reported by Little.[6]

2,3-Dicarboethoxy-2,3-diazabicyclo[2.2.1]hept-5-ene-7-spiro-8,8,9,9-tetramethylcyclopropane (102). A sample of tetramethyl spiro[2.4]hepta-1,3-diene[42] (0.49 g, 3.3 mmol, 1.0 eq) was dissolved in 20 mL methylene chloride and diethylazodicarboxylate (0.63 g, 3.6 mmol, 1.1 eq) was added dropwise under an atmosphere of nitrogen. The reaction mixture was stirred at room temperature for 2.5 h. Filtration through basic alumina, removal of solvent, and flash chromatography[39] (2:1 ether, pentane; R_f=0.3) yielded 0.82 g (78%) of pure product in the form of a colorless oil; ^{1}H NMR ($CDCl_3$) δ 0.95 (s, 6H), 1.00 (s, 6H), 1.09 (t,6H), 4.06 (quartet, 4H), 4.69 (br s, 2H); ^{13}C NMR ($CDCl_3$) δ 14.8, 23.3, 23.8, 59.8, 135.4, 158.4.

2,3-Dicarboethoxy-2,3-diazabicyclo[2.2.1]heptane-7-spiro-8,8,9,9-tetramethylcyclopropane (103). To a sample of **102** (0.12 g, 0.4 mmol) in 20 mL ethanol was added about 2 mL hydrazine. Air was bubbled through the solution at room temperature for 15 h. The solvent was removed and the residue taken up in 35 mL ether. This solution was washed repeatedly with water until the aqueous layer was neutral by pH paper. The organic layer was dried over magnesium sulfate, filtered through basic alumina, and flash chromatographed[39] (2:1 ether, pentane; R_f=0.33) to yield 89 mg of **103** as a white crystalline solid; ^{1}H NMR ($CDCl_3$) δ 1.01 (br s, 12H), 1.24 (t,6H), 1.65–1.83 (m, 4H), 4.10–4.22 (m, 6H); ^{13}C NMR ($CDCl_3$) δ 14.5, 18.6, 19.1, 22.2, 22.9, 28.3, 48.5, 61.5, 61.9, 157.3; anal. C,H,N.

2,3-Diazabicyclo[2.2.1]hept-2-ene-7-spiro-8,8,9,9-tetramethylcyclopropane (88). A solution of potassium hydroxide (0.26 g, 87%, 4.0 mmol, 7.6 eq) in 1 mL 2-propanol (previously purged with nitrogen for 15 min) was brought to reflux under an atmosphere of nitrogen. A solution of carbamate **103** (0.17 g, 0.5 mmol, 1.0 eq) in 1 mL degassed 2-propanol was then added and the mixture heated at reflux for 3 h. After cooling to room temperature, solvent was removed yielding a yellow paste which was then taken up in 3 mL of a saturated sodium bicarbonate solution. The aqueous layer was extracted with methylene chloride (5 x 20 mL). The solvent was then removed and cupric bromide (0.30 g, 1.3 mmol, 2.5 eq) in 0.5 mL water was added. The red precipitate which formed was filtered and taken up in 15 mL methylene chloride. The diazene was liberated by the addition of 5 mL of a 1N solution of ammonium hydroxide. The organic layer was separated and dried over sodium sulfate. Filtration and removal of solvent yielded 0.12 g of a yellow solid. Recrystallization from ethyl acetate gave **88** as a white crystalline solid; mp 101–102 °C; ^{1}H NMR ($CDCl_3$) δ 0.93 (s, 6H), 0.95 (s, 6H), 1.01 (m, 2H), 1.53 (m, 2H), 4.76 (br s, 2H); ^{13}C NMR ($CDCl_3$) δ 18.57, 19.05, 21.07, 21.38, 21.54, 51.00, 76.68; UV (ethanol) λ_{max} 334 nm (ϵ=74), 342 nm (ϵ=74); mass spectrum *m/e* 150 (M–28), 135, 121, 107, 28 (100).

2,3-Diazabicyclo[2.2.1]hept-2-ene-7-spiro-8,8,9,9-tetradeuteriocyclopropane (78). Diazene **78** was prepared by following the procedure of Roth and Enderer.[1] 1,2-Dibromotetradeuterioethane was used to incorporate the deuteria into spiro[2.4]hepta-1,3-diene.[43] Addition of diethylazodicarboxylate, followed by selective reduction of the endocyclic double bond and hydrolysis–oxidation then afforded the desired product.

References for Chapter IV

1. Roth, W.R.; Enderer, K. *Liebigs Ann. Chem.* **1969**, *730*, 82–90; **1970**, *733*, 44–58; see also: Adam, W.; Oppenlander, T.; Zang, G. *J. Org. Chem.* **1985**, *50*, 3303–3312.
2. McElwee-White, L.; Dougherty, D.A. *J. Am. Chem. Soc.* **1984**, *106*, 3466–3474.
3. See Chapter III for details on the ESR spectroscopy of triplet species.
4. Berson, J.A. *Acc. Chem. Res.* **1978**, *11*, 446–453. Berson, J.A. In *Diradicals*; Borden, W.T., Ed.; Wiley: New York, 1982; pp 151–194.
5. Goldberg, A.H. M.S. Thesis, California Institute of Technology, 1982.
6. Little, R.D.; Carroll, G.L. *J. Org. Chem.* **1979**, *44*, 4720–4722.
7. Stone, K.J.; Little, R.D. *J. Org. Chem.* **1984**, *49*, 1849–1853.
8. The expected intensity pattern is 1:10:45:120:210:252:210:120:45:10:1.
9. Lokensgard, D.M.; Dougherty, D.A.; Hilinski, E.F.; Berson, J.A. *Proc. Natl. Acad. Sci. USA.* **1980**, *77*, 3090–3094.
10. Berson, J.A., personal communication.
11. McElwee-White, L. Ph.D. Dissertation, California Institute of Technology, 1984.
12. It is not surprising that direct photolysis is not successful with **85**. This diazene is a derivative of diazabicyclo[2.2.2]oct-2-ene, a ring system known to be relatively photoinert.
13. Buchwalter, S.L.; Closs, G.L. *J. Am. Chem. Soc.* **1979**, *101*, 4688–4693.
14. Snyder, G.J.; Dougherty, D.A. *J. Am. Chem. Soc.* **1986**, *108*, 299–300.
15. Maier, G.; Reisenauer, H.P.; Rohde, B.; Dehnicke, K. *Chem. Ber.*

1983, *116*, 732–740.

16. Recently 1,3-divinyl-1,3-cyclobutanediyl has been observed and a similar experiment shows that it also absorbs light in the same wavelength region. Sponsler, M.B. Ph.D. Dissertation, California Institute of Technology, 1987.

17. Gajewski, J.J. *Hydrocarbon Thermal Isomerizations*; Academic: New York; 1981; pp 90–106.

18. (a) $\Delta H_f^\circ(\mathbf{24})$: Standard group increments (Benson, S.W. *Thermochemical Kinetics*, 2nd ed.; Wiley: New York, 1976) were used to add a cyclopropyl ring to 2,3-diazabicyclo[2.2.1]hept-2-ene ($\Delta H_f^\circ = 49.6$ kcal mol^{-1}; Kao, J.; Huang, T.-N. *J. Am. Chem. Soc.* **1979**, *101*, 5546–5557). Spiro strain (5 kcal mol^{-1}) and ring strain (29 kcal mol^{-1}) were also added. The S_1 and T_1 excited states were placed 84 and 60 kcal mol^{-1} higher (Engel, P.S.; Steel, C. *Acc. Chem. Res.* **1973**, *6*, 275–281). (b) $\Delta H_f^\circ(\mathbf{26})$: The known energy barrier for the bridge-flip process of **43** (29 kcal mol^{-1}; ref. 1) was added to $\Delta H_f^\circ(\mathbf{43})$ obtained by addition of a cyclopropyl ring along with ring strain and spiro strain (10 kcal mol^{-1}) to the known ΔH_f° for bicyclo[2.1.0]pentane (37 kcal mol^{-1}; Chang, S.; McNally, D.; Shary-Tehrany, S.; Hickey, M.J.; Boyd, R.H. *J. Am. Chem. Soc.* **1970**, *92*, 3109–3118). (c) $\Delta H_f^\circ(\mathbf{73})$: Molecular mechanics was used to obtain $\Delta H_f^\circ(\mathbf{93}) = 43$ kcal mol^{-1}. The activation energy for the degenerate rearrangement of methylenecyclobutane (49.5 kcal mol $^{-1}$; Doering, W. von E.; Gilbert, J.C. *Tetrahedron, Supplement No. 7*, 397–414) was added. The additional release of strain due to the bridgehead olefin was estimated at 15 kcal mol^{-1} by molecular mechanics calculations on **93** and its saturated analog.

This puts $\Delta H_f^\circ(\mathbf{73})$ at roughly 79 kcal mol^{-1}. (d) $\Delta H_f^\circ(\mathbf{28})$: $\Delta H_f^\circ(\mathbf{4})$ $= 38.3 + \Delta H_f^\circ($ 1,3-butadiene $) = 64$ kcal mol^{-1} (Feller, D.; Davidson, E.R.; Borden, W.T. *Isr. J. Chem.*, **1983**, *23*, 105–108 and Cox, J.D.; Pilcher, G. *Thermochemistry of Organic and Organometalic Compounds*; Academic: New York, 1970). Addition of an ethano bridge, a methyl group and strain energy (7 kcal mol^{-1}) gives $\Delta H_f^\circ(\mathbf{28})$ as roughly 58 kcal mol^{-1}.

19. See, for example, Chang, M.H.; Dougherty, D.A. *J. Am. Chem. Soc.* **1982**, *104*, 2333–2334.
20. Beckwith, A.L.J.; Ingold, K.U. In *Rearrangements in Ground and Excited States*; de Mayo, P., Ed.; Academic: New York, 1980; Vol. I, pp 161–310.
21. See, for example, ref. 13 and Wilson, R.M.; Geiser, F. *J. Am. Chem. Soc.* **1978**, *100*, 2225–2226; Wilson, R.M.; Rekers, J.W. *J. Am. Chem. Soc.* **1981**, *103*, 206–207. For an alternative analysis see Adam, W.; Hannemann, K.; Hössel, P. *Tet. Lett.*, **1984**, *25*, 181–184.
22. Bell, R.P. *The Tunnel Effect in Chemistry*; Chapman and Hall: New York, 1980.
23. (a) Carpenter, B.K. *J. Am. Chem. Soc.* **1983**, *105*, 1700–1701; Huang, M.-J.; Wolfberg, M. *J. Am. Chem. Soc.* **1984**, *106*, 4039–4040.

    (b) Dewar, M.J.S.; Merz, K.M., Jr.; Stewart, J.J.P. *J. Chem. Soc., Chem. Comm.* **1985**, 166–168.
24. (a) Chang, M.H.; Jain, R.; Dougherty, D.A. *J. Am. Chem. Soc.* **1984**, *106*, 4211–4217. (b) See also, Holt, P.L.; McCurdy, K.E.; Adams, J.S.; Burton, K.A.; Weisman, R.B.; Engel, P.S. *J. Am. Chem. Soc.* **1985**, *107*, 2180–2182.

25. Farneth, W.E.; D'Amore, M.B.; Brauman, J.I. *J. Am. Chem. Soc.* **1976**, *98*, 5546–5552.

26. In rare-gas matrices vibrationally excited states of small molecules can be quite long-lived. See Bondybey, V.E.; English, J.H.; Miller, T.E. *J. Phys. Chem.* **1983**, *87*, 100–1305; Bondybey, V.E.; English, J.H. *J. Chem. Phys.* **1980**, *73*, 87–92.

27. See Chapter II for details on the application of RRKM theory.

28. Bragin, J.; Guthals, D. *J. Phys. Chem.* **1975**, *79*, 2139–2144.

29. See, for example, Brunton, G.; Gray, J.A.; Griller, D.; Barclay, L.R.C.; Ingold, K.U. *J. Am. Chem. Soc.* **1978**, *100*, 4197–4200; Platz, M.S.; Senthilnathan, V.P.; Wright, B.B.; McCurdy, C.W., Jr. *J. Am. Chem. Soc.* **1982**, *104*, 6494–6501.

30. It is *possible* that such a shift is responsible for the formation of cyclobutene in the 185 nm photolysis of bicyclobutane.[31] However, such excitation could lead to upper electronic (or vibrational) states of **13**. Also, paths to cyclobutene that do not involve **13** are feasible.

31. Becknell, A.F.; Berson, J.A.; Srinivasan, R. *J. Am. Chem. Soc.* **1985**, *107*, 1076–1078. Adam, W.; Oppenländer, T.; Zang, G. *J. Am. Chem. Soc.* **1985**, *107*, 3921–3924.

32. Kottis, P.; Lefebvre, R. *J. Chem. Phys.* **1963**, *39*, 393–403. Kottis, P.; Lefebvre, R. *J. Chem. Phys.* **1964**, *41*, 379–393.

33. Fischer, H. In *Free Radicals*; Kochi, J.K., Ed.; Wiley: New York, 1973; Vol. II, pp 446–448.

34. See Borden, W.T. In *Diradicals*; Borden, W.T., Ed.; Wiley: New York, 1982; pp 25–27.

35. Dowd, P. *Acc. Chem. Res.* **1972**, *5*, 242–248. Dowd, P.; Gold, A.;

Sachdev, K. *J. Am. Chem. Soc.* **1968**, *90*, 2715-2716. Claesson, O.; Lund, A.; Gillbro, T.; Ichikawa, T.; Edlund, O.; Yoshida, H. *J. Chem. Phys.* **1980**, *72*, 1463–1470.

36. Lunazzi, L.; Placucci, G.; Grossi, L. *J. Chem. Soc., Chem. Comm.* **1979**, 533–534.

37. Kyburz, R.; Schaltegger, H.; Neuenschwander, M. *Helv. Chim. Acta*, **1971**, *54*, 107–1046.

38. Marullo, N.P.; Alford, J.A. *J. Org. Chem.* **1968**, *33*, 2368–2370.

39. Still, W.C.; Kahn, M.; Mitra, A. *J. Org. Chem.* **1978**, *43*, 2923–2925.

40. Berson, J.A.; Bushby, R.J.; McBride, J.M.; Tremelling, M. *J. Am. Chem. Soc.* **1971**, *93*, 1544–1546.

41. Garbisch, E.W., Jr.; Schildcrout, S.M.; Patterson, D.B.; Sprecher, C.M. *J. Am. Chem. Soc.* **1965**, *87*, 2932–2944.

42. Moss, R.A. *J. Org. Chem.* **1966**, *31*, 3296–3300.

43. Alder, K.; Ache, H.-J.; Flock, F.H. *Chem. Ber.* **1960**, *93*, 1888–1895. Hallam, B.F.; Pauson, P.L. *J. Chem. Soc.* **1958**, 646–650.

APPENDIX C

RESULTS OF RRKM CALCULATIONS

```
BIRADICAL TO BIRADICAL REARRANGEMENT
NO ROTORS, NO OVERALL ROTATION

EZERO =   4.00 KCAL/MOLE     ESTAR =   5.00 KCAL/MOLE

EINC  =   1.00 KCAL/MOLE     REACTION PATH DEGENERACY  =  2.0

  50  RATE CONSTANTS TO BE CALCULATED

NUMBER OF OSCILLATORS IN MOLECULE   NUMBER OF INTERNAL ROTORS IN MOLECULE

                45                         0

FREQUENCIES IN MOLECULE

       400.0      2982.0      2946.0      2921.0      2874.0      1470.0      1446.0      1332.0
      1280.0      1218.0      1188.0      1106.0      1012.0       968.0       883.0       774.0
       755.0       416.0      3054.0      2966.0      2936.0      1465.0      1325.0      1279.0
      1238.0      1198.0      1053.0      1030.0       978.0       922.0       914.0       787.0
      3050.0      1188.0       200.0       922.0       818.0      1218.0      1000.0       200.0
       200.0       854.0       200.0       400.0       787.0

EXTERNAL ROTATIONS TREATED AS INACTIVE

*****STRUCTURE OF THE CRITICAL CONFIGURATION IS SPECIFIED*****

NUMBER OF OSCILLATORS IN COMPLEX   NUMBER OF INTERNAL ROTORS IN COMPLEX

                44                         0

FREQUENCIES IN COMPLEX

       650.0      2982.0      2946.0      2921.0      2874.0      1470.0      1446.0      1332.0
      1280.0      1218.0       787.0      1106.0      1012.0       968.0       200.0       774.0
       755.0       416.0      3054.0      2966.0      2936.0      1465.0      1325.0      1279.0
      1238.0      1198.0      1053.0      1030.0       978.0       922.0       914.0       990.0
      3050.0      1188.0       600.0       922.0      1618.0      1400.0      1025.0       600.0
       600.0       954.0       200.0      1000.0


XXXXXXXXXXXXXXXXXXXXXXXXXXXXXXXXXXXXXXXXXXXXXXXXXXXXXXXXXXXXXXXXXXXXXXXXXXXXXXXXXXXXXXXXXXXXXXXXXXXXXXXX

RATE CONSTANTS CALCULATED USING THESE OPTIONS:      KROT = -1  NANH = 0  NCRIT = 0  JDEN =  0  JSUM =  0

XXXXXXXXXXXXXXXXXXXXXXXXXXXXXXXXXXXXXXXXXXXXXXXXXXXXXXXXXXXXXXXXXXXXXXXXXXXXXXXXXXXXXXXXXXXXXXXXXXXXXXXX
```

ESTAR KCAL/MOLE	EDAG KCAL/MOLE	HARMONIC DENSITY	HARMONIC SUM	HARMONIC RATE CONSTANT
5.00	1.00	.1307E+02	.2063E+01	.9459E+10
6.00	2.00	.4107E+02	.1199E+02	.1751E+11
7.00	3.00	.1207E+03	.5269E+02	.2617E+11
8.00	4.00	.3354E+03	.1972E+03	.3526E+11
9.00	5.00	.8882E+03	.6607E+03	.4460E+11
10.00	6.00	.2255E+04	.2035E+04	.5408E+11
11.00	7.00	.5518E+04	.5857E+04	.6363E+11
12.00	8.00	.1306E+05	.1594E+05	.7317E+11
13.00	9.00	.2999E+05	.4136E+05	.8267E+11
14.00	10.00	.6702E+05	.1029E+06	.9208E+11
15.00	11.00	.1461E+06	.2470E+06	.1014E+12
16.00	12.00	.3111E+06	.5737E+06	.1106E+12
17.00	13.00	.6486E+06	.1294E+07	.1196E+12
18.00	14.00	.1326E+07	.2841E+07	.1285E+12
19.00	15.00	.2661E+07	.6090E+07	.1372E+12
20.00	16.00	.5249E+07	.1276E+08	.1458E+12
21.00	17.00	.1019E+08	.2620E+08	.1542E+12
22.00	18.00	.1948E+08	.5276E+08	.1624E+12
23.00	19.00	.3670E+08	.1044E+09	.1705E+12
24.00	20.00	.6824E+08	.2030E+09	.1784E+12
25.00	21.00	.1253E+09	.3888E+09	.1861E+12
26.00	22.00	.2271E+09	.7338E+09	.1937E+12
27.00	23.00	.4071E+09	.1366E+10	.2011E+12
28.00	24.00	.7218E+09	.2509E+10	.2084E+12
29.00	25.00	.1266E+10	.4551E+10	.2155E+12
30.00	26.00	.2199E+10	.8159E+10	.2224E+12
31.00	27.00	.3783E+10	.1446E+11	.2292E+12
32.00	28.00	.6448E+10	.2537E+11	.2359E+12
33.00	29.00	.1089E+11	.4405E+11	.2424E+12
34.00	30.00	.1825E+11	.7574E+11	.2488E+12
35.00	31.00	.3033E+11	.1290E+12	.2550E+12
36.00	32.00	.5000E+11	.2178E+12	.2612E+12
37.00	33.00	.8182E+11	.3646E+12	.2672E+12
38.00	34.00	.1329E+12	.6053E+12	.2730E+12
39.00	35.00	.2144E+12	.9971E+12	.2788E+12
40.00	36.00	.3435E+12	.1630E+13	.2845E+12
41.00	37.00	.5468E+12	.2645E+13	.2900E+12
42.00	38.00	.8649E+12	.4262E+13	.2954E+12
43.00	39.00	.1360E+13	.6820E+13	.3007E+12
44.00	40.00	.2125E+13	.1084E+14	.3059E+12
45.00	41.00	.3302E+13	.1713E+14	.3110E+12
46.00	42.00	.5102E+13	.2690E+14	.3161E+12
47.00	43.00	.7841E+13	.4198E+14	.3210E+12
48.00	44.00	.1199E+14	.6514E+14	.3258E+12
49.00	45.00	.1823E+14	.1005E+15	.3305E+12
50.00	46.00	.2760E+14	.1543E+15	.3352E+12
51.00	47.00	.4157E+14	.2355E+15	.3397E+12
52.00	48.00	.6231E+14	.3578E+15	.3442E+12
53.00	49.00	.9299E+14	.5407E+15	.3486E+12
54.00	50.00	.1382E+15	.8133E+15	.3529E+12

```
BIRADICAL TO BIRADICAL REARRANGEMENT
NO ROTORS, NO OVERALL ROTATION

EZERO =   6.00 KCAL/MOLE     ESTAR =   7.00 KCAL/MOLE

EINC  =   1.00 KCAL/MOLE     REACTION PATH DEGENERACY  =  2.0

  50  RATE CONSTANTS TO BE CALCULATED

NUMBER OF OSCILLATORS IN MOLECULE   NUMBER OF INTERNAL ROTORS IN MOLECULE

                45                        0

FREQUENCIES IN MOLECULE

       400.0      2982.0      2946.0      2921.0      2874.0      1470.0      1446.0      1332.0
      1280.0      1218.0      1188.0      1106.0      1012.0       968.0       883.0       774.0
       755.0       416.0      3054.0      2966.0      2936.0      1465.0      1325.0      1279.0
      1238.0      1198.0      1053.0      1030.0       978.0       922.0       914.0       787.0
      3050.0      1188.0       200.0       922.0       818.0      1218.0      1000.0       200.0
       200.0       854.0       200.0       400.0       787.0

EXTERNAL ROTATIONS TREATED AS INACTIVE

*****STRUCTURE OF THE CRITICAL CONFIGURATION IS SPECIFIED*****

NUMBER OF OSCILLATORS IN COMPLEX   NUMBER OF INTERNAL ROTORS IN COMPLEX

                44                        0

FREQUENCIES IN COMPLEX

       650.0      2982.0      2946.0      2921.0      2874.0      1470.0      1446.0      1332.0
      1280.0      1218.0       787.0      1106.0      1012.0       968.0       200.0       774.0
       755.0       416.0      3054.0      2966.0      2936.0      1465.0      1325.0      1279.0
      1238.0      1198.0      1053.0      1030.0       978.0       922.0       914.0       990.0
      3050.0      1188.0       600.0       922.0      1618.0      1400.0      1025.0       600.0
       600.0       954.0       200.0      1000.0


XXXXXXXXXXXXXXXXXXXXXXXXXXXXXXXXXXXXXXXXXXXXXXXXXXXXXXXXXXXXXXXXXXXXXXXXXXXXXXXXXXXXXXXXXXXXXXXXXXXXXXXX

RATE CONSTANTS CALCULATED USING THESE OPTIONS:     KROT = -1  NANH = 0  NCRIT = 0  JDEN =  0  JSUM =  0

XXXXXXXXXXXXXXXXXXXXXXXXXXXXXXXXXXXXXXXXXXXXXXXXXXXXXXXXXXXXXXXXXXXXXXXXXXXXXXXXXXXXXXXXXXXXXXXXXXXXXXXX
```

ESTAR KCAL/MOLE	EDAG KCAL/MOLE	HARMONIC DENSITY	HARMONIC SUM	HARMONIC RATE CONSTANT
7.00	1.00	.1207E+03	.2063E+01	.1025E+10
8.00	2.00	.3354E+03	.1199E+02	.2144E+10
9.00	3.00	.8882E+03	.5269E+02	.3556E+10
10.00	4.00	.2255E+04	.1972E+03	.5242E+10
11.00	5.00	.5518E+04	.6607E+03	.7178E+10
12.00	6.00	.1306E+05	.2035E+04	.9341E+10
13.00	7.00	.2999E+05	.5857E+04	.1171E+11
14.00	8.00	.6702E+05	.1594E+05	.1426E+11
15.00	9.00	.1461E+06	.4136E+05	.1697E+11
16.00	10.00	.3111E+06	.1029E+06	.1984E+11
17.00	11.00	.6486E+06	.2470E+06	.2283E+11
18.00	12.00	.1326E+07	.5737E+06	.2594E+11
19.00	13.00	.2661E+07	.1294E+07	.2915E+11
20.00	14.00	.5249E+07	.2841E+07	.3246E+11
21.00	15.00	.1019E+08	.6090E+07	.3584E+11
22.00	16.00	.1948E+08	.1276E+08	.3929E+11
23.00	17.00	.3670E+08	.2620E+08	.4279E+11
24.00	18.00	.6824E+08	.5276E+08	.4635E+11
25.00	19.00	.1253E+09	.1044E+09	.4995E+11
26.00	20.00	.2271E+09	.2030E+09	.5359E+11
27.00	21.00	.4071E+09	.3888E+09	.5726E+11
28.00	22.00	.7218E+09	.7338E+09	.6095E+11
29.00	23.00	.1266E+10	.1366E+10	.6466E+11
30.00	24.00	.2199E+10	.2509E+10	.6838E+11
31.00	25.00	.3783E+10	.4551E+10	.7212E+11
32.00	26.00	.6448E+10	.8159E+10	.7585E+11
33.00	27.00	.1089E+11	.1446E+11	.7960E+11
34.00	28.00	.1825E+11	.2537E+11	.8334E+11
35.00	29.00	.3033E+11	.4405E+11	.8708E+11
36.00	30.00	.5000E+11	.7574E+11	.9081E+11
37.00	31.00	.8182E+11	.1290E+12	.9453E+11
38.00	32.00	.1329E+12	.2178E+12	.9825E+11
39.00	33.00	.2144E+12	.3646E+12	.1020E+12
40.00	34.00	.3435E+12	.6053E+12	.1056E+12
41.00	35.00	.5468E+12	.9971E+12	.1093E+12
42.00	36.00	.8649E+12	.1630E+13	.1130E+12
43.00	37.00	.1360E+13	.2645E+13	.1166E+12
44.00	38.00	.2125E+13	.4262E+13	.1202E+12
45.00	39.00	.3302E+13	.6820E+13	.1238E+12
46.00	40.00	.5102E+13	.1084E+14	.1274E+12
47.00	41.00	.7841E+13	.1713E+14	.1310E+12
48.00	42.00	.1199E+14	.2690E+14	.1345E+12
49.00	43.00	.1823E+14	.4198E+14	.1380E+12
50.00	44.00	.2760E+14	.6514E+14	.1415E+12
51.00	45.00	.4157E+14	.1005E+15	.1450E+12
52.00	46.00	.6231E+14	.1543E+15	.1484E+12
53.00	47.00	.9299E+14	.2355E+15	.1519E+12
54.00	48.00	.1382E+15	.3578E+15	.1553E+12
55.00	49.00	.2044E+15	.5407E+15	.1586E+12
56.00	50.00	.3010E+15	.8133E+15	.1620E+12

```
BIRADICAL TO BIRADICAL REARRANGEMENT
NO ROTORS, NO OVERALL ROTATION

EZERO =  10.00 KCAL/MOLE     ESTAR =  11.00 KCAL/MOLE


EINC  =   1.00 KCAL/MOLE     REACTION PATH DEGENERACY  =  2.0

  50  RATE CONSTANTS TO BE CALCULATED

NUMBER OF OSCILLATORS IN MOLECULE   NUMBER OF INTERNAL ROTORS IN MOLECULE

              45                         0

FREQUENCIES IN MOLECULE

       400.0     2982.0     2946.0     2921.0     2874.0     1470.0     1446.0     1332.0
      1280.0     1218.0     1188.0     1106.0     1012.0      968.0      883.0      774.0
       755.0      416.0     3054.0     2966.0     2936.0     1465.0     1325.0     1279.0
      1238.0     1198.0     1053.0     1030.0      978.0      922.0      914.0      787.0
      3050.0     1188.0      200.0      922.0      818.0     1218.0     1000.0      200.0
       200.0      854.0      200.0      400.0      787.0

EXTERNAL ROTATIONS TREATED AS INACTIVE

*****STRUCTURE OF THE CRITICAL CONFIGURATION IS SPECIFIED*****

NUMBER OF OSCILLATORS IN COMPLEX   NUMBER OF INTERNAL ROTORS IN COMPLEX

              44                         0

FREQUENCIES IN COMPLEX

       650.0     2982.0     2946.0     2921.0     2874.0     1470.0     1446.0     1332.0
      1280.0     1218.0      787.0     1106.0     1012.0      968.0      200.0      774.0
       755.0      416.0     3054.0     2966.0     2936.0     1465.0     1325.0     1279.0
      1238.0     1198.0     1053.0     1030.0      978.0      922.0      914.0      990.0
      3050.0     1188.0      600.0      922.0     1618.0     1400.0     1025.0      600.0
       600.0      954.0      200.0     1000.0


XXXXXXXXXXXXXXXXXXXXXXXXXXXXXXXXXXXXXXXXXXXXXXXXXXXXXXXXXXXXXXXXXXXXXXXXXXXXXXXXXXXXXXXXXXXXXXXXXXXX

RATE CONSTANTS CALCULATED USING THESE OPTIONS:      KROT = -1  NANH = 0  NCRIT = 0  JDEN =  0  JSUM =  0

XXXXXXXXXXXXXXXXXXXXXXXXXXXXXXXXXXXXXXXXXXXXXXXXXXXXXXXXXXXXXXXXXXXXXXXXXXXXXXXXXXXXXXXXXXXXXXXXXXXX
```

ESTAR KCAL/MOLE	EDAG KCAL/MOLE	HARMONIC DENSITY	HARMONIC SUM	HARMONIC RATE CONSTANT
11.00	1.00	.5518E+04	.2063E+01	.2241E+08
12.00	2.00	.1306E+05	.1199E+02	.5505E+08
13.00	3.00	.2999E+05	.5269E+02	.1053E+09
14.00	4.00	.6702E+05	.1972E+03	.1764E+09
15.00	5.00	.1461E+06	.6607E+03	.2712E+09
16.00	6.00	.3111E+06	.2035E+04	.3921E+09
17.00	7.00	.6486E+06	.5857E+04	.5414E+09
18.00	8.00	.1326E+07	.1594E+05	.7208E+09
19.00	9.00	.2661E+07	.4136E+05	.9318E+09
20.00	10.00	.5249E+07	.1029E+06	.1176E+10
21.00	11.00	.1019E+08	.2470E+06	.1454E+10
22.00	12.00	.1948E+08	.5737E+06	.1766E+10
23.00	13.00	.3670E+08	.1294E+07	.2113E+10
24.00	14.00	.6824E+08	.2841E+07	.2496E+10
25.00	15.00	.1253E+09	.6090E+07	.2915E+10
26.00	16.00	.2271E+09	.1276E+08	.3368E+10
27.00	17.00	.4071E+09	.2620E+08	.3858E+10
28.00	18.00	.7218E+09	.5276E+08	.4382E+10
29.00	19.00	.1266E+10	.1044E+09	.4941E+10
30.00	20.00	.2199E+10	.2030E+09	.5535E+10
31.00	21.00	.3783E+10	.3888E+09	.6162E+10
32.00	22.00	.6448E+10	.7338E+09	.6822E+10
33.00	23.00	.1089E+11	.1366E+10	.7515E+10
34.00	24.00	.1825E+11	.2509E+10	.8240E+10
35.00	25.00	.3033E+11	.4551E+10	.8996E+10
36.00	26.00	.5000E+11	.8159E+10	.9783E+10
37.00	27.00	.8182E+11	.1446E+11	.1060E+11
38.00	28.00	.1329E+12	.2537E+11	.1144E+11
39.00	29.00	.2144E+12	.4405E+11	.1232E+11
40.00	30.00	.3435E+12	.7574E+11	.1322E+11
41.00	31.00	.5468E+12	.1290E+12	.1415E+11
42.00	32.00	.8649E+12	.2178E+12	.1510E+11
43.00	33.00	.1360E+13	.3646E+12	.1608E+11
44.00	34.00	.2125E+13	.6053E+12	.1708E+11
45.00	35.00	.3302E+13	.9971E+12	.1810E+11
46.00	36.00	.5102E+13	.1630E+13	.1915E+11
47.00	37.00	.7841E+13	.2645E+13	.2022E+11
48.00	38.00	.1199E+14	.4262E+13	.2132E+11
49.00	39.00	.1823E+14	.6820E+13	.2243E+11
50.00	40.00	.2760E+14	.1084E+14	.2356E+11
51.00	41.00	.4157E+14	.1713E+14	.2471E+11
52.00	42.00	.6231E+14	.2690E+14	.2588E+11
53.00	43.00	.9299E+14	.4198E+14	.2707E+11
54.00	44.00	.1382E+15	.6514E+14	.2827E+11
55.00	45.00	.2044E+15	.1005E+15	.2949E+11
56.00	46.00	.3010E+15	.1543E+15	.3072E+11
57.00	47.00	.4416E+15	.2355E+15	.3198E+11
58.00	48.00	.6453E+15	.3578E+15	.3324E+11
59.00	49.00	.9391E+15	.5407E+15	.3452E+11
60.00	50.00	.1362E+16	.8133E+15	.3581E+11

```
BIRADICAL TO BIRADICAL REARRANGEMENT
NO ROTORS, NO OVERALL ROTATION

EZERO =  20.00 KCAL/MOLE     ESTAR =  21.00 KCAL/MOLE

EINC  =   1.00 KCAL/MOLE     REACTION PATH DEGENERACY  =  2.0

  50  RATE CONSTANTS TO BE CALCULATED

NUMBER OF OSCILLATORS IN MOLECULE   NUMBER OF INTERNAL ROTORS IN MOLECULE

                 45                         0

FREQUENCIES IN MOLECULE

       400.0      2982.0      2946.0      2921.0      2874.0      1470.0      1446.0      1332.0
      1280.0      1218.0      1188.0      1106.0      1012.0       968.0       883.0       774.0
       755.0       416.0      3054.0      2966.0      2936.0      1465.0      1325.0      1279.0
      1238.0      1198.0      1053.0      1030.0       978.0       922.0       914.0       787.0
      3050.0      1188.0       200.0       922.0       818.0      1218.0      1000.0       200.0
       200.0       854.0       200.0       400.0       787.0

EXTERNAL ROTATIONS TREATED AS INACTIVE

*****STRUCTURE OF THE CRITICAL CONFIGURATION IS SPECIFIED*****

NUMBER OF OSCILLATORS IN COMPLEX   NUMBER OF INTERNAL ROTORS IN COMPLEX

                 44                         0

FREQUENCIES IN COMPLEX

       650.0      2982.0      2946.0      2921.0      2874.0      1470.0      1446.0      1332.0
      1280.0      1218.0       787.0      1106.0      1012.0       968.0       200.0       774.0
       755.0       416.0      3054.0      2966.0      2936.0      1465.0      1325.0      1279.0
      1238.0      1198.0      1053.0      1030.0       978.0       922.0       914.0       990.0
      3050.0      1188.0       600.0       922.0      1618.0      1400.0      1025.0       600.0
       600.0       954.0       200.0      1000.0


XXXXXXXXXXXXXXXXXXXXXXXXXXXXXXXXXXXXXXXXXXXXXXXXXXXXXXXXXXXXXXXXXXXXXXXXXXXXXXXXXXXXXXXXXXXXXXXXXXXXXXXXX

RATE CONSTANTS CALCULATED USING THESE OPTIONS:      KROT = -1  NANH = 0  NCRIT = 0  JDEN =  0  JSUM =  0

XXXXXXXXXXXXXXXXXXXXXXXXXXXXXXXXXXXXXXXXXXXXXXXXXXXXXXXXXXXXXXXXXXXXXXXXXXXXXXXXXXXXXXXXXXXXXXXXXXXXXXXXX
```

```
  ESTAR          EDAG          HARMONIC        HARMONIC         HARMONIC
KCAL/MOLE      KCAL/MOLE        DENSITY           SUM         RATE CONSTANT


  21.00          1.00         .1019E+08       .2063E+01        .1214E+05
  22.00          2.00         .1948E+08       .1199E+02        .3691E+05
  23.00          3.00         .3670E+08       .5269E+02        .8606E+05
  24.00          4.00         .6824E+08       .1972E+03        .1733E+06
  25.00          5.00         .1253E+09       .6607E+03        .3162E+06
  26.00          6.00         .2271E+09       .2035E+04        .5370E+06
  27.00          7.00         .4071E+09       .5857E+04        .8624E+06
  28.00          8.00         .7218E+09       .1594E+05        .1324E+07
  29.00          9.00         .1266E+10       .4136E+05        .1958E+07
  30.00         10.00         .2199E+10       .1029E+06        .2806E+07
  31.00         11.00         .3783E+10       .2470E+06        .3914E+07
  32.00         12.00         .6448E+10       .5737E+06        .5334E+07
  33.00         13.00         .1089E+11       .1294E+07        .7120E+07
  34.00         14.00         .1825E+11       .2841E+07        .9333E+07
  35.00         15.00         .3033E+11       .6090E+07        .1204E+08
  36.00         16.00         .5000E+11       .1276E+08        .1530E+08
  37.00         17.00         .8182E+11       .2620E+08        .1920E+08
  38.00         18.00         .1329E+12       .5276E+08        .2380E+08
  39.00         19.00         .2144E+12       .1044E+09        .2918E+08
  40.00         20.00         .3435E+12       .2030E+09        .3543E+08
  41.00         21.00         .5468E+12       .3888E+09        .4263E+08
  42.00         22.00         .8649E+12       .7338E+09        .5086E+08
  43.00         23.00         .1360E+13       .1366E+10        .6022E+08
  44.00         24.00         .2125E+13       .2509E+10        .7077E+08
  45.00         25.00         .3302E+13       .4551E+10        .8263E+08
  46.00         26.00         .5102E+13       .8159E+10        .9587E+08
  47.00         27.00         .7841E+13       .1446E+11        .1106E+09
  48.00         28.00         .1199E+14       .2537E+11        .1269E+09
  49.00         29.00         .1823E+14       .4405E+11        .1448E+09
  50.00         30.00         .2760E+14       .7574E+11        .1645E+09
  51.00         31.00         .4157E+14       .1290E+12        .1861E+09
  52.00         32.00         .6231E+14       .2178E+12        .2096E+09
  53.00         33.00         .9299E+14       .3646E+12        .2351E+09
  54.00         34.00         .1382E+15       .6053E+12        .2627E+09
  55.00         35.00         .2044E+15       .9971E+12        .2925E+09
  56.00         36.00         .3010E+15       .1630E+13        .3246E+09
  57.00         37.00         .4416E+15       .2645E+13        .3591E+09
  58.00         38.00         .6453E+15       .4262E+13        .3960E+09
  59.00         39.00         .9391E+15       .6820E+13        .4354E+09
  60.00         40.00         .1362E+16       .1084E+14        .4775E+09
  61.00         41.00         .1967E+16       .1713E+14        .5222E+09
  62.00         42.00         .2830E+16       .2690E+14        .5697E+09
  63.00         43.00         .4058E+16       .4198E+14        .6201E+09
  64.00         44.00         .5800E+16       .6514E+14        .6734E+09
  65.00         45.00         .8259E+16       .1005E+15        .7297E+09
  66.00         46.00         .1172E+17       .1543E+15        .7890E+09
  67.00         47.00         .1659E+17       .2355E+15        .8514E+09
  68.00         48.00         .2339E+17       .3578E+15        .9171E+09
  69.00         49.00         .3288E+17       .5407E+15        .9859E+09
  70.00         50.00         .4608E+17       .8133E+15        .1058E+10
```

```
BIRADICAL TO BIRADICAL REARRANGEMENT
NO ROTORS, NO OVERALL ROTATION

EZERO =  40.00 KCAL/MOLE     ESTAR =  41.00 KCAL/MOLE

EINC  =   1.00 KCAL/MOLE     REACTION PATH DEGENERACY  =  2.0

  50  RATE CONSTANTS TO BE CALCULATED

NUMBER OF OSCILLATORS IN MOLECULE   NUMBER OF INTERNAL ROTORS IN MOLECULE

                 45                         0

FREQUENCIES IN MOLECULE

      400.0      2982.0      2946.0      2921.0      2874.0      1470.0      1446.0      1332.0
     1280.0      1218.0      1188.0      1106.0      1012.0       968.0       883.0       774.0
      755.0       416.0      3054.0      2966.0      2936.0      1465.0      1325.0      1279.0
     1238.0      1198.0      1053.0      1030.0       978.0       922.0       914.0       787.0
     3050.0      1188.0       200.0       922.0       818.0      1218.0      1000.0       200.0
      200.0       854.0       200.0       400.0       787.0

EXTERNAL ROTATIONS TREATED AS INACTIVE

*****STRUCTURE OF THE CRITICAL CONFIGURATION IS SPECIFIED*****

NUMBER OF OSCILLATORS IN COMPLEX   NUMBER OF INTERNAL ROTORS IN COMPLEX

                 44                         0

FREQUENCIES IN COMPLEX

      650.0      2982.0      2946.0      2921.0      2874.0      1470.0      1446.0      1332.0
     1280.0      1218.0       787.0      1106.0      1012.0       968.0       200.0       774.0
      755.0       416.0      3054.0      2966.0      2936.0      1465.0      1325.0      1279.0
     1238.0      1198.0      1053.0      1030.0       978.0       922.0       914.0       990.0
     3050.0      1188.0       600.0       922.0      1618.0      1400.0      1025.0       600.0
      600.0       954.0       200.0      1000.0


XXXXXXXXXXXXXXXXXXXXXXXXXXXXXXXXXXXXXXXXXXXXXXXXXXXXXXXXXXXXXXXXXXXXXXXXXXXXXXXXXXXXXXXXXXXXXXXXXXXXXXX

RATE CONSTANTS CALCULATED USING THESE OPTIONS:      KROT = -1  NANH = 0  NCRIT = 0  JDEN =  0  JSUM =  0

XXXXXXXXXXXXXXXXXXXXXXXXXXXXXXXXXXXXXXXXXXXXXXXXXXXXXXXXXXXXXXXXXXXXXXXXXXXXXXXXXXXXXXXXXXXXXXXXXXXXXXX
```

ESTAR KCAL/MOLE	EDAG KCAL/MOLE	HARMONIC DENSITY	HARMONIC SUM	HARMONIC RATE CONSTANT
41.00	1.00	.5468E+12	.2063E+01	.2262E+00
42.00	2.00	.8649E+12	.1199E+02	.8312E+00
43.00	3.00	.1360E+13	.5269E+02	.2323E+01
44.00	4.00	.2125E+13	.1972E+03	.5564E+01
45.00	5.00	.3302E+13	.6607E+03	.1200E+02
46.00	6.00	.5102E+13	.2035E+04	.2391E+02
47.00	7.00	.7841E+13	.5857E+04	.4478E+02
48.00	8.00	.1199E+14	.1594E+05	.7972E+02
49.00	9.00	.1823E+14	.4136E+05	.1360E+03
50.00	10.00	.2760E+14	.1029E+06	.2236E+03
51.00	11.00	.4157E+14	.2470E+06	.3563E+03
52.00	12.00	.6231E+14	.5737E+06	.5520E+03
53.00	13.00	.9299E+14	.1294E+07	.8342E+03
54.00	14.00	.1382E+15	.2841E+07	.1233E+04
55.00	15.00	.2044E+15	.6090E+07	.1786E+04
56.00	16.00	.3010E+15	.1276E+08	.2542E+04
57.00	17.00	.4416E+15	.2620E+08	.3557E+04
58.00	18.00	.6453E+15	.5276E+08	.4902E+04
59.00	19.00	.9391E+15	.1044E+09	.6663E+04
60.00	20.00	.1362E+16	.2030E+09	.8940E+04
61.00	21.00	.1967E+16	.3888E+09	.1185E+05
62.00	22.00	.2830E+16	.7338E+09	.1554E+05
63.00	23.00	.4058E+16	.1366E+10	.2017E+05
64.00	24.00	.5800E+16	.2509E+10	.2593E+05
65.00	25.00	.8259E+16	.4551E+10	.3303E+05
66.00	26.00	.1172E+17	.8159E+10	.4173E+05
67.00	27.00	.1659E+17	.1446E+11	.5229E+05
68.00	28.00	.2339E+17	.2537E+11	.6503E+05
69.00	29.00	.3288E+17	.4405E+11	.8032E+05
70.00	30.00	.4608E+17	.7574E+11	.9853E+05
71.00	31.00	.6439E+17	.1290E+12	.1201E+06
72.00	32.00	.8971E+17	.2178E+12	.1456E+06
73.00	33.00	.1246E+18	.3646E+12	.1754E+06
74.00	34.00	.1726E+18	.6053E+12	.2102E+06
75.00	35.00	.2385E+18	.9971E+12	.2507E+06
76.00	36.00	.3285E+18	.1630E+13	.2974E+06
77.00	37.00	.4514E+18	.2645E+13	.3513E+06
78.00	38.00	.6185E+18	.4262E+13	.4131E+06
79.00	39.00	.8454E+18	.6820E+13	.4836E+06
80.00	40.00	.1153E+19	.1084E+14	.5640E+06
81.00	41.00	.1568E+19	.1713E+14	.6551E+06
82.00	42.00	.2127E+19	.2690E+14	.7582E+06
83.00	43.00	.2878E+19	.4198E+14	.8744E+06
84.00	44.00	.3904E+19	.6514E+14	.1000E+07
85.00	45.00	.5265E+19	.1005E+15	.1145E+07
86.00	46.00	.7085E+19	.1543E+15	.1306E+07
87.00	47.00	.9511E+19	.2355E+15	.1485E+07
88.00	48.00	.1274E+20	.3578E+15	.1684E+07
89.00	49.00	.1702E+20	.5407E+15	.1904E+07
90.00	50.00	.2270E+20	.8133E+15	.2148E+07